

Arginine Methylation and RNA Metabolism in Muscle Stem Cells and Beyond

by

Claudia Dominici

Department of Human Genetics

McGill University, Montreal

December 2021

A thesis submitted to McGill University in partial fulfillment of the requirements of the
degree of Doctor of Philosophy

© Claudia Dominici, 2021

Abstract

Post-translational modifications are an important layer of regulation for a wide range of cellular functions. Methylation of arginine residues is critical for the regulation of several of these processes, with complex implications in pathologies. Protein arginine methyl transferases (PRMTs) carry out arginine methylation in the cell and are often overexpressed in cancers making inhibitors of their activity promising therapeutics. Notably, however, single-treatment cancer therapy has limitations due to high toxicity or transient efficiency. Therefore, investigating synergistic combinations that could be delivered at lower doses would be a promising benefit. In the first chapter of this thesis, we identify compounds that synergize with an inhibitor of type I PRMTs, MS023, and increase its toxicity in A549 non-small cell lung carcinoma (NSCLC) cells. We find that poly(ADP)-ribose polymerase (PARP) inhibitors synergize strongly with MS023 to decrease the viability of A549 cells, thus identifying a strong synergistic drug combination that may represent a new therapeutic avenue for PARP inhibitor-resistant cancer cells.

Inhibitors of PRMTs have a wide therapeutic range. In the second chapter of this thesis, we characterize the effect of PRMT1 inhibition on muscle stem cells (MuSCs) and their regenerative capacity. It was previously shown that genetic deletion of PRMT1 in MuSCs produces a highly proliferative phenotype but blocks the process of differentiation. I have now shown that transiently inhibiting PRMT1 achieves enhanced proliferation while still allowing for differentiation capabilities. Enhancing the proliferative capacity of MuSCs can be therapeutically advantageous in patients with muscle wasting disease whose MuSCs precociously differentiate and thus have exhausted MuSC pools. We determine that temporary inhibition of PRMT1 with MS023 allows for accelerated cellular metabolism and extensive MuSC expansion *in vivo*, and

subsequently improves muscle regeneration. Therefore, we identify a small molecule compound which can promote MuSC proliferation while still supporting differentiation capabilities.

In addition to complex post-translational modifications involved in MuSC function during muscle regeneration, there is a network of post-transcriptional regulators which play an important role. The RNA-binding protein Quaking (QKI) acts on a wide range of RNA targets to regulate splicing, mRNA stability and nuclear export of mRNA. In the third chapter of my thesis, I show that QKI regulates asymmetric cell divisions, a process which gives rise to committed MuSCs with muscle regeneration capabilities, via direct binding to integrin alpha-7 pre-mRNA to regulate its alternative splicing. We subsequently showed a severe regeneration defect in QKI knockout mice, and a lack of myogenic progenitor cells on *ex vivo* cultured myofibers. Therefore, we have shown that QKI-mediated alternative splicing is a key part of the machinery required for proper MuSC function and muscle regeneration.

In sum, I highlight the complexity of the physiological outcomes of arginine methylation in cancer and MuSCs. We indicate that PRMT1 inhibition strongly synergizes with PARP inhibitors to induce death in cancer cells, and that it can also act to modify the identity of MuSCs and enhance their regenerative capacity. Furthermore, I identify the QKI RNA binding protein as a key regulator of MuSC function and muscle regeneration.

Résumé

Les modifications post-traductionnelles jouent un rôle important dans la régulation de différentes fonctions cellulaires. La méthylation des résidus d'arginine est une étape cruciale pour la régulation de plusieurs de ces processus, et est fortement impliquée dans les pathologies. Les protéines arginine méthyltransférases (PRMTs) sont les enzymes responsables de la méthylation de l'arginine dans la cellule et sont souvent surexprimées dans les cancers, faisant de leurs inhibiteurs une entrée prometteuse en thérapie. Notamment, la thérapie anticancéreuse à traitement unique a des limites à cause de la toxicité élevée ou de l'efficacité transitoire. Par conséquent, des combinaisons synergiques de drogues, administrées à des doses plus faibles, pourraient être une alternative prometteuse. Dans le premier chapitre de cette thèse, nous avons identifié des composés qui agissent en synergie avec un inhibiteur de PRMT1, MS023 et qui augmentent sa toxicité dans les cellules A549, cancer du poumon à cellules non petites (NSCLC). Nous remarquons une forte synergie entre les inhibiteurs de la poly (ADP-ribose) polymérase (PARP) et MS023 pour diminuer la viabilité des cellules A549, identifiant ainsi une forte combinaison synergique de médicament qui peut représenter une nouvelle voie thérapeutique pour les cellules cancéreuses résistantes aux inhibiteurs de PARP.

Les inhibiteurs des PRMTs constituent une cible thérapeutique importante. Dans le deuxième chapitre de cette thèse, nous avons caractérisé l'effet de l'inhibition de PRMT1 sur les cellules souches musculaires (MuSCs) et leur capacité de régénération. Des travaux antérieurs de notre laboratoire ont montré que l'inhibition de PRMT1 dans les MuSCs bloque le processus de différenciation, tout en évoluant vers un phénotype hautement prolifératif. L'amélioration de la capacité de prolifération des MuSCs peut être thérapeutiquement avantageuse chez les patients atteints d'atrophie musculaire dont les MuSCs se différencient très tôt et épuisent le stock des

MuSCs. Nous avons montré que l'inhibition temporaire de PRMT1 par MS023 accélérât le métabolisme cellulaire et favorisait une expansion étendue des MuSCs *in vivo*, et par conséquent, la régénération musculaire est améliorée. Ainsi, nous avons identifié un inhibiteur important qui peut favoriser la prolifération des MuSCs tout en soutenant leur capacité de différenciation.

En plus des modifications post-traductionnelles impliquées dans la fonction des MuSCs lors de la régénération musculaire, il existe des régulateurs post-transcriptionnels qui jouent un rôle important. La protéine de liaison à l'ARN Quaking (QKI) agit sur un large éventail de cibles d'ARN pour réguler l'épissage, la stabilité de l'ARNm et l'exportation nucléaire de l'ARNm. Dans le troisième chapitre de cette thèse, il a été montré que QKI régule les divisions cellulaires asymétriques ; un processus qui donne naissance à des MuSCs engagées avec des capacités de régénération musculaire, via une liaison directe à la protéine intégrine alpha-7 pour réguler son épissage alternatif. Nous avons ensuite montré que les souris dépourvues de QKI (knock-out QKI) présentent un défaut majeur de régénération et un manque de cellules progénitrices myogéniques sur des myofibres cultivées *ex vivo*. Par conséquent, nous avons montré que l'épissage alternatif médié par QKI est un élément clé de la machinerie requise pour le bon fonctionnement des MuSCs et la régénération musculaire.

En résumé, les chapitres un et deux de cette thèse mettent en évidence la complexité des résultats physiologiques de la méthylation de l'arginine. Nous montrons que l'inhibition de PRMT1 agit comme un synergiseur puissant pour induire la mort des cellules cancéreuses, et peut également agir pour modifier l'identité des MuSCs et améliorer leur capacité de régénération. De plus, nous identifions que la protéine QKI agit comme un régulateur clé de la fonction des MuSCs et de la régénération musculaire.

Table of Contents

ABSTRACT	2
RÉSUMÉ	4
LIST OF ABBREVIATIONS	8
LIST OF FIGURES	12
ACKNOWLEDGEMENTS	13
CONTRIBUTION TO ORIGINAL KNOWLEDGE	15
PREFACE	17
CONTRIBUTION OF THE AUTHORS	18
CHAPTER 1: INTRODUCTION	19
PART 1: MUSCLE STEM CELLS AND MUSCLE REGENERATION	19
1.1 <i>Skeletal muscle</i>	19
1.2 <i>Muscle stem cells</i>	20
1.2.1 Muscle stem cell quiescence	21
1.2.2 Muscle stem cell proliferation: Symmetric and asymmetric division	22
1.2.3 The muscle stem cell niche	24
1.4.4 Muscle stem cell differentiation	25
1.4.5 Muscle stem cell metabolism	26
1.3 <i>Muscle wasting disease</i>	27
1.3.1 Duchenne Muscular Dystrophy (DMD)	27
1.3.2 Aging: Sarcopenia	28
1.3.3 Mouse models of muscle wasting disease	29
PART 2 ARGININE METHYLATION AND SKELETAL MUSCLE	31
2.1 <i>Arginine methylation</i>	31
2.2 <i>Protein Arginine MethylTransferases (PRMTs)</i>	32
2.3 <i>PRMT Structure</i>	32
2.4 <i>PRMT substrates</i>	33
2.5 <i>Readers and erasers of arginine methylation</i>	34
2.6 <i>PRMTs and skeletal muscle stem cells</i>	36
2.6.1 PRMT1 and muscle stem cells	37
2.6.2 CARM1 and skeletal muscle	38
2.6.3 PRMT5 and muscle stem cells	39
2.6.4 PRMT7 muscle stem cells	40
2.7 <i>Beyond muscle stem cells: Arginine methylation and cancer</i>	43
2.7.1 PRMT1 and cancer	43
2.7.2 PRMT5 and cancer	45
2.7.2.1 MTAP deficiency and PRMT5	47
2.7.3 PRMT7 and cancer	47
2.7.4 Inhibitors of PRMTs	48
2.7.5 Substrate sharing of PRMTs	49
PART 3: RNA METABOLISM AND MUSCLE STEM CELLS	52
3.1 <i>RNA binding proteins (RBPs) and their functions</i>	52
3.1.1 Splicing	52
3.1.2 Post-transcriptional mRNA modifications	54
3.3 <i>The Quaking RNA binding protein and its role in muscle</i>	56
HYPOTHESIS AND OBJECTIVES	61
CHAPTER 2: SYNERGISTIC EFFECTS OF TYPE I PRMT AND PARP INHIBITORS AGAINST NON-SMALL CELL LUNG CANCER CELLS	62

2.1 PREFACE	62
2.2 ABSTRACT	63
2.3 BACKGROUND	65
2.4 RESULTS.....	68
2.5 DISCUSSION	88
2.6 CONCLUSIONS	90
2.7 MATERIALS AND METHODS	91
2.8 REFERENCES	96
2.9 SUPPLEMENTAL INFORMATION	101
CHAPTER 3: INHIBITION OF TYPE I PRMTS REFORMS MUSCLE STEM CELL IDENTITY VIA AMPK ACTIVATION, ENHANCING THEIR THERAPEUTIC CAPACITY	104
3.1 PREFACE	104
3.2 ABSTRACT	105
3.3 INTRODUCTION.....	106
3.4 RESULTS.....	108
3.5 DISCUSSION	136
3.6 MATERIALS AND METHODS	142
3.7 REFERENCES	151
3.8 SUPPLEMENTAL INFORMATION	155
CHAPTER 4: MUSCLE STEM CELL POLARITY REQUIRES QKI-MEDIATED ALTERNATIVE SPLICING OF INTEGRIN ALPHA-7 (ITGA7)	165
4.1 PREFACE	165
4.2 ABSTRACT	166
4.3 INTRODUCTION.....	166
4.4 RESULTS.....	168
4.5 DISCUSSION	188
4.6 MATERIALS & METHODS.....	191
4.7 REFERENCES	199
4.8 SUPPLEMENTAL INFORMATION	203
CHAPTER 6: CONCLUSION AND FUTURE DIRECTIONS	218
CHAPTER 7: REFERENCES	229

List of Abbreviations

MuSC	Muscle stem cell
QKI	Quaking
Itga7	Integrin alpha-7
MYHC	Myosin heavy chain
MRF	Myogenic regulatory facto
PAX7	Paired box protein 7
HGFA	hepatocyte growth factor activator
MYF5	Myogenic factor 5
MyoD	Myoblast determination protein 1
WNT7A	Wnt family member 7A
ECM	extra cellular matrix
DLL1	Delta like ligand 1
DLL4	Delta like ligand 4
MYF6	Myogenic factor 6
EGF	Epidermal growth factor
EGFR	Epidermal growth factor receptor
FAP	fibroadipogenic progenitor
TFIID	Transcription factor II D
TAF3	TATA box-binding associated factor 3
TRF3	TATA box-binding related factor 3
FAO	Fatty acid oxidation
OxPhos	Oxidative phosphorylation
SIRT1	Sirtuin 1
NAD	Nicotinamide adenine dinucleotide
LDHA	Lactate dehydrogenase
DMD(gene)	Dystrophin
DMD(disease)	Duchenne muscular dystrophy
MARK2	Microtubule affinity regulating kinase 2
PARD3	Par-3 family cell polarity regulator
CR	Calorie restriction
CTX	Cardiotoxin
PRMT	Protein arginine methyltransferase
PTM	Post translational modification
MMA	Monomethyl arginine
aDMA	Asymmetric dimethylarginine
sDMA	Symmetric dimethylarginine
SAM	S-adenosyl methionine
SAH	S-adenosyl-L-homocysteine

TIM	Triosephosphate isomerase
snRNP	small nuclear ribonucleoprotein
SMN	Survival of motor neuron
TDRD3	Tudor domain containing 3
SPF30	Splicing factor 30
SMA	Spinal muscular atrophy
KDM	Lysine demethylase
PAD4	Peptidyl arginine deiminase 4
HuR	Human antigen R
AMPK	Amp-activated kinase
ULK1	Unc-51 like autophagy activating kinase
PGC-1 α	PPARG coactivator 1 alpha
BRG1	Brahma-related gene 1
DNMT3B	DNA methyltransferase 3b
SBIDDS	Short stature brachydactyly obesity global developmental delay syndrome
SWI/SNF	SWItch/Sucrose non-fermentable
SMARCA4	SWI/SNF Related, Matrix Associated, Actin Dependent Regulator Of Chromatin, Subfamily A, Member 4
EZH2	Enhancer of zeste homologue 1
PCR2	Polycomb repressive complex 2
NHEJ	Non-homologous end joining
PDAC	Pancreatic ductal adenocarcinoma
ST7	Suppression of tumorigenicity 7
NM23	Nucleoside diphosphate kinase 1
NMD	Nonsense-mediated decay
AML	Acute myeloid leukemia
RBMX	RNA binding motif protein X-linked
AKT	Protein kinase B
PIP3	Phosphatidylinositol (3,4,5)-triphosphate
PDK1	Pyruvate dehydrogenase kinase 1
MTAP	Methylthioadenosine phosphorylase
EMT	Epithelial to mesenchyme transition
MAT2a	Methionine adenosyltransferase 2A
MYC	MYC proto-oncogene
FUS	Fused in sarcoma
PABPN1	Poly adenylyate binding protein nuclear 1
RBP	RNA binding protein
KH	K homology
RRM	RNA recognition motif
5'SS	5' splice site

MBNL1	Muscleblind like splicing regulator 1
RBP24	RNA binding protein 24
m ⁶ A	N ⁶ -methyladenosine
METTL3	Methyltransferase 3, N6-adenosine methyltransferase complex catalytic subunit
METTL14	Methyltransferase 14, N6-adenosine methyltransferase subunit
YTH	YT521 homology
RBFOX1	RNA binding protein, fox-1 homolog
MYBPC1	Myosin binding protein C1
Celf1	CUGBP Elav-like family member 1
<i>qk</i> ^v	QKI viable
VSMC	Vascular smooth muscle cells
NSCLC	Non-small cell lung carcinoma
PARPi	PARP inhibitor
PARP	Poly (ADP-ribose) polymerase
DDR	DNA damage response
HR	Homologous recombination
DMSO	Dimethyl sulfoxide
scRNA-seq	single cell RNA sequencing
UMAP	Uniform manifold approximation and projection
TA	Tibialis anterior
AS	Alternative splicing
ASO	Antisense oligonucleotide
TAM	Tamoxifen
SE	Skipped exon
MSE	Multiple skipped exons
RI	Retained intron
A5SS	Alternative 5' splice site
ALE	Alternative last exon
IGV	Integrated Genome Browser
DEG	Differentially expressed genes
DM1	Myotonic dystrophy type I
DGC	Dystrophin glycoprotein complex
QRE	Quaking response element
fGM	Fiber growth media
SSE	Splicing silencer element
DMPK1	Myotonic dystrophy protein kinase 1
CLCN1	Chloride voltage gated channel 1
EDL	Extensor digitorum longus
RT	Room temperature
FACS	Fluorescence activated cell sorting

FDR	False discovery rate
NaCl	Sodium chloride
SETD7	SET domain containing 7, histone lysine methyltransferase
BRCA2	Breast cancer 2
PROTAC	Proteolysis-targeting chimera
AURKA	Aurora kinase A
PTB	Polypyrimidine tract binding protein 1

List of Figures

Figure 1.1. Overview of PRMT contributions to the myogenic process	42
Figure 1.2. PRMT inhibition Dynamics.....	51
Figure 1.3 Summary of QKI structure and functions	60
Figure 2.1. Cell viability screen to identify compounds targeting epigenetic regulators that synergize with MS023. 69	
Figure 2.2. Drug screening analyses by target and molecular pathway reveal the synergistic interaction between MS023 and PARP inhibitors.....	74
Figure 2.3. Combination of MS023 with low concentrations of BMN-673 results in synthetic lethality of A549 lung adenocarcinoma cells.....	77
Figure 2.4. Synergistic effect of MS023 and BMN-673 is dependent on MTAP deficiency in A549 cells.	78
Figure 2.5. BMN-673 also synergizes with PRMT5 inhibitors.	81
Figure 2.6. Accumulation of DNA double-strand breaks in A549 cells treated with MS023 and BMN-673.	85
Figure 2.7. Treatment with MS023 renders PARPi-resistant PEO4 ovarian adenocarcinoma cells sensitive to BMN-673.	88
Supplemental figure S2.1. Validation of the drug screen.	101
Supplemental figure S2.2. MS023 and BMN-673 synergy dependency on MTAP in NSCLC cell lines.....	103
Figure 3.1. Enhanced self-renewal of MS023-treated MuSCs	111
Figure 3.2 Single-cell graph-based clustering analysis.....	117
Figure 3.3 Pseudotime trajectory of pooled, DMSO- and MS023-treated MuSCs.....	121
Figure 3.4 MS023-treated proliferating MuSCs retain oxidative phosphorylation.....	124
Figure 3.5 MS023 treatment of cultured MuSCs maintains high levels of OxPhos via activation of Ampk.....	127
Figure 3.6 MS023 treatment is reversible and allows expanded MuSCs to differentiate ex vivo and in vivo.....	131
Figure 3.7 in vivo administration of MS023 to dystrophic mice improves muscle strength	134
Supplemental Figure S3.1.....	155
Supplemental Figure S3.2.....	156
Supplemental Figure S3.3.....	160
Supplemental Figure S3.4.....	161
Supplemental Figure S3.5.....	162
Supplemental Figure S3.6.....	163
Supplemental Figure S3.7.....	164
Figure 4.1. Mice with QKI-depleted MuSCs exhibit reduced myogenic progenitors and defects in skeletal muscle regeneration.....	170
Figure 4.2. QKI-deficient primary skeletal MuSCs drastically down-regulate markers of terminal differentiation... 176	
Figure 4.3. Components of MuSC polarity establishment undergo AS in QKI-deficient MuSCs.....	180
Figure 4.4 Inclusion of Itga7-X1 (exon 5) is sufficient to induce loss of MuSC polarity and reduction of myogenic progenitors.....	186
Supplemental figure S4.1.	203
Supplemental figure S4.2.	204
Supplemental figure S4.3.	206
Supplemental figure S4.4.	207

Acknowledgements

I would first like to express my gratitude to my supervisor and mentor, Dr. Stéphane Richard. I have grown in many ways since joining your lab, in no small part due to your leadership and expertise. I always appreciated that you encouraged your students to explore their projects with curiosity and independence. One of the biggest strengths I take away from your mentorship is having the confidence to just go for it. I'm sure with all the lessons learned under your guidance that I am prepared for anything that comes next.

I'd like to acknowledge my committee members, Dr. Yojiro Yamanaka, Dr. Michael Witcher, and Dr. Nicolas Dumont, for your support and guidance throughout the years. Admittedly, annual committee meetings can be daunting and intimidating, but I always left them feeling reassured and energized by your valued insights and encouragement.

I would like to thank my collaborators who helped craft the stories that are integral to this thesis. It was a pleasure to work with Dr. Noel Raynal and Dr. Nicolas Sgarioto at the Centre Hospitalier Universitaire Ste-Justine, and with Dr. Jean-Yves Masson and Laura Sesma-Sanz at Université de Sherbrooke to uncover an important synergy between PARP and PRMT inhibitors in cancer cells. I would also like to acknowledge my collaborators for the study of PRMT1 in muscle stem cells, namely Dr. Oscar Villareal for his computational expertise, and Dr. Nicolas Dumont and Dr. Junio Dort for their assistance with *in vivo* studies of PRMT1 inhibition.

My dear lab members. I'm so fortunate to have had a vibrant, supportive, and reliable cohort to complete my PhD with. In addition to learning from your bright minds and sharp scientific thinking, our happy hours and coffee breaks were always a joy and a great opportunity to see what terrific people you all are. Zhenbao, your expertise is unrivaled, and I thank you for always being willing to help and provide input, and for your patience. Nivine, I'm grateful for being able to

confide in you and draw from your experience. My fellow PhD students Ting and Jeesan, your friendship brought a brightness to the last 4 years that I am so grateful for.

This academic endeavour has come with many challenges, some of the toughest I've ever had to face. I consider myself extremely fortunate to be so unconditionally supported by my family. Mom and Dad, even though I know you still have no idea what I actually do, I know that you are always in my corner and rooting for me. Thank you for always encouraging me to pursue what I love - from when I was a kid with a rock tumbler to now, an adult with a science degree. To my parents-in-law Jim and Lisa, thank you for always having a glass of wine ready and for your constant support. My brother Matthew and sister-in-law Natalie, I still laugh when I think back to the enormous gift basket waiting for me in my lobby after my first paper got accepted, thank you for your encouragement. Kyrn, this PhD is a testament to your belief in me. You are always the first to shoulder my complaints, insecurities, and doubts; and you're also the first to celebrate my successes and accomplishments (somehow both involve fuzzy peaches, which is why you're so great ;). Here's to much more fun ahead.

Contribution to original knowledge

The contributions to original knowledge presented in my thesis are highlighted below:

Chapter 2:

- Screen of FDA-approved epigenetic cancer drugs in the A549 non-small cell lung carcinoma cell line revealing top compounds that synergize with type I PRMT inhibitor MS023
- Characterization of synthetic lethality of type I PRMT inhibitors and PARP inhibitors in A549 non-small cell lung carcinoma cell line
- Characterization of synthetic lethality of PRMT5 inhibitors and PARP inhibitors in A549 non-small cell lung carcinoma cell line
- Identification of a treatment strategy for PARP inhibitor-resistant and PARP inhibitor-sensitive ovarian carcinoma cell lines through treatment with PRMT inhibitors
- Identification of DNA damage repair deficiency in inhibitor treated A549 cell line (Type I PRMT inhibitor alone and in combination with a PARP inhibitor)

Chapter 3:

- Characterization of MS023-treated muscle stem cells (MuSCs) at the scRNAseq level revealing novel MuSC subpopulations
- Identification of metabolic regulation by MS023 treatment, creating a previously uncharacterized metabolic state in MuSCs with elevated OxPhos and glycolysis
- Improvement of strength and force generation in a mouse model of Duchenne muscular dystrophy (*mdx*) with MS023 injection

- Enhanced self-renewal and engraftment potential can be obtained with MS023 treatment of *ex vivo* cultured MuSCs
- Long term culture capabilities of MuSCs that retain stemness with MS023 treatment

Chapter 4:

- The first study of Quaking (QKI) deficiency in MuSCs *in vivo*
- Identification of severe muscle regeneration defects in mice with QKI-deficient MuSCs
- QKI is a key regulator of MuSC polarity
- Discovery that QKI is the RNA binding protein which regulates the alternative splicing of integrin alpha-7 (Itga7) embryonic versus adult isoforms (Itga7-X1 and Itga7-X2). Loss of QKI produced the embryonic isoform which is deficient at establishing polarity in the MuSC.
- QKI-mediated loss of polarity leads to defects in asymmetric MuSC division, partially explaining the severe regeneration defects in QKI deficient mice

PREFACE

This is a manuscript-based thesis which includes the text and figures of three original research manuscripts. Chapter 1 consists of a general introduction and literature review. Chapters 2-4 are the core of the thesis and describe the research I conducted under the supervision of Dr. Stéphane Richard for my PhD. Chapter 2 is a published manuscript, Chapter 3 is in preparation to be submitted, and Chapter 4 is a published manuscript. Chapters 2-4 each contain their own preface, abstract, introduction, materials and methods, results, discussion, and references sections. Lastly, Chapter 5 contains a final unifying discussion and Chapter 6 contains conclusions and future directions.

Papers included in this Thesis

Chapter 2

C. Dominici, N. Sgarioto, Z. Yu, L. Sesma-Sanz, J. Y. Masson, S. Richard & N. J. Raynal 2021. Synergistic effects of type I PRMT and PARP inhibitors against non-small cell lung cancer cells. *Clin Epigenetics*, 13, 54.
DOI: 10.1186/s13148-021-01037-1

Chapter 3

C. Dominici, O. Villareal, J. Dort, YC. Wang, E. Heckel, J. Ragoussis, JS. Joyal, N. Dumont, Stéphane Richard. Inhibition of Type I PRMTs Enhances Muscle Stem Cell Therapeutic Capacity. *Manuscript in preparation*.

Chapter 4

C. Dominici and S. Richard 2022. Muscle Stem Cell Polarity Requires QKI-mediated Alternative Splicing of Integrin Alpha-7 (Itga7). *Life Science Alliance*, 5(5):e202101192.
DOI: 10.26508/lsa.202101192.

Contribution of the Authors

Dr. Stéphane Richard supervised all the studies performed in this thesis. I performed the majority of the research, and all writing was done with guidance and support from Dr. Stéphane Richard. The contribution of other authors to this work is as follows:

Chapter 2: The synthetic lethal screen summarized in figures 2.1 and 2.2 was performed in collaboration with Drs. Noel Raynal and Nicolas Sgarioto at Ste. Justine Research Center in Montreal, QC. Generation of MTAP-expressing stable cell lines in figure 2.4 was performed by Dr. Zhenbao Yu, the research associate in our laboratory. Survival curve experiments with PARP-resistant cell lines described in figure 2.7 were performed by Laura Sesma-Sanz in the laboratory of Dr. Jean-Yves Masson at Sherbrooke University in Sherbrooke, QC.

Chapter 3: Dr. Oscar Villareal performed bioinformatics analysis of the scRNAseq data summarized in Figures 3.2 and 3.3. Dr. Junio Dort in the laboratory of Dr. Nicolas Dumont at Ste. Justine Research Center in Montreal, QC, performed MS023 injections in *mdx* mice and we both performed and recorded grip strength and hanging test measurements in Figure 3.7. Dr. Emilie Heckel in the laboratory of Dr. Jean-Sebastien Joyal at Ste. Justine Research Center in Montreal, QC, assisted with the Seahorse experiments by running the Seahorse XF96 Flux Analyzer instrumentation and recording the readouts summarized in Figure 3.4. scRNAseq library preparation was performed by Dr. Yu Chang Wang in the laboratory of Dr. Jiannis Ragoussis at the McGill Genome Center in Montreal, Qc.

Chapter 4: I performed all experiments and analysis.

Chapter 1: Introduction

Part 1: Muscle Stem Cells and Muscle Regeneration

1.1 Skeletal muscle

In adults, muscle exists in three forms: cardiac muscle, smooth muscle, and skeletal muscle (Dave and Varacallo, 2019). Cardiac muscle tissue, also called myocardium, is a striated muscle that lines the walls of the heart and rhythmically contracts in an involuntary manner (Bancroft and Layton, 2013). It is composed of highly branched cardiac muscle cells (also called cardiomyocytes) which are connected to each other by intercalated disks, allowing for the coordinated contraction of myocardium. Cardiac muscle can become damaged resulting in a group of heart diseases known as cardiomyopathies (Bertero and Murry, 2018).

Smooth muscle tissue is found in the walls of vascular and airway tissues, the stomach, and intestines (Wilson, 2011). Smooth muscle is non-striated and contracts in an involuntary manner, and it is made up of spindle-shaped cells with tapered ends called myocytes. Smooth muscle retains contractility after stretching, an important feature for hollow organs such as the stomach (Webb, 2003).

Skeletal muscle is the third form of striated muscle that is responsible for generating force in our bodies and stabilizing our movements. Skeletal muscle is a striated voluntary muscle that is highly vascularized and innervated (Mukund and Subramaniam, 2020). Comprising ~40% of total body weight, skeletal muscle is composed of multi-nucleated myofibers. Myofibers are the main structural unit of skeletal muscle and are bundled together surrounded by the epimysium (Yin et al., 2013). Myofibers can be further categorized into two groups: slow-twitch fibers (type 1) which are resistant to fatigue, and fast-twitch fibers (type 2) which tire more rapidly. Type 2 fast-twitch fibers are further divided into 3 subtypes (2A, 2X, and 2B) which differ based on differential

expression of the structural protein myosin heavy chain (MYHC). Adult skeletal muscle is comprised of varying proportions of fast- and slow-twitch fibers. For example, the triceps muscle found in the arm is majority type 2 fibers, while the soleus leg muscle is almost entire type 1 (Johnson et al., 1973). Interestingly, it has been recently demonstrated that type 2 muscle fiber identity is established early on in development, and the myonuclei within individual muscle fibers have synchronized expression of a single MyHC form which defines their type (Dos Santos et al., 2020).

Skeletal muscle is a highly plastic tissue that can be regenerated in response to exercise or injury (Hodson et al., 2019; Manta et al., 2019). While the multi-nucleated myofibers are post-mitotic, a population of resident muscle stem cells (MuSCs), which reside on the periphery of myofibers beneath the basal lamina, are capable of quickly entering the cell cycle to launch the process of muscle regeneration (Lepper et al., 2011; Relaix et al., 2021; Relaix and Zammit, 2012). These activated MuSCs begin to rapidly proliferate, giving rise to myogenic progenitors which will differentiate and fuse to form multinucleated muscle fibers. Efficient muscle tissue regeneration relies on a wide range of complex cell-intrinsic and -extrinsic factors to guide MuSCs thorough the progression of the myogenic lineage.

1.2 Muscle stem cells

MuSCs are commonly referred to as satellite cells due to their anatomical location on the periphery of individual muscle fibers (Mauro, 1961). MuSCs are generally quiescent under homeostatic muscles. During regeneration, MuSCs rapidly exit quiescence and enter the cell cycle. Progression through the differentiation program is subsequently tightly regulated by a cascade of transcription factors referred to as myogenic regulatory factors (MRFs). MRFs are basic helix-

loop-helix transcription factors which recognize E-box sequences (CANNTG) in the promoter region of target genes (Lassar et al., 1991). Four MRFs named MYF5, MyoD, Myogenin (MYOG) and MRF4 regulate the process of MuSC activation and differentiation, while the paired box transcription factor PAX7 is highly expressed in quiescent MuSCs. The following sections will outline the composition of the molecular machinery that governs MuSC function throughout these processes.

1.2.1 Muscle stem cell quiescence

Quiescent MuSCs are marked by high expression of the transcription factor paired box protein 7 (PAX7) (Yin et al., 2013). In quiescent adult MuSCs, PAX7 activates the transcription of genes required to maintain a stem-like state, including targets which inhibit differentiation (Soleimani et al., 2012). Maintenance of the non-proliferative quiescent state of MuSCs is key for muscle tissue homeostasis. The low turnover frequency of MuSCs in adult tissue is attributed to the low frequency of tumor formation in muscle tissue. In fact, the increased proliferative burden on MuSCs in a degenerative muscle context is accompanied by an increased risk for the development of rhabdomyosarcoma wherein uncontrolled MuSC activation and proliferation leads to tumor growth (Boscolo Sesillo et al., 2019).

One of the major contributors of maintaining MuSC quiescence is canonical Notch signaling. Notch signaling was found to be highly active in quiescent MuSCs, with classical Notch targets Hes1, Hes5, Hes6, Hey1, Hey2, and HeyL being highly elevated compared to activated MuSCs (Bjornson et al., 2012). Deletion of recombining binding protein-Jk (RBP-Jk), a requirement for potentiating Notch signaling, resulted in severe depletion of the MuSC pool, and an inability to regenerate injured muscle *in vivo*. Additionally, loss of Notch signalling in quiescent

MuSCs resulted in spontaneous terminal differentiation of the MuSCs which fused to the mature muscle fiber without passing through S-phase (Mourikis et al., 2012). More recently, it was shown that Notch safeguards MuSC quiescence by inhibiting cell migratory machinery (Baghdadi et al., 2018). Specifically, Notch induces the expression of miR-708, which in turn antagonizes cell migration by downregulating Tensin3 transcripts, a known negative regulator of cell migration.

The transition of quiescent MuSCs to activated and proliferating MuSCs was initially thought to occur immediately without intermediate cell states. However, recent evidence strongly suggests that there are in fact intermediate stages wherein transcriptionally unique MuSCs arise as transitional entities to ease the progression into a proliferative state. It was shown in 2014 that MuSCs transition from quiescence (G_0) to an early activated state termed G_{alert} prior to entering cell cycle (G_1) (Rodgers et al., 2014). Cells in G_{alert} phase were morphologically distinct from G_0 cells, appearing larger and have increased regenerative potential in mice. This transition to G_{alert} was shown to be mediated by hepatocyte growth factor activator (HGFA), which binds to c-Met and activated mTORC1 signaling to initiate the transition (Rodgers et al., 2017).

Following the exit from quiescence, two myogenic regulatory factors (MRFs) are rapidly upregulated to initiate cell cycle: Myogenic factor 5 (MYF5) and myoblast determination protein 1 (MyoD).

1.2.2 Muscle stem cell proliferation: Symmetric and asymmetric division

MuSC proliferation is not a uniform process among cells in the MuSC pool. Once activated, MuSCs either divide symmetrically to replenish the MuSC pool, or divide asymmetrically to produce a committed daughter cell with differentiation capabilities, resulting in a heterogenous pool of MuSCs and their descendants (Yin et al., 2013). Maintaining a balance

between these two types of divisions is critical for preserving muscle tissue homeostasis. Indeed, a hallmark characteristic of muscle wasting disease is the inability to generate myogenic progenitors through asymmetric divisions, which will be discussed further in section 2.3.

Asymmetric MuSC division was first reported when Shinin and colleagues observed in BrdU labelling experiments that the fate-determinant protein Numb segregated to a different daughter cell than the BrdU label (Shinin et al., 2006). The development of a mouse model which crossed *MYF5-Cre* and *Rosa26R-YFP* alleles further facilitated the study of MuSC asymmetric divisions, allowing for cells which express MYF5 to activate Cre recombinase expression and induce expression of the Cre-dependent YFP reporter which is knocked into the highly expressed *Rosa26* locus (Kuang et al., 2007). Visualizing MuSCs that undergo their first division using this mouse demonstrated that MYF5-negative MuSCs can divide symmetrically producing two identical daughter cells along the planar axis which is parallel to the basal lamina. Conversely, when asymmetrical division occurs, one MYF5-negative and one MYF5-positive daughter cell is produced along the apical-basal axis (perpendicular to the basal lamina). It was noted that the MYF5-positive daughter cell was consistently in contact with the fiber, indicating that the MuSC niche plays a role in determining the fate of dividing MuSCs.

A well-established feature of stem cells is their ability to self-renew (Morrison and Kimble, 2006). In MuSCs this process is accomplished through symmetric MuSC division and is required for replenishment of the MuSC pool following injury. Notably, it was shown that symmetric divisions were regulated by the presence of the signaling molecule Wnt family member 7a (*Wnt7a*) within the MuSC niche, which was required to establish planar polarity within the dividing MuSC (Le Grand et al., 2009). A discussion on the importance of the MuSC niche is presented below.

1.2.3 The muscle stem cell niche

The MuSC niche consists of the area between the basal lamina and the sarcolemma membrane of the muscle fiber. The basal lamina is an intricate network of extracellular matrix (ECM) components including laminin and collagen (Sanes, 2003). Importantly, this ECM acts as a source of binding sites for surface integrins on MuSCs such as alpha-7 integrin (Song et al., 1992) (Chapter 4 investigates the effect of alternative splicing of alpha-7 integrin, mediated by the RNA binding protein QKI, on establishing cell polarity). The niche is also a source of various extrinsic signaling cues for the MuSC that are sent by surrounding cell types.

The myofiber itself is capable of sending signals to anchored MuSCs. For example, myofibers express surface markers delta-like 1 (DLL1) and delta-like 4 (DLL4), which in turn act as ligands for NOTCH3 receptors expressed and presented by the MuSC, speculatively to retain quiescence and prevent activation (Low et al., 2018). Furthermore, the expression of myogenic factor 6 (MYF6) exclusively in myofibers causes activation of MYF6 transcriptional targets, such as the epidermal growth factor (EGF), which in turn act as ligands for receptors expressed by MuSCs, such as the epidermal growth factor receptor (EGFR) (Lazure et al., 2020). Lazure and colleagues further show that aberrant EGF signaling from the myofiber interferes with normal EGFR signaling intrinsic to the MuSC, which results in spontaneous exit from quiescence.

The niche is home to other cell types, including endothelial cells, macrophages, and fibroadipogenic progenitor (FAP) cells (Relaix et al., 2021). Interestingly, macrophages infiltrate the MuSC niche following muscle injury to facilitate clearance of damaged tissue, but also to play a role in MuSC activation and differentiation (Arnold et al., 2007). Recently it was shown that macrophages secrete glutamine into the niche which in turn is taken up by MuSCs, triggering

mTOR signaling and promoting proliferation and subsequent differentiation (Shang et al., 2020). Furthermore, macrophage recruitment to the site of injury was shown to be impeded upon the ablation of FAPs, and resulted in impaired MuSC expansion and muscle regeneration, indicating an important level of crosstalk between signaling cells in the MuSC niche (Wosczyzna et al., 2019).

1.4.4 Muscle stem cell differentiation

Myogenic precursor cells which arise from asymmetric MuSC division are characterized by the expression of MYF5 (as mentioned previously), but also by the expression of MyoD (Cooper et al., 1999). MyoD is activated in proliferating myoblasts by FoxO3 and Six1/4 (Grifone et al., 2005). Once expressed, MyoD binds to target gene promoters to induce histone acetylation and subsequent recruitment of RNA polymerase II to initiate gene transcription (Conerly et al., 2016). A key target of MyoD is myogenin, another transcription factor that activates genes required for MuSC differentiation. Interestingly, activation of myogenin by MyoD only occurs under certain spatial conditions. Under proliferating conditions, the MyoD genetic locus is localized to the periphery of the nucleus and is transcriptionally activated by transcription factor II D (TFIID). However, when MuSCs are transitioning towards differentiation into myotubes, the MyoD locus relocates to the lumen of the nucleus, and it activated by TATA-box binding protein associated factor 3/TATA-box-binding protein-related factor (Taf3/Trf3) (Yao et al., 2011), only under these conditions does MyoD activate Myogenin expression to initiate differentiation. The expression of Myogenin leads to repression of MYF5, marking an exit from cell cycle and entrance into the differentiation program (Deato et al., 2008), with subsequent upregulation of genes required for MuSC fusion and terminal differentiation into multinucleated muscle fibers.

Upon terminal differentiation of MuSCs, marked by the formation of myofibers, the final MRF to be expressed in the cascade of myogenic transcription factors is Mrf4. At this stage, MYF5, MyoD, and myogenin are downregulated while Mrf4 expression remains high (Hinterberger et al., 1991)

1.4.5 Muscle stem cell metabolism

Stem cells are endowed with great metabolic flexibility to accommodate their shifting identities as they commit to new cell states (Folmes et al., 2012). MuSCs are no exception, and display shifts in cellular metabolism and preferred energy substrates as they move through activation, proliferation, and differentiation.

Quiescent MuSCs have overall reduced metabolic signatures and favour oxidative metabolism, drawing energy from fatty acid oxidation (FAO) and oxidative phosphorylation (OxPhos). In fact, the reduced metabolic state of quiescent MuSCs allows them to adopt a dormant state post-mortem, enabling them to remain viable and retain regenerative capacity for up to 14- and 17-days post-mortem in mice and humans, respectively (Latil et al., 2012). Sirtuin 1 (SIRT1), a histone deacetylase, was recently identified as an important regulator of quiescent MuSC metabolism. High FAO in quiescence leads to an accumulation of nicotinamide adenine dinucleotide (NAD⁺), which in turn is required to activate SIRT1-mediated deacetylase activity on genes required for the myogenic program, resulting in their repression to maintain quiescence. Interestingly, as MuSCs enter a proliferative state, there is a shift towards glycolysis resulting in reduced cellular NAD⁺, and consequently reduced SIRT1 activity thereby allowing for the expression of genes required for myogenesis (Ryall et al., 2015).

Under proliferating conditions, MuSCs sharply downregulate OxPhos and FAO and switch to glycolysis (L'Honoré et al., 2018). The switch to glycolysis allows for rapid biosynthesis of cellular components required for the proliferative state. Indeed, blocking glycolysis through deletion of the lactate dehydrogenase (LDHA) gene severely limits cell proliferation (Theret et al., 2017).

Entry of MuSCs into the differentiation program is met with a return to OxPhos metabolism, highlighting the complex dynamics of energy metabolism during myogenesis. It was observed that inhibiting mitochondrial function by deleting transcriptional factor A, mitochondria (TFAM), which is required for mitochondrial function and OxPhos, results in differentiation defects (L'Honoré et al., 2018).

1.3 Muscle wasting disease

Muscle wasting diseases are a heterogeneous group of disorders wherein muscle function is impaired resulting in limb weakness, mobility impairments, and/or breathing difficulties. In these diseases, muscle tissue homeostasis is perturbed and MuSCs are continuously activated by extrinsic factors to repair the tissue. Cell-intrinsic defects are also present in a subset of muscle wasting diseases.

1.3.1 Duchenne Muscular Dystrophy (DMD)

DMD is the most severe form of muscle wasting disease, affecting approximately 1 in every 3,500 males, and resulting in death by the 3rd decade of life (Romitti et al., 2015). Progressive muscle wasting is due to a mutation in the dystrophin (DMD) gene, which is expressed in the muscle fiber and is required for its structural integrity (Koenig et al., 1987). Without

functional dystrophin, myofibers are fragile and are constantly undergoing degeneration, resulting in constitutive activation of MuSCs to divide and repair the tissue. Even though MuSC number is higher in dystrophic mice compared to healthy counterparts (Kottlors and Kirschner, 2010), the regenerative capacity of dystrophic MuSCs is severely impaired (Kanagawa et al., 2013).

A new facet of dystrophin's function in DMD was revealed by Dumont and colleagues in a study which defined a role for dystrophin in MuSCs (Dumont et al., 2015b). Dystrophin was shown to be expressed by MuSCs themselves, and not just by the myofibers. In the MuSC, dystrophin acts to establish cell polarity along with other polarity regulators such as microtubule affinity regulating kinase 2 (Mark2) and par-3 family cell polarity regulator (Pard3). The polarization established by dystrophin is required for asymmetric cell division, which gives rise to the myogenic progenitors that are required for muscle regeneration. In the absence of dystrophin, cell polarization is impaired, leading to a reduction in asymmetric cell divisions. The resulting increase in symmetric divisions may contribute to the increased number of MuSCs observed in dystrophic mice, however these cells retain stemness and are unable to differentiate and contribute to muscle regeneration.

1.3.2 Aging: Sarcopenia

Sarcopenia is characterized by a rapid decline in muscle function with aging, leading to reduced mobility and therefore reduced quality of life in elderly patients (Sousa-Victor and Muñoz-Cánoves, 2016). MuSCs undergo age-related decline in their functions due to a plethora of factors, including changes to the aging MuSC niche as well as cell-autonomous alternations. For example, MuSCs isolated from aging mice had an increase in DNA damage compared to healthy individuals, indicating a reduced ability to perform DNA damage repair (Sinha et al.,

2014). Indeed, MuSCs isolated from sarcopenic patients had reduced expression of genes involved in DNA maintenance (Bortoli et al., 2003).

Interestingly, aged mice placed on a calorie-restricted (CR) diet had attenuated development of sarcopenia and more regeneration-competent MuSCs compared to normal-diet counterparts. The MuSCs of CR-fed mice had increased SIRT1 expression, indicating the importance of metabolic regulation in MuSC maintenance (Cerletti et al., 2012).

1.3.3 Mouse models of muscle wasting disease

The development of animal models of muscle disease and injury was pivotal in understanding the molecular mechanisms that drive MuSC function and muscle regeneration. Muscle injury is commonly investigated in rodent models through the local injection of cardiotoxin (CTX) into a single hindlimb muscle (Hardy et al., 2016). The immediate degeneration of muscle tissue allows for an investigation into the response of resident MuSCs and the subsequent regeneration of the damaged tissue. Animal models of muscular dystrophies have been developed and refined to provide an invaluable tool for determining aberrant molecular mechanisms and for developing potential therapies for the disease (Long et al., 2016; McGreevy et al., 2015; Nelson et al., 2016). An extensively used mouse model is the *mdx* mouse, which harbours a mutation in the *DMD* gene encoding dystrophin, thus serving as a model of Duchenne muscular dystrophy (Bulfield et al., 1984).

There is presently no effective treatment for muscle wasting diseases, therefore it is important to understand the molecular underpinnings which guide MuSC function during activation and regeneration of muscle. An emerging key regulator of these processes is the post-translational modification of arginine methylation and, specifically, protein arginine

methyltransferases (PRMTs) that deposit this mark. The following chapter will introduce PRMTs and their role in MuSCs and cancer.

Part 2 Arginine methylation and skeletal muscle

Arginine methylation is an abundant post-translational modification that occurs on RNA binding proteins, histones, DNA damage response proteins, and many other types of proteins. Therefore, PRMTs have extensive roles in myriad cellular processes. Arginine methylation, and in particular protein arginine methyltransferases (PRMTs) are emerging as key regulators of MuSC function and the myogenic process. Consequently, determining where and how PRMTs fit in to MuSC regulation will undoubtedly expand the repertoire of available substrates to target in the development of therapies for muscle wasting diseases. An overview of arginine methylation is given in Part 2 below, along with a summary of PRMT involvement in MuSC function.

2.1 Arginine methylation

The modification of proteins with the covalent attachment of post-translational modifications (PTMs) provides a dynamic regulation of protein stability, localization, and interacting partners ultimately affecting function. Although protein ubiquitination and phosphorylation are the best characterized PTMs, protein methylation is rapidly catching up in importance (Murn and Shi, 2017). The best characterized protein methylation modifications occur on lysine and arginine (Xu and Richard, 2021).

Arginine is an aliphatic α -amino acid with a pKa of 13.8, making it the most basic of all the amino acids, and is positively charged at physiological pH. The arginine side chain contains a guanidino group that gives arginine the potential to form hydrogen bonds or van der Waals interactions with nucleic acids or other proteins (Evich et al., 2016).

The guanidino nitrogen atoms of arginine residues can be methylated (addition of -CH₃ groups) to form three distinct species: ω -N^G-monomethylarginine (MMA), ω -N^G,N^G-asymmetric

dimethylarginine (aDMA), and ω -N^G,N^{'G}-symmetric dimethylarginine (sDMA) (Paik and Kim, 1980). The methylation of arginine is catalyzed by a group of enzymes called protein arginine methyltransferases (PRMTs). PRMTs transfer a methyl group from S-adenosylmethionine (SAM) to the guanidino nitrogen of arginine, creating methylarginine and S-adenosylhomocysteine (SAH) (Bedford and Clarke, 2009).

2.2 Protein Arginine Methyltransferases (PRMTs)

The PRMT family of proteins contains 9 members which are subcategorized into three groups. Type I PRMTs (PRMT1, PRMT2, PRMT3, PRMT4/CARM1, PRMT6, and PRMT8) catalyze the reaction which generates MMA, and can also catalyze the dimethylation reaction that produces aDMA. Type II PRMTs (PRMT5 and PRMT9) also create MMA species, followed by dimethylation to produce sDMA. PRMT7 is the only type III PRMT, and is solely capable of carrying out monomethylation to produce MMA (Guccione and Richard, 2019).

2.3 PRMT Structure

All 9 PRMTs share a similar core structure, with an N-terminal Rossman fold and a C-terminal β -barrel domain. Type I PRMTs fold into a dimeric structure with each monomer subunit forming a SAM-binding and a substrate-binding pocket. PRMT1, the major type I PRMT, exists as a head-to-tail homodimer (Zhang and Cheng, 2003). PRMT5, the representative type II PRMT, also dimerizes through the β -barrel domain, and contains an additional TIM (triose phosphate isomerase) domain which is utilized for interactions with adaptor proteins (Antonysamy et al., 2012). PRMT5 can dimerize with MEP50/WDR77, a stoichiometric partner, to form a heterooctamer and binds with either RIOK1 or pICln to regulate substrate specificity and catalytic

activity (Friesen et al., 2002; Guderian et al., 2011). Type III PRMT7 uniquely exists as a monomer with a more restricted active site, enabling the generation of mono methylated arginines on target proteins (Cura et al., 2014). Interestingly, PRMT7 contains two methyltransferase domains, one truncated and one active, which fold into a ring structure, forming a pseudo-dimer (Hasegawa et al., 2014). A more in depth discussion of the major type I enzyme PRMT1, the major type II enzyme PRMT5, and the type III enzyme PRMT7 and their substrates follows in the proceeding section.

2.4 PRMT substrates

PRMT1 is responsible for the majority of aDMA in the cell, and consequently has a wide range of substrates and is involved in various cellular functions. In fact, ~85% of aDMA species in rat fibroblasts and mouse liver are generated by PRMT1 (Tang et al., 2000). The substrate binding region of PRMT1 is acidic, thus creating a favourable interaction with basic arginine residues, specifically in arginine- and glycine- rich motifs, termed RGG/RG motifs (Thandapani et al., 2013; Zhang and Cheng, 2003). PRMT1 targets both nuclear and cytoplasmic proteins, including DNA damage proteins. The role of PRMT1 in the DNA damage response has implications in cancer (Xu and Richard, 2021), which will be discussed in more detail in section 2.7 of this introduction.

Interestingly, PRMT1 has been shown to methylate the RNA binding protein Quaking (QKI) *in vivo* (Cote et al., 2003). Quaking is the major focus of Chapter 4 and is discussed further in Part 3 of this introduction.

PRMT5 is responsible for the majority of sDMA species in the cell, and dimethylates target arginines in a distributive manner rather than in a processive manner (Wang et al., 2014). After

generating MMA, PRMT5 releases the substrate protein before re-engaging and performing the second methylation event. Similarly to PRMT1, PRMT5 has a preference for substrates with RGG/RG motifs (Blanc and Richard, 2017; Xu and Richard, 2021). Well-known targets of PRMT5 include Sm proteins, which have an integral role in spliceosome assembly (Brahms et al., 2000; Meister et al., 2001). Symmetric dimethylation of the Sm proteins B/B', D1 and D3 is required for their assembly into mature small nuclear ribonucleoproteins (snRNPs). Notably, several studies have established that cells deficient in PRMT5 display striking defects in splicing (Bezzi et al., 2013; Boisvert et al., 2002; Fedoriw et al., 2019; Fong et al., 2019).

Unlike type I and type II PRMTs, PRMT7 has preference for RXR motifs specifically within arginine- and lysine-rich regions of proteins (Feng et al., 2013). Few PRMT7 substrates are confirmed, however MMA undoubtedly has important roles in myriad cellular processes. Among the confirmed substrates of PRMT7 are histones and the non-histone proteins HSP70 and eIF2a. An additional PRMT7 substrate was identified in H4R17, which resulted in allosteric regulation of the neighbouring PRMT5-mediated H4R3me2s mark (Jain et al., 2017).

Overall, the broad range of PRMT targets and downstream mechanistic consequences highlight the importance of arginine methylation in myriad cellular processes. Readers of these arginine methylation marks are important propagators of PRMT-mediated regulation.

2.5 Readers and erasers of arginine methylation

Post translational modifications act a messaging system within the cell, allowing protein machinery known as "readers" to interact with and interpret the modification. A prototype example of reader machinery is the SWI/SNF complex (Lu and Allis, 2017), which remodels nucleosomes

around promoter regions of target genes to regulate transcription (Kwon et al., 1994). Readers are essential for executing protein functions, and different readers exist for different modifications. The reader proteins of arginine methylation are mostly proteins with Tudor domains (Chen et al., 2011).

The Tudor domain was first characterized in *Drosophila* (*Tud*) following a screen for maternal-effect sterility (Boswell and Mahowald, 1985). The Tudor domain is highly conserved amongst species, and typically consists of approximately 60 amino acids which form a β -barrel-like structure. There are approximately 30 Tudor-domain containing proteins in mammals, including the Jumonji demethylase JMJD2 and the p53-binding protein 53BP1, which read mainly histone lysine methylation marks (Lu and Wang, 2013). There are three Tudor domain containing proteins that are known to interact with methylarginines, namely survival of motor neuron (Smn), tudor domain containing 3 (Tdrd3), and splicing factor 30 (Spf30).

Smn contains a single Tudor domain and is associated with the human disease spinal muscular atrophy (SMA) (Friesen et al., 2001; Selenko et al., 2001; Sprangers et al., 2003). Structural studies have shown that the Tudor domain of Smn can interact with both aDMA and sDMA (Liu et al., 2012; Tripsianes et al., 2011). As mentioned previously, spliceosomal proteins are symmetrically dimethylated prior to the assembly of snRNPs. Smn subsequently binds the methylarginines of the splicing factors to further regulate the assembly (Friesen et al., 2001).

Tdrd3 is another methylarginine reader that was shown to bind to methylated arginines on histone tails and promote transcription of target genes (Yang et al., 2010). Additionally, the C-terminal domain of RNA polymerase II is methylated at arginine 1810 by CARM1 prior to transcription initiation, and this methyl mark is read by Tdrd3 (Sims et al., 2011). Tdrd3 can also read both aDMA and sDMA, with a preference for the former (Yang et al., 2010). The cause of

this preference was attributed to a single tyrosine residue within Tdrd3 (Y566), as point mutation of this residue to a tryptophan results in similar affinities for sDMA and aDMA (Sikorsky et al., 2012).

Spf30 shares a 50% identity with Smn (Talbot et al., 1998), and recognizes both aDMA and sDMA (Côté and Richard, 2005). Notably, Spf30 bound most weakly with methylarginines when compared to Smn and Tdrd3 (Liu et al., 2012)

An outstanding question in the field of arginine methylation is whether there are dedicated arginine demethylases, or 'erasers' of arginine methylation. There are lysine demethylases (KDM) of the Jumonji class that have weak activity for methylarginine *in vitro*, however *in vivo* demethylation is not detectable (Walport et al., 2016). There were initial reports that peptidyl arginine deiminase 4 (Pad4) converts methylarginine to citrulline, and releases a methylamine (Wang et al., 2004). However, it was later shown that methylarginine is in fact a poor substrate for PAD4 when compared to unmodified arginines (Kearney et al., 2005). Therefore, arginine methylation appears to be a permanent modification with limited evidence to support its reversibility.

2.6 PRMTs and skeletal muscle stem cells

PRMTs have come to light as major players in muscle stem cell function and skeletal muscle regeneration and physiology. The following sections will further detail the contributions of individual PRMTs to these important processes (summarized in figure 1.1)

2.6.1 PRMT1 and muscle stem cells

PRMT1 has demonstrated effect in the regulation of MuSC function. A key step in the initiation of MuSC differentiation is the activation of MyoD, a major myogenic regulatory factor (Kassar-Duchossoy et al., 2004; Rudnicki et al., 1993). Blanc et al showed that PRMT1 is directly involved in the activation of MyoD expression in committed progenitors by methylating the SIX1/4 coactivator, EYA1 (Blanc et al., 2017). PRMT1 deficient myoblasts harbor hypomethylated EYA1, which is incapable of binding to the MyoD promoter and subsequently activating transcription. As a result, PRMT1 deficient myoblasts are highly proliferative and can be expanded in culture but are unable to terminate differentiation. In vivo, this translates into a muscle regeneration defect due to an inability of PRMT1 knockout MuSCs to differentiate into mature muscle fibers after injury. This study points to an indirect epigenetic regulation of MuSC differentiation by PRMT1. Given the well-studied coactivator function of PRMT1 through methylation of histones, it is also likely that PRMT1 has a direct epigenetic regulation of MuSC function that has yet to be uncovered.

MyoD protein plays a major regulatory role in MuSCs and the post-translational modifications required for its function, such as phosphorylation and acetylation, were established early on. Phosphorylation of MyoD by Cdk1/2 was shown to modulate its stability, resulting in rapid degradation (Song et al., 1998). On the other hand, acetylation of MyoD is required for its DNA binding and transcriptional activation abilities (Sartorelli et al., 1999). Interestingly, MyoD was more recently shown to be methylated by PRMT1 at R121. Similar to acetylation, arginine methylation by PRMT1 is important for the DNA binding and transcriptional activation activity

of MyoD. In this study, specific deletion of R121 led to the loss of MyoD-mediated activation of Myogenin (Liu et al., 2019).

2.6.2 CARM1 and skeletal muscle

Another Type I PRMT, CARM1 (also called PRMT4), plays a role in regulating the asymmetric division of MuSCs. Activated MuSCs can divide symmetrically for self-renewal or divide asymmetrically giving rise to a committed progenitor cell. Kawabe and colleagues revealed that CARM1 methylates multiple arginines in the N-terminus of PAX7 in committed muscle progenitor cells (Kawabe et al., 2012). The methylated PAX7 is then capable of recruiting the histone methyltransferase complex and initiating MYF5 transcription, followed by entry into the myogenic program (Kawabe et al., 2012).

CARM1 is also involved in the muscular defects observed in spinal muscular atrophy (SMA). In a mouse model of SMA, *Smn2B*^{-/-} mice, CARM1 levels are elevated in muscle tissue. As a result, the RNA binding protein human antigen R (HuR) does not properly respond to muscle injury, and target mRNAs are deregulated. Interestingly, the SMA-causing mutation E134K within the survival of motor neuron (*Smn*) protein resides in the *Smn* tudor domain. Recapitulation of this mutation coupled with CARM1 depletion in muscle cells interfered with *Smn*-HuR interaction (Ravel-Chapuis et al., 2021).

AMP-activated protein kinase (*Ampk*) has a demonstrated role in regulating skeletal muscle size, hypertrophy, and atrophy (Thomson, 2018). An important regulator of *Smn* expression in muscle is the *Ampk*-p38-*Pgc-1α* signalling axis (Ng et al., 2019). Interestingly, *Ampk* was shown to be methylated by CARM1 in skeletal muscle, subsequently mediating *Ampk* signaling during muscle inactivation caused by denervation. Muscle-specific deletion of CARM1

resulted in reduced muscle atrophy following muscle denervation, and reduced activation of key AMPK downstream targets including Unc-51 like autophagy activating kinase 1 (Ulk1), Acetyl-coenzyme A carboxylase, and peroxisome proliferator-activated receptor gamma coactivator 1-alpha (Pgc-1 α) (Stouth et al., 2020). Indeed, Ampk is a strong regulator of autophagy in skeletal muscle (Kjøbsted et al., 2018), and these findings shed light on the role of PRMTs in this signaling axis in mature skeletal muscle. Chapter 2 of my thesis will investigate the role of PRMT1-mediated Ampk function at the level of the muscle stem cell.

2.6.3 PRMT5 and muscle stem cells

PRMT5 was initially shown to be an epigenetic regulator of MuSC function by initiating Brahma-related gene-1 (Brg1)-dependent chromatin remodeling necessary for active transcription of Myogenin, a regulator of terminal MuSC differentiation (Dacwag et al., 2007). Later, however, it was also shown to act as a critical regulator of MuSC proliferation.

Zhang and colleagues performed a loss-of-function screen and identified 120 genes which were required for MuSC survival. Interestingly, PRMT5 was a top hit, and further study revealed that MuSC-specific deletion of PRMT5 in mice not only blocked MuSC proliferation, but also impeded muscle regeneration. They showed that PRMT5 epigenetically silences expression of the cell cycle inhibitor p21. As a result, removal of PRMT5 led to a slowing down of MuSC proliferation (Zhang et al., 2015). These studies provide an interesting starting point for the characterization of PRMT5 as an important regulator of MuSC function.

2.6.4 PRMT7 muscle stem cells

The function of PRMT7 in MuSCs was only recently investigated. It was discovered that whole body PRMT7 *-/-* mice had severe muscle regeneration defects upon muscle injury. Furthermore, PRMT7-deficient MuSCs were unable to terminate differentiation, explaining the *in vivo* regeneration defect, and instead underwent premature cellular senescence. The PRMT7 knock-out MuSCs were found to have increased levels of the cell cycle inhibitor cyclin-dependent kinase inhibitor 1 (p21), and decreased levels of the p21 repressor DNA methyl transferase 3b (Dnmt3b) (Blanc et al., 2016).

Recently, Jeong et al showed that PRMT7 deficiency in myoblasts leads to a block in differentiation (Jeong et al., 2019). The authors discovered that PRMT7 directly promotes MyoD-mediated MuSC differentiation through methylating and thereby activating p38MAPK, which in turn promotes MyoD activity (Jeong et al., 2019). The muscles of whole body PRMT7 knockout mice were shown in another study to have diminished oxidative metabolism with reduced endurance, consistent with a downregulation of PCG1 α expression in myoblasts, and exacerbated age-related obesity (Jeong et al., 2016).

A novel intellectual disability syndrome has been characterized wherein compound heterozygous or homozygous variants in the PRMT7 gene leads to short stature, brachydactyly, intellectual development disability and seizures (SBIDDS syndrome) (Agolini E, 2018; Akawi et al., 2015; Birnbaum et al., 2019). One of the presentations of this syndrome is muscle tone abnormalities, including ataxia, hypotonia, dystonia and spasticity. Together with the evidence that loss of PRMT7 leads to weakened muscles (Jeong et al., 2016) and incomplete muscle

regeneration (Blanc et al., 2016), these studies point to a strong contribution of PRMT7 to MuSC function.

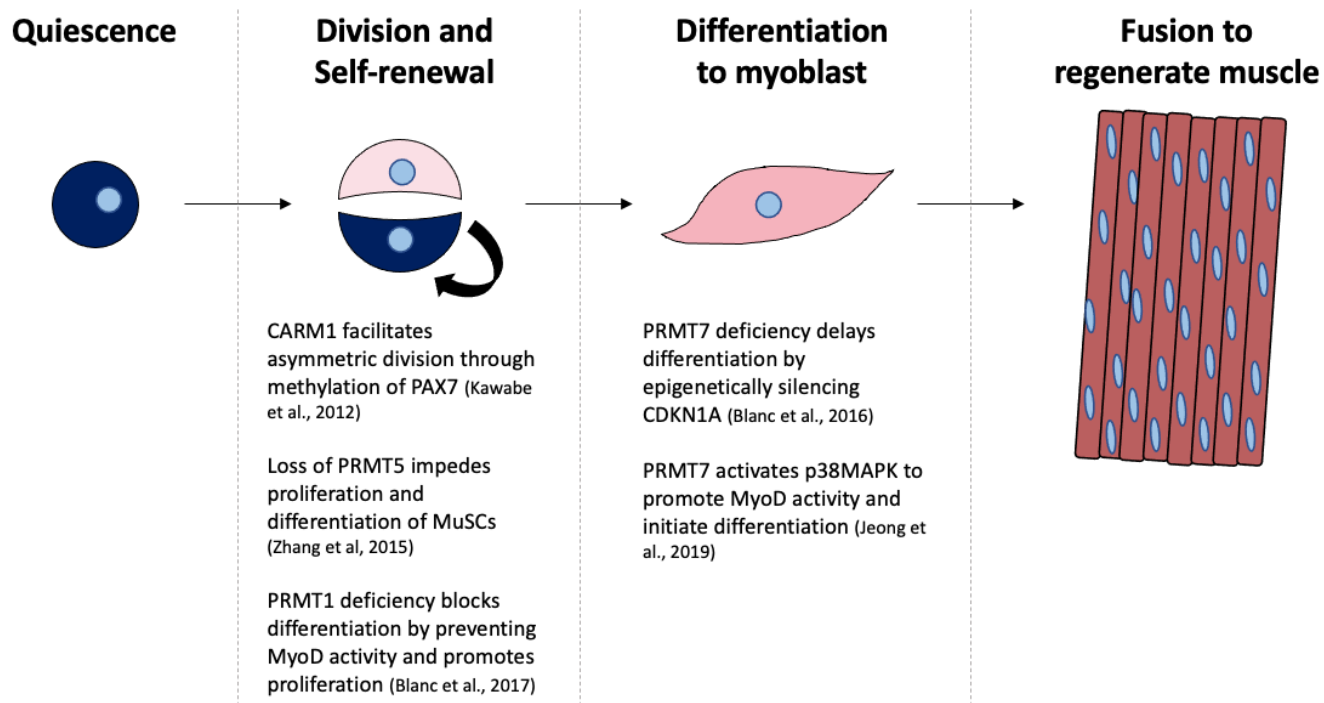


Figure 1.1. Overview of PRMT contributions to the myogenic process

An overview of the diverse roles of PRMTs in MuSC function. As quiescent MuSCs are activated upon muscle injury, they begin to proliferate prior to initiating the differentiation program, leading to the generation of mature muscle tissue to replace damaged tissue. PRMTs have been implicated in the proliferative and self-renewal capacity of MuSCs, as well as in the differentiation of MuSCs into mature muscle.

2.7 Beyond muscle stem cells: Arginine methylation and cancer

Interestingly, cancer cells mimic some stem cell qualities, such as maintaining the capacity for ongoing self-renewal and growth (Ben-Porath et al., 2008; Kim et al., 2010; Wong et al., 2008). The field of arginine methylation is of growing importance in the realm of cancer research and has been unfolding as a key therapeutic target in several types of cancer (Guccione and Richard, 2019; Xu and Richard, 2021). The discussion below will summarize the contributions of PRMTs to various cancer cell types.

2.7.1 PRMT1 and cancer

Increased expression of PRMT1 is a common feature in a broad range of cancer cell types, with implications in aberrant gene activation and DNA damage repair promoting cancer cell growth and survival.

A recent study showed that PRMT1 expression is upregulated in colorectal cancer and is involved in its progression (Yao et al., 2021). The major histone mark deposited by PRMT1, H4R3me2a, recruits the ATPase subunit of the SWItch/sucrose non-fermentable (SWI/SNF) complex, SWI/SNF related, matrix associated, actin dependent regulator of chromatin, subfamily A, member 4 (Smarca4), which in turn induces chromatin remodelling to promote the proliferative and invasive qualities of colorectal cancer cells. Specifically, the epidermal growth factor receptor (EGFR) is a major target of PRMT1/Smarca4 transcriptional activation, and elevated PRMT1/Smarca4 expression in colorectal cancer patients is positively correlated with EGFR expression and poor prognosis (Yao et al., 2021).

Furthermore, PRMT1 was shown to directly methylate EGFR in the endoplasmic reticulum/golgi area of the cell prior to the localization of EGFR to the cellular membrane (Liao

et al., 2015). This methylation event leads to reduced overall survival of colorectal cancer patients. Methylation of R198 and R200, located within the extracellular domain of EGFR, enhanced binding to EGF substrate, leading to aberrant EGFR signaling activation in colorectal cancer cells (Liao et al., 2015).

Enhancer of zeste homolog 2 (Ezh2) plays a functional role in depositing the histone methylation signature H3K27me3 that is required for gene silencing, specifically acting as the enzymatic subunit of the polycomb repressive complex 2 (PCR2) (Di Croce and Helin, 2013). Ezh2 has broad implications in cancer, with gain- and loss-of-function mutations as well as overexpression of Ezh2 have been associated with cancer progression (Kim and Roberts, 2016). Interestingly, Ezh2 is asymmetrically dimethylated at R342 by PRMT1, and this mark was shown to inhibit phosphorylation of the nearby threonine 345 and 487 (T345 and T487) by Cdk1 (Li et al., 2020). PRMT1-mediated methylation of Ezh2 subsequently resulted in downregulation of target gene expression, leading to increased breast cancer cell invasiveness and metastasis (Li et al., 2020).

PRMT1 is involved in the DNA damage response. Mre11, an important DNA damage protein involved in dsDNA break repair, contains an RGG/RG motif that is methylated by PRMT1 (Boisvert et al., 2005a). Methylation of Mre11 has subsequently been shown to be important for its role in regulating cell cycle checkpoint, proliferation, DNA repair (Boisvert et al., 2005b; Yu et al., 2009). Furthermore, PRMT1 was shown to methylate and regulate the DNA-binding function of 53BP1, a protein involved in promoting non-homologous end joining (NHEJ)-mediated dsDNA break repair (Boisvert et al., 2005c). Given the crucial role PRMT1 plays in the DNA damage response, it is not surprising that certain cancer cells are dependent on PRMT1-mediated DNA damage repair to promote tumor growth. Pancreatic ductal adenocarcinoma

(PDAC) is increasing in incidence and has limited therapeutic interventions available, resulting in a low survival rate of 5 years (Ying et al., 2016). A recent RNAi-based *in vivo* functional screen of patient-derived PDAC cells identified PRMT1 as a requirement for PDAC cell survival (Giuliani et al., 2021). The authors found that global inhibition of aDMA resulted in a significant downregulation of DNA damage response components, leading to genomic instability and inhibition of tumor cell growth, thus highlighting the potential of type I PRMT inhibitors in cancer therapeutics.

2.7.2 PRMT5 and cancer

PRMT5 is demonstrated to be involved in various cancer types and is emerging as a viable option for drug targeting. An early study indicated PRMT5 as a regulator of genes involved in tumor progression. By depositing H4R3me2s and H3R8me2s histone marks, PRMT5 associates with the SWI/SNF chromatin remodelling complex to repress the expression of tumor suppressor genes, including suppressor of tumorigenicity 7 (St7) and nonmetastatic 23 (Nm23) (Pal et al., 2004). DNA damage response and mRNA splicing have been thoroughly shown to be key pathways regulated by PRMT5.

PRMT5 is overexpressed in a subset of myeloproliferative neoplasms (Liu et al., 2011), and dual inhibition of PRMT5 and Jak1/2 resulted in reduced methylation of the PRMT5 target E2f1, leading to downregulation of DNA damage response genes and cancer cell death (Pastore et al., 2020). Furthermore, PRMT5 was shown to upregulate the expression of DNA damage response genes in prostate cancer cells in concert with pICln. Inhibiting PRMT5 in these cells subsequently resulted in sensitization to DNA damaging agents (Owens et al., 2020).

Major splicing defects are observed in cells with PRMT5 deficiency (Fong et al., 2019). One notable splicing event that is sensitive to PRMT5 deficiency occurs within the Mdm4 transcript, resulting in a short isoform that undergoes nonsense-mediated decay (NMD) due to the generation of a premature stop codon (Bezzi et al., 2013). NMD is utilized by the cell as a surveillance mechanism to selectively target mRNAs with a premature termination codon for degradation (Schweingruber et al., 2013).

MDM4 is a repressor of p53, and thus full length Mdm4 is required for tumor suppression. Furthermore, the role of PRMT5 in splicing is a requirement for the survival of acute myeloid leukemia cells (Radzishchanskaya et al., 2019). The major splicing regulator Srsf1 is methylated by PRMT5, and loss of PRMT5 results in alternative splicing of key genes required for acute myeloid leukemia (AML) cell survival. Interestingly, it was recently shown that PRMT5 methylates the RNA binding motif protein X-linked (RBMX) which is required for the interaction of RBMX with Srsf1 (Cai et al., 2021a). Disruption of this interaction in PRMT5-deficient cells hindered Srsf1 binding to MDM4 pre-mRNA and resulted in reduced Mdm4 protein levels.

Interestingly, there is growing evidence to suggest that the AKT signaling pathway and cellular metabolism is regulated by arginine methylation. AKT, also called Protein Kinase B, is frequently overexpressed in many types of cancers, and its overactivation leads to uncontrolled cell growth (Song et al., 2019). Recently it was shown that PRMT5 directly methylates AKT at R391. This event is required to mediate the interaction between AKT and phosphatidylinositol 3,4,5 triphosphate (PIP3), which results in translocation of Akt to the cell membrane where it is activated by phosphoinositide-dependent kinase-1 (PDK1). Deficient methylation of AKT R391 was sufficient to reduce AKT kinase activity and inhibit tumorigenesis (Yin et al., 2021). The involvement of PRMT1 in muscle stem cell metabolism is explored in Chapter 3.

2.7.2.1 MTAP deficiency and PRMT5

Cancer cells with a deficiency in methylthioadenosine phosphorylase (MTAP) create a strong dependency for PRMT5 activity. MTAP is an enzyme involved in the methionine salvage pathway whose genomic location is directly adjacent to the tumor suppressor genes *Cdkn2a* and *Cdkn2b*. Therefore, MTAP is commonly co-deleted in several types of cancers, including ~40% of non-small cell lung carcinoma (NSCLC) patients (Schmid et al., 1998). As a result, the metabolite that is normally processed by MTAP, methylthioadenosine (MTA), accumulates in the cell, and acts as a strong inhibitor of PRMT5 activity (Kryukov et al., 2016; Marjon et al., 2016; Mavrakis et al., 2016). MTAP-negative cancer cells harbour an intrinsic reduction of PRMT5 activity that can be exploited by using inhibitors of other PRMTs to reduce arginine methylation levels in the cell below a threshold of tolerability (Fedoriw et al., 2019; Gao et al., 2019). This unique vulnerability of MTAP-negative cancer cells is further explored in Chapter 2 of this thesis.

2.7.3 PRMT7 and cancer

Evidence to suggest that PRMT7 can regulate the epithelial to mesenchyme transition (EMT) in breast cancer cells was presented when it was shown that PRMT7 inhibits the expression of E-cadherin. PRMT7 directly bound to the promoter of E-cadherin and altered the histone methylation profile by elevating H4R3me2s. The repressive mark subsequently led to reduced E-cadherin expression which facilitated EMT of breast cancer cells. Interestingly, the explanation for how the PRMT5-mediated H4R3me2s mark could potentially be regulated by PRMT7 binding was provided later on. As mentioned previously, the monomethylation of H4R17 by PRMT7

regulates PRMT5 activity at the nearby H4R3 by creating an allosterically permissive environment (Jain et al., 2017).

2.7.4 Inhibitors of PRMTs

Given the extensive implications of PRMTs in cancer detailed above, PRMTs serve as key therapeutic targets with several drugs being tested in clinical trials, as reviewed recently (Wu et al., 2021).

To date, many promising inhibitors have been established for PRMTs. For example, MS023 is a potent and selective small-molecule inhibitor of type I PRMTs, with no activity against type II and type III PRMTs and DNA methyltransferases (Eram et al., 2016). MS023 is used in Chapter 3 to demonstrate enhanced self-renewal of MuSCs, however inhibition of type I PRMTs is also an attractive candidate in various types of cancer. In fact, type I PRMT inhibition with GSK3368715 is in phase I clinical trials for the treatment of diffuse large B-cell lymphoma and solid tumors (ClinicalTrials.gov identifier numbers NCT03666988). A selective inhibitor of the Type I PRMT4, TP-064, has been developed with indications for multiple myeloma (Nakayama et al., 2018).

Several inhibitors targeting PRMT5 are developed and being tested in the clinic, JNJ-64619178 and GSK3326595 are currently in phase I clinical trials (ClinicalTrials.gov identifier numbers NCT03573310 and NCT03614728, respectively) for patients with advanced cancers. Inhibitors of PRMT5 are particularly potent in cells with defective splicing machinery (Fong et al., 2019). Furthermore, cancer cells with MTAP loss are particularly sensitive to PRMT5 inhibition, as discussed in section 2.7.2.1. A recent development has identified another vulnerability in MTAP-deficient cells which acts through PRMT5, wherein targeting the metabolic

enzyme methionine adenosyl transferase 2 α (MAT2a) results in reduced SAM levels, thus impairing PRMT5 activity (Kalev et al., 2021).

Notably, while the focus of PRMT drug development has been targeted to type I and type II PRMTs, an inhibitor against type III PRMT7 has been developed which occupies the SAM-binding site of PRMT7, thus selectively inhibiting PRMT7-mediated MMA (Szewczyk et al., 2020). The inhibitor, SGC3027, is delivered as a prodrug that gets converted to SGC8158 by intracellular reductases.

2.7.5 Substrate sharing of PRMTs

Given the common recognition motif shared by type I and type II PRMTs (RGG/RG), it is unsurprising that type I PRMT1 and type II PRMT5 share common substrates. As mentioned in the previous section, H4R3 is a common substrate of PRMT1 and PRMT5, and has different functional consequences on gene expression depending on methylation status (me2a versus me2s). There are additional shared substrates of the two major type I and type II PRMTs, including MYC proto-oncogene (MYC) (Favia et al., 2019), E2F transcription factor 1 (E2f1) (Zheng et al., 2013), and several RNA binding proteins such as fused in sarcoma (FUS) (Chitiprolu et al., 2018; Tradewell et al., 2012) and polyadenylated-binding protein 1 (PABPN1) (Martin et al., 2010).

PRMT7 and PRMT5 share H4 as a common substrate wherein PRMT7-mediated MMA allosterically regulates the ability of PRMT5 to methylate a neighbouring arginine (Jain et al., 2017). Intriguingly, methylation of Sm proteins by PRMT5 is affected by PRMT7 expression (Gonsalvez et al., 2007), further suggesting a crosstalk between PRMT5 sDMA and PRMT7 MMA.

The discovery of shared substrates provided the first insights into potential redundancy between the two major PRMTs. It was eventually demonstrated that loss of PRMT1 resulted in a global increase of MMA and sDMA (Dhar et al., 2013), suggesting that there was substrate scavenging occurring between type I and II PRMTs. This is thought to be due in part to PRMT1 depositing the majority of arginine methylation, thus PRMT1 inhibition makes a wide range of substrates available to PRMT5-mediated methylation. An overview of Type I PRMT and PRMT5 inhibition dynamics is given in Figure 1.2.

The discovery of inhibitors of arginine methylation has facilitated the characterization of cancer cell vulnerabilities, such as MTAP deletion as described above. An additional example is cells with defects in splicing, which are particularly sensitive to both type I PRMT and PRMT5 inhibitors (Fedoriw et al., 2019; Fong et al., 2019).

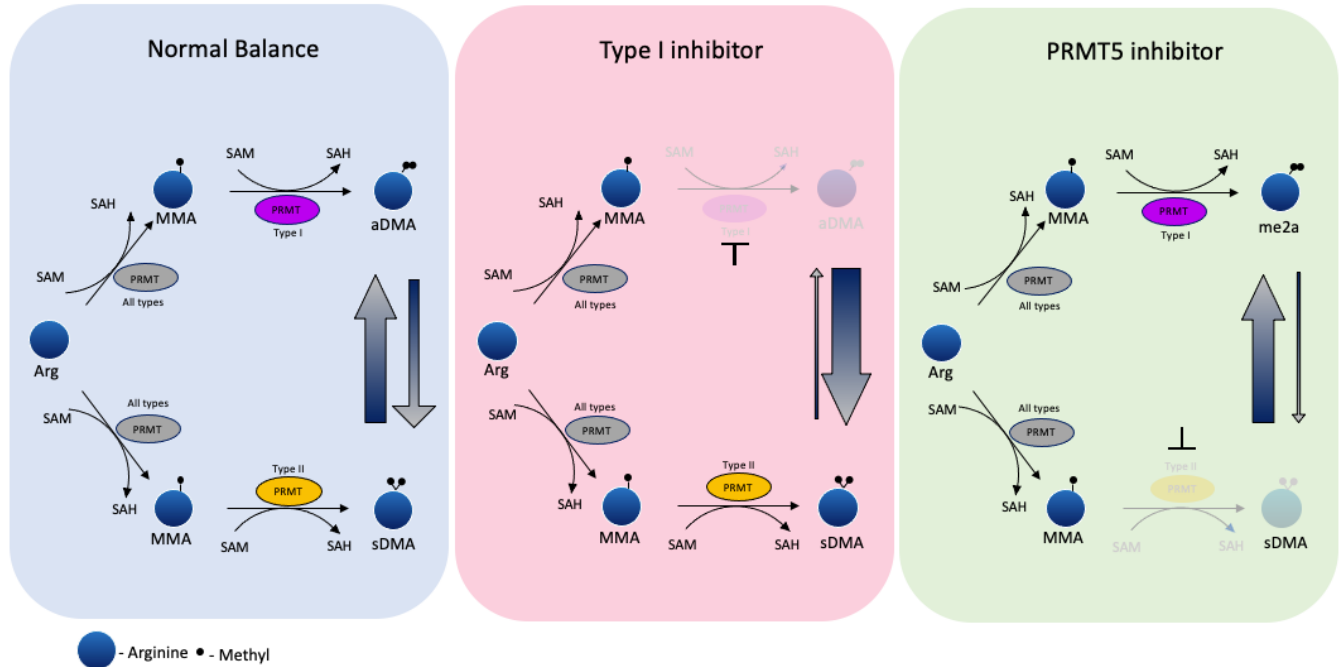


Figure 1.2. PRMT inhibition Dynamics

Arginine residues on peptides can be asymmetrically dimethylated by Type I PRMTs, or symmetrically dimethylated by Type II PRMTs. All Type I and Type II PRMTs can deposit a monomethyl group on arginine (MMA). Pharmacological inhibition of Type I PRMTs results in a global reduction in asymmetric dimethylarginine species (aDMA), accompanied by an upregulation of monomethyl arginine and symmetric dimethylarginine (MMA and sDMA, respectively) species. Conversely, pharmacological inhibition of PRMT5, the major Type II PRMT, results in a global decrease in sDMA.

Part 3: RNA Metabolism and Muscle Stem Cells

In addition to complex post-translational modifications involved in MuSC function during muscle regeneration, there is a network of post-transcriptional regulators which play an important role. Post-transcriptional processing of pre-mRNA transcripts is carried out by RNA-binding proteins, which have diverse functions in the cell.

3.1 RNA binding proteins (RBPs) and their functions

Post-transcriptional processing of mRNA diversifies the transcriptomic profile of the cell. RNA binding proteins (RBPs) are crucial modifiers of this layer of regulation and play a role throughout the lifespan of RNA; from its initial transcription, to splicing and translation, and in some cases, its decay.

Typically, RBPs require RNA binding domains in order to interact with RNA. Common RNA binding domains include the K-homology (KH) domain, the RNA recognition motif (RRM), and the DEAD box helicase domain (Gerstberger et al., 2014). These domains can interact with specific target RNA sequences or specific structural motifs. Interestingly, this family of proteins are more evolutionarily conserved than transcription factors, indicating an important "housekeeping" role for RBPs (Gebauer et al., 2021).

Once bound to their RNA substrates, RBPs carry out a wide range of functions, some of which are summarized below.

3.1.1 Splicing

Transcription of a gene generates a precursor messenger RNA (pre-mRNA) molecule that undergoes splicing to remove intronic sequences and fuse together exons which comprise the

coding sequence of the gene. 5' ends of the intronic sequences contain a GU sequence that serves as a splicing donor site, while the 3' end contains an AG sequence acceptor site. The splicing reaction is carried out by the spliceosomal complex which is comprised of five small ribonucleoproteins (snRNPs). The U1 and U2 snRNPs bind to intronic sequences and recruit U4/U6/U5 snRNP trimer. The intronic 5' splice site (5'SS) is taken by U1 to U6, resulting in folding towards U2 and the formation of a branchpoint at the adenosine which attacks the 5'SS, thereby freeing the 5' exon. The freed 5' exon now attacks the 3'SS, finally excising a lariat intron and a mature mRNA species (Wilkinson et al., 2020).

Exon/intron boundaries can be read in different ways by the spliceosomal machinery resulting in alternative splicing patterns which stray from the canonical removal of intronic sequences. These alternatively spliced transcripts may contain skipped exons, retained introns, or different 5' and 3' untranslated sequences. Alternative splicing can therefore change the reading frame of transcripts and give rise to different protein isoforms (Baralle and Giudice, 2017).

Alternative splicing can be tissue-specific with different functional outcomes that depend on the landscape of RBPs, which include splicing factors, present in the cell. For example, in brain cells, almost 400 mRNA transcripts undergo extensive alternative splicing with no change to overall expression level, indicating that splicing is the key regulator of expression of those genes (Dillman et al., 2013). In cardiac muscle tissue development, alternative splicing of muscle-specific transcripts is dependent on changing expressions levels of RBPs such as muscleblind-like protein 1 (MBNL1) and RNA-binding protein 24 (Rbp24) (Giudice and Cooper, 2014), indicating a further level of splicing dynamics that is temporally-regulated.

3.1.2 Post-transcriptional mRNA modifications

Post-translational modifications have complex interplay with post-transcriptional modifications in the cell. mRNA can be methylated, producing *N*⁶-methyladenosine (m⁶A) (Desrosiers et al., 1974), and interestingly it was shown that PRMT1 methylates enzymes required for depositing this mark. Nearly three decades after the discovery of m⁶A, the enzyme responsible generating the vast majority of it in the cell was cloned and termed methyltransferase-like protein 3 (Mettl3) (Bokar et al., 1997). The m⁶A mark is best known to be associated with RNA instability (Sommer et al., 1978), however has more recently been shown to have functions in mRNA translation, splicing, and phase separation.

As with post-translational modifications, the m⁶A post-transcriptional modification has writers, readers, and erasers. The writer of the majority of m⁶A species in the cell is a heterodimer formed by Mettl3 and methyltransferase-like protein 14 (Mettl14) (Wang et al., 2016a; Wang et al., 2016b). Mettl14 binds directly to mRNA targets and allosterically activates Mettl3, which is catalytically active and methylates the bound substrate. Inactivation of either Mettl3 or Mettl14 results in loss of ~90% of total m⁶A in the cell (Geula et al., 2015), highlighting the major role of the heterodimer in depositing post-transcriptional modifications. Notably, the m⁶A mark can be read by proteins containing the YT521 homology (YTH) domain, as revealed by RNA pulldown experiments, and is required for cell fate decisions (Dominissini et al., 2012).

PRMT1 methylates Mettl14 at R255, and this methylation event was required for Mettl14 function, as introducing a R255K mutation in mouse embryonic stem cells (ESCs) resulted in a significant global reduction of m⁶A. Depletion of R255 methylation by PRMT1 affected endoderm differentiation of the mouse ESCs.

3.2 RBPs and alternative splicing in muscle stem cell function

Alternative splicing (AS) occurs in a highly tissue-specific manner, and skeletal muscle has the third highest number of AS events, behind the brain and testis (Castle et al., 2008). AS is a crucial part of the myogenic process. One of the earliest known and best studied cases examples of AS in MuSCs is with the myocyte enhancer factor 2C (Mef2c) and Mef2d transcripts (Nakka et al., 2018). Both undergo extensive regulation at the transcriptional and alternative splicing level, and Mef2d splicing in MuSCs produces a tissue-specific isoform that is indispensable for MuSC differentiation (Sebastian et al., 2013). The MuSC surface marker integrin alpha-7 (Itga7) has two alternatively spliced isoforms wherein exons 5 and 6 are mutually exclusive, and these two variants are differentially regulated during muscle development. The Itga7-X1 isoform (inclusion of exon 5) is observed in embryogenesis during the development of skeletal muscle, while the Itga7-X2 isoform is found in adult skeletal muscle (Collo et al., 1993; Song et al., 1993; von der Mark et al., 2002; Ziober et al., 1993). In chapter 4, we show that the expression of the Itga7-X1 isoform in adult MuSCs results in the loss of MuSC polarity and provides evidence that maintaining a high Itga7-X2/Itga7-X1 isoform ratio is a requirement for MuSC polarity.

The process of MuSC differentiation is a highly orchestrated, temporally regulated process. It is therefore unsurprising that the RBPs which regulate AS in the MuSC must also behave in a time-sensitive manner (Boutz et al., 2007). A prototype example of this is RNA binding fox-1 homolog 1 (Rbfox1). Rbfox1 is expressed at low levels in the MuSC and is rapidly upregulated during myogenesis (Pedrotti et al., 2015). When Rbfox1 is present, it binds to key transcripts involved in MuSC differentiation such as Mef2d and myosin-binding protein-C (Mybpc1) to facilitate inclusion of the required exons (Runfola et al., 2015).

Localization of RBPs within the cells is one of many layers of regulation which affect RBP splicing activity. For example, the CUGBP Elav-like family member 1 (Celf1) RNA binding protein, known to be involved in the AS of developmentally regulated transcripts (Ladd et al., 2001), displays enhanced nuclear localization, while MBNL1 protein is sequestered to nuclear foci in myotonic dystrophy cells. The aberrant localization of these two important RBPs results in a perturbed splicing network that contributes to the pathogenesis of myotonic dystrophy.

Indeed, AS is intricately involved in muscular diseases. For example, sequestration of MBNL1 to nuclear foci as described earlier has multiple functional implications in myotonic dystrophy. Namely, the second last exon of the DMD transcript (exon 78) is alternatively spliced in the absence of MBNL1, leading to the formation of the embryonic form of dystrophin. The presence of this embryonic version in adult muscle leads to compromised muscle fiber integrity and maintenance (Rau et al., 2015).

The complex network of AS observed in MuSCs during myogenesis is still being untangled, and further studies are required to have a complete understanding of how this network is regulated. The RBP Quaking is well known to be a key regulator of AS in various cell types, however its role in MuSC is just starting to come to light. A more detailed overview of QKI is provided in the following section.

3.3 The Quaking RNA binding protein and its role in muscle

The RBP Quaking (QKI) binds to its response element (QRE) (ACUAAAY...(1-20)...UAAY) (Galarneau and Richard, 2005) on a wide range of RNA targets. QKI pre-mRNA undergoes extensive splicing around the 3' end of its gene to generate 4 isoforms: QKI-5, QKI-6, QKI-7, and QKI-7b. The four QKI isoforms differ only in their C-terminal 35 amino acids which

are encoded by *qkl* exons 7 and 8 (Kondo et al., 1999). Localization differs among the isoforms, as QKI-5 contains a nuclear localization signal (NLS) while QKI-6 and QKI-7/b do not (Pilotte et al., 2001). All QKI isoforms contain a QUA1 domain responsible for dimerization (Chen et al., 1997; Chen and Richard, 1998), and a continuous KH-QUA2 domain that engages in RNA binding (Ryder et al., 2004). QKI also contains a proline rich (Y-rich) motif, which can be required for Src kinase-mediated phosphorylation (Zhang et al., 2003) (Figure 1.3A). The QKI isoforms are expressed ubiquitously throughout various cell types in the body, and as such have a broad range of cellular functions to regulate mRNA, splicing, nuclear export, and stability (Figure 1.3B) (Darbelli and Richard, 2016).

QKI was shown to participate in myelination of the central nervous system (CNS) by mediating nuclear export of the myelin basic protein (MBP) transcript (Larocque et al., 2002). QKI bound to the 3' UTR of MBP mRNA, and overexpression of QKI-5 in oligodendrocytes retained MBP transcripts in the nucleus. Binding of QKI to the 3'UTR of mRNA transcripts has been shown to regulate their stability. For example, QKI-6 binds to the 3'UTR of the actin-interacting protein (Aip-1) leading to a shorter half-life of the AIP-1 mRNA. QKI-5 was shown to bind to the 3'UTR of Stat3 to increase its stability, thereby promoting VEGF signaling and increasing endothelial cell differentiation (Cochrane et al., 2017). Extensive changes to alternative splicing networks have been noted in several cellular contexts with QKI deficiency, including muscle stem cells, neurons, microglia, and cancer cells (Darbelli and Richard, 2016; Lee et al., 2021).

The name of the Quaking gene itself originates from the phenotype observed in mice with severe shaking behaviour and reduced myelination throughout the CNS (Sidman et al., 1964), called quaking viable (*qk^v*) mice, which were later determined to have a genetic deletion in the promoter region of the quaking (*qkl*) gene (Ebersole et al., 1996). While other genes were encoded

in the deleted region of the quaking viable mice, it was later shown that it was the reduced expression of the QKI proteins that specifically caused the myelination defects. Studies using a conditional QKI knockout mouse wherein QKI was deleted in adult oligodendrocytes only (*PLP-CreERT2*) showed a disruption in myelin/axon interactions as a result of a reduction in the expression of Neurofascin-155 in the oligodendrocytes (Darbelli et al., 2016).

In addition to its extensive function in the CNS, QKI has been implicated in various other human diseases, including Schizophrenia (McInnes and Lauriat, 2006), Multiple Sclerosis (Lee et al., 2020; Wu et al., 2001), and cancer (He et al., 2020; Iwata et al., 2017; Li et al., 2002; Shi et al., 2019; Zhang et al., 2018). Interestingly, a role for QKI in muscle stem cell maintenance and adult muscle regeneration has been described and will be discussed further in Chapter 4.

With such diverse functions in RNA metabolism, QKI is involved in complex processes of many different cell types, including oligodendrocytes (Darbelli et al., 2016), microglia (Lee et al., 2020), and cardiac smooth muscle (Chen et al., 2021a). In fact, the role of QKI in smooth muscle functions has been recently well characterized. Chen and colleagues showed that QKI was critical for the alternative splicing program in developing heart, with muscle-specific components of the Z-disc being a key target (Chen et al., 2021a). Furthermore, QKI is regulated by microRNA-214 (miR-214) in vascular smooth muscle cells (VSMCs). When miR-214 is elevated under cobalt chloride-induced hypoxic conditions in mice, QKI is repressed leading to senescence of VSMCs (Chen et al., 2020).

Despite being well characterized in smooth muscle function, the role of QKI in skeletal MuSCs and during skeletal myogenesis is not well characterized. A study in C2C12 cells, an immortalized mouse myoblast cell line, described a QKI-regulated alternative splicing network during differentiation into myotubes (Hall et al., 2013). In this study, siRNA was used to

knockdown QKI, and splicing-sensitive microarray identified 406 cassette exons which were altered in QKI-deficient C2C12 cells, with about half being included and half being excluded. The authors also noted that the expression of QKI protein increased throughout differentiation of the C2C12 myoblasts, indicating that QKI may be required for this process. However, the role of QKI in primary MuSCs and during *in vivo* muscle regeneration has not been previously characterized, and is addressed in Chapter 4.

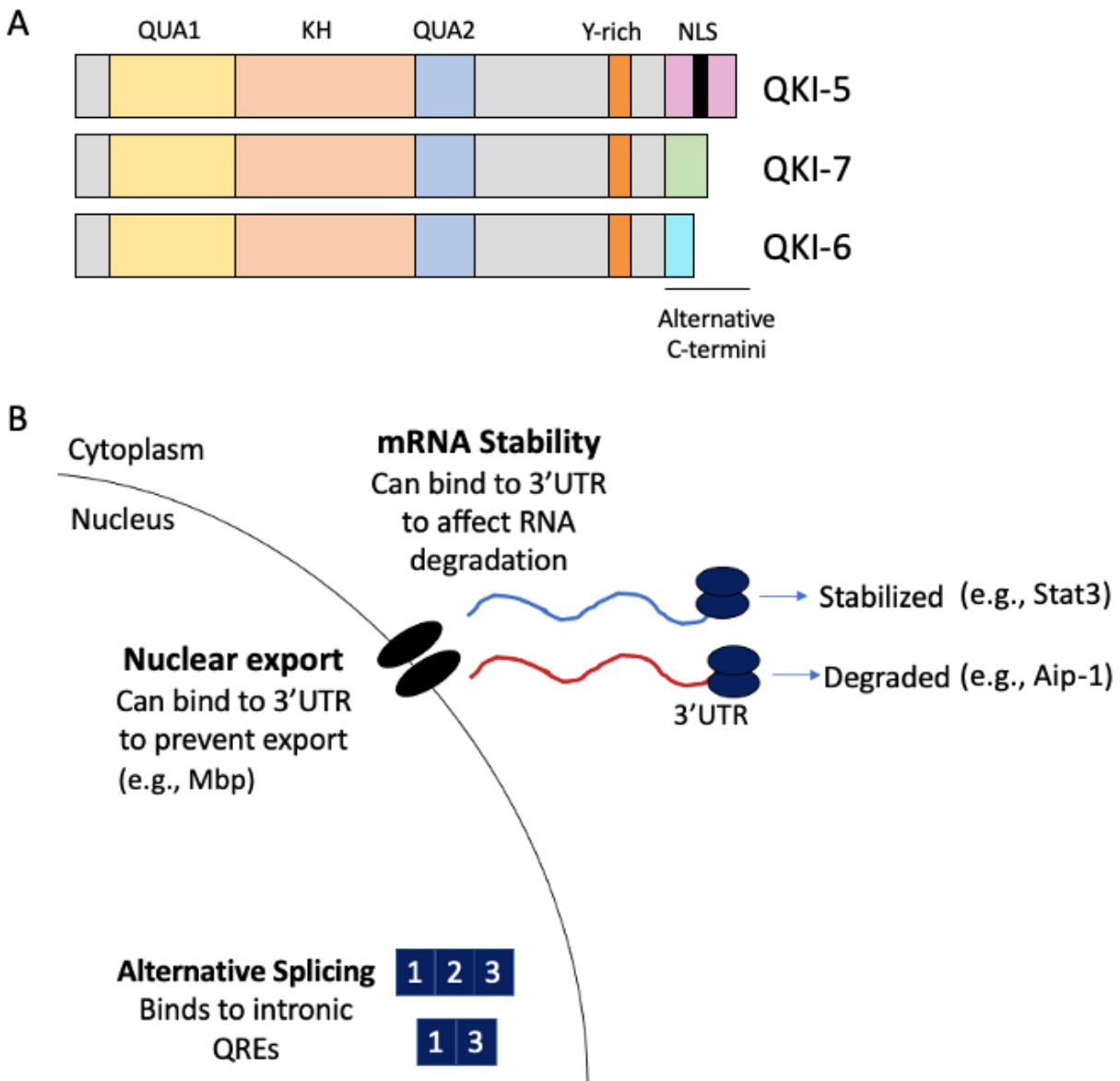


Figure 1.3 Summary of QKI structure and functions

A) Overview of the three main QKI isoforms, highlighting the alternative C-termini. NLS: Nuclear localization signal. KH: K homology. **B)** Graphical summary of the various functions of QKI in the nucleus and cytoplasm. QRE: Quaking response element. 3'UTR: three prime untranslated region.

Hypothesis and objectives

Chapter 2:

Hypothesis: We hypothesize that type I PRMT inhibition can synergize with other epigenetic drugs to kill cancer cells.

Objectives: Perform a cell viability screen in the non-small cell lung carcinoma cell line A549 to identify compounds might synergize with MS023, a type I PRMT inhibitor. Functionally validate the identified compounds *in vitro*.

Chapter 3:

Hypothesis: Transient inhibition of PRMT1 with MS023 can achieve increased proliferation while still allowing for differentiation capabilities of muscle stem cells (MuSCs)

Objectives: Perform scRNAseq on MuSCs treated with MS023. Test engraftment and regeneration capabilities of MS023-treated MuSCs expanded *ex vivo*. Determine if there is any therapeutic effect of MS023 in a dystrophic mouse model.

Chapter 4:

Hypothesis: The RNA binding protein QKI is required for *in vivo* muscle regeneration and targets important regulators of MuSC differentiation for alternative splicing.

Objectives: Generate a conditional QKI knockout mouse wherein QKI is deleted only in MuSCs. Perform regeneration experiments to determine effect of QKI deficiency *in vivo*. Perform RNAseq on purified wildtype and QKI-knockout MuSCs to identify key QKI targets which may be related to regeneration phenotype.

Chapter 2: Synergistic effects of type I PRMT and PARP inhibitors against non-small cell lung cancer cells

Claudia Dominici, Nicolas Sgarioto, Zhenbao Yu, Laura Sesma, Jean-Yves Masson, Stéphane Richard and Noël J-M Raynal

Clinical Epigenetics, March 10; 13(1):54 (2021). DOI 10.1186/s13148-021-01037-1

¹Segal Cancer Center, Lady Davis Institute for Medical Research and Gerald Bronfman Department of Oncology and Departments of Biochemistry, Human Genetics and Medicine, McGill University, Montréal, Québec, Canada H3T 1E2.

²Département de Pharmacologie and Physiologie, Université de Montréal, and Research Centre of the Sainte-Justine University Hospital, Montréal, Québec, Canada H3T 1C5.

³Genome Stability Laboratory, CHU de Québec Research Center, Oncology Division; Department of Molecular Biology, Medical Biochemistry and Pathology; Laval University Cancer Research Center, 9 McMahan, Québec City, Québec, Canada G1R S3S.

*Corresponding authors: stephane.richard@mcgill.ca; noel.raynal@umontreal.ca

2.1 Preface

Synergistic drug combinations are commonly used in the treatment of cancer, with the goal of reducing the dose and therefore the toxicity of the individual components. Typically, synergistic drugs are selected to exploit an intrinsic vulnerability present in the cancer cell. In chapter 2 of this thesis, Dominici et al. describe a novel synergy between inhibitors of PARP and PRMT enzymes and show that the combination treatment is lethal to cancer cells with an MTAP deficiency.

2.2 Abstract

Background: Non-small cell lung carcinoma (NSCLC) is a leading cause of cancer-related death and represents a major health burden worldwide. Current therapies for NSCLC include chemotherapy, immunotherapy, and targeted molecular agents such as tyrosine kinase inhibitors and epigenetic drugs such as DNA methyltransferase inhibitors. However, survival rates remain low for patients with NSCLC, especially those with metastatic disease. A major cause for therapeutic failure is drug resistance, highlighting the need for novel therapies and combination strategies. Given that epigenetic modulators such as protein arginine methyltransferases (PRMTs) are frequently overexpressed in cancers, PRMT inhibitors are a promising class of cancer therapeutics. We screened a library of epigenetic and anticancer drugs to identify compounds that would synergize with MS023, a type I PRMT inhibitor, in decreasing the viability of methylthioadenosine phosphorylase (MTAP)-negative NSCLC cells.

Results: Among 181 compounds, we identified PARP inhibitors (PARPi) as having a strong synergistic interaction with type I PRMT inhibition. The combination of MS023 and the PARP inhibitor BMN-673 (Talazoparib) demonstrated strong synergistic interaction at low nanomolar concentrations in MTAP-negative NSCLC cell lines A549, SK-LU-1 and HCC4006. The re-introduction of MTAP decreased the sensitivity of the combination therapy in A549. The combination therapy resulted in elevated γ -H2AX foci indicating increased DNA damage causing decreased cell viability. Lastly, the combination therapy was effective in PARPi resistant ovarian cancer cells, suggesting that type I PRMT inhibitors could mitigate PARPi resistance, thus potentially having an important clinical impact for cancer treatment.

Conclusions: These findings identify a novel cancer drug combination therapy, which is more potent than the separate single-agent therapies. Thus, combining PARP inhibitors and type I

PRMT inhibitors represents a new therapeutic opportunity for MTAP-negative NSCLC and certain cancer cells resistant to PARP inhibitors.

2.3 Background

Lung cancer is the leading cause of cancer-related death worldwide and is highly taxing on health care systems (Siegel et al., 2018). The vast majority (about 85%) of lung cancer cases are of the non-small cell lung cancer (NSCLC) subtype (Molina et al., 2008). Early-stage NSCLC is addressed with surgery, however later stages NSCLC present a challenge that is not adequately met with current therapeutics (Herbst et al., 2018; Vansteenkiste et al., 2014). Myriad oncogenic pathways have been identified in patients with NSCLC with varying degrees of penetration, such as aberrations in receptor tyrosine kinase signalling, mTOR signalling, and components of the cell cycle (Ding et al., 2008; Herbst et al., 2018). While deficiencies in these well-studied pathways create an opening for targeted molecular therapies, the complex etiology of NSCLC presents a challenge in developing a unified therapy that can be extended to a broad range of patients. Targeting the epigenetic regulation with small molecule inhibitors provides a promising avenue in the development of successful therapies. Indeed, inhibitors of epigenetic modulators are actively being pursued (Schiffmann et al., 2016; Shi et al., 2019). Unfortunately, single agent delivery of epigenetic inhibitors has been met with limited success due to high toxicity or impermanent effects (Juergens et al., 2011; Vansteenkiste et al., 2008). Therefore, delivering combinations of synergic epigenetic inhibitors at lower doses represents a suitable alternative. In fact, the success observed with targeting DNA methyltransferases (DNMTs) in combination with histone deacetylases (HDACs) in NSCLC provides a rationale for uncovering other combinations of epigenetic modifiers, which can be developed into effective therapies (Cameron et al., 1999; Huang et al., 2012).

Arginine methylation is an abundant post-translational modification identified in many proteins including histones, RNA-binding proteins, transcription factors and their coregulators,

and DNA damage repair proteins (Guccione and Richard, 2019). Arginine methylation is mediated by a family of nine protein arginine methyltransferases (PRMTs) (Bedford and Clarke, 2009). PRMTs transfer methyl groups from S-adenosylmethionine (SAM) to the guanidino nitrogens of arginine, generating methylated arginines and S-adenosylhomocysteine (SAH) as a by-product. PRMTs are divided into three subtypes (Bedford and Clarke, 2009): type I catalyzes the formation of monomethylarginine (MMA) before a dimethylation reaction to produce asymmetric dimethylarginine (aDMA). PRMT1 is the type I enzyme responsible for the majority of aDMA. Type II enzymes also generate MMA as an intermediate for the production of symmetric dimethylarginine (sDMA), with PRMT5 being the major enzyme generating this modification. PRMT7 is only known type III enzyme only able to generate MMA (Feng et al., 2013). The early discovery of a transcriptional co-activator function of PRMT1 and PRMT4 (CARM1) linked arginine methylation to the field of epigenetics (Chen et al., 1999; Wang et al., 2001). In addition, arginine methylation is known to be linked to double strand DNA break (DSB) repair through methylating the DNA damage proteins and affecting cell cycle checkpoints (Boisvert et al., 2005; Clarke et al., 2017; Hamard et al., 2018; Yu et al., 2009).

Overexpression of PRMTs resulting in altered methylarginine patterns is a common feature of cancer cells (Yang et al., 2014), and therefore PRMTs may serve as key therapeutic targets for intervention, as reviewed recently (Guccione and Richard, 2019). Promising small-molecule inhibitors are developed for several PRMTs (Chan-Penebre et al., 2015; Eram et al., 2016; Fedoriw et al., 2019; Nakayama et al., 2018; Szewczyk et al.). Notably, the type I PRMT inhibitor GSK3368715 is in phase I clinical trials for the treatment of diffuse large B-cell lymphoma and solid tumors (clinicaltrials.gov identifier number: NCT03666988). Additionally, PRMT5 inhibitors JNJ-64619178 and GSK3326595 are currently in phase I clinical trials

(ClinicalTrials.gov identifier numbers NCT03573310 and NCT03614728, respectively) for patients with advanced cancers.

Substrate scavenging exists between type I and II PRMTs, leading to a global increase in MMA and sDMA, when PRMT1 is deleted (Dhar et al., 2013). This interplay between type I and type II PRMTs has recently been shown to have therapeutic value for cancer treatment and thus, it is not surprising that PRMT1 is synthetic lethal to PRMT5 deletion (Fedoriw et al., 2019; Fong and al., 2019; Gao et al., 2019). Since PRMTs require SAM as a methyl donor, they are inextricably linked to methionine metabolism. The enzyme 5-methylthioadenosine phosphorylase (MTAP) is a key component of the methionine salvage pathway. Due to its genomic proximity to the tumor suppressor genes CDKN2A and CDKN2B, the MTAP gene is commonly co-deleted in human cancer. This genetic deletion is found in ~40% of NSCLC patients (Schmid et al., 1998). Interestingly, MTAP-deleted cancer cells accumulate the metabolite methylthioadenosine (MTA), which is a high-affinity inhibitor of PRMT5 activity (Kryukov et al., 2016; Marjon et al., 2016; Mavrakis et al., 2016). MTAP-negative A549 cells have elevated levels of MTA, resulting in endogenous PRMT5 inhibition (Kryukov et al., 2016; Marjon et al., 2016; Mavrakis et al., 2016). As a result, inhibition of PRMT1 with the recently developed inhibitor of type I PRMTs, MS023 (Eram et al., 2016) or GSK3368715, is inherently optimal at reducing cell viability of MTAP-negative cells such as A549 (Fedoriw et al., 2019; Fong et al., 2019; Gao et al., 2019).

Herein, we aimed to identify compounds that synergized with MS023 and elevated its cytotoxicity in the A549 NSCLC cell line. A library of epigenetic and anticancer compounds was screened, and we measured viability in the presence or absence of MS023. We identified several poly(ADP)-ribose polymerase (PARP) inhibitors that had a strong synergistic interaction with type I PRMT inhibition in A549 cells. This synergistic effect was partially attenuated in A549 cells

stably transfected with MTAP expressing lentiviral vectors. Furthermore, we show that MS023 and the PARP inhibitor BMN-673 (Talazoparib) also synergized in SK-LU-1 and HCC4006 NSCLC cell lines. The combination therapy produced a significant increase in the accumulation of γ -H2AX foci indicating increased DNA damage, which was responsible for decreased viability. Furthermore, we show that MS023 lessened the resistance to PARPi in the PEO ovarian cancer cell line, indicating a degree of robustness to the synergy of BMN-673 and MS023 in cancer cells. Our data identify a new combination therapy using type I PRMT (MS023) and PARP (BMN-673; Talazoparib) inhibitors to effectively promote cell death of NSCLC.

2.4 Results

Cell viability screen with epigenetic/anticancer library identifies compounds that synergize with the type I PRMT inhibitor, MS023

Since PRMT overexpression has been implicated in various human cancers and deficiency of PRMT activity can inhibit cancer cell proliferation and lead to cell death (Yang et al., 2014), we initiated a small molecule library screen to identify epigenetic/anticancer drugs, which can cause synthetic lethality in combination with MS023, an inhibitor of type I PRMTs (Eram et al., 2016). The ChemSelleck Epigenetic compound library is composed of 181 compounds with epigenetic and anticancer activities that is divided into 6 main families; angiogenesis (2.2%), cell cycle (3.9%), cell signalling (10.5%), JAK/STAT (12.7%), DNA damage (17.1%), and epigenetics (53.6%). The cell line chosen for screening was A549, a human MTAP-negative NSCLC cell line (Fig. 2.1a).

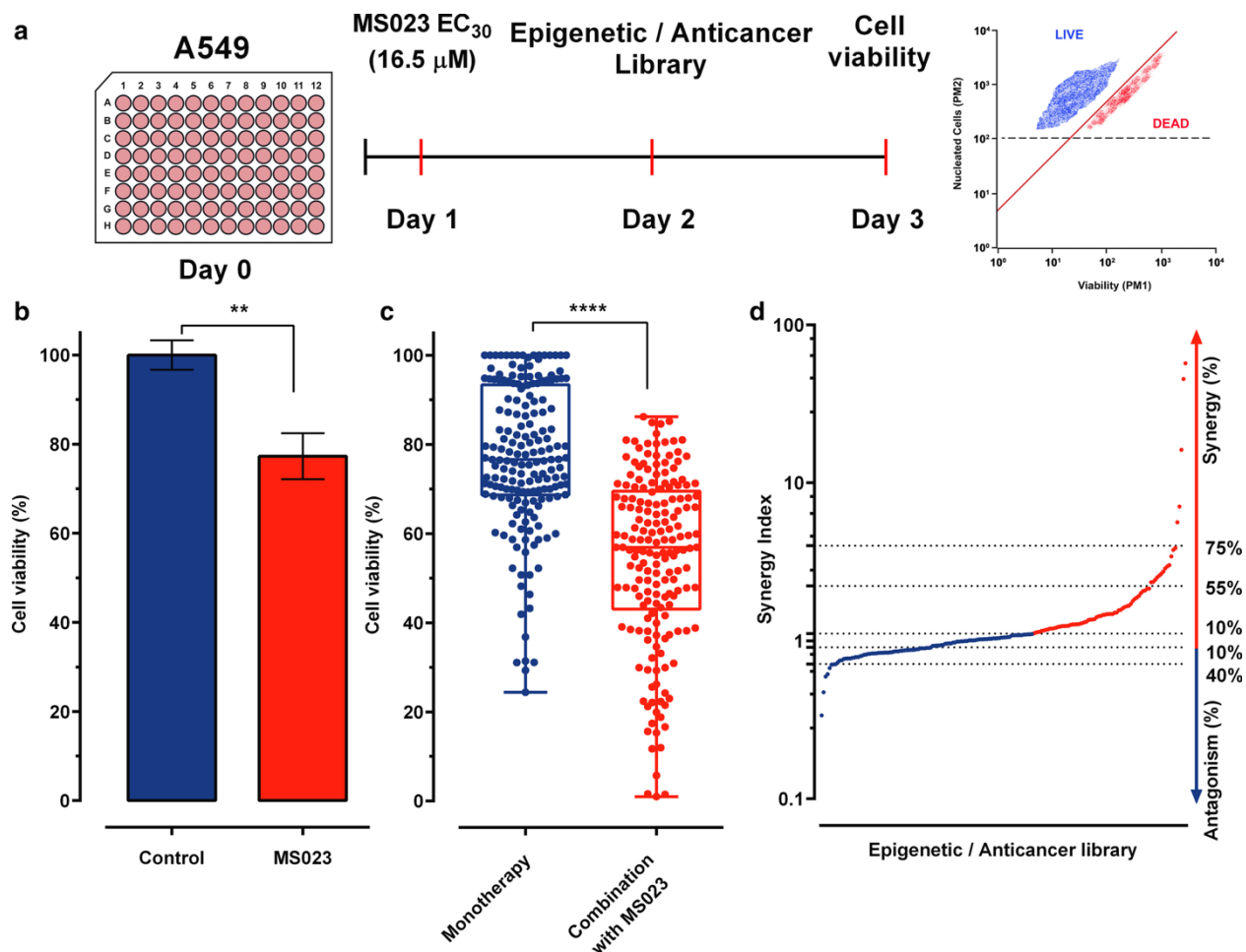


Figure 2.1. Cell viability screen to identify compounds targeting epigenetic regulators that synergize with MS023.

A Scheme of the method used to measure synergy of MS023 with drugs from the Epigenetic/Anticancer compound library. Plates were seeded (20 K cells/well) and treated the next day with MS023 or DMSO. Drugs from the Epigenetic/Anticancer compound library were added on the following day. On day 3, viability was analyzed by flow cytometry using Guava® ViaCount™ Reagent. **B** Cell viability of A549 cells treated with DMSO (blue) or MS023 16.5 μM (red) through the screen. Cell viability was expressed as a percentage relative to DMSO-treated cells. Treatment with MS023 significantly ($p = 0.0034$ Wilcoxon matched-pairs signed rank test)

decreased cell viability by 23% between vehicle condition (DMSO: 100.0 ± 3.3 ; $n = 12$) and MS023 treatment (77.3 ± 5.2 ; $n = 11$). **C** Drug screening results showing the distribution of viability of A549 cells after treatment with the drug library in monotherapy (10 μ M, 24 h) or with a 24 h pre-treatment with MS023 (16.5 μ M). Each dot represents cell viability (%) of a compound for each condition (monotherapy vs combination with MS023) relative to vehicle treated cells. Mean viability is significantly decreased by 23% (77.2 ± 16.4 vs. 54.2 ± 19.4 ; unpaired, nonparametric, Mann–Withney analysis, $p < 0.001$) indicating a global effect of MS023 pre-treatment on cell viability. For this representation, 3 drugs (CX-6258-HCL; Pirarubicin; MC1568) produced 1% cell viability and were excluded for the analyses in both conditions. **D** Synergy index obtained after the sequential combination of the MS023 followed by the Epigenetic/Anticancer drug library. A synergy index of 1.12 was set as a threshold for all combination to be considered synergistic

We first performed multiple dose–response experiments after a 24 h MS023 exposure and measured dose-dependent cell viability inhibition. We selected 16.5 μM as the concentration of MS023 to be used for the screen, which resulted in a 23% decrease in A549 cell viability (Fig. 2.1b). For drug screening, A549 cells were pre-treated with 16.5 μM MS023 for 24 h, and then exposed for an additional 24 h to the drug library at 10 μM . Cell viability was measured by flow cytometry using Viacount reagent, which distinguishes between viable, pre-apoptotic and dead cells based on the differential permeability of DNA-binding dyes. For all screened compounds, the mean cell viability was $77.2 \pm 16.4\%$ in monotherapy (Fig. 2.1c). Pre-treatment with MS023 (16.5 μM , 24 h) followed by epigenetic/ anticancer compounds (10 μM , 24 h) produced a global and significant 25% reduction ($p < 0.001$) in cell viability to $54.2 \pm 19.4\%$, indicating a general sensitization effect of MS023 (Fig. 2.1c). We then calculated a synergy index displaying quantitatively synergistic and antagonistic drug interactions with MS023 by normalizing cell viability of drug combination data to cell viability of each compound alone, allowing result comparison between each drug combination (Fig. 2.1d). We observed that 58 (42%), 13 (10%), and 5 (3%) compounds produced synergistic synthetic cell death by more than 10%, 55%, and 75%, respectively. Antagonist interactions by more than 10 and 40%, were produced by 47 (30%) and 8 (4%) compounds, respectively (Fig. 2.1d). Confirmation experiments of 40 compounds (20 most active and 20 less active compounds) showed a validation rate of 70% (28/40; Additional file 1: Figure S2.1). These experiments indicate that MTAP-deficient A549 NSCLC cells are sensitized to epigenetic/anticancer drugs following type I PRMT inhibitor pre-treatment.

To identify pharmacological effects from groups of drugs with similar targets, we evaluated the synergy index by regrouping drugs based on target pathways (Fig. 2.2a), or molecular targets (Fig. 2.2b). Pie charts are showing the percentage of drugs among each target pathways and

molecular targets (Fig. 2.2a, b). Within each target pathway or molecular target sub-groups, we calculated an enrichment score per class by normalizing the effect of each sub-group to the number of compounds per category. Thus, the enrichment score takes into account the percentage of synergy of each compound and its own weight in its sub-group. An enrichment score above 1 suggests a category that synergizes with MS023. When classified by target pathways, mean synergy index per class showed that compounds belonging to DNA damage pathway (enrichment score = 1.68) were the most synergistic with MS023 followed by JAK/STAT (enrichment score = 1.10). In contrast, epigenetics (enrichment score = 0.96), cell signaling (enrichment score = 0.74), cell cycle (enrichment score = 0.51), and angiogenesis (enrichment score = -1.12) drug classes had low enrichment scores (< 1) and low to antagonistic synergistic index (Fig. 2.2a).

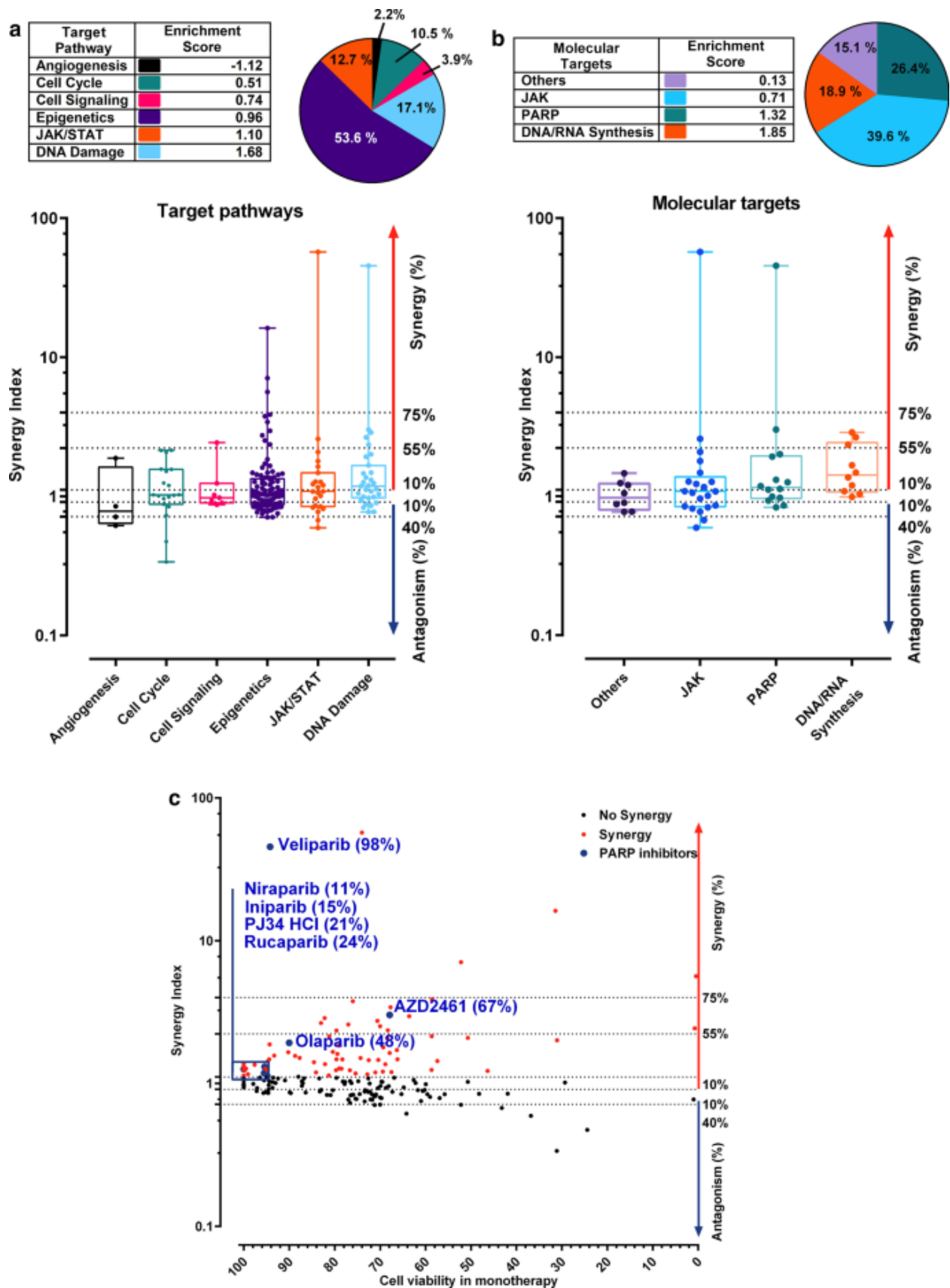


Figure 2.2. Drug screening analyses by target and molecular pathway reveal the synergistic interaction between MS023 and PARP inhibitors.

A Synergy Index distribution of the drugs classified by target pathways. Table indicates the enrichment score of each family after the combination screen. Pie chart shows the repartition of each family in the library. Violin plots are classified by target pathways and ordered by enrichment score. Compounds associated with “JAK/STAT” and “DNA Damage” pathways respectively present an enrichment score of 1.10 and 1.68, respectively, suggesting a synergistic interaction with MS023. **B** Synergy Index distribution of the drugs classified by Molecular targets. Table indicates the enrichment score of each target family within the screen. Pie chart shows the repartition of each family in the library. Violin plots are classified by Molecular targets and ordered by enrichment score. Compounds inhibiting “PARP” and “DNA/RNA Synthesis” present an enrichment of 1.32 and 1.85 respectively, and seems more prone to synergise with MS023. **C** Synergy indexes of each compound are plotted in function of their cell viability in monotherapy. PARP inhibitors are indicated in the graph

The two most enriched target pathways were DNA damage and JAK/STAT. When grouping based on molecular targets, compounds targeting DNA/RNA synthesis had the highest mean synergy index (enrichment score = 1.85) followed by PARP inhibitors (PARPi, enrichment score = 1.32; Fig. 2.2b). Interestingly, approved PARPi (Veliparib, Niraparib, and Olaparib) and PARPi in development (Iniparib, PJ34 HCl, and AZD2461) showed synergistic interactions with MS023, without causing cytotoxicity in monotherapy, suggesting a potentiation effect (Compounds that potentiate the effect of MS023 are found on the left-hand side of the graph, Fig. 2.2c). Overall, our screen in the MTAP-negative A549 NSCLC cell line showed that PARPi exhibited a high synergistic interaction with a type I PRMT inhibitor, which may be easily combined in a clinical setting to increase therapeutic efficacy (Fig. 2.2a–c). Observing enrichment in this drug class prompted further investigation into the synergistic potential between PARPi and the type I PRMT inhibitor MS023.

Combination of MS023 with low concentrations of the PARP inhibitor BMN-673 (Talazoparib) results in synthetic lethality of A549 NSCLC cells

To confirm the activity of PARPi identified in our screens, we performed MTT-based cell viability assays (Fig. 2.3a). We used BMN-673 (Talazoparib), one of the recently approved PARPi, which displays high potency by trapping PARP to DNA lesions (Hopkins et al., 2015; Hoy, 2018). We used lower doses of MS023 while increasing treatment duration to 7 days as previously reported to significantly impact A549 cell viability (Gao et al., 2016). We found that even at very low concentrations of BMN-673 (0.3 nM), the combination of the two inhibitors significantly killed more than 80% of the cells (Fig. 2.3b). We calculated the synergy score using the Bliss Synergy method and found that BMN-673 combined with MS023 produced a synergistic

effect on cell death (Fig. 2.3c). These results demonstrate a significant synergistic effect at very low concentrations of PARP and type I PRMT inhibitors. Next, we asked whether the MTAP deficiency in A549 cells could play a role in the synergistic interaction between type I PRMT and PARP inhibitors. A549 cells were stably transfected with an MTAP expression vector and we generated two clones (A549 MTAP #1 and #2), which re-expressed the MTAP protein as visualized by immunoblotting (Fig. 2.4a). To confirm the restored MTAP enzymatic activity, we measured symmetric arginine dimethylation (SDMA) levels by immunoblotting. MTAP re-expression in A549 clones #1 and #2 had an increase in SDMA levels, consistent with earlier findings that MTAP reduces MTA levels and de-represses PRMT5 inhibition (Fig. 2.4b) (Fedoriw et al., 2019; Kryukov et al., 2016; Marjon et al., 2016; Mavrakis et al., 2016).

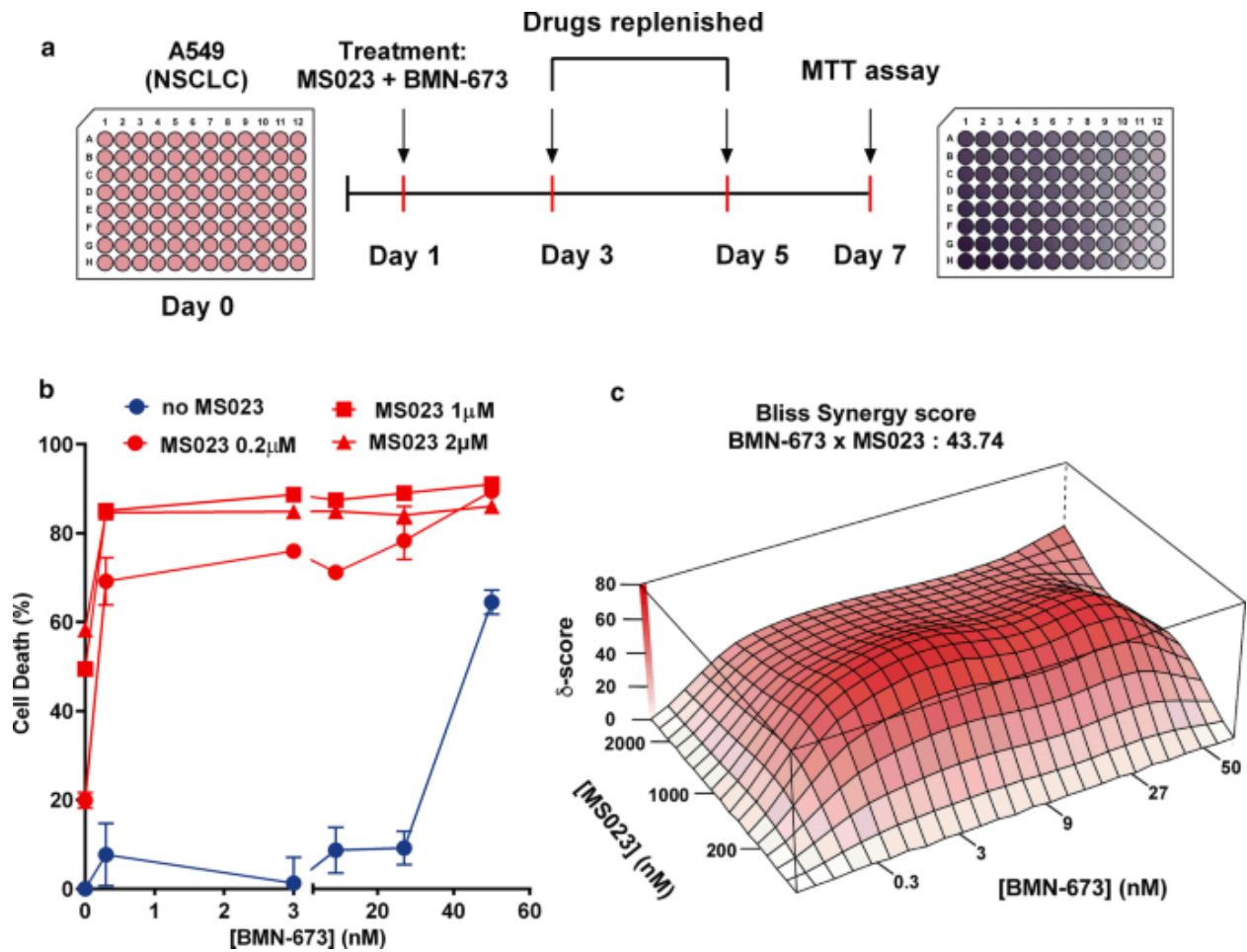


Figure 2.3. Combination of MS023 with low concentrations of BMN-673 results in synthetic lethality of A549 lung adenocarcinoma cells.

A Schematic for generating cell viability curves using the MTT assay. **B** Cell viability curves from A549 cells treated with a range of BMN-673 (0.3–60 nM) alone (blue line), or in combination with 0.2, 1, or 2 μ M MS023 (red line) ($n = 3$). **C** The open-source R package SynergyFinder was used to visualize the dose–response of the combination of BMN-673 and MS023 in A549 cells and to calculate Bliss synergy scores. The Bliss synergy score is presented on the z-axis of the Bliss graph and is used to determine concentrations at which synergy occurs. Highest Bliss synergy score is highlighted in the graph

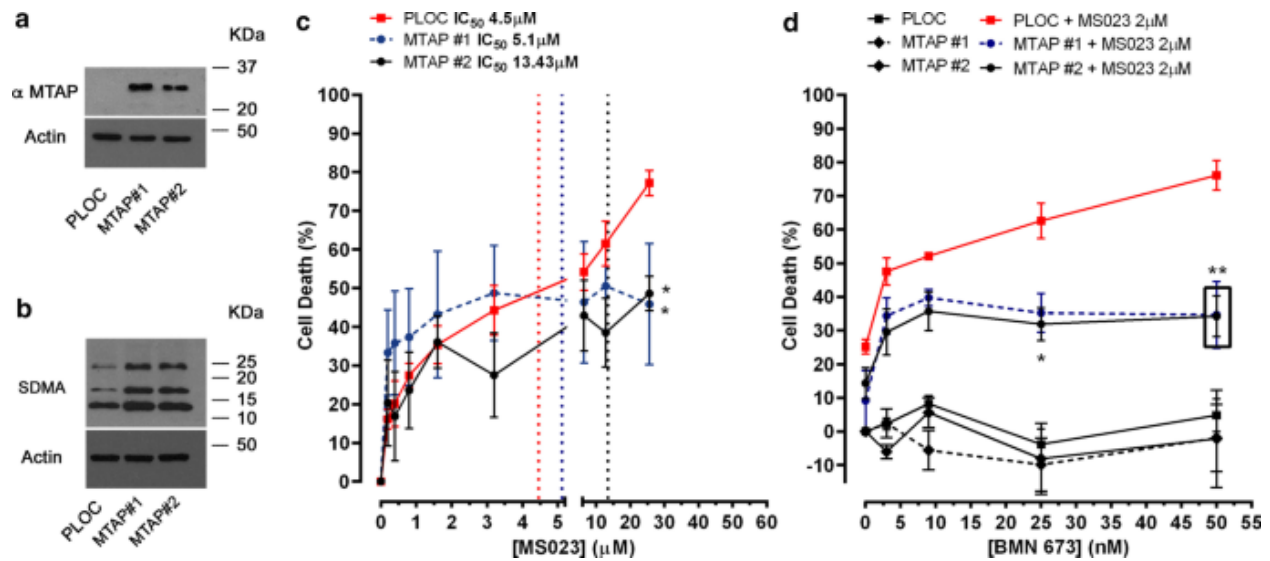


Figure 2.4. Synergistic effect of MS023 and BMN-673 is dependent on MTAP deficiency in A549 cells.

A Immunoblotting of A549 cells infected with the empty lentivector (pLoc) or pLoc-MTAP. Clones #1 and #2 show the re-expression of MTAP using anti-MTAP antibodies. Antibodies against β -actin were used to show equivalent loading. The molecular mass markers are shown in kDa. **B** Same as panel A except the cellular lysates were immunoblotted with anti-SDMA and β -actin antibodies as indicated. **C** MTT cell viability assays were performed with A549 (PLOC) and A549 (MTAP #1, #2) treated with a range of MS023 concentrations. Dotted vertical lines represent IC₅₀ values (n = 3). (*p < 0.05, two-way ANOVA) indicates a statistical difference PLOC and MTAP clones. **D** Cell viability curves as determined by MTT assay of the A549 clones treated with a range of BMN-673 in combination 2 μ M MS023 (n = 4). ** (p < 0.01, two-way ANOVA) indicates a statistical difference PLOC and MTAP clones

First, we performed MTT assays in control (PLOC) and MTAP-expressing (clones #1, #2) A549 cells (Fig. 2.4c) to determine their sensitivity to MS023. The presence of MTAP reduced cell death induced by MS023 (PLOC-IC50: 4.4 μ M; MTAP#1-IC50: 5.1 μ M; MTAP#2-IC50: 13.4 μ M). Then, A549 cells were treated with low dose MS023 (2 μ M) and various doses of PARPi BMN-673 in the absence (PLOC) or in presence of MTAP (Fig. 2.4d). Interestingly, the presence of MTAP reduced cell death by at least 50% after exposure to the combination of MS023 and BMN-673 (at 25 and 50 nM), demonstrating that MTAP desensitizes A549 cell to the drug combination. To further explore the potential of the combination, we used two other MTAP-deficient NSCLC cell lines, SK-LU-1 and HC4006. Similarly to A549 cells, MTAP-expression conferred resistance to MS023-induced cell death in both cell lines as shown by increased IC50 values (Additional file 1: Figure S2.2A-D). Interestingly, the combination of MS023 and BMN-673 produced synergistic cell death in SK-LU-1 and HCC4006 (Additional file 1: Figure S2.2E-H). In contrast to A549 cells, MTAP expression in SK-LU-1 and HC4006 cells did not alter cell death induced by the drug combination, suggesting the involvement of other mechanisms (Additional file 1: Figure S2.2E, F). It is noteworthy that SK-LU-1 and HCC4006 cells (with or without MTAP) had slower doubling times than A549 cells suggesting that the impact of PARPi is likely to be dependent on the number of cell divisions. Additional experiments need to address these issues in the context of combination PRMTi and PARPi.

Next we asked whether inhibitors of other types of PRMTs, such as PRMT5 (EPZ015666 and GSK591) could synergize with PARPi BMN-673. Cell death was measured in A549 cells using the Viacount reagent after treatment with MS023 (2 μ M), EPZ015666 (2.5–5 μ M), and GSK591 (2.5–5 μ M) alone or in combination with BMN-673 (0.3–50 nM; Fig. 2.5a). Interestingly, the type I PRMT inhibitor (MS023) demonstrated superiority to induce cell death in combination

with the lowest dose of PARPi (0.3 nM), as compared to PRMT5 inhibitors. However, higher doses of PARPi enhanced the activity of both PRMT5 inhibitors (producing synergistic Bliss synergy scores), as also observed by others (Hamard et al., 2018), suggesting some redundancy between PRMT1 and PRMT5 pathways (Fig. 2.5b, c). Overall, the data support the rationale to combine PRMT inhibitors with PARPi to induce lung cancer cell death at low doses.

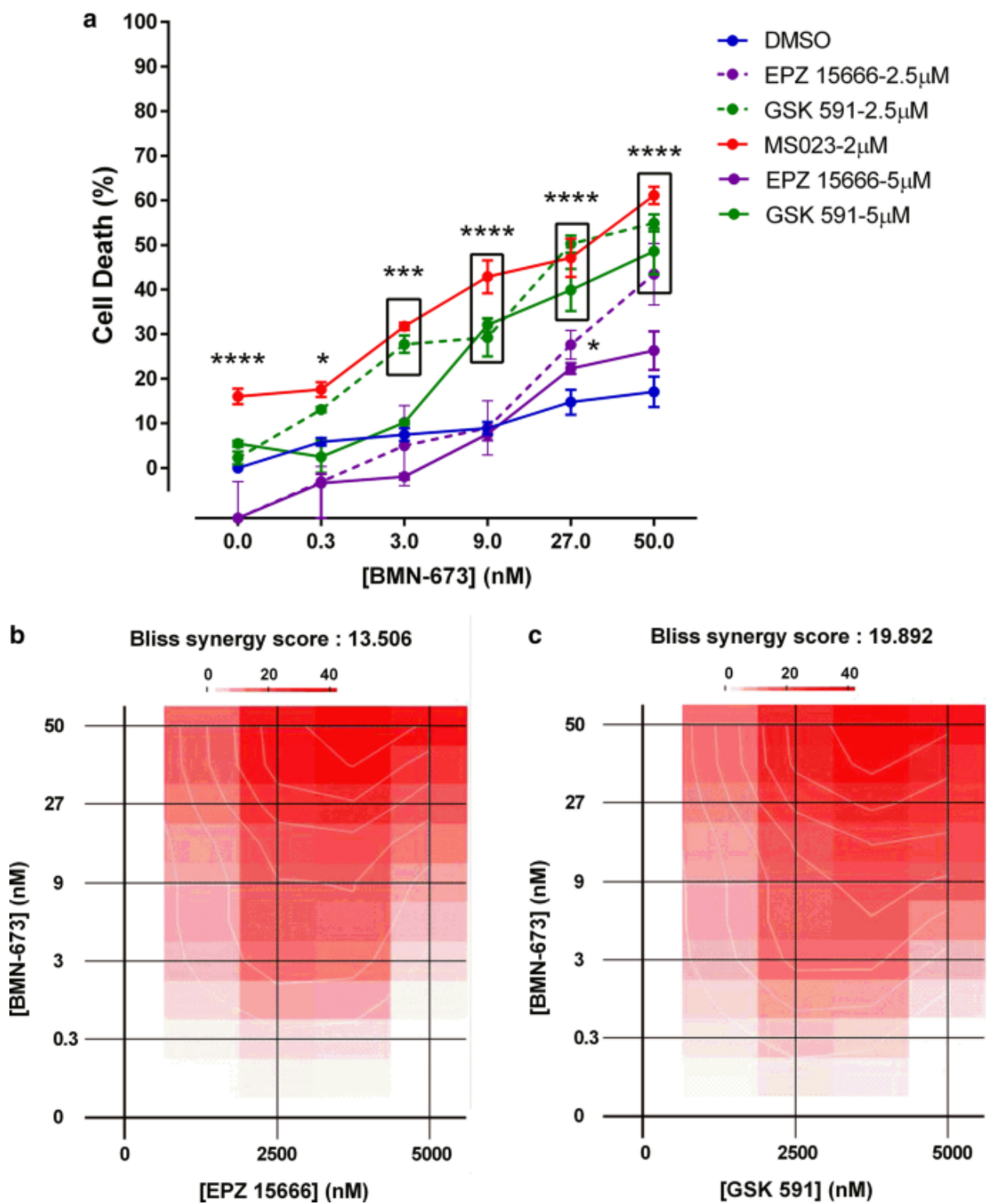


Figure 2.5. BMN-673 also synergizes with PRMT5 inhibitors.

A A549 cells were treated for 7 days with DMSO, MS023 or either the PRMT5 inhibitor EPZ015666 or GSK-591 in presence of absence of BMN-673. Cell death was measured using the Viacount reagent (* $p < 0.05$; *** $p < 0.001$; **** $p < 0.0001$; two-way ANOVA). **B** Synergy map showing the interaction between EPZ15666 and BMN-673 in A549 cells. **c** Synergy map showing the interaction between GSK-591 and BMN-673 in A549 cells

A549 cells treated with a combination of MS023 and BMN-673 accumulate γ -H2AX foci. PARP inhibitors are well-known for generating synthetic lethality in BRCA-mutant breast and ovarian cancer cells, which is largely attributed to a deficiency in homologous recombination (HR) (Ashworth, 2008; Bryant et al., 2005; Farmer et al., 2005; Fong et al., 2009). Considering that both PRMTs and PARPs are functionally involved in the DNA damage response, we performed γ -H2AX foci analysis to monitor DNA damage in A549 cells. Treatment for 7 days with either MS023 (2 μ M) or BMN-673 (50 nM) induced γ -H2AX foci formation, as observed by immunofluorescence (Fig. 2.6a). These observations suggest that the single drug treatments were able to induce a certain level of DNA damage on their own. The combination therapy using both inhibitors led to a significant increase in γ -H2AX foci, implying increased DNA damage being responsible for the reduced viability (Fig. 2.6a). More precisely, low concentrations of BMN-673 (1–50 nM) produced a significant increase in the percentage of cells (1 nM, 24.8%; 50 nM, 40.4%) with greater than five γ -H2AX ($p < 0.0001$), as compared to untreated cells (3.9%; Fig. 2.6b). Low concentrations of MS023 (0.2–2 μ M) produced similar effects (0.2 μ M, 19.6%; 2.0 μ M, 27.6%; Fig. 2.6b). The combination of BMN-673 (50 nM) and MS023 (2 μ M) produced a significant increase in the percentage of cells (69.5%) with greater than five γ -H2AX foci ($p < 0.001$; Fig. 2.6b). Overall, the data show that the drug combination of PARP and type I PRMT inhibitors elevate cytotoxicity by augmenting DNA damage in MTAP-negative A549 cells.

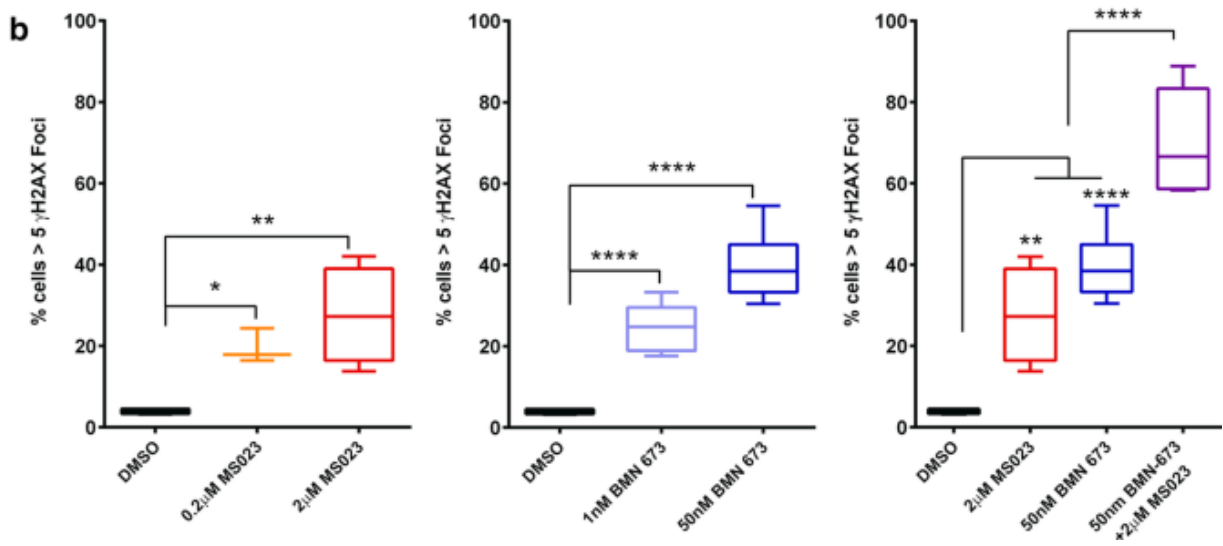
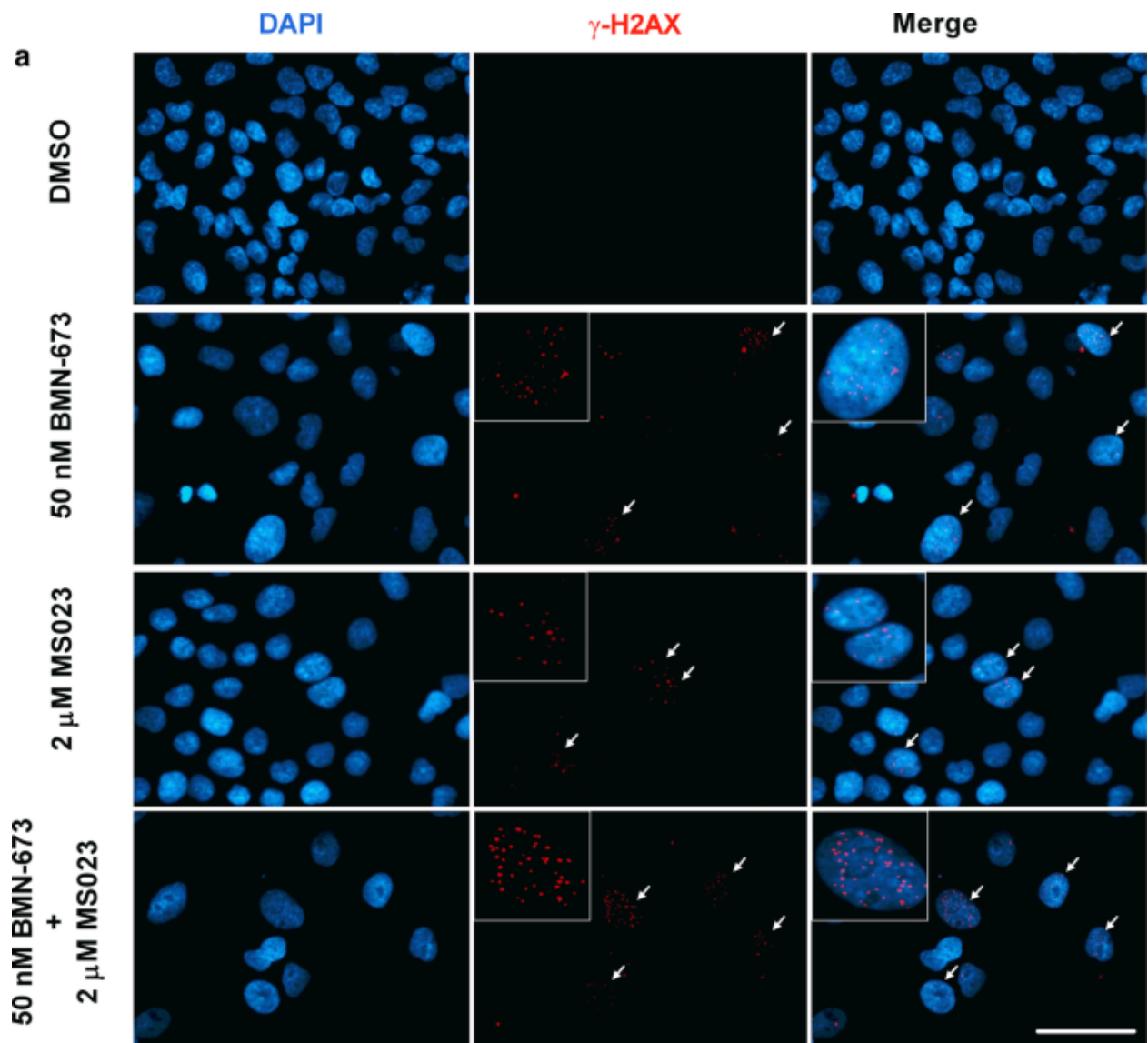


Figure 2.6. Accumulation of DNA double-strand breaks in A549 cells treated with MS023 and BMN-673.

A Representative images of A549 cells treated with the indicated drug and concentrations for 7 days and stained for γ -H2AX. Scale bar represents 50 μ m in all images. White arrows indicate cells with > 5 γ -H2AX foci. **B** Quantification of γ -H2AX foci in treated A549 cells. Box-and-whisker plots represent the percentage of cells with > 5 γ -H2AX foci, taken from a minimum total of 200 cells in each treatment group. ANOVA was used to compare treatment versus DMSO control, p values are presented within the graphs

PRMT inhibitors restore PARP inhibitor sensitivity

We asked whether the synergic relationship between MS023 and BMN-673 could be extended to PARPi-resistant cells. We used the ovarian cancer cell lines PEO1 and PEO4, which are derived from the same patient (Wolf et al., 1987). PEO1 cells are BRCA2-deficient and show sensitivity to PARPi, MS023 and their combination (Fig. 2.7a). PEO4 cells have a secondary BRCA2 mutation, which restores BRCA2 expression and are therefore resistant to BMN-673 alone (Fig. 2.7b). Interestingly, we observed a synergistic effect of the combination of MS023 and BMN-673 not only on the PEO1 cells, but also in the PEO4 BMN-673-resistant cells, as demonstrated by the high bliss score values in both cell lines (Fig. 2.7c, d). These results indicate that type I PRMT inhibition in combination with PARPi may be used to treat tumors that present resistance to PARPi through HR restoration (Fig. 2.7e).

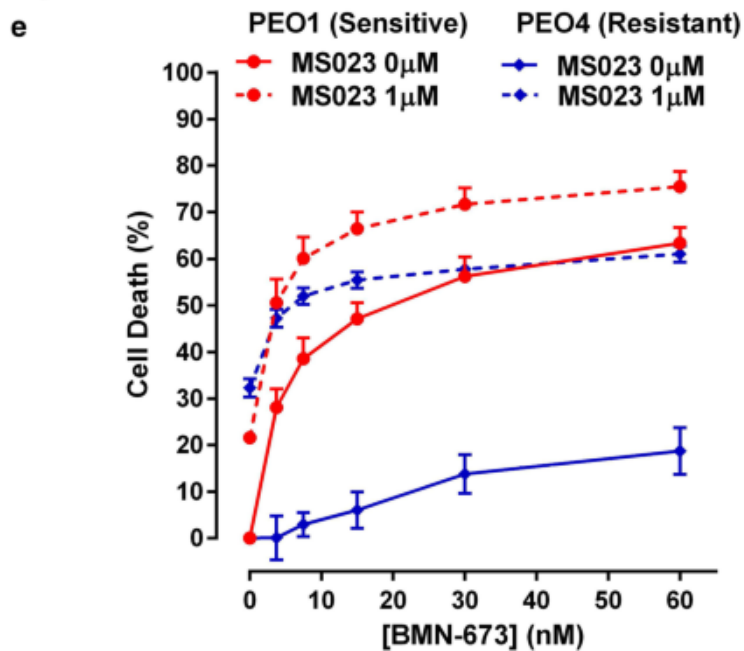
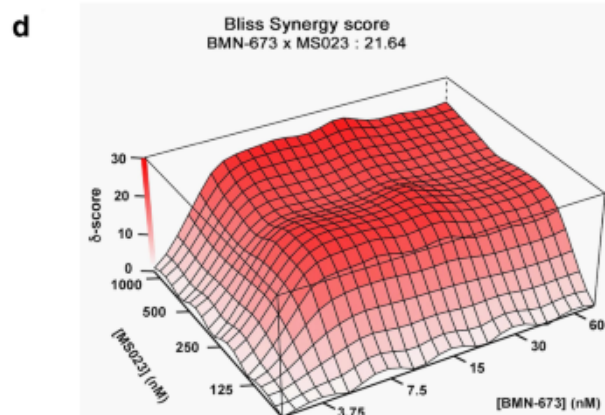
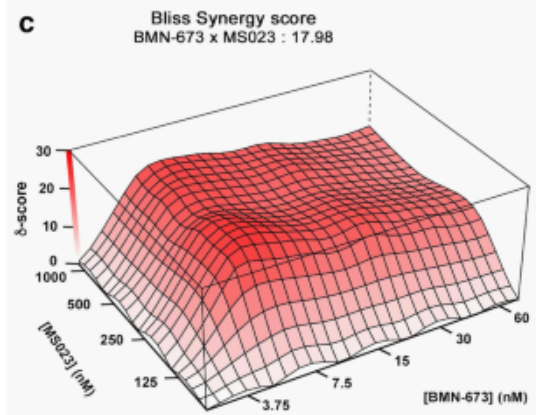
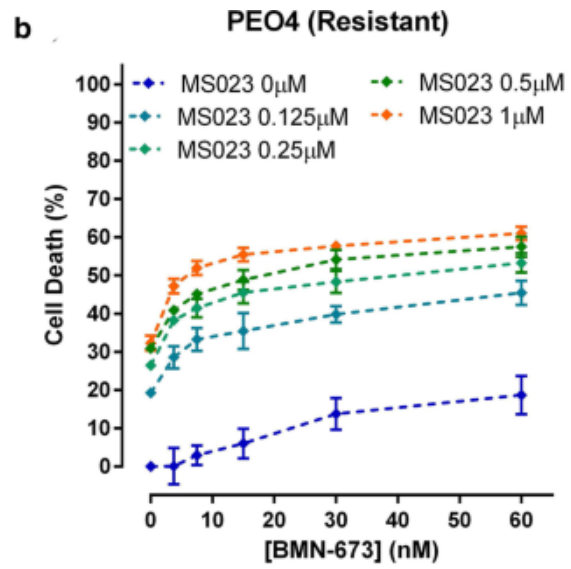
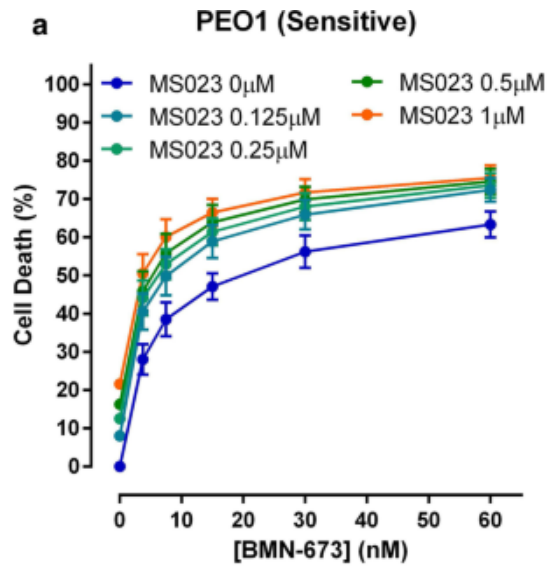


Figure 2.7. Treatment with MS023 renders PARPi-resistant PEO4 ovarian adenocarcinoma cells sensitive to BMN-673.

A,B Cell viability curves from PEO1 (a) and PEO4 (b) cells treated with a range of BMN-673 (3.75–60 nM) alone, or in combination with 0.125, 0.25, 0.5, or 1 μ M MS023. **C,D** The open-source R package SynergyFinder was used to visualize the dose–response of the combination of BMN-673 and MS023 in PEO1 (c) and PEO4 (d) cells and to calculate Bliss synergy scores. The Bliss synergy score is presented on the z-axis of the Bliss graph and is used to determine concentrations at which synergy occurs. **E** Cell viability curves from PEO1 (red) and PEO4 (blue) cells treated with a range of BMN-673 (3.75–60 nM) alone, or in combination with 1 μ M MS023

2.5 Discussion

In the present manuscript, we performed a chemical screen to identify epigenetic and anticancer drugs that synergize with a type I PRMT inhibitor, MS023. Homozygous deletion of the MTAP gene is frequently (~ 40%) seen in lung cancer patients (Schmid et al., 1998), and leads to elevated levels of MTA, a metabolite known to act as an endogenous inhibitor of PRMT5 activity (Kryukov et al., 2016; Marjon et al., 2016; Mavrakis et al., 2016). As such, MTAP-deficient cancer cells are inherently sensitive to inhibition of PRMT1 (Fedoriw et al., 2019; Fong and al., 2019; Gao et al., 2019). As resistance occurs frequently in NSCLCs, we aimed to identify additional compounds that could function in combination therapy with MS023 to significantly increase its cytotoxicity in the MTAP-negative A549 cell line. We identified several PARPi that had a strong synergy index with type I PRMT inhibition. We further examined the combination of MS023 and the PARP inhibitor BMN-673 (Talazoparib), and observed strong synergistic interaction at low nM concentrations in MTAP-negative A549, SK-LU-1 and HCC4006 NSCLC

cells. The re-introduction of MTAP decreased the sensitivity of the combination therapy in A549 cells. Importantly, PARP inhibitor sensitive and resistant cells (PEO1, PEO4) were both sensitive to the combination therapy of MS023 and BMN-673. These data suggest that type I PRMT inhibitors may have a wide therapeutic window targeting certain NSCLC and ovarian cancers in combination with PARP inhibitors.

PARPs are a family of enzymes with at least 18 members that catalyze the addition of poly(ADP-ribose) to various biological molecules. The most well-studied member of the PARP family, PARP1, plays an important role in DNA damage repair and is able to catalyze poly (ADP-ribose) chains (Caron et al., 2019; O'Sullivan et al., 2019). Inhibitors of PARP generate synthetic lethality in BRCA1- and BRCA2-mutant breast/ovarian cancer cells (Ashworth, 2008; Bryant et al., 2005; Farmer et al., 2005; Fong et al., 2009). Four PARP inhibitors have been approved by regulatory agencies, including Olaparib and Rucaparib in BRCA-mutated ovarian cancer; Niraparib in epithelial ovarian, fallopian tube and primary peritoneal cancer; and Talazoparib in BRCA-mutated breast cancer (Dréan et al., 2016; Lord and Ashworth, 2017). Importantly, several compounds are being pursued as promising combinatorial agents with PARPi in several types of cancers (Färkkilä et al., 2020; Konstantinopoulos et al., 2019; Lampert et al., 2020; Pulliam et al., 2018). Defining additional inhibitors that will work in combination with PARPi is paramount since resistance to PARPi single agent can occur through increased drug efflux, reactivation of homologous recombination, restoration of replication fork stability, or loss of DNA double-strand break resection inhibition (Ronato et al., 2020).

We now identify type I PRMT inhibitors as functioning to kill NSCLC. Type I PRMT inhibition or PRMT1 deficiency is known cause DNA damage with homologous recombination defects (Yu et al., 2009). Thus, it is likely that MS023 creates HR defects similar to what is

observed in BRCA-mutated cancers, thereby creating a vulnerability for PARPi. The combination of MS023 and PARP inhibitors can be used to ablate HR-proficient cancers. Indeed, PARP inhibitors have also been used in combination with other agents to treat HR-proficient cancers (Amin et al., 2015; Dréan et al., 2016; Ibrahim et al., 2012; Mo et al., 2016)

At sites of DNA damage, negatively charged PARylated proteins including PARP1 itself may recruit positively charged RGG/RG motif-containing methylated proteins. Arginine methylation plays a key role in the DNA damage response (DDR), and is known to occur at the RGG/RG motifs on several DDR proteins, including MRE11, 53BP1, and BRCA1 (Auclair and Richard, 2013; Guendel et al., 2010; Gurunathan et al., 2015; Vadnais et al., 2018; Yang et al., 2014). Therefore, arginine methylation of these proteins may affect their interactions with chains of PAR. Collectively, the combination of lack of arginine methylation and PARylation leads to DNA repair defects, causing synthetic lethality in MTAP-negative NSCLC.

2.6 Conclusions

As with any chemotherapy, the potential cytotoxicity of PARPi either alone or in combination with other agents needs to be considered. Importantly, we show that low concentrations of BMN-673 PARPi (0.3 nM) were sufficient to kill lung cancer cells in combination with MS023. As demonstrated in our present study, the PARP and PRMT combination may be useful for recombination (HR) repair-deficient and proficient cancers. Due to the redundancy of PRMT1 and PRMT5 pathways, we also demonstrated that PARPi were effective in combination with PRMT5 inhibitors. Indeed, PARPi have been shown to synergize with PRMT5 inhibitors (Hamard et al., 2018). In sum, our findings show that targeting PRMTs in combination with PARP inhibitors presents as a new therapy option for NSCLC cancers that are HR-proficient.

2.7 Materials and Methods

Cell culture and generation of stable cell lines

Lung carcinoma cells A549 (ATCC CCL-185), SK-LU-1 (ATCC HTB57) and HCC4006 (ATCC CRL-2871) were cultured in F12K, DEMEM and RPMI-1640 (GE Healthcare Life Sciences, Canada) respectively, supplemented with 10% of FBS (Wisent, Canada), and maintained in a humidified incubator with 5% CO₂ at 37 °C. Cells were regularly checked for mycoplasma infection and kept at low passages. Cell lines re-expressing MTAP were generated by infecting the MTAP-deficient cell lines A549, SK-LU-1 and HCC4006 with human MTAP lentivirus (pLoc-MTAP). The MTAP-infected cells were treated with 3 µg/ml blasticidin and single clones were selected. MTAP expression was confirmed by Western blot using anti-MTAP antibody (Cell Signaling Technology, 4158). As a control, the cells were also infected with lentiviral empty vector (pLoc) and a pool of blasticidin-resistant cells were selected. Ovarian adenocarcinoma cells PEO1 and PEO4 were a kind gift from Scott H. Kaufmann (Mayo Clinic). Cells were cultured in OSE (Wisent, Canada) supplemented with 10% of FBS (Wisent, Canada), and maintained in a humidified incubator with 5% CO₂ at 37 °C. For combination survival assays, PEO1 and PEO4 cells were seeded at 3,000 cells/well in flat bottom black 96-well plates (Corning). One day after plating, cells were treated with the indicated concentrations of MS023 (Cayman Chemical) and/or BMN-673 (SelleckChem, S7048), or an equivalent concentration of vehicle (DMSO, Sigma-Aldrich). Media containing inhibitors or DMSO were replenished every 48 h. Six days after the first treatment, Hoechst 33342 (Thermo Fischer Scientific, H3570) was added at a final concentration of 10 µg/ml and the plates were returned to the incubator for 30 min. The wells were imaged using a Cytation5 plate imager (BioTek) and the nuclei counted using Gen5 software. To

normalize the results, the number of nuclei in the inhibitor-treated wells was divided by the number of nuclei of the DMSO-treated wells.

Epigenetic drug screen and synergy index calculation

For screening purposes, A549 cells were seeded at 20 K cells/well in flat-bottom 96-well plates (Sarstedt). One day after, cells were treated with 16.5 μ M MS023 (Cayman Chemical) or an equivalent concentration of vehicle (DMSO, Sigma-Aldrich). The next day, 181 drugs from the SelleckChem epigenetic library (Epigenetics Compound Library (96-well)-Z203065-100 μ L1900) were added at 10 μ M for 24 h. Each plate contained controls to assess the individual effects of DMSO and MS023 on cells. On the third day, cell viability was measured using Viacount (Luminex, 4000-0040) on Guava flow cytometer (Millipore) as follows. Media was collected for each well and kept aside for later, cells were rinsed in 200 μ l PBS without calcium (Wisent) and incubated with 0.25% trypsin (Gibco) for 5 min at 37 °C. Media of each well was added to stop trypsinization and mixed thoroughly with Integra 96-well automated pipettor. One control well (DMSO) was heat-killed to obtain a total cell death control. Viacount solution (25 μ l) was added and mixed to each well, as suggested per manufacturer guidelines. After incubation (5 min at room temperature, in the dark), cell viability was analyzed on the Guava flow cytometer. The drug library was screened in monotherapy, as previously described. The Synergy Index (SI) is calculated as follows: $SI = (\text{Viability in monotherapy} \times \text{MS023 Viability effect}) / \text{Viability in combination}$. We also calculated a synergy/antagonism percentage value to associate a score to the combination as compared to monotherapy. The synergy/antagonism percentage is calculated as follows $(1 - (1/\text{Synergy Index})) * 100$.

Enrichment score was calculated to express relative effect of a drug class to other drug classes present in the library. Enrichment score is the ratio of its enrichment index and the global index of

the whole screen. To calculate the enrichment index, we created a frequency table of each drug response per group. The matrix is composed of 21 bins from -100 to 100, with a step of 10. Then, we calculate the representative percentage (weight) of each bin per group (bin weight = bin frequency / total number of compounds per group), to create 21 pairs per group. Finally, we sum up for each group the product of each (bin, weight) pairs. The global index is calculated the same way. The enrichment score corresponds to the ratio of each group index divided by the global index: a score > 1 shows an enrichment whereas a score < 1 shows the opposite.

MTT assay

A549, SK-LU-1 and HCC4006 stable cells infected with MTAP or empty lentiviral vectors were treated as described above with different dosage of inhibitors for 7 days. For treatment, the type I PRMT inhibitor MS023 was dissolved in DMSO to prepare a 3 mM stock solution, and cells were treated with a final concentration of 0.2–2 μM as indicated. The PARP1/2 inhibitor BMN-673 (SelleckChem, S7048) was also dissolved in DMSO to prepare a 3 mM stock solution, and cells were treated with a final concentration of 0.3–50 nM as indicated. For treatment, cells were seeded on day zero and inhibitors or DMSO were added after 16 h. Media and inhibitors or DMSO were replenished every 48 h. Cell viability was assessed using the MTT assay kit (Abcam, ab211091) according to manufacturer's instructions. Briefly, cells were grown in a 96-well plate and each treatment group was repeated in triplicate. On the 7th day, media was carefully aspirated and 100 μl of 1X MTT reagent was added to each well, and the plate was incubated for 3 h at 37 $^{\circ}\text{C}$. Following incubation, 150 μl of MTT solvent was added to each well and incubated at room temperature on an orbital shaker for 15 min prior to reading absorbance at OD = 590 nm. To normalize absorbance values, each value for the inhibitor-treated wells was divided by the absorbance of the DMSO-treated wells. Absorbance values are proportional to cell number, so

percent cell death was determined by subtracting the normalized values from 1. An evaluation of the drug combination effect was carried out using the Bliss Independence dose–response calculation (Ianevski et al., 2020; Liu et al., 2018).

Immunofluorescence

A549 cells were cultured on glass coverslips under the cell culture treatment conditions described above for the MTT assay. On day 7, coverslips were transferred to a solution of 4% paraformaldehyde in PBS and fixed for 15 min at room temperature. Cells were then permeabilized with 0.2% Triton X-100, 0.125 M glycine in PBS for 12 min at room temperature. Blocking followed for 1 h at room temperature with 2% BSA, 2% horse serum and 0.1% Triton X-100 in PBS. γ -H2AX foci were detected using anti-gamma H2A.X (Abcam, ab11174) diluted 1:1000 in blocking buffer and incubated at 4 °C for 16 h. Cells were washed three times with PBS for 10 min and incubated with secondary antibody (AlexaFluor anti-mouse 488 nm) diluted 1:400 for 45 min in the dark at room temperature. Cells were then washed three times for 10 min with PBS. Finally, coverslips were inverted and mounted onto a microscope slide with Immu-Mount (Fisher Scientific) and DAPI for counterstain. Slides were imaged on a Zeiss Axio Imager M1 microscope (Carl Zeiss, Thornwood NY), and resulting images were analyzed using Zeiss' ZEN Digital imaging suite software. A minimum of 200 cells per treatment condition were imaged, and cells with > 5 γ H2AX foci were quantified and divided by total number of cells as determined by DAPI counterstain.

Statistical analyses

Statistical significance was determined using GraphPad Prism version 6.0 software to perform unpaired t tests, where p values less than 0.05 were accepted as significant.

Availability of Data and Materials:

All data generated or analysed during this study are included in this published article and its supplementary information files.

Acknowledgements:

We thank Marielle Huot for generating the Bliss graphical representation.

Funding:

This work was funded by Canadian Institute of Health Research Grants: FDN-154303 to SR; NRF 173588 to NJ-MR, and FDN-388879 to JYM and by Charles-Bruneau Foundation. CD holds a Fonds de recherche du Québec en Santé studentship award. JYM is a Tier I Canada Research Chair in DNA repair and Cancer Therapeutics. NJ-MR holds a Junior 2 Research Scholar Award from the Fonds de recherche du Québec en Santé.

Author Information:

Segal Cancer Center, Lady Davis Institute for Medical Research and Gerald Bronfman Department of Oncology and Departments of Biochemistry, Human Genetics and Medicine, McGill University, Montréal, QC, H3T 1E2, Canada

Claudia Dominici, Zhenbao Yu & Stéphane Richard

Département de Pharmacologie et Physiologie, Université de Montréal, and Research Centre of the Sainte-Justine University Hospital, Montréal, QC, H3T 1C5, Canada

Nicolas Sgarioto & Noël J.-M. Raynal

Genome Stability Laboratory, CHU de Québec Research Center, Oncology Division, Department of Molecular Biology, Medical Biochemistry and Pathology, Laval University Cancer Research Center, 9 McMahan, Québec, QC, G1R 3S3, Canada

Laura Sesma-Sanz & Jean-Yves Masson

Contributions:

CD and ZY performed MTT assays and immunochemistry experiments, NS performed the drug screening and drug screening analysis. LSS performed the ovarian cell lines experiment. CD, LSS, ZY, NS, JYM, SR, and NJ-MR designed experiments, analyzed data and wrote the manuscript. All authors read and approved the final manuscript

Corresponding Authors:

Correspondence to Stéphane Richard or Noël J.-M. Raynal.

2.8 References

- Amin, O., Beauchamp, M.C., Nader, P.A., Laskov, I., Iqbal, S., Philip, C.A., Yasmeeen, A., and Gotlieb, W.H. (2015). Suppression of Homologous Recombination by insulin-like growth factor-1 inhibition sensitizes cancer cells to PARP inhibitors. *BMC cancer* *15*, 817.
- Ashworth, A. (2008). A synthetic lethal therapeutic approach: poly(ADP) ribose polymerase inhibitors for the treatment of cancers deficient in DNA double-strand break repair. *Journal of clinical oncology : official journal of the American Society of Clinical Oncology* *26*, 3785-3790.
- Auclair, Y., and Richard, S. (2013). The role of arginine methylation in the DNA damage response. *DNA repair* *12*, 459-465.
- Bedford, M.T., and Clarke, S.G. (2009). Protein arginine methylation in mammals: who, what, and why. *Molecular cell* *33*, 1-13.
- Boisvert, F.-M., Déry, U., Masson, J.-Y., and Richard, S. (2005). Arginine methylation of MRE11 by PRMT1 is required for DNA damage checkpoint control. *Genes & Dev* *19*, 671-676.
- Bryant, H.E., Schultz, N., Thomas, H.D., Parker, K.M., Flower, D., Lopez, E., Kyle, S., Meuth, M., Curtin, N.J., and Helleday, T. (2005). Specific killing of BRCA2-deficient tumours with inhibitors of poly(ADP-ribose) polymerase. *Nature* *434*, 913-917.
- Cameron, E.E., Bachman, K.E., Myohanen, S., Herman, J.G., and Baylin, S.B. (1999). Synergy of demethylation and histone deacetylase inhibition in the re-expression of genes silenced in cancer. *Nature genetics* *21*, 103-107.
- Caron, M.-C., Sharma, A.K., O'Sullivan, J., Myler, L.R., Ferreira, M.T., Rodrigue, A., Coulombe, Y., Ethier, C., Gagné, J.-P., Langelier, M.-F., *et al.* (2019). Poly(ADP-ribose) polymerase-1 antagonizes DNA resection at double-strand breaks. *Nature communications* *10*, 2954.
- Chan-Penebre, E., Kuplast, K.G., Majer, C.R., Boriack-Sjodin, P.A., Wigle, T.J., Johnston, L.D., and *et al.* (2015). A selective inhibitor of PRMT5 with in vivo and in vitro potency in MCL models. *Nature chemical biology* *11*, 432-437.
- Chen, D., Ma, H., Hong, H., Koh, S.S., Huang, S.M., Schurter, B.T., Aswad, D.W., and Stallcup, M.R. (1999). Regulation of transcription by a protein methyltransferase. *Science (New York, NY)* *284*, 2174-2177.
- Clarke, T.L., Sanchez-Bailon, M.P., Chiang, K., Reynolds, J.J., Herrero-Ruiz, J., Bandejas, T.M., Matias, P.M., Maslen, S.L., Skehel, J.M., Stewart, G.S., *et al.* (2017). PRMT5-Dependent

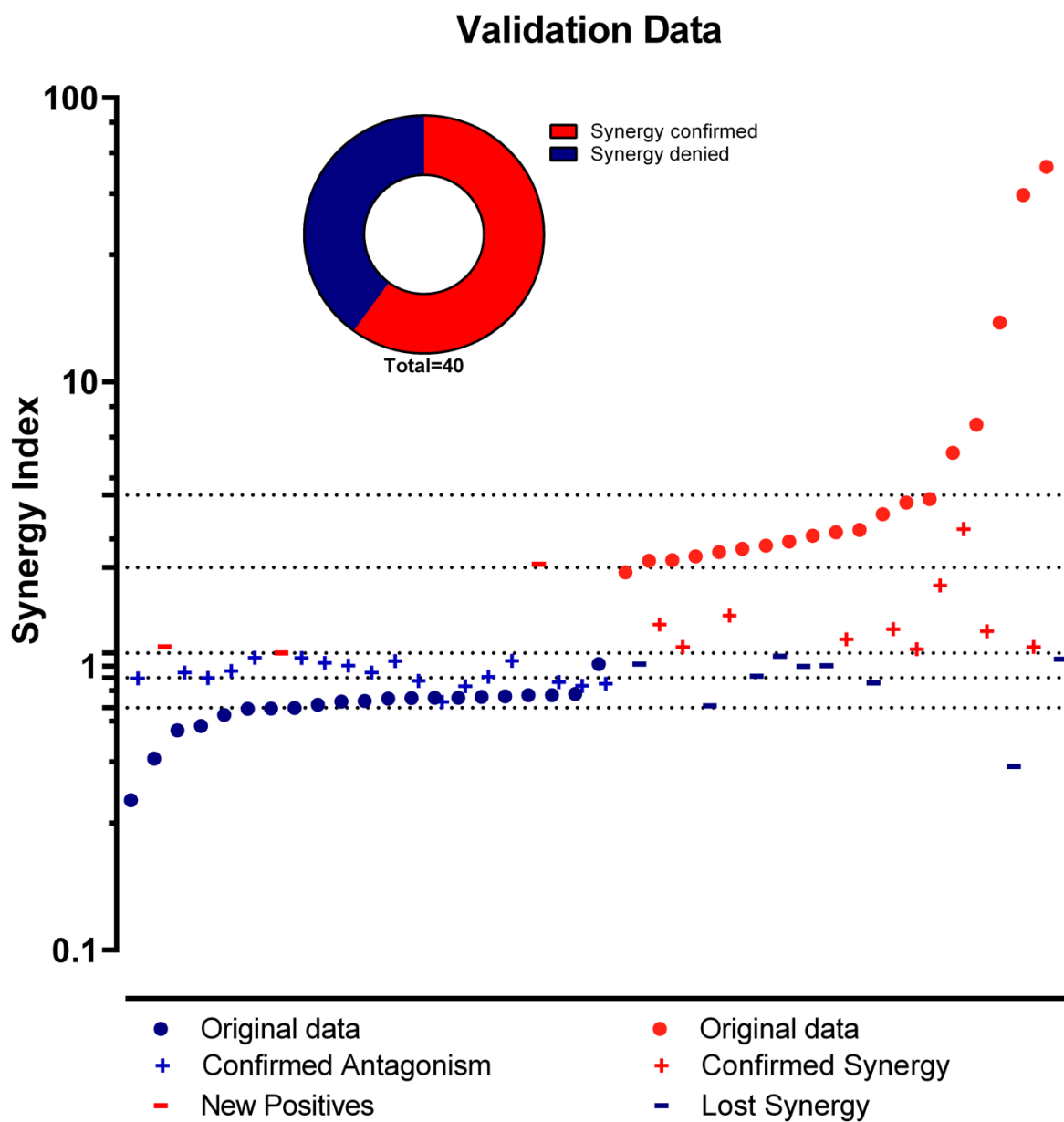
- Methylation of the TIP60 Coactivator RUVBL1 Is a Key Regulator of Homologous Recombination. *Molecular cell* 65, 900-916.
- Dhar, S., Vemulapalli, V., Patananan, A.N., Huang, G.L., Di Lorenzo, A., Richard, S., Comb, M.J., Guo, A., Clarke, S.G., and Bedford, M.T. (2013). Loss of the major Type I arginine methyltransferase PRMT1 causes substrate scavenging by other PRMTs. *Scientific reports* 3, 1311.
- Ding, L., Getz, G., Wheeler, D.A., Mardis, E.R., McLellan, M.D., Cibulskis, K., Sougnez, C., Greulich, H., Muzny, D.M., Morgan, M.B., *et al.* (2008). Somatic mutations affect key pathways in lung adenocarcinoma. *Nature* 455, 1069-1075.
- Dréan, A., Lord, C.J., and Ashworth, A. (2016). PARP inhibitor combination therapy. *Critical reviews in oncology/hematology* 108, 73-85.
- Eram, M.S., Shen, Y., Szewczyk, M., Wu, H., Senisterra, G., Li, F., Butler, K.V., Kaniskan, H.U., Speed, B.A., Dela Sena, C., *et al.* (2016). A Potent, Selective, and Cell-Active Inhibitor of Human Type I Protein Arginine Methyltransferases. *ACS chemical biology* 11, 772-781.
- Färkkilä, A., Gulhan, D.C., Casado, J., Jacobson, C.A., Nguyen, H., Kochupurakkal, B., Maliga, Z., Yapp, C., Chen, Y.A., Schapiro, D., *et al.* (2020). Immunogenomic profiling determines responses to combined PARP and PD-1 inhibition in ovarian cancer. *Nature communications* 11, 1459.
- Farmer, H., McCabe, N., Lord, C.J., Tutt, A.N., Johnson, D.A., Richardson, T.B., Santarosa, M., Dillon, K.J., Hickson, I., Knights, C., *et al.* (2005). Targeting the DNA repair defect in BRCA mutant cells as a therapeutic strategy. *Nature* 434, 917-921.
- Fedoriw, A., Rajapurkar, S.R., O'Brien, S., Gerhart, S.V., Mitchell, L.H., Adams, N.D., Rioux, N., Lingaraj, T., Ribich, S.A., Pappalardi, M.B., *et al.* (2019). Anti-tumor Activity of the Type I PRMT Inhibitor, GSK3368715, Synergizes with PRMT5 Inhibition through MTAP Loss. *Cancer cell*.
- Feng, Y., Maity, R., Whitelegge, J.P., Hadjikyriacou, A., Li, Z., Zurita-Lopez, C., Al-Hadid, Q., Clark, A.T., Bedford, M.T., Masson, J.Y., *et al.* (2013). Mammalian protein arginine methyltransferase 7 (PRMT7) specifically targets RXR sites in lysine- and arginine-rich regions. 288, 37010-37025.
- Fong, J.Y., and al., e. (2019). Therapeutic targeting of RNA splicing catalysis through inhibition of protein arginine methylation. *Cancer cell* 36, 194-209.
- Fong, J.Y., Pignata, L., Goy, P.A., Kawabata, K.C., Lee, S.C., Koh, C.M., Musiani, D., Massignani, E., Kotini, A.G., Penson, A., *et al.* (2019). Therapeutic Targeting of RNA Splicing Catalysis through Inhibition of Protein Arginine Methylation. *Cancer cell* 36, 194-209.e199.
- Fong, P.C., Boss, D.S., Yap, T.A., Tutt, A., Wu, P., Mergui-Roelvink, M., Mortimer, P., Swaisland, H., Lau, A., O'Connor, M.J., *et al.* (2009). Inhibition of poly(ADP-ribose) polymerase in tumors from BRCA mutation carriers. *The New England journal of medicine* 361, 123-134.
- Gao, G., Zhang, L., Villarreal, O.D., He, W., Su, D., Bedford, E., Moh, P., Shen, J., Shi, X., Bedford, M.T., *et al.* (2019). PRMT1 loss sensitizes cells to PRMT5 inhibition. *Nucleic acids research*.
- Gao, Y., Zhao, Y., Zhang, J., Lu, Y., Liu, X., Geng, P., Huang, B., Zhang, Y., and Lu, J. (2016). The dual function of PRMT1 in modulating epithelial-mesenchymal transition and cellular senescence in breast cancer cells through regulation of ZEB1. *Scientific reports* 6, 19874.
- Guccione, E., and Richard, S. (2019). The regulation, functions and clinical relevance of arginine methylation. *Nature reviews Molecular cell biology* 20, 642-657.

- Guendel, I., Carpio, L., Pedati, C., Schwartz, A., Teal, C., Kashanchi, F., and Kehn-Hall, K. (2010). Methylation of the tumor suppressor protein, BRCA1, influences its transcriptional cofactor function. *PloS one* *5*, e11379.
- Gurunathan, G., Yu, Z., Coulombe, Y., Masson, J.Y., and Richard, S. (2015). Arginine methylation of hnRNPUL1 regulates interaction with NBS1 and recruitment to sites of DNA damage. *Scientific reports* *5*, 10475.
- Hamard, P.-J., Santiago, G.E., Liu, F., Karl, D.L., Martinez, C., Man, N., Mookhtiar, A.K., Duffort, S., Greenblatt, S., Verdun, R.E., *et al.* (2018). PRMT5 Regulates DNA Repair by Controlling the Alternative Splicing of Histone-Modifying Enzymes. *Cell reports* *24*, 2643-2657.
- Herbst, R.S., Morgensztern, D., and Boshoff, C. (2018). The biology and management of non-small cell lung cancer. *Nature* *553*, 446-454.
- Hopkins, T.A., Shi, Y., Rodriguez, L.E., Solomon, L.R., Donawho, C.K., DiGiammarino, E.L., Panchal, S.C., Wilsbacher, J.L., Gao, W., Olson, A.M., *et al.* (2015). Mechanistic Dissection of PARP1 Trapping and the Impact on In Vivo Tolerability and Efficacy of PARP Inhibitors. *Molecular cancer research : MCR* *13*, 1465-1477.
- Hoy, S.M. (2018). Talazoparib: First Global Approval. *Drugs* *78*, 1939-1946.
- Huang, Y., Vasilatos, S.N., Boric, L., Shaw, P.G., and Davidson, N.E. (2012). Inhibitors of histone demethylation and histone deacetylation cooperate in regulating gene expression and inhibiting growth in human breast cancer cells. *Breast cancer research and treatment* *131*, 777-789.
- Ianevski, A., Giri, A.K., and Aittokallio, T. (2020). SynergyFinder 2.0: visual analytics of multi-drug combination synergies. *Nucleic acids research*.
- Ibrahim, Y.H., García-García, C., Serra, V., He, L., Torres-Lockhart, K., Prat, A., Anton, P., Cozar, P., Guzmán, M., Grueso, J., *et al.* (2012). PI3K inhibition impairs BRCA1/2 expression and sensitizes BRCA-proficient triple-negative breast cancer to PARP inhibition. *Cancer discovery* *2*, 1036-1047.
- Juergens, R.A., Wrangle, J., Vendetti, F.P., Murphy, S.C., Zhao, M., Coleman, B., Sebree, R., Rodgers, K., Hooker, C.M., Franco, N., *et al.* (2011). Combination epigenetic therapy has efficacy in patients with refractory advanced non-small cell lung cancer. *Cancer discovery* *1*, 598-607.
- Konstantinopoulos, P.A., Barry, W.T., Birrer, M., Westin, S.N., Cadoo, K.A., Shapiro, G.I., Mayer, E.L., O'Ceirbhail, R.E., Coleman, R.L., Kochupurakkal, B., *et al.* (2019). Olaparib and α -specific PI3K inhibitor alpelisib for patients with epithelial ovarian cancer: a dose-escalation and dose-expansion phase 1b trial. *The Lancet Oncology* *20*, 570-580.
- Kryukov, G.V., Wilson, F.H., Ruth, J.R., Paulk, J., Tsherniak, A., Marlow, S.E., Vazquez, F., Weir, B.A., Fitzgerald, M.E., Tanaka, M., *et al.* (2016). MTAP deletion confers enhanced dependency on the PRMT5 arginine methyltransferase in cancer cells. *Science (New York, NY)* *351*, 1214-1218.
- Lampert, E.J., Zimmer, A.S., Padget, M.R., Cimino-Mathews, A., Nair, J.R., Liu, Y., Swisher, E.M., Hodge, J.W., Nixon, A.B., Nichols, E., *et al.* (2020). Combination of PARP inhibitor olaparib, and PD-L1 inhibitor durvalumab, in recurrent ovarian cancer: a proof-of-concept phase 2 study. *Clinical cancer research : an official journal of the American Association for Cancer Research*.
- Liu, Q., Yin, X., Languino, L.R., and Altieri, D.C. (2018). Evaluation of drug combination effect using a Bliss independence dose-response surface model. *Stat Biopharm Res* *10*, 112-122.

- Lord, C.J., and Ashworth, A. (2017). PARP inhibitors: Synthetic lethality in the clinic. *Science* (New York, NY) *355*, 1152-1158.
- Marjon, K., Cameron, M.J., Quang, P., Clasquin, M.F., Mandley, E., Kunii, K., McVay, M., Choe, S., Kernytsky, A., Gross, S., *et al.* (2016). MTAP Deletions in Cancer Create Vulnerability to Targeting of the MAT2A/PRMT5/RIOK1 Axis. *Cell reports* *15*, 574-587.
- Mavrakis, K.J., McDonald, E.R., 3rd, Schlabach, M.R., Billy, E., Hoffman, G.R., deWeck, A., Ruddy, D.A., Venkatesan, K., Yu, J., McAllister, G., *et al.* (2016). Disordered methionine metabolism in MTAP/CDKN2A-deleted cancers leads to dependence on PRMT5. *Science* (New York, NY) *351*, 1208-1213.
- Mo, W., Liu, Q., Lin, C.C., Dai, H., Peng, Y., Liang, Y., Peng, G., Meric-Bernstam, F., Mills, G.B., Li, K., *et al.* (2016). mTOR Inhibitors Suppress Homologous Recombination Repair and Synergize with PARP Inhibitors via Regulating SUV39H1 in BRCA-Proficient Triple-Negative Breast Cancer. *Clinical cancer research : an official journal of the American Association for Cancer Research* *22*, 1699-1712.
- Molina, J.R., Yang, P., Cassivi, S.D., Schild, S.E., and Adjei, A.A. (2008). Non-small cell lung cancer: epidemiology, risk factors, treatment, and survivorship. *Mayo Clinic proceedings* *83*, 584-594.
- Nakayama, K., Szewczyk, M.M., Dela Sena, C., Wu, H., Dong, A., Zeng, H., Li, F., de Freitas, R.F., Eram, M.S., Schapira, M., *et al.* (2018). TP-064, a potent and selective small molecule inhibitor of PRMT4 for multiple myeloma. *Oncotarget* *9*, 18480-18493.
- O'Sullivan, J., Tedim Ferreira, M., Gagné, J.P., Sharma, A.K., Hendzel, M.J., Masson, J.Y., and Poirier, G.G. (2019). Emerging roles of eraser enzymes in the dynamic control of protein ADP-ribosylation. *Nature communications* *10*, 1182.
- Pulliam, N., Fang, F., Ozes, A.R., Tang, J., Adewuyi, A., Keer, H., Lyons, J., Baylin, S.B., Matei, D., Nakshatri, H., *et al.* (2018). An Effective Epigenetic-PARP Inhibitor Combination Therapy for Breast and Ovarian Cancers Independent of BRCA Mutations. *Clinical cancer research : an official journal of the American Association for Cancer Research* *24*, 3163-3175.
- Ronato, D.A., Mersaoui, S.Y., Busatto, F.F., Affar, E.B., Richard, S., and Masson, J.Y. (2020). Limiting the DNA Double-Strand Break Resectosome for Genome Protection. *Trends in biochemical sciences*.
- Schiffmann, I., Greve, G., Jung, M., and Lübbert, M. (2016). Epigenetic therapy approaches in non-small cell lung cancer: Update and perspectives. *Epigenetics* *11*, 858-870.
- Schmid, M., Malicki, D., Nobori, T., Rosenbach, M.D., Campbell, K., Carson, D.A., and Carrera, C.J. (1998). Homozygous deletions of methylthioadenosine phosphorylase (MTAP) are more frequent than p16INK4A (CDKN2) homozygous deletions in primary non-small cell lung cancers (NSCLC). *Oncogene* *17*, 2669-2675.
- Shi, Y.X., Sheng, D.Q., Cheng, L., and Song, X.Y. (2019). Current Landscape of Epigenetics in Lung Cancer: Focus on the Mechanism and Application. *Journal of oncology* *2019*, 8107318.
- Siegel, R.L., Miller, K.D., and Jemal, A. (2018). Cancer statistics, 2018. *CA: a cancer journal for clinicians* *68*, 7-30.
- Szewczyk, M.M., Ishikawa, Y., Organ, S., Sakai, N., Li, F., Halabelian, L., Ackloo, S., Couzens, A.L., Eram, M., Dilworth, D., *et al.* (2020). Pharmacological inhibition of PRMT7 links arginine monomethylation to the cellular stress response. *Nature communications* *11*, 2396.
- Vadnais, C., Chen, R., Fraszczak, J., Yu, Z., Boulais, J., Pinder, J., Frank, D., Khandanpour, C., Hebert, J., Dellaire, G., *et al.* (2018). GFI1 facilitates efficient DNA repair by regulating PRMT1 dependent methylation of MRE11 and 53BP1. *Nature communications* *9*, 1418.

- Vansteenkiste, J., Crinò, L., Doms, C., Douillard, J.Y., Faivre-Finn, C., Lim, E., Rocco, G., Senan, S., Van Schil, P., Veronesi, G., *et al.* (2014). 2nd ESMO Consensus Conference on Lung Cancer: early-stage non-small-cell lung cancer consensus on diagnosis, treatment and follow-up. *Annals of oncology : official journal of the European Society for Medical Oncology* 25, 1462-1474.
- Vansteenkiste, J., Van Cutsem, E., Dumez, H., Chen, C., Ricker, J.L., Randolph, S.S., and Schöffski, P. (2008). Early phase II trial of oral vorinostat in relapsed or refractory breast, colorectal, or non-small cell lung cancer. *Investigational new drugs* 26, 483-488.
- Wang, H., Huang, Z.-Q., Xia, L., Feng, Q., Erdjument-Bromage, H., Strahl, B.D., Briggs, S.D., Allis, C.D., Wong, J., Tempst, P., *et al.* (2001). Methylation of histone H4 at arginine 3 facilitates transcriptional activation by nuclear hormone receptor. *Science (New York, NY)* 293, 853-857.
- Wolf, C.R., Hayward, I.P., Lawrie, S.S., Buckton, K., McIntyre, M.A., Adams, D.J., Lewis, A.D., Scott, A.R., and Smyth, J.F. (1987). Cellular heterogeneity and drug resistance in two ovarian adenocarcinoma cell lines derived from a single patient. *Int J Cancer* 39, 695-702.
- Yang, J.H., Chiou, Y.Y., Fu, S.L., Shih, I.Y., Weng, T.H., Lin, W.J., and Lin, C.H. (2014). Arginine methylation of hnRNPK negatively modulates apoptosis upon DNA damage through local regulation of phosphorylation. *Nucleic acids research* 42, 9908-9924.
- Yu, Z., Chen, T., Hebert, J., Li, E., and Richard, S. (2009). A mouse PRMT1 null allele defines an essential role for arginine methylation in genome maintenance and cell proliferation. *Molecular and cellular biology* 29, 2982-2996.

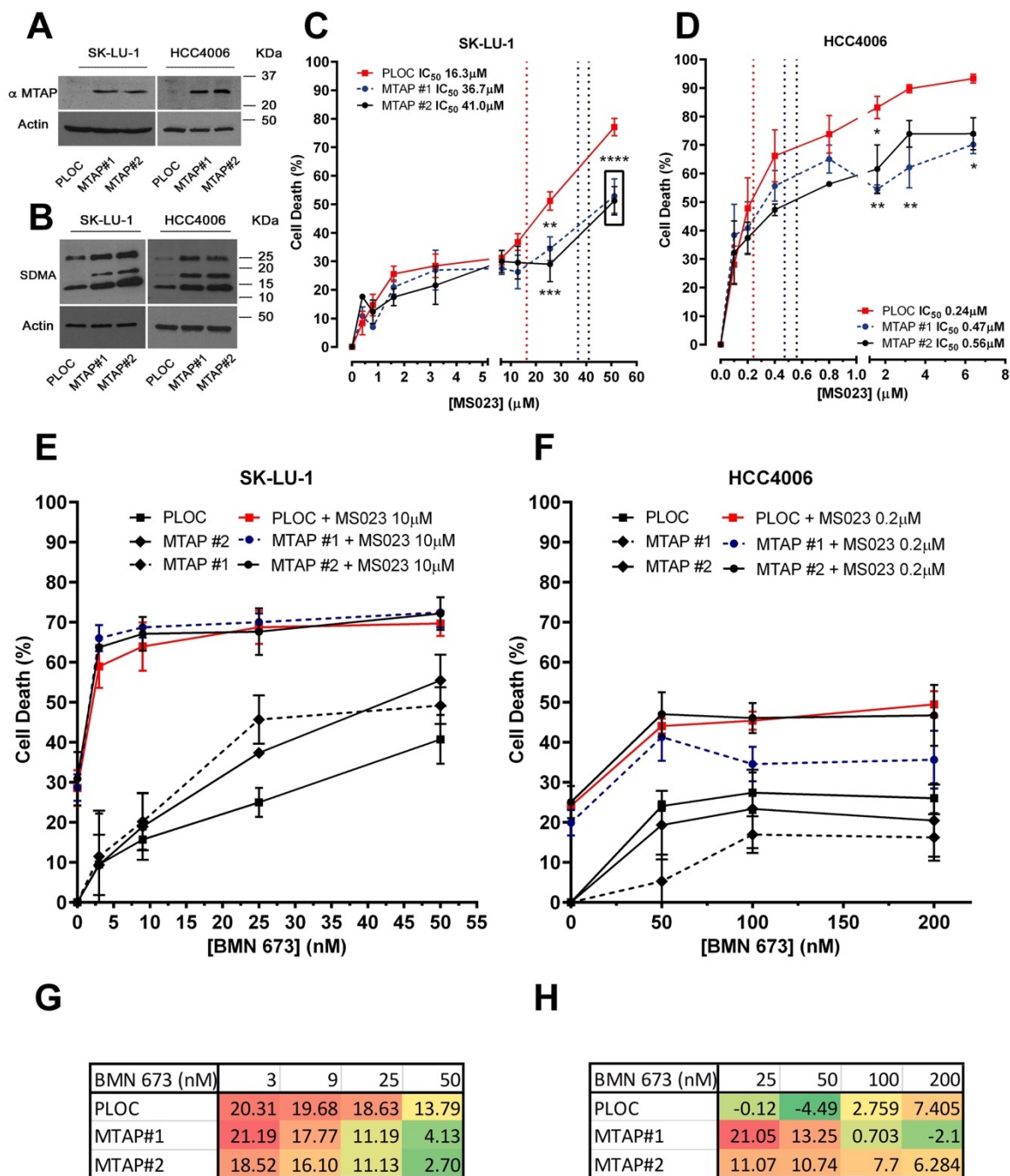
2.9 Supplemental information



Supplemental figure S2.1. Validation of the drug screen.

Graphic showing original data from the screen (plain circle) highest (20) and lowest (20) hits. Results from the validation are labelled with (+) if validation was confirmed or (-) if validation

failed. Pie chart summarizes result of validation process; 28 of 40 compounds matched the primary output, leading to a validation rate for the screen of 70%.



Supplemental figure S2.2. MS023 and BMN-673 synergy dependency on MTAP in NSCLC cell lines.

A Immunoblotting of SK-LU-1 and HCC4006 cell lines infected with the empty lentivector (pLoc) or pLoc-MTAP. Clones #1 and #2 show the re-expression of MTAP using anti-MTAP antibodies. Antibodies against β -actin were used to show equivalent loading. The molecular mass markers are shown in kDa. **B** Same as panel A except the cellular lysates were immunoblotted with anti-SDMA and β -actin antibodies as indicated. **C-D** Cell death curves as determined by MTT assay of the SK-LU-1 and HCC4006 clones treated with a range of MS023 concentrations. Dotted vertical lines represent IC50 values for each cell line (SK-LU-1: n=5; HCC4006: n=4). Stars (*: p < 0.05; **: p < 0.01; ***: p < 0.001, ****: p < 0.0001; two-way ANOVA). **E-F** Cell death curves as determined by MTT assay of the SK-LU-1 and HCC4006 clones treated with a range of BMN-673 in combination 10 μ M MS023 (SK-LU-1, n=4) or 0.2 μ M MS023 (HCC4006, n=6). **G-H** Bliss synergy scores calculated for BMN-673 and MS023 combination treatment in SK-LU-1 and HCC4006 cells, respectively.

Chapter 3: Inhibition of Type I PRMTs Reforms Muscle Stem Cell Identity via Ampk activation, Enhancing their Therapeutic Capacity

Claudia Dominici^{1,4}, Oscar Villareal¹, Junio Dort⁶, Yu Chang Wang⁷, Emilie Heckel⁶, Jiannis Ragoussis⁷, Jean-Sebastien Joyal⁶, Nicolas Dumont⁶, Stéphane Richard^{1,2,3,4,5*}

¹Segal Cancer Center, Lady Davis Institute for Medical Research and ²Gerald Bronfman Department of Oncology and Departments of ³Medicine, ⁴Human Genetics and ⁵Biochemistry, McGill University, Montréal, Québec, Canada H3T 1E2

⁶Sainte-Justine University Hospital Research Center, Montréal University, Montréal, Québec, Canada H3T 1C5

⁷Genome Quebec Innovation Centre, Montreal, Quebec, Canada.

*Corresponding author: stephane.richard@mcgill.ca

3.1 Preface

Purified and *ex vivo* cultured MuSCs spontaneously differentiate in culture, creating a substantial barrier to the understanding of what mechanisms maintain their stemness, as well as impeding re-engraftment therapies for muscle wasting diseases. In the present study, Dominici et al characterize the effect of the type I PRMT inhibitor, MS023, on MuSCs. Treatment with MS023 achieves and maintains a stem-like state as indicated by transcriptional and metabolic profiling, thereby identifying MS023 as a promising inhibitor for muscle wasting disease.

3.2 Abstract

In skeletal muscle, muscle stem cells (MuSC) are the main cells responsible for regeneration upon injury. In diseased skeletal muscle, it would be therapeutically advantageous to replace defective MuSCs, or rejuvenate them with drugs to enhance their self-renewal and ensure long-term regenerative potential. One limitation of the replacement approach has been the inability to efficiently expand MuSCs *ex vivo*, while maintaining their stemness and engraftment abilities. Herein, we show that inhibition of type I protein arginine methyltransferases (PRMTs) with MS023 increases the proliferative capacity of *ex vivo* cultured MuSCs. Single cell RNA sequencing (scRNAseq) of *ex vivo* cultured MuSCs revealed the emergence of novel subpopulations in MS023-treated cells which are defined by elevated PAX7 expression and markers of MuSC quiescence - both features of enhanced self-renewal. Furthermore, the scRNAseq identified MS023-specific subpopulations to be metabolically reprogrammed with upregulated glycolysis and oxidative phosphorylation (OxPhos). We identify AMP kinase (Ampk) to be activated in MS023 cells, and depletion of Ampk by siRNA reversed the proliferative phenotype of MS023-treated MuSCs. Transplantation of MuSCs treated with MS023 had a better ability to repopulate the MuSC niche and contributed more robustly to muscle regeneration following injury. Interestingly, the preclinical mouse model of Duchenne muscular dystrophy had increased bilateral grip strength 10 days after a single intraperitoneal dose of MS023. These findings suggest that type I PRMT inhibition metabolically reprograms MuSCs resulting in improved self-renewal and muscle regeneration fitness.

3.3 Introduction

Skeletal muscle is a dynamic tissue that can regenerate following injury. Muscle stem cells (MuSCs) reside on the periphery of muscle fibers in skeletal muscle, and are activated following injury to drive muscle regeneration (Lepper et al., 2011; Relaix and Zammit, 2012). Major challenges arise when attempting to manipulate MuSCs *ex vivo*. Purified MuSCs spontaneously differentiate upon *ex vivo* expansion (Fu et al., 2015a; Sacco et al., 2008), limiting the potential of CRISPR-based applications and stem cell engraftment therapy. Cell-intrinsic defects in patients with Duchenne muscular dystrophy (DMD) prevent MuSCs from maintaining a proper balance between stem cell self-renewal and differentiation, ultimately leading to depletion of regeneration-competent MuSCs (**Bentzinger et al., 2014; Dumont et al., 2015b; Wang et al., 2013**).

MuSCs have metabolic flexibility that allows them to adapt to demands presented by their changing environments (Relaix et al., 2021). Indeed, metabolic signatures are strong contributors to the heterogeneity observed in isolated MuSCs (Cho and Doles, 2017).

Several emerging findings have indicated that the metabolic state of the MuSC is inextricably tied to its function and fate. Quiescent MuSCs predominantly rely on fatty acid oxidation (FAO) and oxidative phosphorylation (OxPhos) (Machado et al., 2017). Interestingly, Ryall and colleagues showed that increased cellular levels of NAD⁺ generated by oxidative metabolism in quiescent MuSCs activated the deacetylase activity of Sirtuin 1 (SIRT1), which in turn repressed differentiation genes required for the myogenic program. Deletion of SIRT1 in MuSCs *in vivo* resulted in deregulation of their myogenic fate and reduced muscle fiber size (Ryall et al., 2015).

While glycolysis remains very low in quiescent cells, it is upregulated as MuSCs begin to proliferate following activation, representing a metabolic shift in activated MuSCs (L'Honoré et

al., 2018; Ryall et al., 2015). Interestingly, retaining mitochondrial OxPhos in proliferating MuSCs by genetically deleting p107, a repressor of mitochondrial gene expression, enhances their proliferative rate (Bhattacharya et al., 2021).

It has been repeatedly shown that *ex vivo* cultured MuSCs are vastly inferior at engrafting and contributing to muscle regeneration when compared to freshly isolated MuSCs, indicating the importance of retaining stemness for MuSC engraftment and muscle regeneration (Montarras et al., 2005; Sakai et al., 2017). The dynamic regulation of metabolic state during the transition from MuSC quiescence to proliferation therefore presents a unique avenue to regulate MuSC regenerative capacity.

Arginine methylation is a regulator of MuSC proliferation and function, and is carried out by protein arginine methyltransferases (PRMTs) (Xu and Richard, 2021). The PRMT family comprises of nine members which are classed according to their catalytic activity: type I enzymes (ex: PRMT1) catalyze arginine asymmetrical dimethylation (ADMA), type II enzymes (ex: PRMT5) catalyze arginine symmetrical dimethylation (SDMA), and the unique type III enzyme PRMT7 catalyzes arginine monomethylation (MMA) (Bedford and Clarke, 2009).

It was shown that PRMT1 in MuSCs functions through the activation of MyoD expression in committed progenitors by methylating the SIX1/4 coactivator, EYA1 (Blanc et al., 2017). PRMT1 deficient MuSCs are highly proliferative and can be expanded in culture. However, these MuSCs are unable to terminate differentiation, leading to a severe muscle regeneration defect *in vivo* following muscle injury (Blanc et al., 2017). Moreover, it was shown that PRMT5 regulates MuSC proliferation by epigenetically downregulating expression of the cell cycle inhibitor p21 (Zhang et al., 2015). Deletion of PRMT5 in MuSCs blocked their expansion *ex vivo* and caused defects in muscle regeneration *in vivo*. PRMT7 also functions in the myogenic process and is

required for MuSC self-renewal and muscle regeneration (Blanc et al., 2016). Deletion of PRMT7 in MuSCs caused persistent p21 expression, leading to cellular senescence and failure to regenerate muscle.

Interestingly, there is growing evidence to suggest a role for PRMTs in cellular metabolism. Knockdown of PRMT5 was shown to activate the Lkb1/Ampk/mTOR pathway in esophageal squamous cell carcinoma (Chen et al., 2021b). PRMT5 was also shown to directly methylate protein kinase B (also called Akt) to regulate its kinase activity (Yin et al., 2021).

Given the importance of the metabolic state in maintaining MuSC stemness and the enhanced MuSC proliferation observed with PRMT1 deficiency, we aimed to determine whether small molecule inhibition of type I PRMTs would affect cellular metabolism and fulfil the requirements of generating a stem-like MuSC in culture with subsequent regenerative capabilities. Small molecule inhibitors of epigenetic regulators are a promising avenue to pursue in the treatment of muscle wasting diseases, as several inhibitors have already been identified which enhance MuSC self-renewal. Namely, an inhibitor of eIF2 α dephosphorylation (Zismanov et al., 2016), and an inhibitor of Setd7-mediated lysine methylation (Judson et al., 2018), were shown to have beneficial effects.

Herein, we show that MS023, an inhibitor of type I PRMTs, fulfils the requirements of a reversible inhibitor which maintains the stemness of cultured MuSCs, while allowing for engraftment and regenerative capabilities.

3.4 Results

Type I PRMT inhibitor MS023 enhances self-renewal and *in vitro* expansion of MuSCs

We isolated whole muscle fibers from 6 to 8 week old C57BL/6 wild type mice and stained them for the myogenic transcription factor PAX7 (Seale et al., 2000; Soleimani et al., 2012), and the proliferation marker ki67. The number of PAX7/ki67 double-positive cells increased significantly in the presence of MS023 for 48 h (Figure 3.1A, 3.1B). We observed a significant increase in the number of clusters with 3 or more cells with MS023 treatment (Figure 3.1B). These data show that type I PRMT inhibition causes *in vitro* MuSC expansion. To determine the activation state of these fiber-associated MuSCs, we examined fibers after 48 h in culture for the expression of PAX7 and the myogenic regulator transcription factor, MyoD (Rudnicki et al., 1993; Troy et al., 2012). Interestingly, MS023 treatment restricted the proportion of committed PAX7^{neg}/MyoD^{pos} cells, while expanding the proportion of activated and cycling cells (PAX7^{pos}/MyoD^{pos}, Figure 3.1C, D).

MuSCs spontaneously differentiate into non-cycling myoblasts and lose their stemness *in vitro* (Montarras et al., 2005; Ryall et al., 2015; Sacco et al., 2008). The enhanced proliferation of MuSCs observed with type I PRMT inhibition on muscle fibers prompted us to examine whether similar effects could be achieved with FACS-purified MuSCs cultured *in vitro*. MuSCs incubated with MS023 for 48 h had reduced aDMA containing proteins, as visualized by immunoblotting (Supplemental Figure S3.1A), and had increased proliferative capacity of MuSCs, as determined by ki67 immunofluorescence (Supplemental Figure S3.1B) and by FACS analysis of ki67-PE intracellularly-stained MuSCs (Supplemental Figure S3.1C). These data are consistent with what was observed in muscle fiber-associated MuSCs (Figure 3.1A-C). Importantly, immunofluorescence analysis of myogenic markers in cultured MuSCs revealed that MS023 treatment prevented initiation of differentiation, as indicated by the significantly reduced sub-population of committed PAX7^{neg}/MyoD^{pos} cells compared to control DMSO culture (13% versus

31%, respectively) (Figure 3.1E, F). Additionally, there was an increase in the proportion of cells that have retained their stemness by delaying expression of MyoD (PAX7^{pos}/MyoD^{neg}) in the MS023-treated samples compared to DMSO (40% versus 9%, Figure 3.1E, F). Similar proportions were observed with fiber-associated MuSCs (34% versus 14%, Figure 3.1C, D). Furthermore, we observed that the impediment of precocious differentiation afforded by treatment with MS023 led to enhanced long-term culture capabilities of MuSCs up to the 14th passage (Supplemental Figure S3.1D). Altogether, these findings indicate that treatment with MS023 maintained cultured MuSCs in a stem-like state.

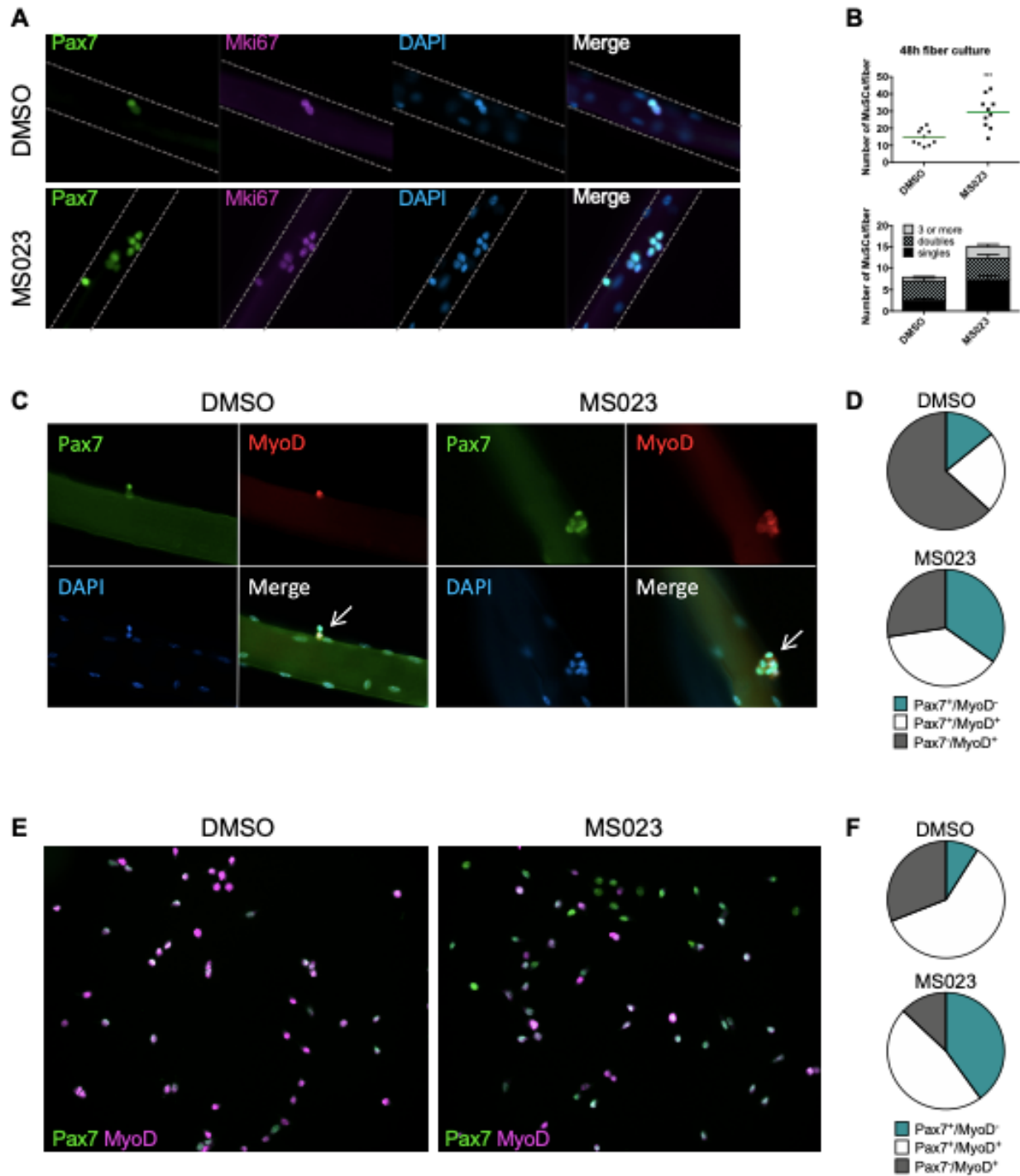


Figure 3.1. Enhanced self-renewal of MS023-treated MuSCs

(A) Muscle fibers cultured for 48h with MS023 or DMSO. PAX7 identifies MuSCs, and ki67 identifies proliferating cells. (B) Quantification of total MuSCs per fiber. 30 fibers were counted

per condition, horizontal bar represents average number of MuSCs per fiber (n=3 mice per condition). (C) Muscle fibers cultured for 48h with MS023 or DMSO. 30 fibers counted per condition (n=3 mice per condition). (D) Quantification of PAX7/MyoD expressing MuSCs from (C). (E) PAX7/MyoD immunofluorescence staining of cultured myoblasts treated with MS023 or DMSO for 48h (F) Quantification of PAX7/MyoD expressing cells from (E).

Transcriptionally distinct MuSC sub-populations emerge under PRMT1 repression

To identify subpopulations of MuSCs generated by MS023, we performed single-cell RNA sequencing (scRNA-seq). MuSCs were purified from 8 week-old wild type C57BL/6 mice in biological duplicates immediately after 1) isolation (termed d0; sample day 0), and 2) culture in growth medium for 4 days with 0.033% DMSO as control (sample d4) or with 1 μ M MS023 (sample d4MS023), and 3) grown in growth media for 6 days with 0.033% DMSO removed at day 4 (sample d6), or 6 days in culture with 1 μ M MS023 removed at day 4 (sample d6MS023rd4). Cells were collected at these time points and processed on the 10x Genomics Chromium platform for scRNA-seq. Data filtering and analysis was performed using the Seurat package for scRNAseq analysis (Butler et al., 2018). After filtering out low-quality cells, approximately 4,000 cells (average, 3,887 \pm 44 cells) from each sample were retained for subsequent analysis. A Pearson correlation of >0.97 (Supplemental Figure S3.2A) was obtained between replicates and we chose to include a replicate for each time point for analysis.

Dimensionality reduction was performed using uniform manifold approximation and projection (UMAP) on pooled cells from all samples, resulting in 10 distinct subpopulations of myogenic cells (labelled 0-9, Supplemental Figure S2B). We then visualized the distribution of individual samples within the UMAP embedding (Figure 3.2C, Supplemental Figure S3.2C). To

determine the identity of the 10 subpopulations, we examined the expression of *PAX7* and the bHLH transcription factors *Myod1*, *MYF5* and *Myog* (Figure 3.2B).

Two populations of *PAX7* and *MYF5* expressing cells were observed which we called quiescence 1 and 2 (Q1 and Q2), while the two populations that expressed both *Myod1* and *Myog* were called differentiated myoblasts 1 and 2 (DM1 and DM2, Figure 2D). The remaining *Myod1* populations we named myoblast clusters 1 to 5 (M1-M5), and the last one C1 for committed 1 (Figure 3.2A). The freshly isolated MuSCs of day 0 (d0) segregated into Q1 and Q2 (Supplemental Figure S3.2D), which in addition to *PAX7* and *MYF5*, expressed markers of MuSC quiescence (*Fos*, *Egr1*, *Jun*), and early activation markers (*MyoD1*, *Mt1*, *Mt2*, Figure 2E). Our Q1 and Q2 populations are similar to quiescence and early activation populations reported recently from freshly isolated (De Micheli et al., 2020; Dell'Orso et al., 2019; van Velthoven et al., 2017). The two *Myog* expressing clusters expressed other markers of early differentiation (*Acta2*; DM1), and late differentiation (*Tnnt3*, *Myh11*, *Acta1*; DM2) (Figure 3.2E). An enrichment for cell cycle and proliferation markers was found throughout the remaining 5 undifferentiated myoblast clusters (*Cdk1*, *Ccnd1*, *Mki67*, *Top2a*, *Birc5*, and *Cenpa*; M1-M5) (Figure 3.2E).

The control DMSO day 4 (d4) sample was distributed among 3 subpopulations of myoblasts (M1, M2, and M4), while two additional days in culture day 6 (d6) contained M1, M2, and M4, but also had differentiated clusters DM1 and DM2 (Figure 3.2C, 3.2D Supplemental Figure S3.2E). In comparison, day 4 with MS023 (d4MS023) was distributed uniquely among clusters M3 and M5. Day 6 MS023 removed at day 4 (d6MS023rd4) had clusters of day 4 MS023 treatment, as well as DM1 and DM2 DM2 (Figure 3.2C, 3.2D Supplemental Figure S3.2E). Notably, d6MS023rd4 had nearly twice as many cells in DM1 (20.8%) as d6 (11.5%) (Figure 3.2D), indicating that MS023 inhibition was reversible and cells enter the differentiation program

more efficiently. In addition, all samples had in common a small subpopulation of cells (<200 cells) in cluster C1.

Analysis of the top 100 enriched genes in each cluster revealed distinct transcriptional profiles. For example, the d4MS023-occupied cluster M5 was enriched for cell cycle markers (*Cdk1*, *Cdk4*, *Ccnd3*) and other markers of proliferation (*Mki67*, *Birc5*, *Top2a*). The other d4MS023-occupied cluster M3 retained some markers of proliferation (*Ccnd1*), however also expressed the cell cycle inhibitor *Cdkn2a* and the structural muscle gene *Myl6*, in addition to a strong enrichment for ribosomal genes (over 20% of the top100 markers belonged to the ribosomal protein family, a feature that is unique to cluster M3). Therefore, clusters M3 and M5 are unique to MS023-treated MuSCs and represent robust proliferation clusters with extensive ribosomal protein expression.

The top 100 enriched genes in each sample were also investigated (see heatmap Supplemental Figure S3.2J). Interestingly, d4MS023 genes were strongly enriched for the reactome pathways of respiratory electron transport, the citric acid cycle, and formation of ATP. In contrast, d4 was enriched for the reactome pathways of RNA metabolism, translation, and mRNA splicing (Supplemental Figure S3.2H, S3.2I).

The d4 cluster M2 shared many of the same gene enrichments as cluster M5 (*Cdk1*, *Mki67*, *Birc5*, *Top2a*). Conversely, the other d4 cluster M4 down-regulated these genes while maintaining expression of replication-dependent transcripts such as *Ube2c* and *Dut*, indicating increased heterogeneity in cycling cells compared to d4MS023. The final d4 cluster M1 resembled the transitional d4MS023 cluster M3 in that it expressed a mix of cell cycle (*Ccnd1*) and differentiation (*Myl6*) markers, however lacked the enrichment of ribosomal genes observed in M3.

It was important to note is the stark difference in the pathway enrichment signatures of the transitional clusters M1 (d4) and M3 (d4MS023). The genes which were uniquely enriched in cluster M3 were strongly associated with protein synthesis (eg. *Rps9*, *Eef1g*, *Uba52*) (Supplemental Figure S3.2H, I). In contrast, the enriched genes unique to cluster M1 were associated with cellular response to toxic substance and cellular detoxification (*Anxa1*, *Txn1*, *Hmox1*, *Prdx5*) (Supplemental Figure S3.2H, I).

We further investigated the distribution of expression levels for *PAX7*, *MYF5*, *MyoD*, and *MYOG* across clusters and samples (Supplemental Figure S3.2F, G). We observed a unique expression pattern for *PAX7* in d4MS023 and d6MS023rd4 samples (Supplemental Figure S3.2G). In d4 MuSCs, cells were divided into two populations, *PAX7*-negative (expression level 0) and *PAX7*-positive (standard distribution around expression level 1). In d6 myoblasts, *PAX7*-positive cells maintain the same level of *PAX7* expression, but a higher proportion of cells became *PAX7*-negative, consistent with canonical *PAX7* expression during MuSC differentiation (Yin et al., 2013). Meanwhile, with MS023 treatment, three subpopulations emerged. The *PAX7*-positive cells in d4MS023 and d4MS023rd4 were divided into two groups, both of which had higher *PAX7* expression levels than their untreated counterparts and were more comparable with day 0 (quiescent) MuSC *PAX7* expression levels (Supplemental Figure S3.2G).

Together, these findings suggest that the MuSC subpopulations generated by MS023 treatment possess several unique features. Day 4 MS023 cells had proliferating signatures, less heterogeneity and were localized mainly within one cluster (cluster M5), unlike day 4 DMSO proliferating cells which were divided into two clusters (clusters M2 and M4), each with different expression profiles of cell cycle regulators. Cluster M5 had a striking enrichment for genes involved in cellular metabolism that was unique to M5. Furthermore, the day 4 MS023 transitional

cluster M3 had a strong enrichment for genes involved in mRNA translation which was not observed in the day 4 DMSO transitional cluster M1. Analysis of expression level patterns in d4MS023 cells indicated a subpopulation of MuSCs with elevated *PAX7* expression compared to day 4 DMSO control cells. Therefore, through repression of type I PRMTs with MS023, we have reprogrammed MuSCs to acquire a unique and previously uncharacterized identity.

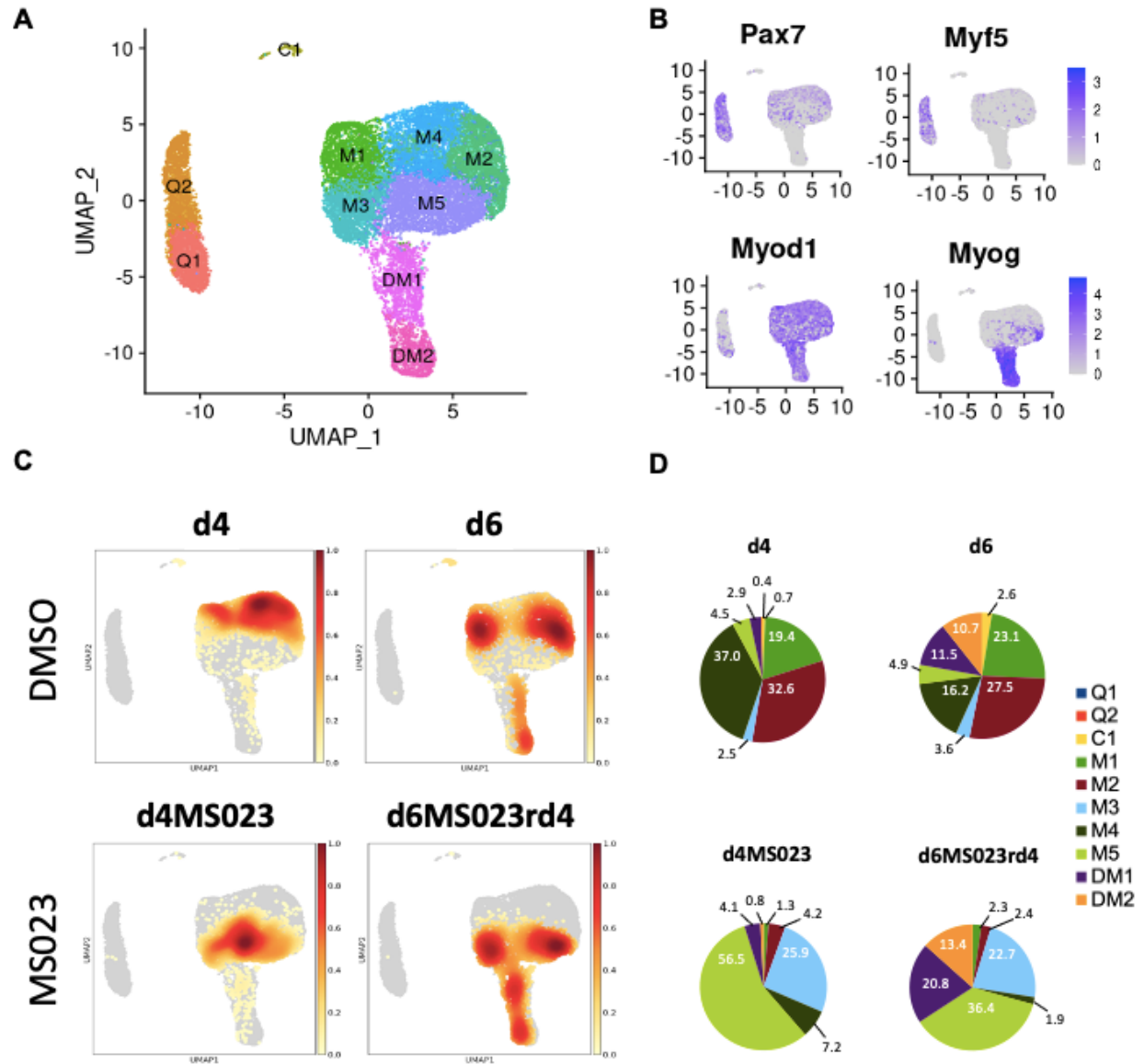


Figure 3.2 Single-cell graph-based clustering analysis

(A) UMAP embedding representation for all cells. (B) Gene expression density on the UMAP embedding plot of myogenic markers PAX7, MYF5, MyoD, and Myogenin. (C) Distribution of cells from each sample within the UMAP embedding representation. (D) Proportion of cells from each sample belonging to each of the 10 identified clusters.

Trajectory analysis reveals temporally distinct expression patterns in MuSCs treated with MS023 with unique enrichment for energy metabolism

Using the Monocle v2.16.0 R package (Trapnell et al., 2014), we conducted trajectory analysis on 3 groups of samples to obtain hierarchical links between clusters: (1) all samples; (2) d0, d4, d6; (3) d0, d4MS023, d6MS023rd4. Monocle analysis placed each cell from the 9 clusters (Q1/Q2, M1-5, and DM1/2) onto a pseudotime axis based on differential gene expression patterns. The trajectory analysis of all samples pooled produced a pseudotime axis with a single branchpoint and 3 cell states which we labelled Q for quiescence, M for myoblast, and DM for differentiating myoblast (Figure 3.3A). Cells from the Q1 and Q2 clusters were found at the beginning of pseudotime, cells from the M1-5 clusters populated the area around the branchpoint, and cells from DM1/2 mainly populated the upward-oriented branch, following an overall trajectory of Q1/2→M1-5→DM1/2 (Figure S3.3A).

Day 0 cells populated the beginning of pseudotime, with d4 and d4MS023 cells appearing shortly after. d6 and d6MS023rd4 cells had a similar distribution as d4 and d4MS023, with the exception of having increased density around the terminus of the upward-oriented branch (Supplemental Figure S3.3A). Interestingly, d4MS023 and d6MS023rd4 cells emerge later along the pseudotime axis than d4 and d6 cells and appeared closer to the branchpoint (Supplemental Figure S3.3A).

We examined the genes which were significantly differentially regulated across the branchpoint of the pooled sample trajectory to confirm whether this split is representative of the molecular events which determine whether MuSCs will commit to differentiation or continue to proliferate. As expected, genes involved in the myogenic process were highly upregulated along the branch that diverges upwards along the trajectory (eg. *Tnnt1*, *Tnnt2*, *Acta1*, *Myog*), while genes

involved in cell cycle and proliferation were upregulated along the branch that diverges downwards along the trajectory (eg. *Mki67*, *Cdca8*, *Top2a*, *Birc5*) (Supplemental Figure S3.3B, C).

Trajectory analysis was also performed on a subset of samples (d0→d4→d6; DMSO trajectory and d0→d4MS023→d4MS023rd4; MS023 trajectory) to identify treatment-specific alterations in the molecular events which drive fate-determining decisions (Figure 3.3B). Both the DMSO and MS023 trajectories retained a single branch point indicating that the overall lineage patterns were conserved.

Closer inspection of genes which were significantly differentially regulated across the branchpoint in the DMSO and MS023 trajectories revealed a unique signature in the MS023-trajectory. The list of genes which changed significantly across the branchpoint for both trajectories (7094 for the DMSO trajectory, 7616 for the MS023 trajectory) were filtered for genes which were unique to each condition. The DMSO trajectory had 1,517 unique genes, while the MS023 trajectory had 2037 unique genes (Supplemental Figure S3.3D). Interestingly, the MS023 trajectory-unique genes revealed an enrichment for oxidative phosphorylation and mitochondrial ATP synthesis (Figure 3.3F, 3.3G), consistent with cluster marker analysis for MS023-specific clusters (Supplemental Figure S3.2G, S3.2H: *electron transport*, *ATP synthesis*). Expression of select genes involved in the mitochondrial electron transport chain (*Ndua2*, *Ndufa4*, *Uqcr10*, *Cox4II*, *Cox5b*, *Cox8a*, *Atp5c1*, *AtpIf1*, *Atp5j2*) were further examined for expression level within the scRNAseq UMAP plot, and it was confirmed that they were elevated in MS023-specific clusters (Figure 3.4A). Moreover, RT-qPCR analysis of a subset of these genes confirmed they were upregulated in d4MS023 MuSCs compared to d4 MuSCs (Supplemental Figure S3.4A).

Therefore, these pathways both define the unique identity of MS023-treated MuSCs, and serve as driving forces in their fate-determination.

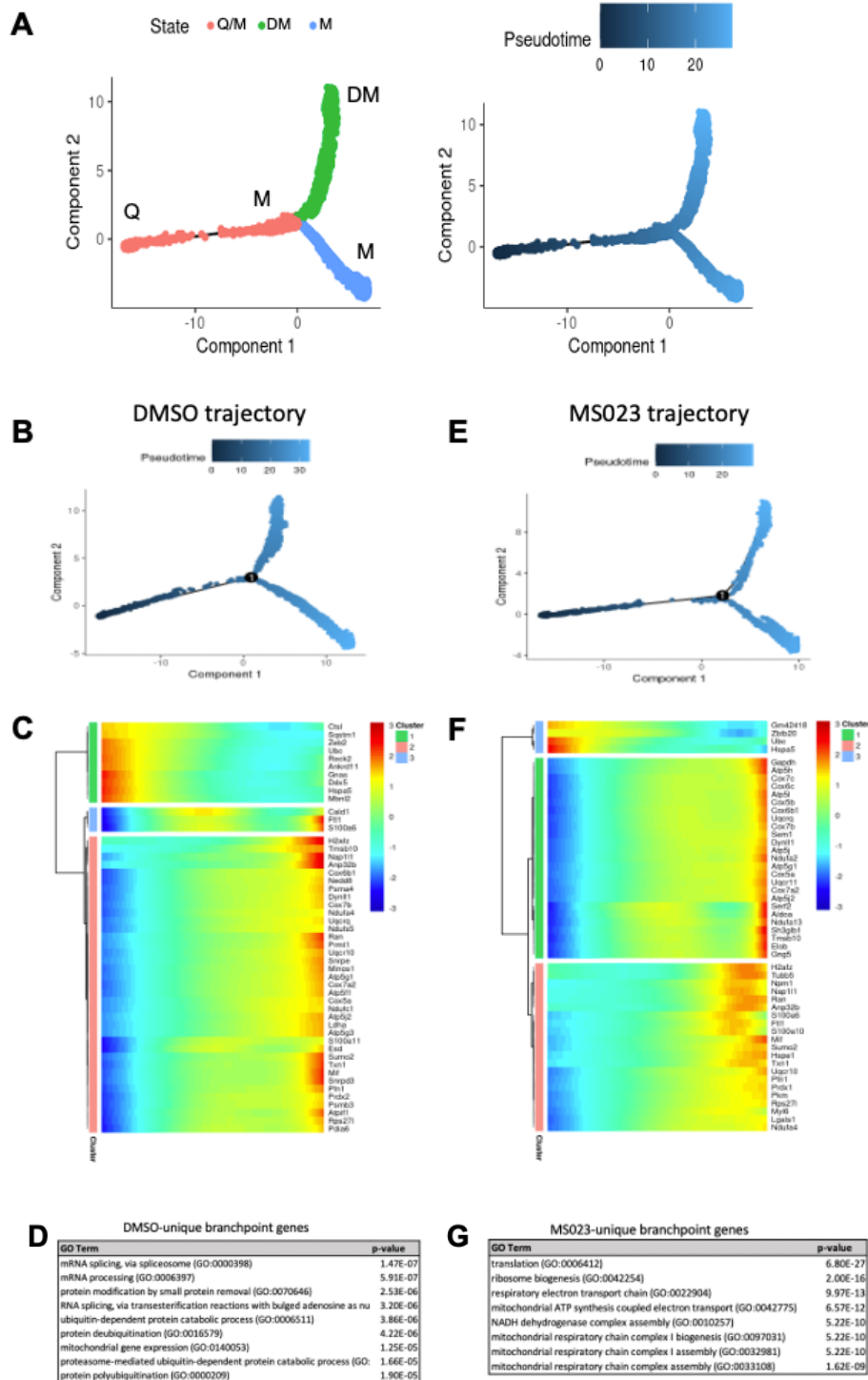


Figure 3.3 Pseudotime trajectory of pooled, DMSO- and MS023-treated MuSCs

(A) Trajectory of all cells depicting three cell states. Pseudotime starts at the left endpoint of the plot. Q: Quiescence. M: Proliferating myoblast. DM: Differentiating myoblast. **(B-D)** Monocle trajectory of day-0 and DMSO-treated samples **(B)**, heatmap of top differentially regulated genes across pseudotime **(C)** and GO enrichment analyses of DMSO-unique branchpoint genes **(D)**. **(E-G)** Monocle trajectory of day-0 and MS023-treated samples **(E)**, heatmap of top differentially regulated genes across pseudotime **(F)** and GO enrichment analyses of MS023-unique branchpoint genes **(G)**.

MS023-treated proliferating MuSCs retain oxidative phosphorylation and have elevated glycolysis

The transition of MuSC from quiescence to proliferation is accompanied by a sharp reduction in oxidative metabolism and a shift towards glycolysis (L'Honoré et al., 2018; Ryall et al., 2015). Therefore, the retention of a transcriptional signature indicating high levels of mitochondrial oxidative phosphorylation in MS023-treated cells was unexpected. We sought to validate these findings in *ex vivo* cultured MuSCs by performing metabolic analysis with Seahorse Extracellular Flux Analyzer (Agilent). We isolated MuSCs from C57BL/6 wildtype mice and seeded them onto matrigel-coated 96-well plates and treated with 1 μ M MS023 or DMSO for 48 hours (n= 3 mice per treatment condition). Oxygen consumption rate (OCR) was first measured to characterize mitochondrial bioenergetics (Figure 3.4B). As predicted, MS023-treated MuSCs displayed increased OCR measurements at nearly all timepoints (Figure 3.4B, $p= 0.000001 - 0.02$), with significantly elevated basal respiration ($p= 0.006$) and maximal respiration ($p= 0.04$), and a trend of increased ATP production (approaching statistical significance, $p=0.1$). To confirm an increase in mitochondrial biogenesis, d4 and d4MS034 MuSCs were stained with MitoTracker CMXRos (ThermoFisher Scientific). The average intensity of the MitoTracker signal was significantly increased in d4MS023 cells (Figure 3.4C, 3.4D, $p < 0.0001$)

We next determined whether markers of glycolysis were also differentially regulated in MS023-treated MuSCs. Indeed, several of the marker genes for MS023-specific clusters were components of glycolysis which displayed increased expression compared to clusters of DMSO-treated cells (*Hkl1*, *Eno1*, *Pfkm*, *Gapdh*, *Pkm*, *Slc2a1*; Supplemental Figure S3.4B). We next performed extracellular acidification rate (ECAR) analysis as an indicator of glycolysis again using the Seahorse Extracellular Flux Analyzer. MS023-treated cells were strikingly more

glycolytic than DMSO-treated cells (Supplemental Figure S3.4C). Glycolysis, glycolytic capacity, and glycolytic reserve were all significantly increased ($p= 0.02$, $p= 0.004$ and $p= 0.001$, respectively) (Supplemental Figure S3.4C). As further indicators of glycolysis, the growth media supernatant of d4 and d4MS023 cultured cells was analyzed using a Nova Biomedical Bioprofile 400 analyzer (Cambridge Scientific). As expected, d4MS023 cells had significantly higher levels of glucose uptake (measured as grams/liter per 10,000 cells, $p= 0.004$). Additionally, the glycolytic byproduct lactate was present in higher concentrations d4MS023 media and was undetectable in the d4 media (Supplemental Figure S3.4D).

Collectively, these findings indicate that MS023-treated MuSCs utilize both OxPhos and glycolysis at elevated levels compared to untreated control cells to boost cellular metabolism, suggesting a possible mechanism through which enhanced proliferation is supported.

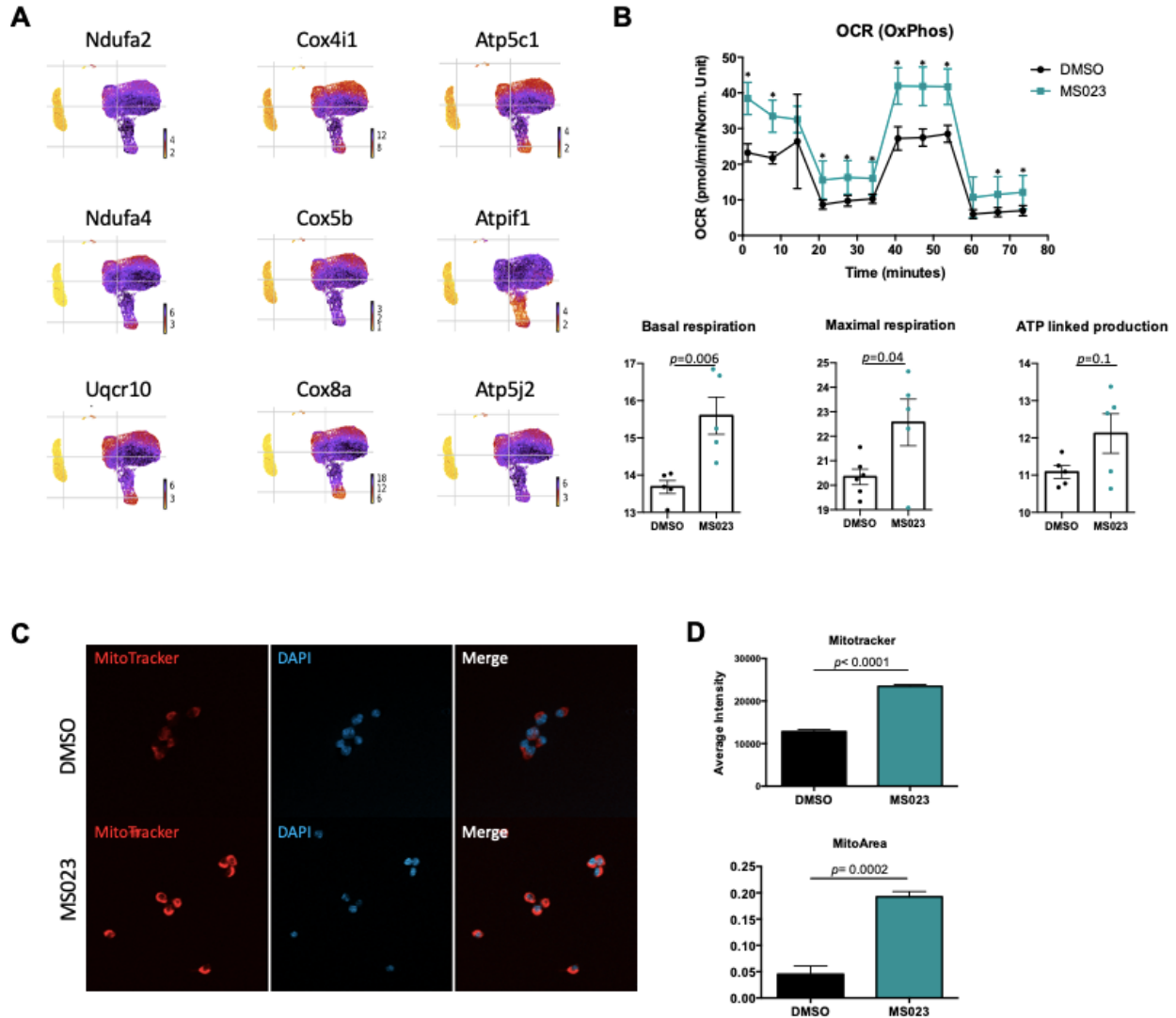


Figure 3.4 MS023-treated proliferating MuSCs retain oxidative phosphorylation

(A) UMAP plots showing expression of components of the electron transport chain localized to MS023 clusters. (B) Seahorse XF96 analysis of oxygen consumption rate (OCR) in DMSO and MS023-treated freshly isolated primary MuSCs and quantification of basal respiration, maximal respiration, and ATP-linked production. Error bars represent mean \pm SEM from 7 individual wells per condition. (C) MitoTracker staining (red) of freshly isolated MuSCs treated with DMSO (upper panel) or MS023 (lower panel) and counterstained with DAPI to visualize nuclei. Minimum 200 cells quantified per condition from 3 independent experiments (D) (upper panel) Quantification of

MitoTracker signal intensity of cells from (C), error bars represent mean \pm SEM from 3 individual replicates, > 200 nuclei quantified per condition ($p < 0.0001$). (lower panel) Quantification of MitoArea as determined by Image J ($p = 0.0002$).

MS023 treatment of cultured MuSCs maintains high levels of OxPhos via activation of Ampk

Ampk is a master regulator of mitochondrial homeostasis (Herzig and Shaw, 2018). Therefore, we hypothesized that the unexpected capacity of MS023-treated MuSCs for enhanced mitochondrial OxPhos was through activation Ampk. We isolated MuSCs from wildtype C57BL/6 mice and cultured them *ex vivo* for 4 days with MS023 or DMSO. Western blot was performed on whole cell lysates for total Ampk and the active form p-Ampk (T172). While total Ampk protein levels were unaltered, p-Ampk was markedly increased in MS023-treated MuSCs (Figure 3.5A). Ampk is known to activate genes required for mitochondrial biogenesis through activation of the nuclear transcription factor Nrf1 (Marin et al., 2017). Notably, total Nrf1 protein was also increased in MS023 treated cells (Figure 3.5A), a further indication that Ampk is activated upon MS023 treatment.

To further confirm Ampk activation, we looked at the scRNAseq expression of known Ampk downstream targets in MS023-treated MuSCs. Ampk is known to regulate autophagy genes (Kim et al., 2011) and Foxo3 transcriptional targets (Greer et al., 2007). Indeed, MS023-treated MuSCs had elevated expression of genes involved in autophagy (*Atg5*, *Lamp1*, *Lamp2*, *Sqstm1*), and Foxo3 transcriptional targets (*Wipi1*, *Wipi2*) (Supplemental Figure S3.5A). Therefore, these data indicate that Ampk is activated, and its downstream targets are upregulated in MS023-treated cells.

Given the increased activation of Ampk in MS023-treated MuSCs, we wondered whether Ampk acts as a potential upstream node of the self-renewal phenotype observed with MS023 treatment. Therefore, primary wildtype MuSCs were isolated from C57BL/6 mice and expanded for 48h with MS023 or DMSO. After 48h, MuSCs were transfected with siRNA directed against Ampk and cultured for a further 48h with DMSO or MS023. Cells were then fixed and analyzed

for PAX7 and ki67 expression with immunofluorescence. Cells treated with MS023 in the siLuc control displayed dramatically increased numbers of ki67⁺ cells, as expected (76.1 ± 0.61% in MS023 versus 34.69 ± 4.22% in DMSO). Treatment with siAmpk in DMSO-treated cells led to a decrease in proliferating cells (34.69 ± 4.22% in DMSO siLuc versus 20.19 ± 1.06% in DMSO siAmpk). Interestingly, treatment with siAmpk in MS023-treated cells caused a drastic reduction in the number of proliferating cells (76.1 ± 0.61% in MS023 siLuc versus 25.39 ± 7.59% in MS023 siAmpk) (Figure 3.5D).

Together these findings indicate that Ampk acts as an upstream regulator of the MS023-induced phenotype of enhanced self-renewal in MuSCs, as knockdown of Ampk results in reversal of the MS023 proliferation phenotype.

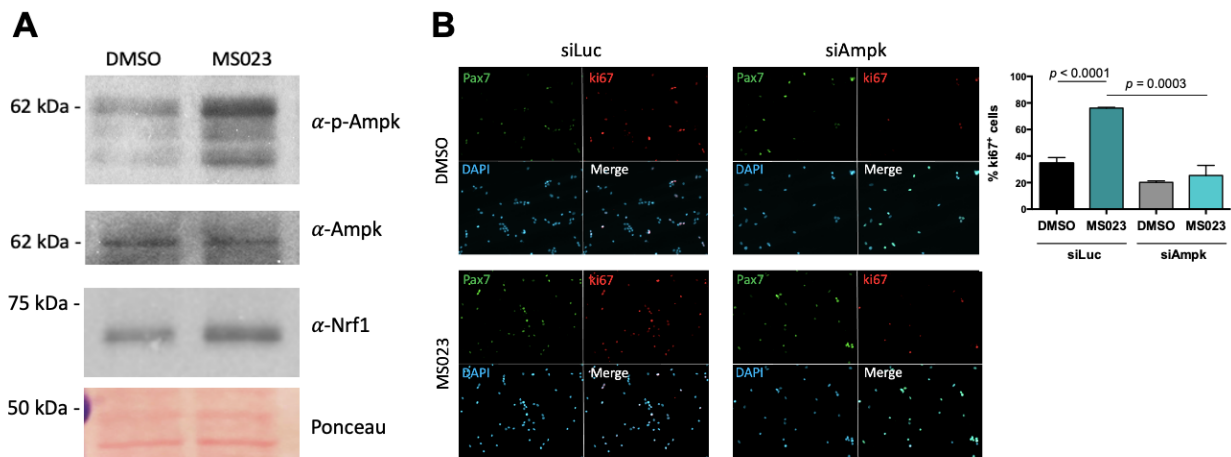


Figure 3.5 MS023 treatment of cultured MuSCs maintains high levels of OxPhos via activation of Ampk

(A) Immunoblotting of whole cell lysate from day 4 DMSO and MS023 treated MuSCs. Molecular weight markers are indicated on the left, and the immunoblotting antibody is indicated on the right.

(B) (left) Immunofluorescence of freshly sorted MuSCs treated with DMSO or MS023, plus siAmpk or siLuc control. The cells were stained using PAX7 (green) and ki67 (red) and were counterstained with DAPI (blue). (right) Quantification of the ki67 positive cells. Error bars represent mean \pm SEM from 3 independent experiments, >200 nuclei quantified per condition.

***In vitro* expanded MS023-treated MuSCs retain the potential to become mature myoblasts**

We next wanted to validate that removal of MS023 created conditions which are permissive to terminal differentiation. Primary MuSCs were cultured under four conditions before switching to differentiation media: (1) for four days with DMSO, (2) washout for additional two days without DMSO (DMSOwo), (3) for four days with MS023, and (4) washout for additional two days without MS023 (MS023wo). Cells treated for four days were switched to differentiation media with the continued presence of DMSO or MS023. Washout cells were switched to differentiation media without DMSO or MS023. Expectedly, cells differentiated in the presence of MS023 had an impaired ability to form multinucleated myotubes and had a poor fusion index of 19% compared to the 77% fusion index observed with DMSO treated MuSCs (Figure 3.6A, 3.6B). Interestingly, MS023wo cells had completely restored their ability to terminate differentiation, with their fusion index of 76% being comparable to that of DMSOwo cells (78%) (Figure 3.6C, 3.6D).

Together, these experiments define MS023 as a reversible inhibitor of type I PRMT activity which enhances MuSC proliferation and self-renewal while still allowing for full differentiation capabilities upon removal of the compound.

Type I PRMT inhibitor MS023 enhances MuSC engraftment

We next sought to confirm that MS023 washout conditions create a pool of MuSCs that are regeneration-competent upon engraftment into an injured muscle *in vivo*. Primary MuSCs were isolated from a β -actin-GFP reporter mouse (C57BL/6-Tg(CAG-EGFP)10sb/J, Jackson Laboratory 003291, FACS gating strategy in Supplemental Figure S3.6B, S3.6C), and treated with MS023 or DMSO *in vitro* for 6 days to allow for expansion. Following culture, 15,000 GFP⁺ myoblasts from each group were injected into the tibialis anterior (TA) muscle of wild type mice.

One day after stem cell injection, the TA was injured with cardiotoxin (CTX). After 3 weeks, mice were sacrificed and GFP⁺ differentiated muscle fibers were quantified following cross-sectional staining of the injured TA muscle (n=3 mice per condition) (Supplemental Figure S3.6A). Interestingly, the mice which received MS023-treated MuSCs had more GFP⁺ mature muscle fibers than the mice which received DMSO-treated MuSCs (88 fibers/section \pm 32 for MS023 versus 31 fibers/section \pm 14 for DMSO, $p= 0.02$) (Figure 3.6E, 3.6F). These data indicate that MS023-treated MuSCs were able to regain their ability differentiate *in vivo* following Type I PRMT de-repression and contribute more robustly to muscle regeneration following injury.

We next wanted to determine whether MS023-treated engrafted cells were able to repopulate the niche. Therefore, we repeated the engraftment experiment with MS023 and DMSO-treated GFP⁺ MuSCs, and this time re-isolated MuSCs three weeks after CTX injection. Strikingly, MS023-treated MuSC engraftment yielded a 6.8 fold increase in the number of GFP⁺ following muscle regeneration ($p=0.004$) (Figure 3.6G, 3.6H).

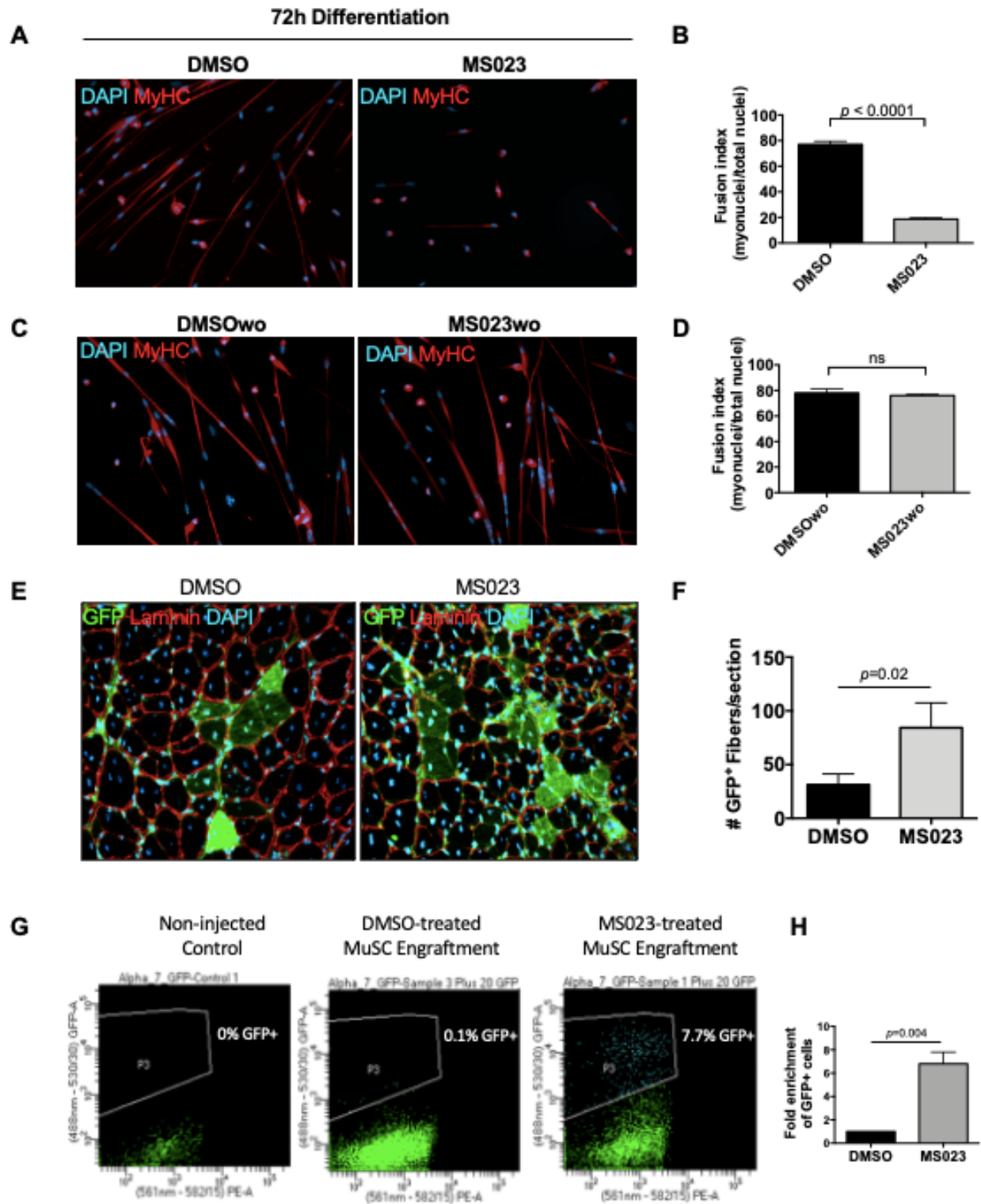


Figure 3.6 MS023 treatment is reversible and allows expanded MuSCs to differentiate *ex vivo* and *in vivo*.

(A) Immunofluorescence of MyHC counterstained with DAPI in primary myotubes that were differentiated in the presence of DMSO or MS023 following 4 days of treatment with DMSO or MS023. (B) Fusion index calculated as the ratio of nuclei within the myotube to total nuclei from >200 nuclei per condition, error bars represent mean \pm SEM from 3 individual replicates. (C) Immunofluorescence of MyHC counterstained with DAPI in primary myotubes that were differentiated in the absence of DMSO or MS023 following 4 day of treatment with DMSO or MS023 and 2 days of washout. (D) Fusion index calculated as the ratio of myonuclei to total nuclei from >200 nuclei per condition, error bars represent mean \pm SEM from 3 individual replicates. (E) Immunofluorescence of GFP⁺ myofibers following transplantation of 15,000 DMSO or MS023-treated MuSCs. (F) Quantification of GFP⁺ myofibers. Error bars represent mean \pm SEM from 3 individual biological replicates. (G) (left) Representative FACS plots of re-isolated MuSCs following engraftment and muscle regeneration. P3 represents the population of purified GFP⁺ MuSCs. (H) Fold enrichment of MS023-treated MuSC re-isolation compared to DMSO. Error bars represent mean \pm SEM from 3 individual biological replicates.

MS023 injection increases muscle strength in *mdx* mice

Patients with Duchenne muscular dystrophy (DMD) lack functional dystrophin, a structural protein which is required to connect mature myofibers to the extracellular matrix. The resulting muscle tissue is vulnerable to injury and is caught in constant cycles of muscle degeneration and regeneration (Serrano et al., 2011). The *Dmd^{mdx}* mice harbor a spontaneous mutation in the gene encoding dystrophin, and are therefore commonly used as a model for DMD (Bulfield et al., 1984; Ryder-Cook et al., 1988).

To determine whether MS023 could provide any therapeutic benefits in a dystrophic context, we delivered 80 mg/kg of MS023 or vehicle via intraperitoneal injection to $n=6$ *mdx* mice once a day for 3 days. Tail pieces were collected 48h after the final injection and whole tissue lysate was analyzed for aDMA- and sDMA-containing proteins using immunoblotting. We observed reduced aDMA proteins and a subsequent increase in sDMA proteins in MS023-treated mice compared to vehicle-treated mice (Supplemental Figure S3.7A). At 10 and 20 days following the final injection, 2-paw and 4-paw grip strength measurements were taken. Additionally, endurance was tested by placing mice on a wire grid and inverting them so that the amount of time spent hanging could be recorded (Figure 3.7A for schematic). We observed a 50% increase in 2-paw grip strength ($p= 0.0113$) and a 45% increase ($p= 0.0089$) in 4-paw grip strength in the MS023-treated mice versus those that received vehicle at the 10-day time point (Figure 3.7B). The hanging test to measure endurance showed a positive trend towards increased endurance at the 10-day time point in MS023 versus vehicle-treated mice, however this was not statistically significant ($p=0.1$) (Supplemental Figure S3.7B). A final measurement was performed at the 32-day endpoint, during which mice were placed under terminal anesthesia and the extensor digitorum longus (EDL) hindlimb muscle was isolated and used to generate a force/frequency curve. Interestingly, this

experiment revealed that MS023-treated mice responded with a ~30% increase in force compared to their vehicle-treated counterparts ($p = 0.00727$) (Figure 3.7C). Moreover, we observed a reduction in the variation of the minimum ferret measurements of fibers from TA cross sections of MS023-treated mice ($p = 0.04$) (Figure 3.7D). These findings indicate that transient repression of PRMT1 with MS023 can offer a therapeutic avenue to explore for enhancing MuSC proliferation while still maintaining the ability to differentiate to mature muscle fibers, thus providing improved muscle strength.

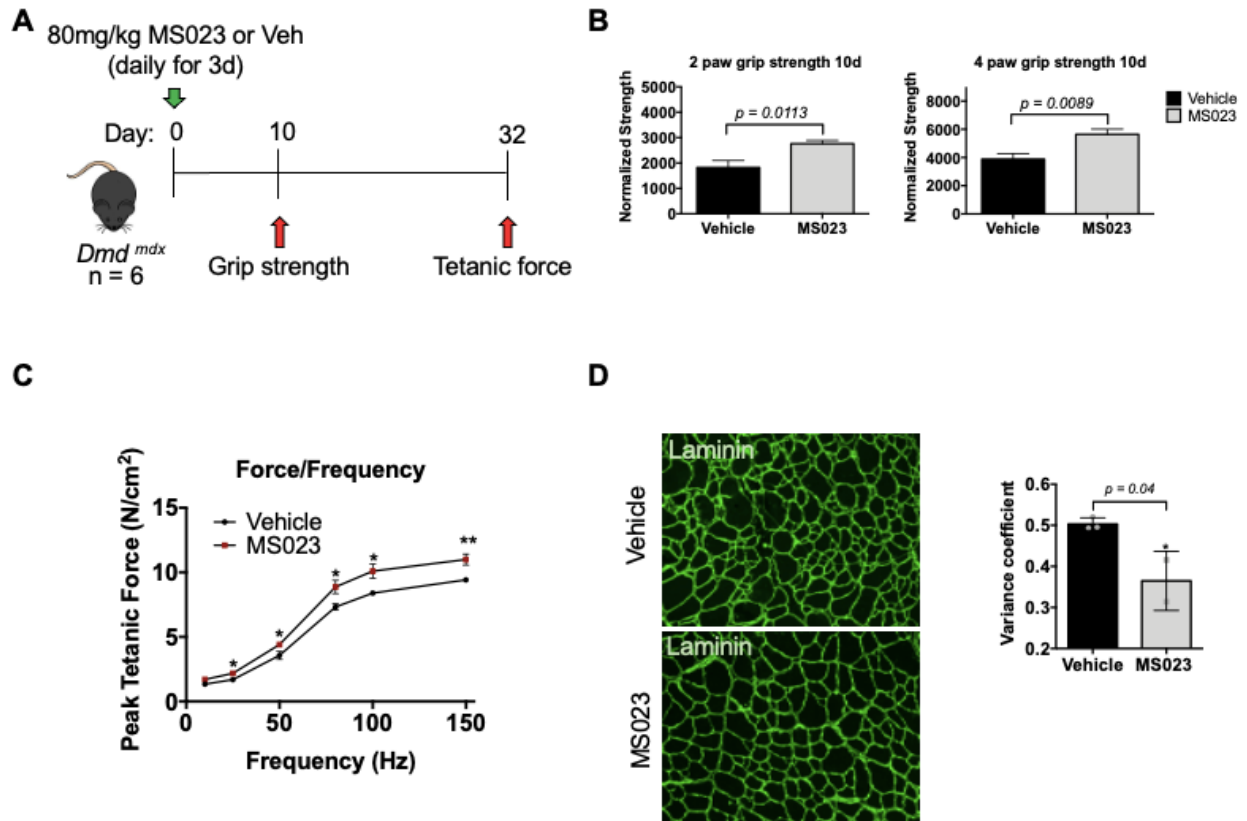


Figure 3.7 *in vivo* administration of MS023 to dystrophic mice improves muscle strength

(A) Experimental schema. (B) Normalized grip strength measurements taken from two forelimbs and all 4 limbs of mice treated with vehicle or MS023 10 days after the last injection. Error bars

represent mean \pm SEM from 6 biological replicates. **(C)** Force/frequency curve generated for mice treated with vehicle or MS023. **(D)** Representative cross-sectional area of TA muscles isolated from mice treated with vehicle or MS023 and immunostained with anti-laminin antibodies to visualize myofibers. **(E)** Quantification of the variance coefficient of TA muscle minimum fiber Feret measurement from mice treated with vehicle or MS023. Error bars represent mean \pm SEM from 6 biological replicates, >200 fibers measured per mouse)

3.5 Discussion

In the present manuscript, we show that inhibition of type I PRMTs promoted the *in vitro* proliferation of PAX7-positive MuSCs as visualized by ki67 staining. scRNA-seq analysis of these MS023 treated MuSCs identified new transitional clusters. These MS023-specific subpopulations harboured unique transcriptional signatures of stemness and energy metabolism. The MS023 treated MuSCs exhibited elevation of both glycolysis and OxPhos. Moreover, the MS023 treated cells displayed increased AMP kinase (Ampk) activation. The knockdown of Ampk resulted in reversal of the MS023-induced proliferation phenotype. Engrafted MuSCs treated with MS023 were better at regenerating injured muscle and at repopulating the niche. A single treatment of the *mdx* mouse model of DMD with MS023 resulted in enhanced grip strength and force generation. Therefore, repression of type I PRMTs reforms the metabolic state of cultured MuSCs to enhance their capacity for self-renewal *ex vivo* and maintain their ability to robustly participate in muscle regeneration. These findings demonstrate that type I PRMT inhibitors may serve as viable treatment options for skeletal muscle diseases.

Inhibition of type I PRMTs in MuSCs activates Ampk and results in elevated energy metabolism and self-renewal. The ability to tailor energy metabolism to the specific demands of cell proliferation and differentiation is known as metabolic plasticity, and is required for maintaining tissue homeostasis (Folmes et al., 2012). The transition from quiescence to proliferation is regulated by a shift from OxPhos to glycolysis (Pala et al., 2018; Ryall et al., 2015). During MuSC quiescence, high levels of NAD⁺ are generated by oxidative metabolism which in turn activates Sirtuin 1 (SIRT1) to deacetylate and repress expression of differentiation genes required for the myogenic program (Ryall et al., 2015). The shift from OxPhos to glycolysis upon exit from quiescence results in reduced NAD⁺ levels and subsequent activation of differentiation

genes. Furthermore, it has been shown that entry to the process of terminal differentiation is mediated by the activation of pyruvate dehydrogenase (PDH), marking a switch from glycolysis to OxPhos (Hori et al., 2019). Ampk is a major energy sensor in the cell, regulating energy balance and metabolic state (Hardie et al., 2016). Null alleles of Ampk have contributed to the understanding of its role in MuSC function (Fu et al., 2015b; Theret et al., 2017). It was shown that Ampk-deficient MuSCs did not effectively respond to injury and failed to shift towards glycolysis upon exit from quiescence, resulting in proliferation defects and impaired muscle regeneration (Fu et al., 2015b). A second study showed that deleting Ampk following the expansion of MuSCs conferred a switch to OxPhos and enhanced self-renewal (Theret et al., 2017), indicating that cellular reprogramming for self-renewal requires elevated oxidative metabolism. Although PRMT1 has many substrates, we show that siRNA knockdown of Ampk alone was sufficient to reverse the MS023-mediated increase in proliferation. Activated Ampk simultaneously stimulates autophagy and mitochondrial biogenesis, thus maintaining mitochondrial homeostasis (Herzig and Shaw, 2018). Our data show that maintaining active Ampk in day 4 cultured MuSCs through inhibition of type I PRMTs elevates OxPhos and enhances self-renewal, and stimulates expression of autophagic markers (Atg5, Lamp1, Lamp2, Sqstm1). Interestingly, transcriptional activation of mitochondrial biogenesis was shown to be regulated by the Ampk-Nrf1 signaling axis (Marin et al., 2017) and we show that Nrf1 protein is elevated in MS023-treated MuSCs.

Treatment of MuSCs with MS023 results in metabolic reprogramming of MuSCs, supporting a role for PRMT1 as a metabolic coactivator. PRMT1 was shown to interact with Ampk in skeletal muscle during the early stages of muscle atrophy (Stouth et al., 2018). Moreover, CARM1 directly methylates Ampk to regulate its activity during muscle response to denervation

(Stouth et al., 2020). PRMT1 has also been shown to play a signaling role to regulate thermogenesis. PRMT1 acts through the transcriptional co-activator PGC-1 α in human and mouse adipocytes to regulate thermogenic fat activation, and PRMT1-deficient mice were unable to induce the thermogenic program following cold exposure (Qiao et al., 2019). Methylation of PGC-1 α by PRMT1 was also shown to stimulate mitochondrial biogenesis (Teyssier et al., 2005). Additionally, PRMT1-mediated methylation positively regulates the insulin receptor (IR)-phosphatidylinositol 3-kinase (PI3-K) pathway which is required for glucose transport in skeletal muscle (Iwasaki and Yada, 2007). Overexpression of PRMT1 in the liver under hypoxic conditions causes hypermethylation of FoxO1 and increased translocation to the nucleus, resulting in reduced glucose uptake (Bayen et al., 2018). Therefore, these findings indicate that PRMT1 methylates key regulators of cellular metabolism and highlight a cross-talk between metabolic effectors and PRMTs.

scRNA-seq analysis of MS023 treated MuSCs identified new transitional clusters which harboured unique transcriptional signatures of stemness and energy metabolism. DMSO clusters M1/M2/M4 and MS023 clusters M3/M5 were both enriched for proliferation markers (Cdk1, Mki67), and M3/M5 also uniquely harboured elevated metabolic genes including components of the ETC (Atp5k, Cox5a, Ndufa2) and components of glycolysis (Eno1, Gapdh). The simultaneous elevation of both glycolytic and OxPhos components in MS023 subpopulations likely contributes to the enhanced proliferation phenotype. MuSC subpopulations have been characterized at the single-cell level during muscle regeneration, revealing regulatory mechanisms that guide the transition from quiescence to activation, proliferation, and differentiation. A general progressive elevation of metabolic enzyme expression has been noted from low levels in MuSCs isolated from uninjured muscle, to slightly elevated levels in MuSCs isolated from acutely injured muscle (60h

after injury), to the highest levels in cultured proliferating MuSCs (Dell'Orso et al., 2019). A more in-depth analysis of MuSC subpopulations throughout muscle regeneration investigated additional time points after injury (2, 5, and 7 days) and generated a hierarchical continuum model of MuSCs throughout the regeneration process, with a focus on ligand-receptor cell communication networks (De Micheli et al., 2020). Additionally, analysis of young and aged MuSCs revealed that, while they have similar transcriptional signatures, aged MuSCs display delayed activation state dynamics when exiting quiescence, thus preventing them from entering the differentiation program as efficiently as young MuSCs (Kimmel et al., 2020). It has been previously reported that the quiescent MuSCs captured by scRNAseq exist in two groups, one 'quiescent' and one 'early activation', wherein the early activation group highly expresses Fos and Jun while down-regulating Hox genes (van den Brink et al., 2017). Our Q1 and Q2 clusters are in alignment with these two states (Q1 - quiescence; Q2 - early activation), and bare transcriptional similarities to our MS023-specific clusters M3 and M5, such as upregulated Fos and Jun, as well as high levels of PAX7. Notably, capture of rare transient MuSC states remains difficult due to poor sampling or limited cell number. To overcome these issues, one study evaluated 365,000 single cells/nuclei from over 100 combined datasets, allowing for the characterization of short-lived MuSC subpopulations that emerge throughout the myogenic process (McKellar et al., 2021). We show that MS023 treatment generates unique subpopulations of self-renewing MuSCs that have not been previously identified, suggesting that transient cell states may be also amplified through treatment with other epigenetic inhibitors, thus facilitating a more in-depth understanding of their function and contributions to muscle regeneration.

PRMTs are known as epigenetic regulators, and we show that type I PRMT inhibition leads to activation of Ampk which induces metabolic reprogramming favouring proliferation and self-

renewal, providing another example of targeting epigenetic regulators to modulate signaling within the cell. It has been shown that inhibition of the epigenetic modulator Setd7 enhances the proliferation of cultured MuSCs while retaining their stemness by preventing transport of β -catenin into the nucleus, thereby failing to activate the differentiation program (Judson et al., 2018). Taken together, these findings suggest that inhibiting epigenetic methyltransferases can affect MuSC fate through a wide range of targets. Activation of Ampk has also been known to repress protein synthesis via inhibition of mTORC1 signaling (Hindupur et al., 2015). Interestingly, it was shown that repression of protein synthesis is required for maintenance of quiescence in MuSCs. Treatment of MuSCs with an eIF2 α phosphorylation inhibitor resulted in global repression of protein synthesis, and subsequent maintenance of stemness (Zismanov et al., 2016).

We report heightened engraftment capabilities of MS023-treated MuSCs accompanied by high PAX7 expression levels. It has been shown that freshly isolated MuSCs retain high PAX7 expression levels and are superior at engrafting compared to cultured MuSCs (Montarras et al., 2005; Sacco et al., 2008). Generating stable PAX7 expression in myogenic precursor cells with lentiviral delivery of transgenes is a strategy for enhancing engraftment potential following *ex vivo* expansion of MuSCs (Kim et al., 2021), although this approach may be hampered by safety concerns. Therefore, we have identified an additional strategy for increasing PAX7 expression and improving engraftment efficiency and self-renewal of *ex vivo* expanded MuSCs through inhibition of type I PRMTs. Furthermore, our findings show that injection of MS023 in the dystrophic mouse model *mdx* led to enhanced muscle strength with effects lasting up to 30 days, suggesting that the transient increase in MuSC proliferation and self-renewal afforded by MS023 treatment has lasting effects that could benefit patients with muscle wasting disease.

In sum, we report that inhibition of type I PRMTs elevates cellular metabolism in MuSCs. Activation of Ampk stimulates mitochondrial biogenesis and increases OxPhos, generating a more stem-like MuSC with enhanced self-renewal and engraftment capabilities.

3.6 Materials and Methods

Mice

C57BL/6J (Jackson Laboratory 000664) were the wild type mice used for MuSC FACS purification for scRNA-seq, muscle fiber isolation, and for all other *in vitro* experiments.

β -Actin GFP mice (C57BL/6-Tg(CAG-EGFP)10sb/J, Jackson Laboratory 003291) were used to obtain GFP^{Pos} MuSCs for further implantation experiments. Mice lacking dystrophin expression (C57BL/10ScSn-*Dmd*^{mdx}/J, Jackson Laboratory 001801) were used for intraperitoneal MS023 injection and muscle physiology assessment. The experiments with the *Dmd*^{mdx} mice were performed at Ste-Justine and were approved by the CHU Sainte-Justine Research Ethics Committee and performed in compliance with the Comité Institutionnel des Bonnes Pratiques Animales en Recherche (CIBPAR; approval number 2020-2668) in accordance with the Canadian Council on Animal Care guidelines. All other mouse husbandry and experiments were conducted in accordance with the Institutional Animal Care and Use Committee (IACUC) of McGill University. All animal procedures conducted at McGill were approved by the Animal Welfare Committee of McGill University (protocol #3506).

Primary MuSC isolation

Skeletal muscle tissue was isolated from the abdominal and diaphragm muscles of wild type mice and muscle stem cells were isolated as previously described using fluorescence activated cell sorting (FACS) (Pasut et al., 2012). Briefly, dissected muscles were minced with dissection scissors and digested with collagenase/dispase solution (2.4U/ml collagenase D, 2.4U/ml Dispase II in Ham's F10 media) at 37°C for 1h. Digested tissue was triturated and filtered through a 40 μ M cell strainer. Cells were pelleted for 18 min at 1800 rpm and resuspended in 2% BSA/PBS. Cells were stained for 15 min at room temperature with ITGA7-Alexa647 (R&D systems) for positive

selection, and PE-CD45 (Invitrogen), PE-CD11b (Invitrogen), PE-CD31 (BD Pharmigen), and PE-ScaI (BD Pharmigen) for negative selection. Hoechst was used to gate the living cells. Cells were washed once with 2% BSA/PBS and pelleted prior to final resuspension and one last filter through a 40 μ M cell strainer. ITGA7+/CD45-/CDCD11b-/Sca1-/Hoechst+ cells were sorted in to full myoblast growth media using the FACSARIAIII cell sorter (BD Biosciences).

Myoblast growth and differentiation culture

Purified MuSCs were seeded onto collagen-coated plates and expanded in growth media (Ham's F10 media with 20% FBS, 2.5 ng/mL human recombinant bFGF, and 1% Penicillin/Streptomycin) at 37°C and 5% CO₂. Media was replenished every two days. To differentiate myoblasts into myotubes, myoblasts were grown to 90% confluency in growth media, washed twice with 1X PBS, and switched to differentiation media (DMEM, 1% FBS, and 1% Penicillin/Streptomycin). For inhibitor treatment, cells were incubated with 0.033% DMSO or 1 μ M MS023 (Sigma) in 0.033% DMSO and media was replenished every second day for the duration of the indicated treatment time.

Western blot

Proteins from total cell or tissue lysate (50 mM HEPES [pH 7.4], 150 mM NaCl, and 1% Triton X-100) were resolved on SDS 8-15% polyacrylamide gels and transferred onto nitrocellulose membranes using the Trans-Blot turbo transfer system (BioRad). Membranes were blotted with the primary antibodies against aDMA (Millipore), SDMA (Millipore), and β -Actin (Sigma) overnight at 4°C. Following 3 washes in TBST, membranes were incubated with HRP-conjugated secondary antibodies (Sigma) for 45 min and visualised on X-ray films with Western Lightning Plus ECL (Perkin Elmer).

Cultured myoblast immunofluorescence

Myoblasts expanded in growth media were seeded onto collagen-coated glass coverslips (VWR) in 6-well plates. Coverslips were transferred to a 12-well plate containing 4% paraformaldehyde (PFA) and cells were fixed for 15 min at room temperature. Cells were then permeabilized with 0.2% Triton X-100, 0.125M glycine in PBS for 12 min at room temperature (RT). Incubation with blocking buffer (2% BSA, 5% horse serum and 0.1% Triton X-100) proceeded for 1 h at RT. Primary antibodies were diluted in blocking buffer to detect PAX7 (Developmental Studies Hybridoma Bank, 1:100), MyoD (Santa Cruz Biotechnology, 1:200), or ki67 (abcam, 1:1000). After 16h incubation at 4°C, cells were washed 3 times with 1X PBS for 10 min. Secondary antibody (AlexaFluor anti-mouse or anti-rabbit 488nm or 568nm) was used at a dilution of 1:400 in blocking buffer for 45 min in the dark at RT. Cells were washed 3 times for 10 min with 1X PBS. Finally, the cover slips were transferred to a microscope slide and mounted with ProLong Gold Antifade Mountant with DAPI (ThermoFisher Scientific). Cells were then visualized on a Zeiss Axio Imager M1 microscope (Carl Zeiss, Thornwood NY), and resulting images were analyzed using Zeiss' ZEN Digital imaging suite software.

Muscle fiber isolation and culture

Wild type mice were sacrificed and their extensor digitorum longus (EDL) muscles were dissected using standard dissection techniques. Isolated muscles were incubated with 0.4% collagenase (Sigma) in DMEM for 30 min at 37°C and 5% CO₂. Whole muscle was then triturated with a plastic disposable Bohr pipette to dissociate individual fibers from the whole muscle as described previously (Gallot et al., 2016). To mimic activating conditions, fibers were cultured in fiber growth media (DMEM plus 20% FBS, 1% chick embryo extract, 2.5 ng/mL bFGF, 1% penicillin/streptomycin) at 37°C and 5% CO₂. For quiescent satellite cell analysis, fibers were fixed immediately following dissociation using 4% PFA prepared fresh in 1X PBS.

Muscle fiber immunofluorescence

Cultured muscle fibers from wild type mice were fixed in 4% paraformaldehyde PFA and washed twice with 1X PBS. Fibers were then permeabilized with 0.2% Triton X-100, 0.125M glycine in PBS for 15 min at RT. Blocking followed for one hour at room temperature with 2% BSA, 5% horse serum and 0.1% Triton X-100. Primary antibodies were diluted in blocking buffer to detect PAX7 (Developmental Studies Hybridoma Bank, 1:100), MyoD (Santa Cruz Biotechnology, 1:200), ki67 (abcam, 1:1000). After 16h incubation at 4°C, fibers were washed 3 times with 1X PBS for 10 min. Secondary antibody (AlexaFluor anti-mouse or anti-rabbit 488nm or 568nm) was used at a dilution of of 1:400 in blocking buffer for 45 min in the dark at RT. Fibers were washed 3 times for 10 min with 1X PBS. Finally, the fibers were transferred to a microscope slide outlined using an ImmEdge hydrophobic barrier pen and mounted with ProLong Gold Antifade Mountant with DAPI (ThermoFisher Scientific). Fiber-associated satellite cells were then visualized on a Zeiss Axio Imager M1 microscope (Carl Zeiss, Thornwood NY), and resulting images were analyzed using Zeiss' ZEN Digital imaging suite software.

scRNA-seq sample preparation and computational analysis

Each biological replicate for the scRNA-seq corresponded to one wild type C57BL/6 mouse. The purified MuSCs were cultured in Ham's F10 (Gibco) with 20% FBS (HyClone), 2.5 ng/mL human recombinant bFGF (Gibco), 1% Penicillin/Streptomycin (Wisent Inc.) with 0.033% DMSO or 1 μ M MS023 in 0.033% DMSO. The medium was changed on day 2 and day 4 of culturing. The purified MuSCs from each replicate were stained for viability with calcein-AM and ethidium-homodimer1 (P/ N L3224 Thermo Fisher Scientific). scRNA libraries were generated using the GemCode Single- Cell Instrument (10x Genomics, Pleasanton, CA, USA) and Single Cell 3' Library & Gel Bead Kit v2 and Chip Kit (P/N 120236 P/N 120237 10x Genomics). The sequencing

ready libraries were purified with SPRIselect, quality controlled for sized distribution and yield (LabChip GX Perkin Elmer), and quantified using qPCR (KAPA Biosystems Library Quantification Kit for Illumina platforms P/N KK4824) as previously described (Couturier et al., 2020). Libraries were subsequently shipped and sequenced using Illumina NovaSeq6000 at IGM Genomics Center, UCSD, San Diego, CA. Cell barcodes and UMI (unique molecular identifiers) barcodes were demultiplexed and paired-end reads were first aligned to the mouse genome (mm10) using the Cell Ranger software v3.1.0 (10X Genomics, <https://support.10xgenomics.com/single-cell-gene-expression/software/pipelines/latest/what-is-cell-ranger>). Pre-processing was then carried out with the Seurat v3.2.0 R package (Butler et al., 2018). Genes detected in less than 3 cells as well as cells containing less than 200 genes detected were removed. Cells were further filtered out for each sample based on the distribution of genes detected as well as the percentage of mitochondrial counts to balance the number of cells per sample to ~4000, and the raw count matrices of all samples were merged. Read counts for each cell were then normalized by the cell total, multiplied by 10000 and natural-log transformed. The expression of the 2000 genes with highest cell-to-cell variation was standardized and the heterogeneity associated with mitochondrial contamination was regressed out. Principal component analysis was performed on the scaled data and the top 10 principal components were used to construct a K-nearest neighbor cell graph. Clustering of cells was carried out through the Louvain algorithm with the granularity parameter set to 0.4 and visualized with the Uniform Manifold Approximation and Projection (UMAP) (Becht et al., 2019) dimensional reduction technique using the Scanpy v1.5.2 python module (Wolf et al., 2018). Cluster biomarkers were identified using the Wilcoxon Rank Sum test. Cell trajectories across pseudotime were analyzed by the Monocle v2.16.0 R package (Trapnell et al., 2014). Cell progress was defined by differentially expressed genes based on the clusters identified

by Seurat. The dimensionality of the data was reduced through the Discriminative Dimensionality Reduction with Trees (DDRTree) algorithm to two dimensions and the cells were ordered along the trajectory according to pseudotime. Genes with branch-dependent expression were identified through the branched expression analysis modeling (BEAM) test. RNA velocity analysis was performed by the scVelo v0.2.2 python module (Bergen et al., 2020). Spliced and unspliced mRNAs were first distinguished through the velocity v0.17.17 python module (La Manno et al., 2018). Velocities representing the direction and speed of cell motion were then computed and projected onto the UMAP embedding.

Oxygen consumption rate and extracellular acidification measurements

Oxygen consumption rates (OCR) and extracellular acidification rate (ECAR) were measured using a Seahorse XFe96 Flux Analyzer and analyzed with Wave 2.6.0 software (Agilent Technologies). FACS sorted muscle stem cells were seeded in a matrigel-coated 96-well plate and cultured with MS023 or DMSO for 48 h. Cells were incubated in MitoStress test assay media (DMEM 5030 media, 10mM glucose, 1mM sodium pyruvate, 2mM glutamine, PH7.4) or GlycoStress test assay media (DMEM 5030 media, 2mM glutamine, pH 7.4) 1 h prior to OCR and ECAR measurements, respectively. Oligomycin (3mM, Sigma-Aldrich), carbonyl cyanide-p-trifluoromethoxy-phenylhydrazone (FCCP; 1mM, Abcam) and rotenone-antimycin A (RAA; 2.5mM, Sigma-Aldrich) were added to cells to measure OCR parameters while glucose (10mM, Sigma-Aldrich), Oligomycin (1mM, Sigma-Aldrich) and 2-DG (100mM) were used to measure ECAR parameters. Following the assay, cells were stained with crystal violet and nuclei were counted in each well for normalization.

MuSC engraftment and muscle histology

Primary MuSCs were FACS-purified from donor GFP mice and cultured with MS023 or DMSO for 5 days. Cells were then trypsinized, resuspended in 1X PBS, and pelleted for 10 min at 1,800 RPM. Cell pellets were resuspended in 1ml of 1X PBS and counted using a haemocytometer. 15,000 cells from each condition were then injected into the TA muscle of wild type mice. Recipient mice were also injected with 50 μ l of 10 μ M cardiotoxin (CTX) 24h prior to MuSC engraftment to induce muscle regeneration. Recipient mice were sacrificed 3 weeks after CTX injection, and the TA muscles were dissected and fixed in 2% PFA at 4°C for 16 h. Fixed TA muscles were then embedded in OCT and frozen prior to cryosectioning onto a glass microscope slide. Resulting tissue sections were permeabilized for 12 min with 0.2% Triton X-100, 0.125M glycine in PBS at RT. Blocking followed with M.O.M blocking reagent (Vector Laboratories) for 1 h at RT. Primary antibodies were diluted in blocking reagent to detect PAX7 (Developmental Studies Hybridoma Bank, 1:10) and laminin (Sigma, 1:50). After 16h incubation at 4°C, sections were washed 3 times with 1X PBS for 10 min. Secondary antibody (AlexaFluor anti-mouse or anti-rabbit 488nm or 568nm) was used at a dilution of 1:400 in blocking reagent for 45 min in the dark at RT. Sections were then washed 3 times for 10 min with 1X PBS. Tissue sections were mounted with ProLong Gold Antifade Mountant with DAPI (ThermoFisher Scientific) and covered with a coverslip. Visualization was performed on a Zeiss Axio Imager M1 microscope (Carl Zeiss, Thornwood NY), and resulting images were analyzed using Zeiss' ZEN Digital imaging suite software.

MS023 injection in mdx mice

12-week old *mdx* mice received an intraperitoneal injection of 80 mg/kg MS023 (Sigma) dissolved in 50 μ l N-methyl-2-pyrrolidone, 200 μ l Captisol, 200 μ l polyethylene glycol 400 and 550 μ l PBS once per day for three consecutive days. As control, 12-week old mice received vehicle (50 μ l N-

methyl-2-pyrrolidone, 200 μ l Captisol, 200 μ l polyethylene glycol 400 in 550 μ l PBS) alone. Grip strength and hanging test measurements were taken at 10 and 20 days after the final injection. 29 days after the final injection, mice were anesthetized and sacrificed for endpoint *in situ* force measurements. Tail pieces were collected 48h after the last injection and lysed for western blot analysis with anti-aDMA and anti-sDMA and β -actin antibodies.

Grip strength measurements and hanging test

Peak grip strength was measured for the front two paws and for all four limbs using a Bioseb Grip Strength Test instrument. Each mouse was placed on the rod (2 paws) or mesh (4 paws) and pulled from the tail three times. The highest measurement was retained for subsequent analysis. To assess endurance, mice were placed on a plastic mesh taped to a hollow cylinder. The cylinder was slowly inverted over soft bedding to allow mice to grip the mesh, and the amount of time each mouse remained suspended before falling onto the bedding was recorded 3 times. The longest time measurement was retained for analysis.

In situ force measurements of mdx mice

Proximal and distal tendons of the EDL were attached with silk suture (3.0) and the muscle was carefully isolated and placed in a buffered physiological solution (Krebs-Ringer supplemented with glucose and bubbling carbogen gas) maintained at 25°C. The muscles were attached to an electrode at one end, and to a lever arm at the other end (300C-LR dual-mode lever; Aurora Scientific, Canada). Optimal muscle length (L_0) was determined and gradually adjusted until the maximum isometric twitch tension was achieved, at which point the muscles were allowed a 10 min equilibration in the bath prior the contractile measurement. Muscles were stimulated at 25V at different frequencies (10, 25, 50, 80, 100, 150 Hz; 2 min rest between each stimulation) to obtain a force-frequency curve. Thereafter, muscle length and weight were measured. Muscle specific

muscle force (N/cm^2) was determined using the following formula: (force (N) x fiber length (0.44 x L_0 for the EDL muscle) x muscle density ($1.06 \text{ g}/\text{cm}^3$))/muscle mass (g) (Dufresne et al., 2016; Dumont and Frenette, 2013).

DECLARATION OF INTERESTS

The authors declare no competing interests.

ACKNOWLEDGEMENTS

The authors would like to thank Chris Young and Mathew Duguay at the LDI Flow Cytometry Facility for their assistance with FACS experiments. We would also like to thank Dr. Vahab Soleimani for thoughtful discussions. The research was funded by Canadian Institute of Health Research FDN-154303 to S.R. C.D. holds a studentship from the fonds de la recherche en santé du Québec (FRQS).

AUTHOR CONTRIBUTIONS

C.D conceptualized the project, conducted the experiments, and wrote the paper. S.R. conceptualized the project, secured funding, supervised the research, and wrote the paper. O.V. performed bioinformatics analysis of scRNAseq data. N.D. critically reviewed the paper and supervised the *mdx* injection experiments. J.D performed the *mdx* injections and C.D and J.D recorded strength measurements. J.J supervised the Seahorse experiments, and E.H. and C.D performed the Seahorse experiments and analysis. Y.C. performed the library preparations of the scRNAseq samples under supervision of J.R.

3.7 References

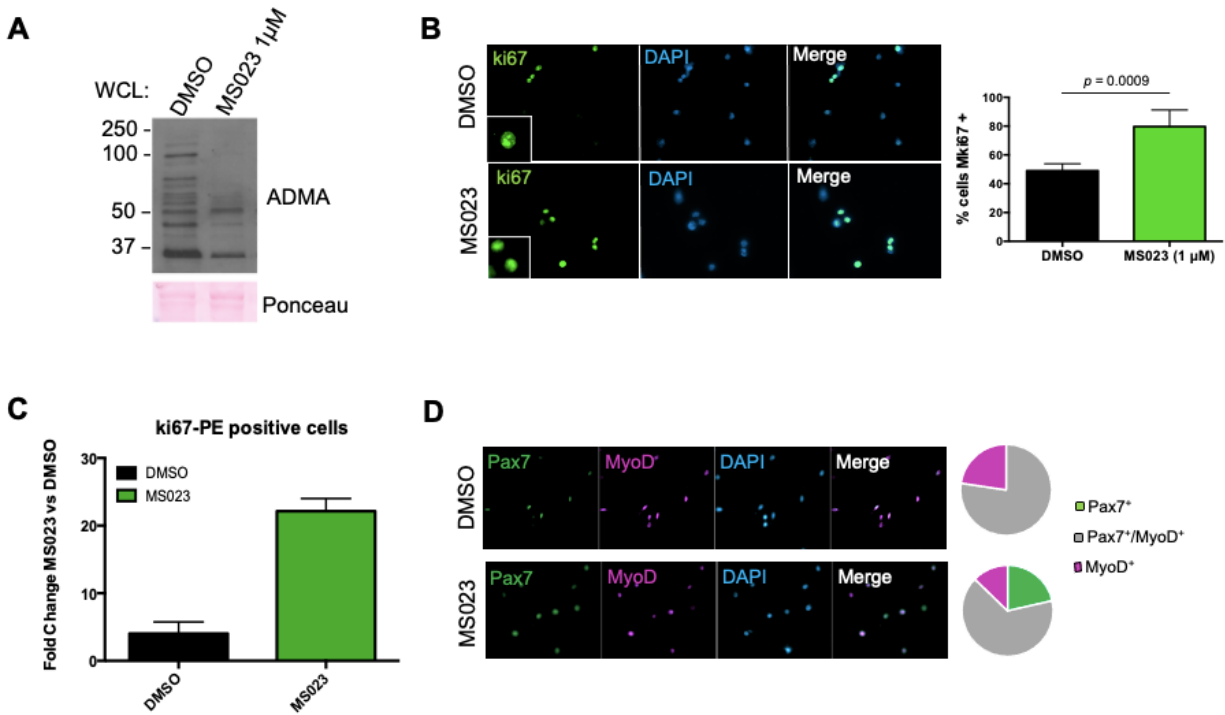
- Bayen, S., Saini, S., Gaur, P., Duraisamy, A.J., Kumar Sharma, A., Pal, K., Vats, P., and Singh, S.B. (2018). PRMT1 promotes hyperglycemia in a FoxO1-dependent manner, affecting glucose metabolism, during hypobaric hypoxia exposure, in rat model. *Endocrine* 59, 151-163.
- Bedford, M.T., and Clarke, S.G. (2009). Protein arginine methylation in mammals: who, what, and why. *Molecular cell* 33, 1-13.
- Bentzinger, C.F., von Maltzahn, J., Dumont, N.A., Stark, D.A., Wang, Y.X., Nhan, K., Frenette, J., Cornelison, D.D., and Rudnicki, M.A. (2014). Wnt7a stimulates myogenic stem cell motility and engraftment resulting in improved muscle strength. *The Journal of cell biology* 205, 97-111.
- Bhattacharya, D., Shah, V., Oresajo, O., and Scimè, A. (2021). p107 mediated mitochondrial function controls muscle stem cell proliferative fates. *Nature communications* 12, 5977.
- Blanc, R.S., Vogel, G., Chen, T., Crist, C., and Richard, S. (2016). PRMT7 Preserves Satellite Cell Regenerative Capacity. *Cell reports* 14, 1528-1539.
- Blanc, R.S., Vogel, G., Li, X., Yu, Z., Li, S., and Richard, S. (2017). Arginine Methylation by PRMT1 Regulates Muscle Stem Cell Fate. *Molecular and cellular biology* 37.
- Bulfield, G., Siller, W.G., Wight, P.A., and Moore, K.J. (1984). X chromosome-linked muscular dystrophy (mdx) in the mouse. *Proceedings of the National Academy of Sciences of the United States of America* 81, 1189-1192.
- Butler, A., Hoffman, P., Smibert, P., Papalexi, E., and Satija, R. (2018). Integrating single-cell transcriptomic data across different conditions, technologies, and species. *Nature biotechnology* 36, 411-420.
- Chen, Y.-r., Li, H.-n., Zhang, L.-j., Zhang, C., and He, J.-g. (2021). Protein Arginine Methyltransferase 5 Promotes Esophageal Squamous Cell Carcinoma Proliferation and Metastasis via LKB1/AMPK/mTOR Signaling Pathway. *Frontiers in Bioengineering and Biotechnology* 9.
- Cho, D.S., and Doles, J.D. (2017). Single cell transcriptome analysis of muscle satellite cells reveals widespread transcriptional heterogeneity. *Gene* 636, 54-63.
- Couturier, C.P., Ayyadhury, S., Le, P.U., Nadaf, J., Monlong, J., Riva, G., Allache, R., Baig, S., Yan, X., Bourgey, M., *et al.* (2020). Single-cell RNA-seq reveals that glioblastoma recapitulates a normal neurodevelopmental hierarchy. *Nature communications* 11, 3406.
- De Micheli, A.J., Laurilliard, E.J., Heinke, C.L., Ravichandran, H., Fraczek, P., Soueid-Baumgarten, S., De Vlaminck, I., Elemento, O., and Cosgrove, B.D. (2020). Single-Cell Analysis of the Muscle Stem Cell Hierarchy Identifies Heterotypic Communication Signals Involved in Skeletal Muscle Regeneration. *Cell reports* 30, 3583-3595.e3585.
- Dell'Orso, S., Juan, A.H., Ko, K.D., Naz, F., Perovanovic, J., Gutierrez-Cruz, G., Feng, X., and Sartorelli, V. (2019). Single cell analysis of adult mouse skeletal muscle stem cells in homeostatic and regenerative conditions. *Development (Cambridge, England)* 146.
- Dumont, N.A., Wang, Y.X., von Maltzahn, J., Pasut, A., Bentzinger, C.F., Brun, C.E., and Rudnicki, M.A. (2015). Dystrophin expression in muscle stem cells regulates their polarity and asymmetric division. *Nature medicine* 21, 1455-1463.
- Folmes, C.D., Dzeja, P.P., Nelson, T.J., and Terzic, A. (2012). Metabolic plasticity in stem cell homeostasis and differentiation. *Cell stem cell* 11, 596-606.

- Fu, X., Xiao, J., Wei, Y., Li, S., Liu, Y., Yin, J., Sun, K., Sun, H., Wang, H., Zhang, Z., *et al.* (2015a). Combination of inflammation-related cytokines promotes long-term muscle stem cell expansion. *Cell research* 25, 1082-1083.
- Fu, X., Zhu, M.J., Dodson, M.V., and Du, M. (2015b). AMP-activated protein kinase stimulates Warburg-like glycolysis and activation of satellite cells during muscle regeneration. *The Journal of biological chemistry* 290, 26445-26456.
- Gallot, Y.S., Hindi, S.M., Mann, A.K., and Kumar, A. (2016). Isolation, Culture, and Staining of Single Myofibers. *Bio-protocol* 6.
- Greer, E.L., Oskoui, P.R., Banko, M.R., Maniar, J.M., Gygi, M.P., Gygi, S.P., and Brunet, A. (2007). The energy sensor AMP-activated protein kinase directly regulates the mammalian FOXO3 transcription factor. *The Journal of biological chemistry* 282, 30107-30119.
- Hardie, D.G., Schaffer, B.E., and Brunet, A. (2016). AMPK: An Energy-Sensing Pathway with Multiple Inputs and Outputs. *Trends in cell biology* 26, 190-201.
- Herzig, S., and Shaw, R.J. (2018). AMPK: guardian of metabolism and mitochondrial homeostasis. *Nature Reviews Molecular Cell Biology* 19, 121-135.
- Hindupur, S.K., González, A., and Hall, M.N. (2015). The opposing actions of target of rapamycin and AMP-activated protein kinase in cell growth control. *Cold Spring Harbor perspectives in biology* 7, a019141.
- Hori, S., Hiramuki, Y., Nishimura, D., Sato, F., and Sehara-Fujisawa, A. (2019). PDH-mediated metabolic flow is critical for skeletal muscle stem cell differentiation and myotube formation during regeneration in mice. *FASEB journal : official publication of the Federation of American Societies for Experimental Biology* 33, 8094-8109.
- Iwasaki, H., and Yada, T. (2007). Protein arginine methylation regulates insulin signaling in L6 skeletal muscle cells. *Biochemical and biophysical research communications* 364, 1015-1021.
- Judson, R.N., Quarta, M., Oudhoff, M.J., Soliman, H., Yi, L., Chang, C.K., Loi, G., Vander Werff, R., Cait, A., Hamer, M., *et al.* (2018). Inhibition of Methyltransferase Setd7 Allows the In Vitro Expansion of Myogenic Stem Cells with Improved Therapeutic Potential. *Cell stem cell* 22, 177-190.e177.
- Kim, H., Selvaraj, S., Kiley, J., Azzag, K., Garay, B.I., and Perlingeiro, R.C.R. (2021). Genomic Safe Harbor Expression of PAX7 for the Generation of Engraftable Myogenic Progenitors. *Stem cell reports* 16, 10-19.
- Kim, J., Kundu, M., Viollet, B., and Guan, K.-L. (2011). AMPK and mTOR regulate autophagy through direct phosphorylation of Ulk1. *Nature cell biology* 13, 132-141.
- Kimmel, J.C., Hwang, A.B., Scaramozza, A., Marshall, W.F., and Brack, A.S. (2020). Aging induces aberrant state transition kinetics in murine muscle stem cells. *Development (Cambridge, England)* 147.
- L'Honoré, A., Commère, P.H., Negroni, E., Pallafacchina, G., Friguet, B., Drouin, J., Buckingham, M., and Montarras, D. (2018). The role of Pitx2 and Pitx3 in muscle stem cells gives new insights into P38 α MAP kinase and redox regulation of muscle regeneration. *eLife* 7.
- Lepper, C., Partridge, T.A., and Fan, C.M. (2011). An absolute requirement for PAX7-positive satellite cells in acute injury-induced skeletal muscle regeneration. *Development (Cambridge, England)* 138, 3639-3646.
- Machado, L., Esteves de Lima, J., Fabre, O., Proux, C., Legendre, R., Szegedi, A., Varet, H., Ingerslev, L.R., Barrès, R., Relaix, F., *et al.* (2017). In Situ Fixation Redefines Quiescence and Early Activation of Skeletal Muscle Stem Cells. *Cell reports* 21, 1982-1993.

- Marin, T.L., Gongol, B., Zhang, F., Martin, M., Johnson, D.A., Xiao, H., Wang, Y., Subramaniam, S., Chien, S., and Shyy, J.Y. (2017). AMPK promotes mitochondrial biogenesis and function by phosphorylating the epigenetic factors DNMT1, RBBP7, and HAT1. *Science signaling* *10*.
- McKellar, D.W., Walter, L.D., Song, L.T., Mantri, M., Wang, M.F.Z., De Vlaminck, I., and Cosgrove, B.D. (2021). Large-scale integration of single-cell transcriptomic data captures transitional progenitor states in mouse skeletal muscle regeneration. *Communications biology* *4*, 1280.
- Montarras, D., Morgan, J., Collins, C., Relaix, F., Zaffran, S., Cumano, A., Partridge, T., and Buckingham, M. (2005). Direct isolation of satellite cells for skeletal muscle regeneration. *Science (New York, NY)* *309*, 2064-2067.
- Pala, F., Di Girolamo, D., Mella, S., Yennek, S., Chatre, L., Ricchetti, M., and Tajbakhsh, S. (2018). Distinct metabolic states govern skeletal muscle stem cell fates during prenatal and postnatal myogenesis. *Journal of cell science* *131*.
- Pasut, A., Oleynik, P., and Rudnicki, M.A. (2012). Isolation of muscle stem cells by fluorescence activated cell sorting cytometry. *Methods in molecular biology (Clifton, NJ)* *798*, 53-64.
- Qiao, X., Kim, D.I., Jun, H., Ma, Y., Knights, A.J., Park, M.J., Zhu, K., Lipinski, J.H., Liao, J., Li, Y., *et al.* (2019). Protein Arginine Methyltransferase 1 Interacts With PGC1 α and Modulates Thermogenic Fat Activation. *Endocrinology* *160*, 2773-2786.
- Relaix, F., Bencze, M., Borok, M.J., Der Vartanian, A., Gattazzo, F., Mademtzoglou, D., Perez-Diaz, S., Prola, A., Reyes-Fernandez, P.C., Rotini, A., *et al.* (2021). Perspectives on skeletal muscle stem cells. *Nature communications* *12*, 692.
- Relaix, F., and Zammit, P.S. (2012). Satellite cells are essential for skeletal muscle regeneration: the cell on the edge returns centre stage. *Development (Cambridge, England)* *139*, 2845-2856.
- Rudnicki, M.A., Schnegelsberg, P.N., Stead, R.H., Braun, T., Arnold, H.H., and Jaenisch, R. (1993). MyoD or Myf-5 is required for the formation of skeletal muscle. *Cell* *75*, 1351-1359.
- Ryall, J.G., Dell'Orso, S., Derfoul, A., Juan, A., Zare, H., Feng, X., Clermont, D., Koulis, M., Gutierrez-Cruz, G., Fulco, M., *et al.* (2015). The NAD(+)-dependent SIRT1 deacetylase translates a metabolic switch into regulatory epigenetics in skeletal muscle stem cells. *Cell stem cell* *16*, 171-183.
- Ryder-Cook, A.S., Sicinski, P., Thomas, K., Davies, K.E., Worton, R.G., Barnard, E.A., Darlison, M.G., and Barnard, P.J. (1988). Localization of the mdx mutation within the mouse dystrophin gene. *The EMBO journal* *7*, 3017-3021.
- Sacco, A., Doyonnas, R., Kraft, P., Vitorovic, S., and Blau, H.M. (2008). Self-renewal and expansion of single transplanted muscle stem cells. *Nature* *456*, 502-506.
- Sakai, H., Fukuda, S., Nakamura, M., Uezumi, A., Noguchi, Y.T., Sato, T., Morita, M., Yamada, H., Tsuchida, K., Tajbakhsh, S., *et al.* (2017). Notch ligands regulate the muscle stem-like state *ex vivo* but are not sufficient for retaining regenerative capacity. *PloS one* *12*, e0177516.
- Seale, P., Sabourin, L.A., Girgis-Gabardo, A., Mansouri, A., Gruss, P., and Rudnicki, M.A. (2000). PAX7 is required for the specification of myogenic satellite cells. *Cell* *102*, 777-786.
- Serrano, A.L., Mann, C.J., Vidal, B., Ardite, E., Perdiguero, E., and Muñoz-Cánoves, P. (2011). Cellular and molecular mechanisms regulating fibrosis in skeletal muscle repair and disease. *Current topics in developmental biology* *96*, 167-201.
- Soleimani, V.D., Punch, V.G., Kawabe, Y., Jones, A.E., Palidwor, G.A., Porter, C.J., Cross, J.W., Carvajal, J.J., Kockx, C.E., van, I.W.F., *et al.* (2012). Transcriptional dominance of PAX7 in adult myogenesis is due to high-affinity recognition of homeodomain motifs. *Developmental cell* *22*, 1208-1220.

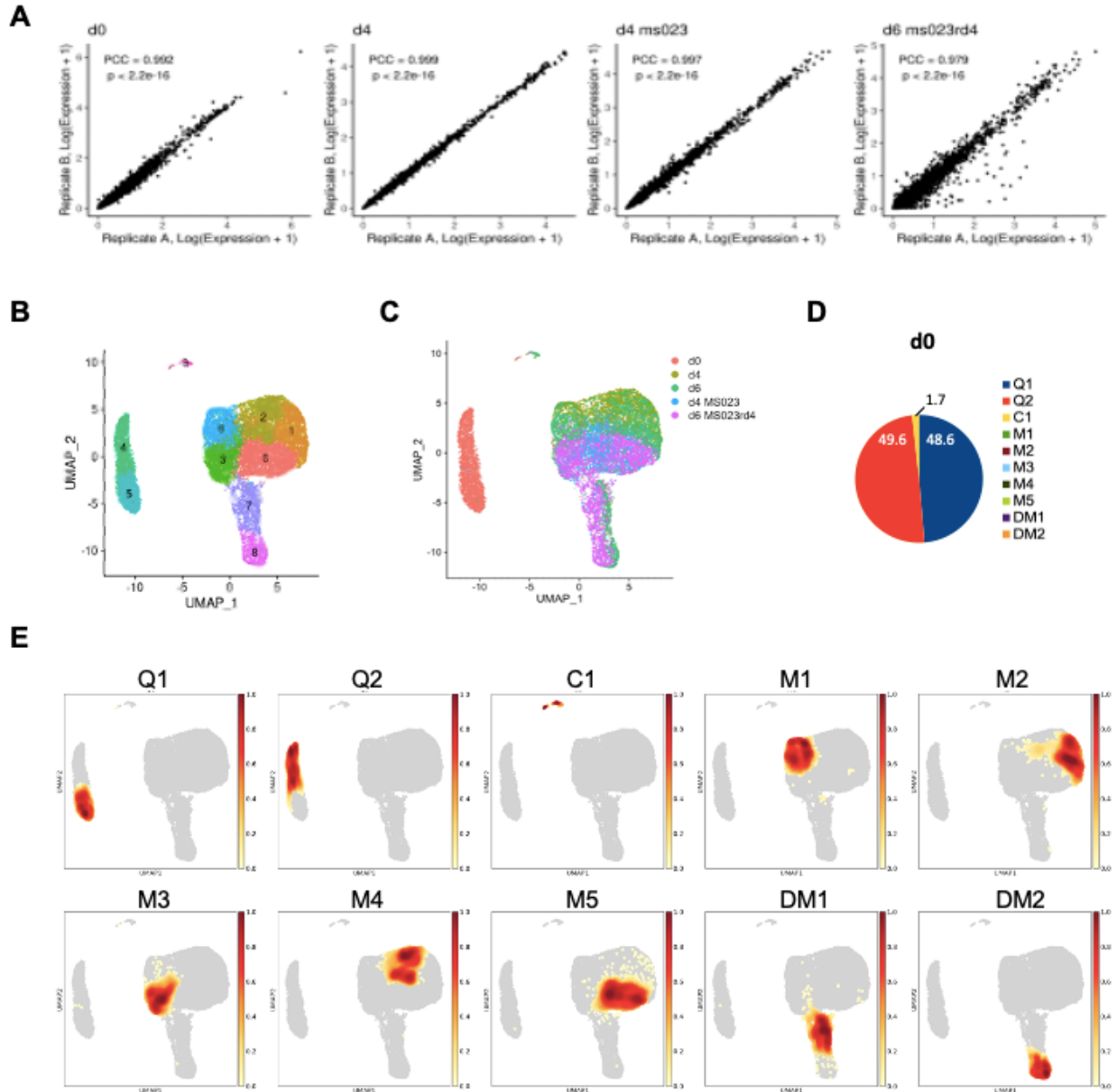
- Stouth, D.W., Manta, A., and Ljubicic, V. (2018). Protein arginine methyltransferase expression, localization, and activity during disuse-induced skeletal muscle plasticity. *American journal of physiology Cell physiology* 314, C177-c190.
- Stouth, D.W., vanLieshout, T.L., Ng, S.Y., Webb, E.K., Manta, A., Moll, Z., and Ljubicic, V. (2020). CARM1 Regulates AMPK Signaling in Skeletal Muscle. *iScience* 23, 101755.
- Teyssier, C., Ma, H., Emter, R., Kralli, A., and Stallcup, M.R. (2005). Activation of nuclear receptor coactivator PGC-1 α by arginine methylation. *Genes & development* 19, 1466-1473.
- Theret, M., Gsaier, L., Schaffer, B., Juban, G., Ben Larbi, S., Weiss-Gayet, M., Bultot, L., Collodet, C., Foretz, M., Desplanches, D., *et al.* (2017). AMPK α 1-LDH pathway regulates muscle stem cell self-renewal by controlling metabolic homeostasis. *The EMBO journal* 36, 1946-1962.
- Trapnell, C., Cacchiarelli, D., Grimsby, J., Pokharel, P., Li, S., Morse, M., Lennon, N.J., Livak, K.J., Mikkelsen, T.S., and Rinn, J.L. (2014). The dynamics and regulators of cell fate decisions are revealed by pseudotemporal ordering of single cells. *Nature biotechnology* 32, 381-386.
- Troy, A., Cadwallader, A.B., Fedorov, Y., Tyner, K., Tanaka, K.K., and Olwin, B.B. (2012). Coordination of satellite cell activation and self-renewal by Par-complex-dependent asymmetric activation of p38 α / β MAPK. *Cell stem cell* 11, 541-553.
- van den Brink, S.C., Sage, F., Vértesy, Á., Spanjaard, B., Peterson-Maduro, J., Baron, C.S., Robin, C., and van Oudenaarden, A. (2017). Single-cell sequencing reveals dissociation-induced gene expression in tissue subpopulations. *Nature methods* 14, 935-936.
- van Velthoven, C.T.J., de Morree, A., Egner, I.M., Brett, J.O., and Rando, T.A. (2017). Transcriptional Profiling of Quiescent Muscle Stem Cells In Vivo. *Cell reports* 21, 1994-2004.
- Wang, Y.X., Bentzinger, C.F., and Rudnicki, M.A. (2013). Treating muscular dystrophy by stimulating intrinsic repair. *Regenerative medicine* 8, 237-240.
- Wang, Y.X., Feige, P., Brun, C.E., Hekmatnejad, B., Dumont, N.A., Renaud, J.M., Faulkes, S., Guindon, D.E., and Rudnicki, M.A. (2019). EGFR-Aurka Signaling Rescues Polarity and Regeneration Defects in Dystrophin-Deficient Muscle Stem Cells by Increasing Asymmetric Divisions. *Cell stem cell* 24, 419-432.e416.
- Xu, J., and Richard, S. (2021). Cellular pathways influenced by protein arginine methylation: Implications for cancer. *Molecular cell*.
- Yin, H., Price, F., and Rudnicki, M.A. (2013). Satellite cells and the muscle stem cell niche. *Physiological reviews* 93, 23-67.
- Yin, S., Liu, L., Brobbey, C., Palanisamy, V., Ball, L.E., Olsen, S.K., Ostrowski, M.C., and Gan, W. (2021). PRMT5-mediated arginine methylation activates AKT kinase to govern tumorigenesis. *Nature communications* 12, 3444.
- Zhang, T., Gunther, S., Looso, M., Kunne, C., Kruger, M., Kim, J., Zhou, Y., and Braun, T. (2015). Prmt5 is a regulator of muscle stem cell expansion in adult mice. *Nature communications* 6, 7140.
- Zismanov, V., Chichkov, V., Colangelo, V., Jamet, S., Wang, S., Syme, A., Koromilas, A.E., and Crist, C. (2016). Phosphorylation of eIF2 α Is a Translational Control Mechanism Regulating Muscle Stem Cell Quiescence and Self-Renewal. *Cell stem cell* 18, 79-90.

3.8 Supplemental Information



Supplemental Figure S3.1

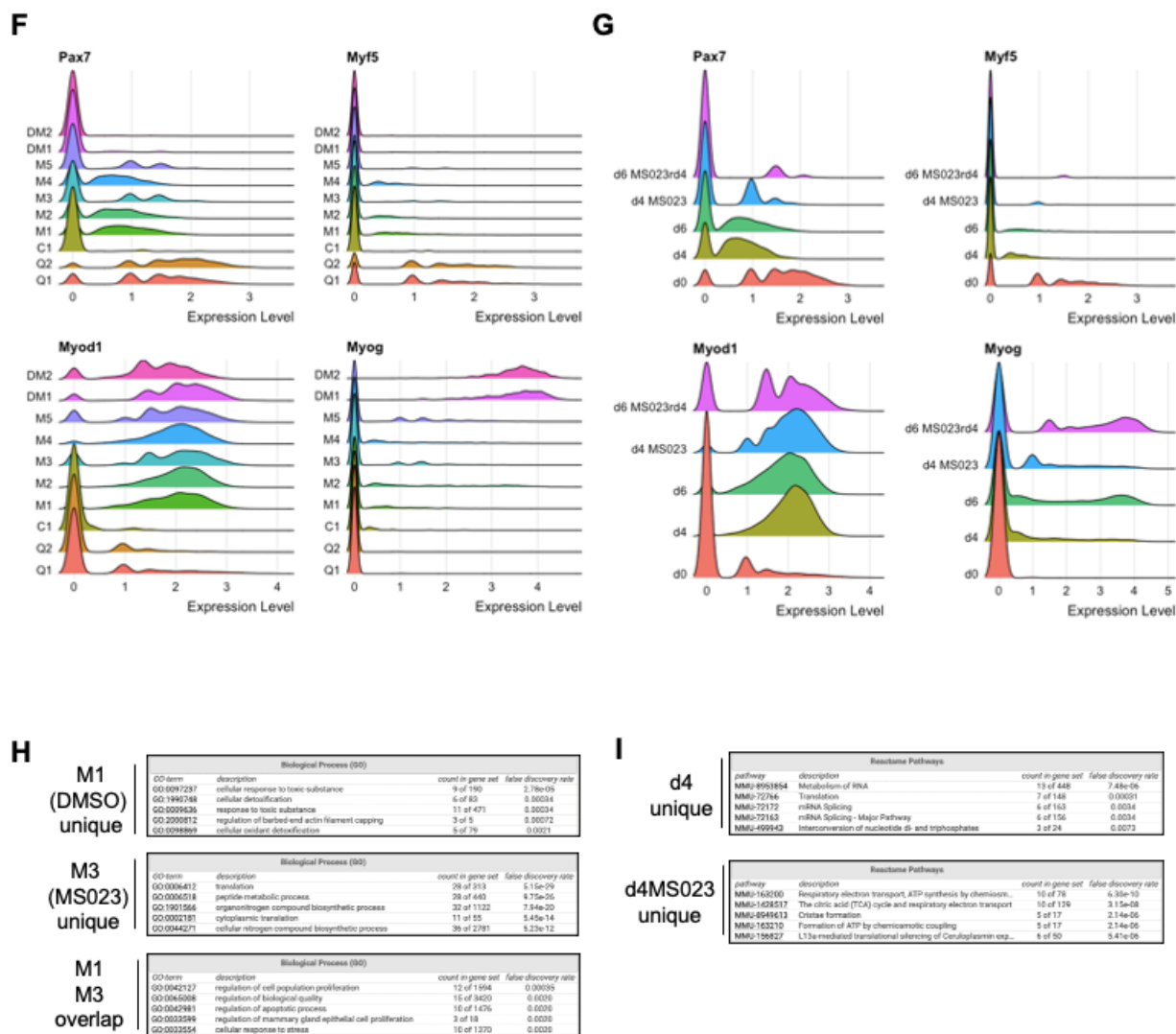
(A) Western blot of total asymmetric dimethyl arginine (aDMA) from whole cell lysate of primary myoblasts treated with MS023 (1 μ M) or DMSO. (B) Ki67 immunofluorescence of MS023-treated primary myoblasts. Error bars represent mean \pm SEM from 3 individual experiments, minimum of 200 cells per condition counted. (C) Ki67-PE immunostained MS023-treated primary myoblasts analyzed with FACS, foldchange of mean intensity calculated compared to DMSO-treated cells. Error bars represent mean \pm SEM from 3 individual replicates. (D) (left) Immunofluorescence of 14th passage MuSCs with DMSO or MS023 treatment, PAX7 (green), MyoD (purple), counterstained with DAPI. (right) Pie chart representing quantification of PAX7 and MyoD expression from cells in left panel.



Supplemental Figure S3.2

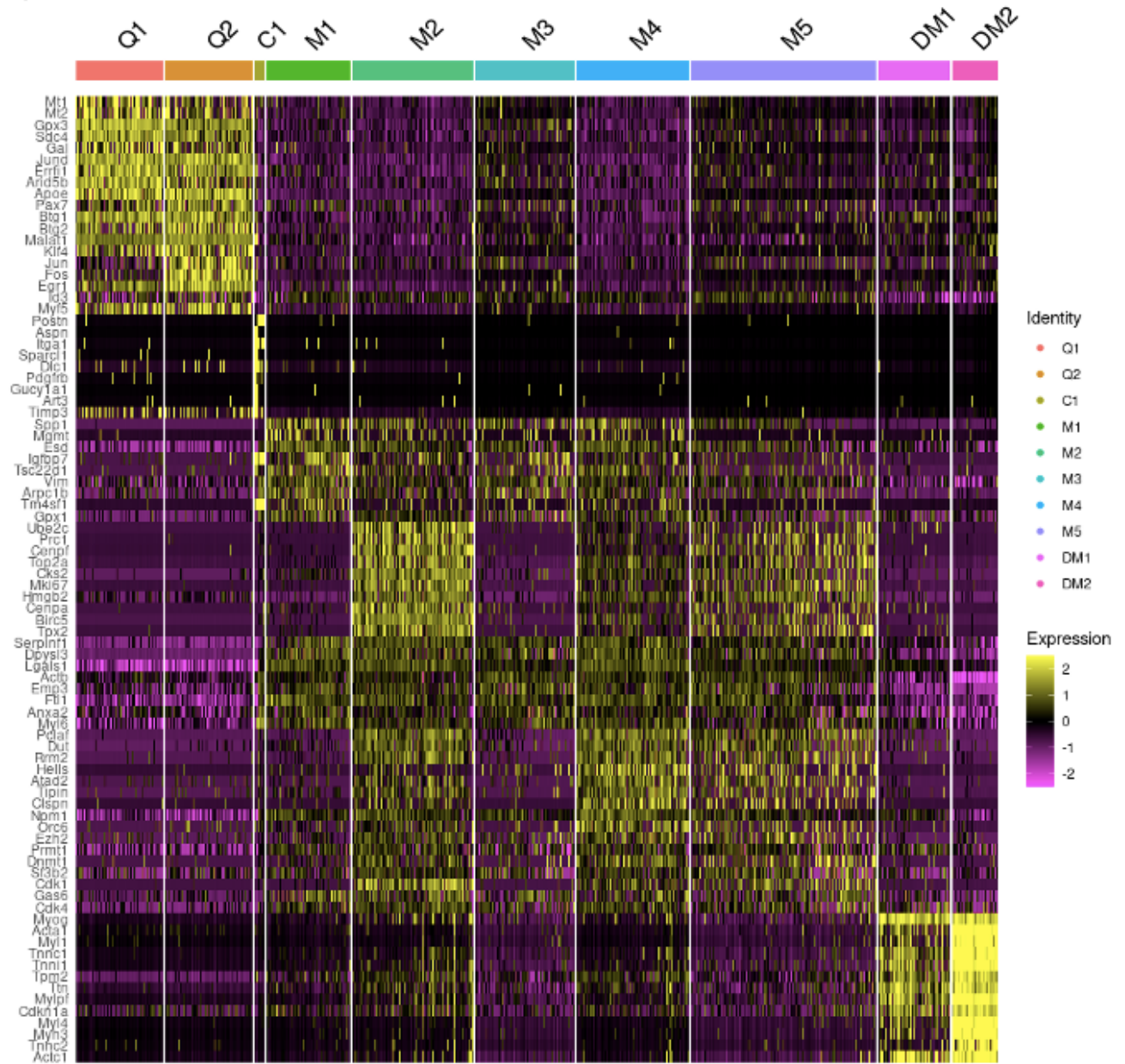
(A) Reproducibility of average gene expression across biological replicates represented as Pearson correlation coefficients. (B) UMAP plot labelled with clusters 0-9. (C) Distribution of individual samples mapped onto the UMAP embedding representation for all cells. (D) Distribution of cells from d0 across the clusters represented in a pie chart. Cluster colour legend indicated on the right.

(E) Distribution of individual clusters mapped onto the UMAP embedding representation for all cells.

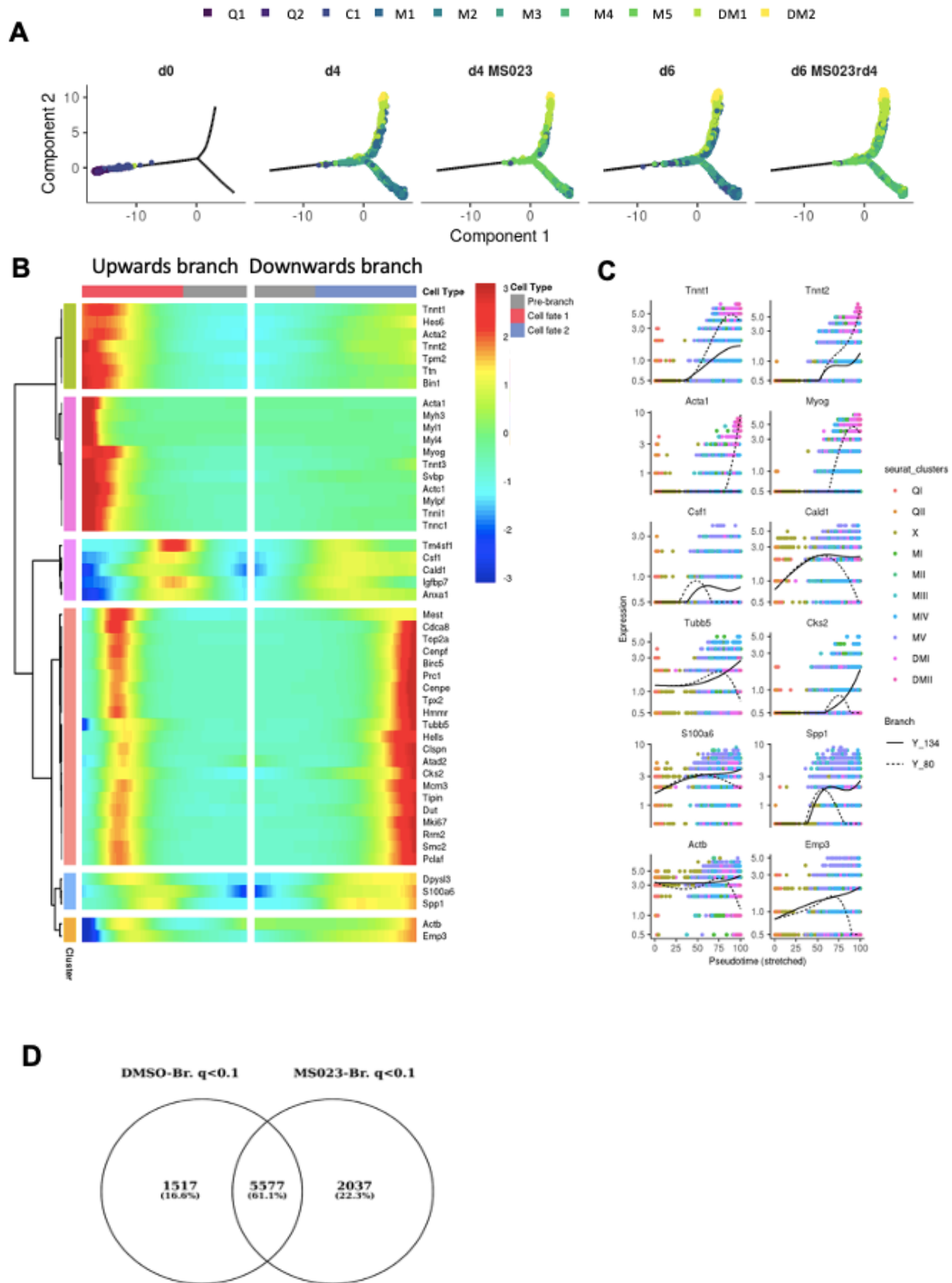


Supplemental Figure S3.2 (Cont'd)

(F) Expression RidgePlots of key myogenic markers PAX7, MYF5, MyoD (Myod1) and Myog separated by cluster. (G) Expression RidgePlots of key myogenic markers PAX7, MYF5, MyoD (Myod1) and Myog separated by sample.

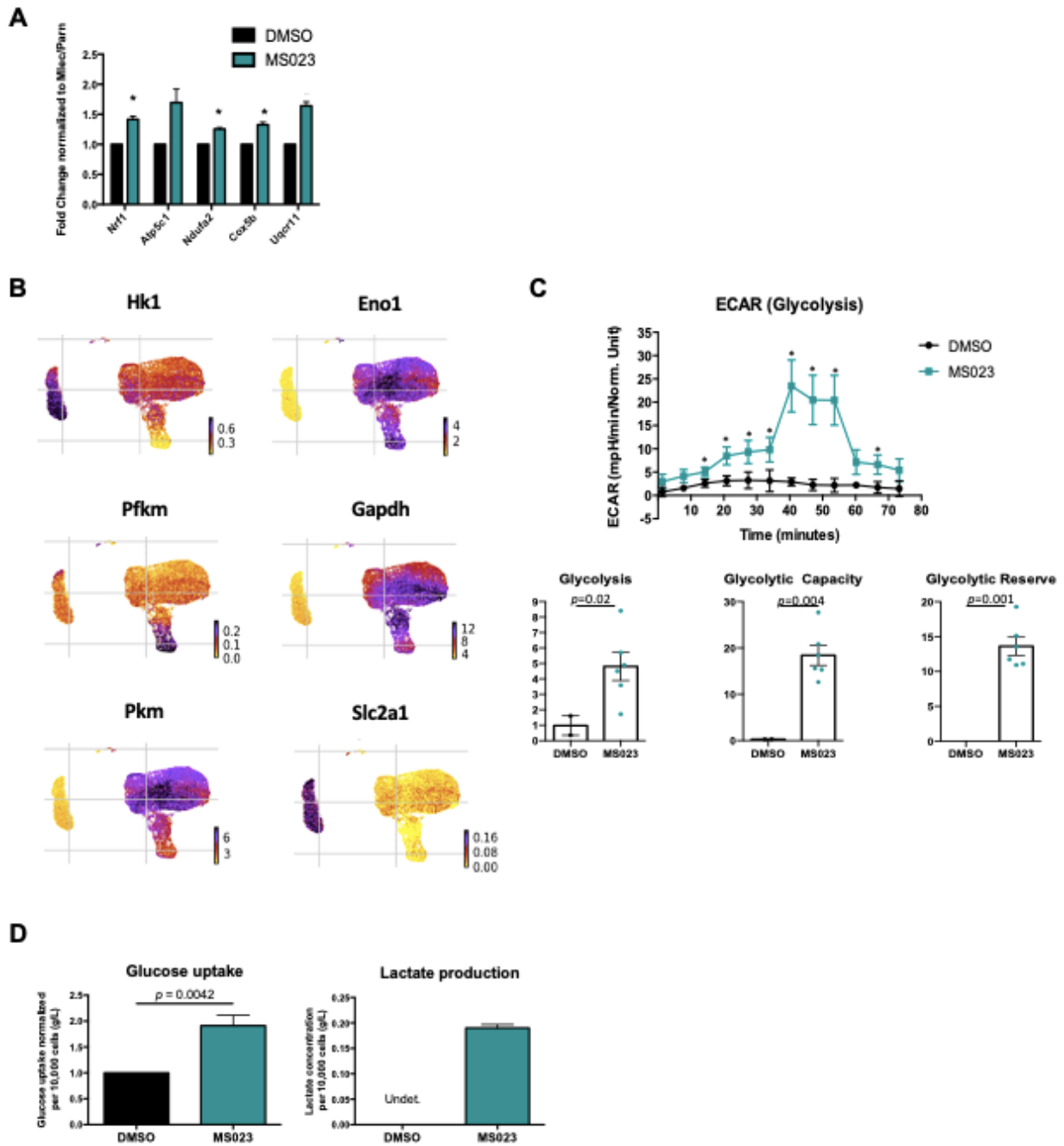
J**Supplemental Figure S3.2 (Cont'd)**

(J) Heatmap of the top 100 enriched genes in each cluster



Supplemental Figure S3.3

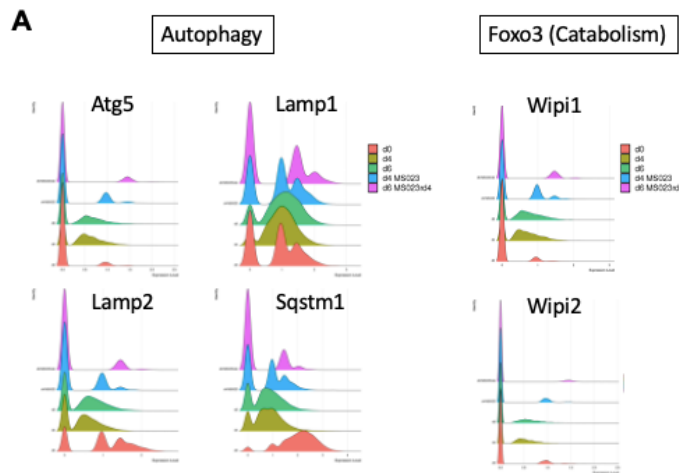
(A) Cell trajectories for each sample and cluster, with the pseudotime starting at the left endpoint of the plot. (B) Heatmap of significantly differentially expressed genes across the branchpoint of the pooled sample trajectory. (C) Distributions in the kinetic trends of each lineage for the expression for selected genes (D) Venn diagram of overlapping differentially regulated genes across the branch point of the DMSO and MS023 trajectories with a q value <0.1 .



Supplemental Figure S3.4

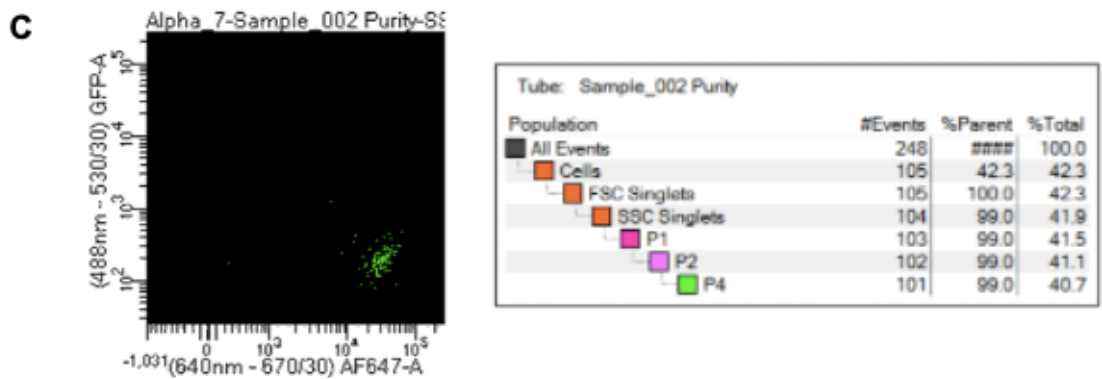
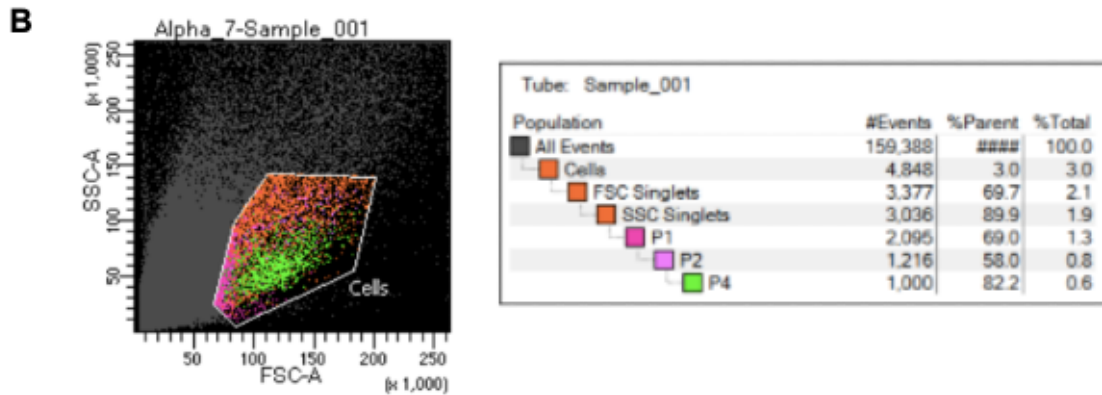
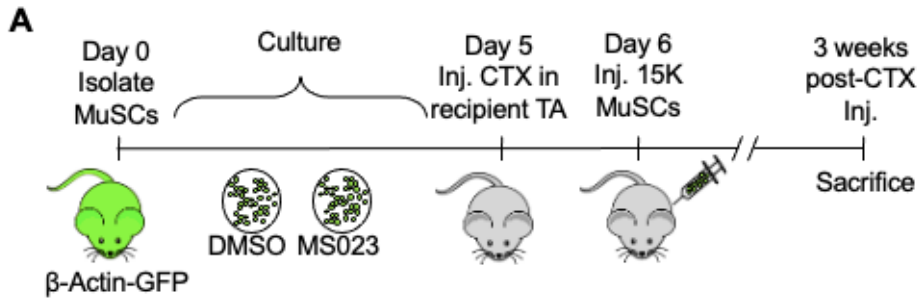
(A) Fold change of selected OxPhos genes in response to treatment with MS023. Bulk RNA was isolated from freshly purified primary myoblasts. Error bars represent mean \pm SEM from 3 biological replicates. (B) UMAP plots showing expression of components of glycolysis localized

to MS023 clusters. (C) Seahorse XF96 analysis of extracellular acidification rate (ECAR) in DMSO and MS023-treated freshly isolated primary MuSCs and quantification of glycolysis, glycolytic capacity, and glycolytic reserve. Error bars represent mean \pm SEM from 7 individual wells per condition. (D) Measurement of glucose uptake (left) and lactate production (right) as quantified from the media of d4 (DMSO) and d4MS023 (MS023) MuSCs. Error bars represent mean \pm SEM from 3 independent experiments.



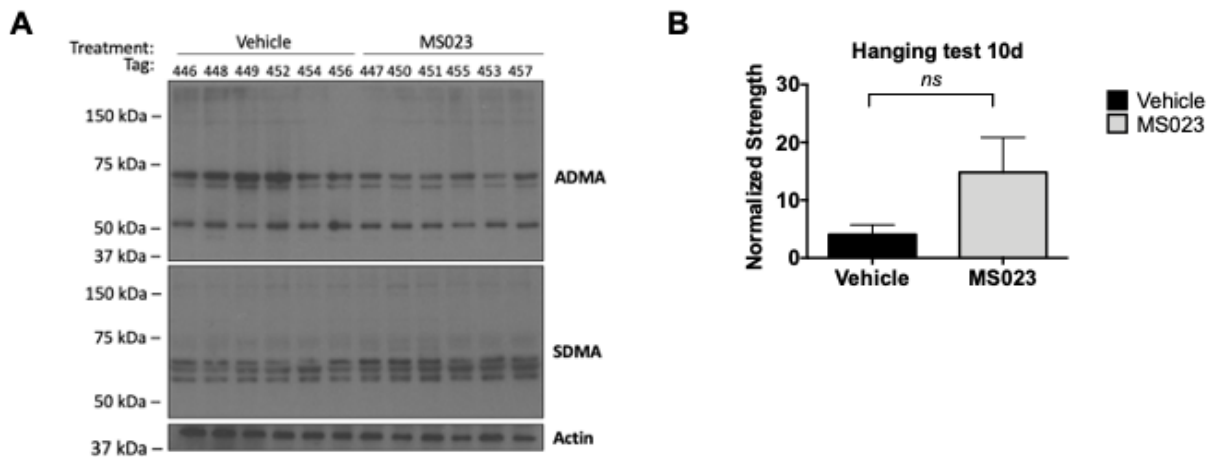
Supplemental Figure S3.5

(A) Expression RidgePlots of components of Ampk-regulated autophagy (left) and Foxo3 transcriptional targets (right) across samples.



Supplemental Figure S3.6

(A) Experimental outline for MuSC engraftment (B) FACS plot of primary purified MuSCs represented as P4 (0.6% of the total population) (C) Purity of sorted cells (99%)



Supplemental Figure S3.7

(A) Whole tissue lysate from tail pieces of mice treated with Vehicle or MS023 probed with antibodies against total asymmetric dimethyl arginine (ADMA), symmetric dimethyl arginine (SDMA), and actin for loading control. (B) Hanging test measurements taken from mice treated with vehicle or MS023 at 10d post-injection. Error bars represent mean \pm SEM from 6 biological replicates.

Chapter 4: Muscle Stem Cell Polarity Requires QKI-mediated Alternative Splicing of Integrin Alpha-7 (Itga7)

Claudia Dominici and Stéphane Richard

Life Sci Alliance. 2022 Feb 14;5(5):e202101192. DOI: 10.26508/lsa.202101192

Segal Cancer Center, Lady Davis Institute for Medical Research and Gerald Bronfman
Department of Oncology and Departments of Medicine, Human Genetics and Biochemistry,
McGill University, Montréal, Québec, Canada H3T 1E2

*Corresponding author: stephane.richard@mcgill.ca

4.1 Preface

Muscle regeneration relies on the differentiation of MuSCs into mature myoblasts. The process is launched when activated MuSCs undergo division, which can be symmetrical or asymmetrical. Asymmetrical division requires polarization of the MuSC prior to division and gives rise to a stem-like daughter cell which repopulates the stem cell pool, and a more committed myogenic progenitor cell which goes on to differentiate into mature muscle. The role of alternative splicing in establishing cell polarity and carrying out asymmetric cell division has not been well studied. In chapter 4 of this thesis, Dominici et al. investigate the role of the RNA binding protein QKI in the regulation of splicing during MuSC asymmetric division.

4.2 Abstract

Muscle stem cells (MuSCs) have the ability to carry out the specialized function of cell polarization, which is required for the production of one repopulating cell and one myogenic progenitor cell with muscle regeneration capabilities. The mechanisms which regulate proteins involved in establishing MuSC polarity such as *Dmd* and *Itga7* are currently not well understood. Herein, we define the RNA binding protein Quaking (QKI) as a major regulator alternative splicing (AS) of key MuSC polarity factors including *Dmd*, *Itga7*, *Mark2*, and *Numb*. We generate a conditional QKI knockout mouse, and for the first time it is shown *in vivo* that deficiency of QKI in MuSCs results in a loss of the myogenic progenitor cell population leading to striking regeneration defects following injury of skeletal muscle. Transcriptomic analysis of QKI-deficient MuSCs identifies QKI as a regulator of the previously uncharacterized splicing events which give rise to the mutually exclusive *Itga7*-X1 and -X2 isoforms. We observe increased X1 expression in QKI-deficient MuSCs and recapitulate this splicing event using antisense oligonucleotide (ASO) directed against a quaking binding site within the *Itga7* mRNA. Interestingly, recreating this single splicing event is detrimental to the polarization of *Itga7* and *Dmd* proteins, and leads to a drastic reduction of the myogenic progenitor population, highlighting the significance of QKI-mediated AS of *Itga7* in maintaining MuSC polarity. Altogether, these findings define a novel role for QKI as a post-transcriptional regulator of MuSC polarity.

4.3 Introduction

Muscle regeneration is a complex process which begins with the activation of tissue-resident quiescent muscle stem cells (MuSCs) (Montarras et al., 2013). Following muscle injury or disease, activated MuSCs may divide symmetrically to replenish the MuSC pool, or

asymmetrically to give rise to one repopulating stem cell and one myogenic progenitor cell (Kuang et al., 2007). Lineage progression of myogenic progenitor cells ends with terminal differentiation and fusion to construct new muscle fibers, thus completing muscle regeneration (Chargé and Rudnicki, 2004; Gurevich et al., 2016; Le Grand and Rudnicki, 2007; Relaix and Zammit, 2012). The specific subcellular localization of certain proteins is a requirement for asymmetric MuSC division. For example, dystrophin (Dmd) deficient MuSCs were observed to have asymmetric division defects, a result of faulty localization of polarity-determining proteins Mark2 and Pard3, leading to a loss of myogenic progenitor cells (Dumont et al., 2015b). More recently, it has been shown that treatment of MuSCs with exogenous epidermal growth factor (EGF) leads to polarized activation of the EGF receptor-Aurora kinase A signaling pathway which then drives asymmetric MuSC division (Wang et al., 2019b). Additionally, the Numb protein segregates to one daughter cell during mitosis, along with an unequal distribution of template DNA to provide different identities to the resulting daughter cells (Shinin et al., 2006). These findings lay important groundwork towards a better understanding of the complexities of asymmetric MuSC division. However, the role of post-transcriptional regulatory networks mediated by RNA binding proteins (RBPs) in cell polarity and asymmetric MuSC division is not understood.

The QKI RNA binding protein belongs to the hnRNP K homology (KH)-type family of RBPs (Ebersole et al., 1996; Lukong et al., 2008). QKI is a specific RBP recognizing the following the QKI response element (QRE): ACUAAY (1-20) UAAY (Y; C/U) (Galarneau and Richard, 2005) as a dimer (Beuck et al., 2012; Chen and Richard, 1998; Teplova et al., 2013). QKI is known to regulate RNA metabolism (Darbelli and Richard, 2016), in part, by influencing pre-mRNA splicing (Wu et al., 2002). There are three main isoforms named QKI-5, QKI-6, and QKI-7 for the length of their mRNAs which encode identical proteins except for the last 35 amino acids of their

C-terminus (Darbelli and Richard, 2016; Ebersole et al., 1996). QKI-5 contains a C-terminal nuclear localization signal, while QKI-6 and QKI-7 do not (Pilotte et al., 2001). QKI-deficient cells have defects in alternative splicing (AS) networks, mainly contributed to the lack of the nuclear QKI-5 isoform (Chen et al., 2021a; de Bruin et al., 2016; Hall et al., 2013; Lee et al., 2020; van der Veer et al., 2013; Zong et al., 2014).

The role of the QKI proteins and AS, in general, in MuSC physiology is not well understood. In the present study, we report that deletion of QKI in mouse MuSCs leads to a lack of production of myogenic progenitors resulting in muscle regeneration defects following injury. Transcriptomic analysis identified aberrant splicing of regulators of MuSC asymmetric division, including *Itga7*, *Dmd*, *Mark2*, and *Numb*. Indeed QKI-deficient MuSCs were unable to polarize *Itga7* and *Dmd* prior to division. Interestingly, using a 2'-O-methyl antisense oligonucleotide (ASO) to mask the QRE within *Itga7* intron 4 near the 3' splice site of exon 5 was sufficient to induce loss of polarized localization of *Dmd* and *Itga7* proteins, as observed in QKI-deficient MuSCs. These findings define QKI as a regulator of *Itga7* AS, which is required for MuSC polarity and the production of myogenic progenitors following MuSC activation.

4.4 Results

QKI-5 is expressed during the activation of primary skeletal MuSCs and throughout myogenesis.

To define the role of QKI-5 mediated AS during the early stages of activation when MuSCs exit quiescence and begin to proliferate, we confirmed its expression in myofiber-associated MuSCs. The first MuSC division on an *ex vivo* cultured myofiber occurs after approximately 40h after isolation and by 72h the MuSCs have proliferated extensively (Dumont et al., 2015b). To monitor QKI-5 expression at these critical times, we isolated myofibers from C57BL/6 mice and

cultured them for 0 (quiescent), 24, 48, or 72h. Myofibers were co-immunostained with anti-QKI-5 antibody and antibodies against MuSC markers PAX7 (at 0h) or MyoD (at 24, 48, and 72h) to identify MuSCs. We observed that nuclear QKI-5 was expressed at all time points (Figure 4.1A), indicating its presence throughout the activation and proliferation phases of MuSCs in their niche during *ex vivo* myofiber culture.

We next interrogated QKI-5 expression throughout myogenesis of primary MuSCs. Primary MuSCs were purified from C57BL/6 mice and differentiated *in vitro* with reduced serum media for 24, 48, and 72h. Total cell lysates were immunoblotted with antibodies against QKI-5 and the terminal differentiation marker myosin heavy chain (MyHC) to confirm that MuSCs were differentiated. QKI-5 protein was increased immediately after 24h of differentiation and persisted through 72h (Figure 4.1B). Together, these data show that the expression of QKI-5 increases during MuSC differentiation.

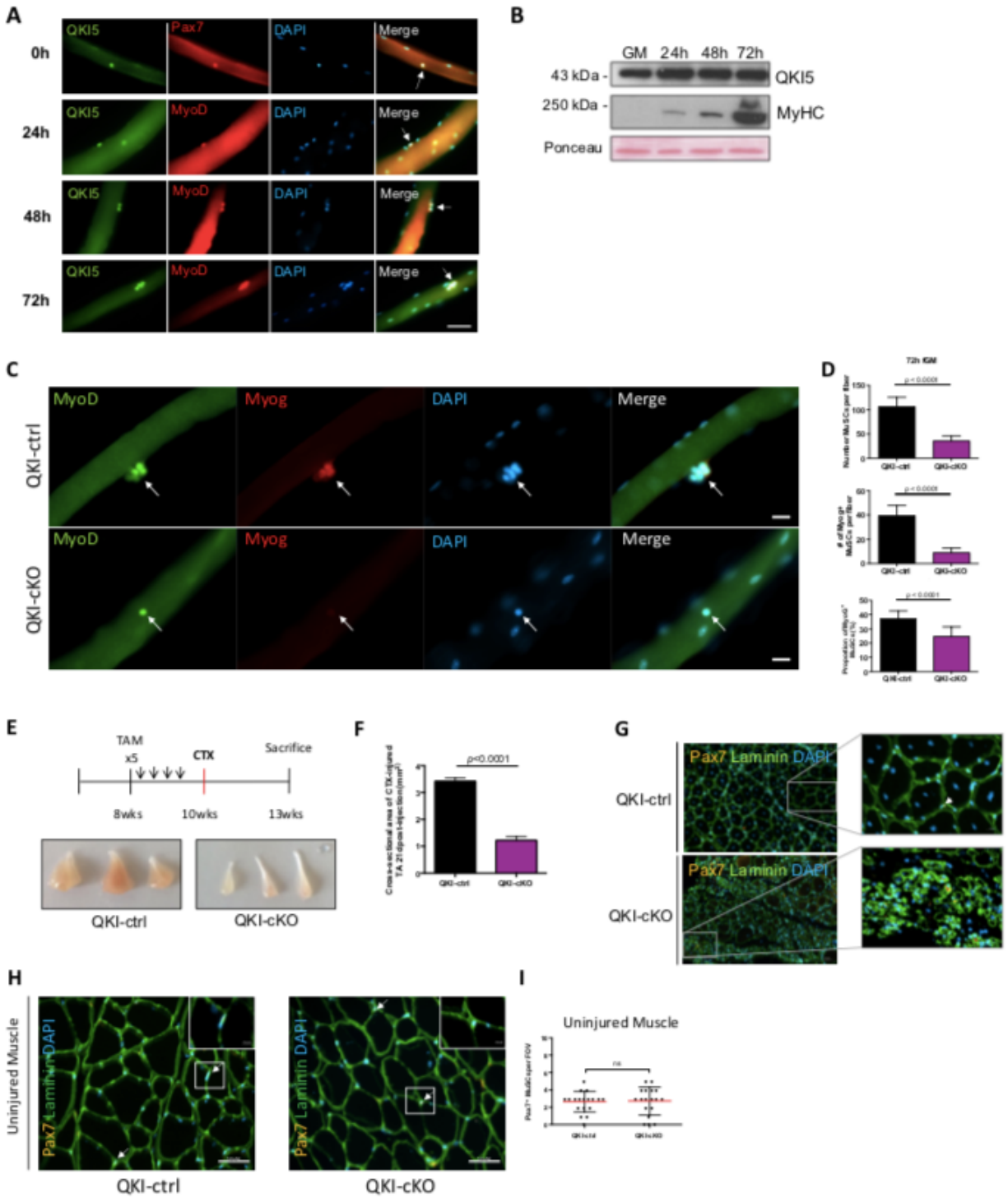


Figure 4.1. Mice with QKI-depleted MuSCs exhibit reduced myogenic progenitors and defects in skeletal muscle regeneration.

(A) Representative immunofluorescence images of myofibers isolated from wild type mice and immunostained for QKI-5 (green), and co-stained with appropriate MuSC markers (Pax7 and MyoD; Red), counterstained with DAPI. Fibers were fixed immediately after isolation (0h, quiescent MuSCs), and after 24, 48, and 72h of culture. White arrows denote MuSCs. Scale white bar represents 50 μ m. (B) Western blot of QKI-5 protein expression during a differentiation time course of primary mouse MuSCs (GM denotes growth media; 24h to 72h represent time in differentiation media; MyHC is myosin heavy chain). Ponceau red was used to show equal protein loading. (C) Muscle fibers isolated from QKI-ctrl and QKI-cKO mice and cultured in fGM for 72h, stained with MyoD (green), Myogenin (red), and counterstained with DAPI (blue) and merged. Scale bar represents 10 μ m. (D) Quantification of Myogenin-expressing MuSCs (upper panel) and total MuSCs (middle panel) from (C) (n = 3 biological replicates, minimum 1,000 cells quantified per condition, $p < 0.0001$, unpaired student's t-test). Proportion of Myog⁺ MuSCs from (C, lower panel) (n = 3 biological replicates, minimum 1,000 cells quantified per condition, $p < 0.0001$, unpaired student's t-test). (E) Timeline of tamoxifen (TAM) injections (once daily for 5 days) to induce conditional QKI knockout in MuSCs of QKI^{2lox/2lox}:Pax7^{CreERT2/+} or QKI^{2lox/2lox}:Pax7^{+/+} as ctrl, followed by cardiotoxin (CTX) injection in the TA hindlimb muscle to induce muscle injury. Three weeks after injury, the mice were sacrificed and their TA muscles isolated (n=6 biological replicates, 3 replicates depicted in bottom panels). (F) Quantification of cross-sectional area in mm² of TA muscles from QKI-ctrl and QKI-cKO mice in (E). (G) Representative immunofluorescence cross-sectional images of TA muscles 3 weeks after CTX injury from QKI-ctrl and QKI-cKO. Laminin (green) stains muscle fiber edges, Pax7 (orange) indicates MuSCs, counterstained with DAPI (blue) (n=6). (H) Cross-section of uninjured contralateral TA muscle of QKI-ctrl and QKI-cKO mice, laminin (green), Pax7 (orange), and

DAPI (blue). Pax7⁺ MuSCs magnified in insets. Scale bars represent 50 μ m. (I) Quantification of Pax7⁺ MuSCs per field of view (FOV) in QKI-ctrl and QKI-cKO TA cross sections represented in (H).

Mice with QKI-depleted MuSCs exhibit reduced myogenic progenitors and defects in skeletal muscle regeneration.

Since QKI-5 is expressed during MuSC activation and differentiation, we examined whether its presence was necessary for these processes. Conditional QKI knockout mice were generated by crossing QKI^{2lox/2lox} mice with PAX7^{CreERT2/+} mice (Murphy et al., 2011) to deplete QKI in MuSCs (QKI^{2lox/2lox};PAX7^{CreERT2/+}, herein referred to as QKI-cKO, Supplemental Figure S4.1A). QKI^{2lox/2lox}; PAX7^{+/+} littermates were used as controls, herein referred to as QKI-ctrl. Daily injections of 4-hydroxytamoxifen (TAM) for 5 days were performed on QKI-ctrl and QKI-cKO mice, and myofibers were isolated and cultured *ex vivo* for 72h revealing QKI ablation in MuSCs by immunostaining of QKI-5 (Supplemental Figure S4.1B). Interestingly, the total number of MuSCs per myofiber at 72h was reduced in QKI-cKO (35.5 ± 10.7) compared to QKI-ctrl mice (106.3 ± 18.5) (Figure S4.1C, S4.1D). In contrast, the number of MuSCs was not significantly altered shortly after activation at 24h of culture with 6.8 ± 0.4 in QKI-ctrl versus 7.2 ± 0.4 in QKI-cKO mice, nor was PAX7/MyoD expression status (Supplemental Figure S4.1C, S4.1D). We then quantified the number of differentiating myogenic progenitors based on immunostaining of the differentiation marker, myogenin (Myog). We observed a drastic reduction in the number of Myog⁺ MuSCs per QKI-cKO myofibers (8.8 ± 4.0) compared to QKI-ctrl (39.4 ± 8.5) (Figure 4.1C, 4.1D). These findings indicate that QKI deficiency does not negatively affect viability or

early stages of MuSC activation prior to the first cell division but has a marked effect on the expansion of myogenic progenitors on *ex vivo* cultured myofibers.

We reasoned that the reduced number of myogenic progenitors in QKI-cKO mice might influence muscle regeneration after cardiotoxin (CTX) injury of the tibialis anterior (TA) hindlimb muscle. Therefore, we injected CTX into the TA hindlimbs of QKI-ctrl and QKI-cKO mice (Figure 4.1E). Three weeks after injection, QKI-cKO mice had a remarkably reduced TA size with cross-sectional area of $1.2 \text{ mm}^2 \pm 0.07$ in QKI-cKO versus $3.4 \text{ mm}^2 \pm 0.06$ in QKI-ctrl (Figures 4.1E, 4.1F), and disorganized muscle fiber architecture (Figure 4.1G). Notably, the uninjured contralateral TA muscle which also contained QKI-deficient MuSCs did not have significantly different PAX7⁺ MuSC number ($2.7/\text{field of view (FOV)} \pm 0.3$ in QKI-ctrl, $2.7/\text{FOV} \pm 0.4$ in QKI-cKO) or muscle fiber architecture (Supplemental Figure S4.1E, S4.1F), consistent with our observation of unchanged MuSC number in cultured myofibers at 24h (Supplemental Figure S4.1D). Together, these data suggest that QKI is required for the generation of myogenin-expressing myogenic progenitor and muscle regeneration following injury.

QKI-deficient primary skeletal MuSCs drastically down-regulate markers of terminal differentiation.

To determine the AS events regulated by QKI-5 in MuSCs, we injected TAM daily for 5 days into QKI-ctrl and QKI-cKO mice, and purified MuSCs for *ex vivo* expansion. Following 72h in culture, total RNA was isolated and paired-end RNA-sequencing was performed (n=3 biological replicates) (Figure 4.2A). CRE-mediated deletion of *QKI* exon 2 was confirmed with RT-qPCR (Supplemental Figure S4.2A). Differentially expressed genes (DEGs) were revealed following analysis with Cufflinks v2.2.1 (Trapnell et al., 2010) and AS analysis was carried out using rMATS

v4.0.2 software (Shen et al., 2014). A PCA plot was generated following dimensionality reduction performed using the CummeRbund software package (Trapnell et al., 2012) (Supplemental Figure S4.2B), and gene expression was visualized with distribution of FPKM scores (Supplemental Figure S4.2C) and pairwise scatterplot (Supplemental Figure S4.2D) across QKI-ctrl and QKI-cKO MuSC samples. There was approximately 400 DEGs and 600 AS events (ASEs) in purified MuSCs from QKI-ctrl and QKI-cKO mice (Figure 2B). Volcano plot analysis of DEGs revealed 167 downregulated genes and 231 upregulated genes (absolute log₂ fold change >1.2, FDR <0.05, base mean >20) (Figure 2C). Pathway enrichment analysis was performed on the QKI-mediated DEGs using the Enrichr software (Chen et al., 2013; Kuleshov et al., 2016) (Figure 2D). Genes that were downregulated in QKI-cKO MuSCs were enriched for ‘muscle contraction’ and ‘actin-myosin filament sliding’ terms, which describe known functions of fully differentiated muscle (Figure 2E). Among the downregulated genes were key structural components of muscle, including *Myl1*, *Myl4*, *Myh3*, *Mylph*, *Sspn*, and *Mybph*. The downregulation of these targets was further validated with quantitative PCR (Figure 2F). The depletion of these muscle differentiation markers corroborates with defects in the number of myogenic progenitors and muscle regeneration observed in QKI-cKO mice.

Differential AS events identified in QKI-cKO MuSCs were further categorized into skipped exon (SE, 68%), multiple skipped exon (MSE, 11%), retained intron (RI, 5%), alternative 3' splice site (A3SS, 11%), and alternative 5' splice site (A5SS, 4%) (Supplemental Figure S4.2E). All significant SE events were visualized on integrative genome (IGV) browser v2.8.13 (Robinson et al., 2011). Of the skipped exon events, we observed 92 incidences of alternative last exon (ALE) usage and 191 microexon splicing events (Supplemental Figure S4.2F). Our group has recently reported that QKI also regulates the splicing of microexons in microglia cells, and we have found

38 of these events were conserved in MuSCs (Lee et al., 2020). Furthermore, approximately 65% of the AS exons in QKI-cKO MuSCs had QRE sequences in the neighbouring introns, and 45% of these QREs were located within 200 nucleotides of the exon, indicating that regulation of these AS events may be influenced directly by QKI. Overall, our transcriptomic analysis identified a dysregulated AS network in QKI-deficient primary MuSCs.

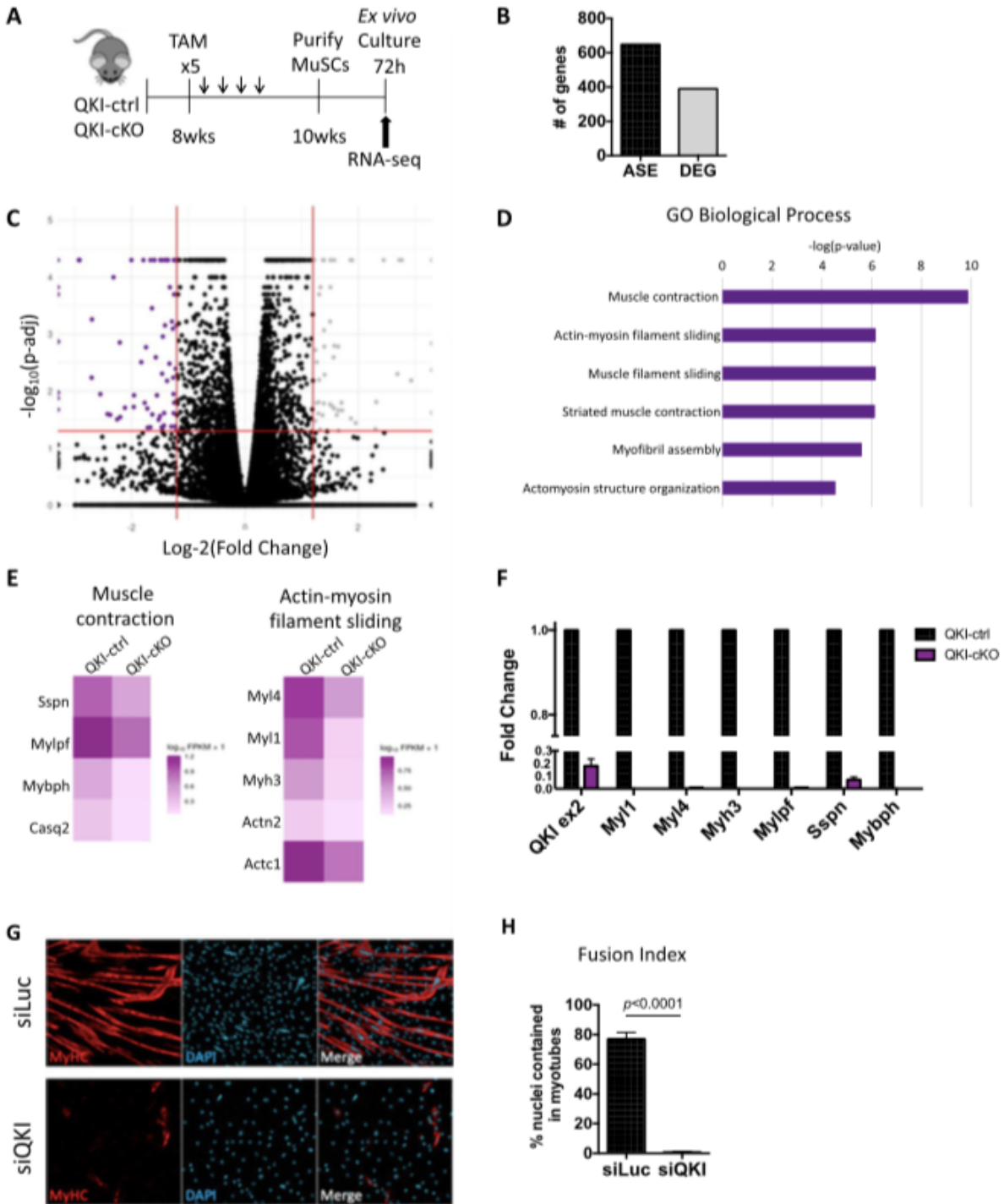


Figure 4.2. QKI-deficient primary skeletal MuSCs drastically down-regulate markers of terminal differentiation.

(A) Timeline for TAM-induced knockout of QKI in MuSCs, MuSC purification and culture prior to RNA isolation for RNA-seq (n=3 biological replicates). (B) Total alternative splicing events (ASE) and differentially expressed genes (DEG) in QKI-cKO MuSCs compared to QKI-ctrl. (C) Volcano plot showing differentially regulated transcripts of QKI-ctrl and QKI-cKO MuSCs. Vertical lines represent log₂ fold change cut-off of value 1.2, and horizontal lines represent FDR cut-off value 0.05. (D) Pathway enrichment analysis of GO biological processes carried out using Enrichr software of significantly downregulated genes in QKI-cKO versus QKI-ctrl MuSCs. (E) Heatmaps show the downregulation of genes selected from enriched gene sets corresponding to *muscle contraction* and *actin-myosin filament sliding* terms. Colour scale represents log₁₀(fpkm)+1 values. (F) Quantitative PCR confirmation of selected downregulated myogenic differentiation markers in QKI-cKO MuSCs compared to QKI-ctrl from (E), and exon 2 of QKI transcript to confirm knockdown (Error bars represent mean +/- SEM, n = 3 biological replicates). (G) Immunofluorescence of C2C12 myotubes differentiated for 72h in the presence of siQKI or siLuc control. Myosin heavy chain is in red and the slides were counterstained with DAPI (blue). (H) Fusion index of myotubes from (G) calculated as percentage of nuclei within myotubes (Error bars represent mean +/- SEM, n = 3 independent experiments, $p < 0.0001$).

The transcripts of asymmetric division components undergo dysregulated AS in QKI-deficient MuSCs.

Establishing polarity within the MuSC is a precursor to asymmetric cell division, and asymmetric cell division is a source of myogenic progenitor cells during muscle regeneration (Yin et al., 2013). Polarity-determining proteins such as dystrophin (Dmd) and Mark2 localize to one side of the MuSC prior to asymmetric cell division (Dumont et al., 2015b). Additionally, Numb

segregates to one daughter cell during MuSC asymmetric division to unevenly distribute template DNA to the two daughter cells (Shinin et al., 2006). Further analysis of AS events observed in QKI-cKO MuSCs revealed AS patterns in *Dmd* (exon 78 exclusion), *Mark2* (exon 15 inclusion), and *Numb* (exon 9 inclusion). Notably, AS of *Dmd* exon 78 is known to occur in patients with myotonic dystrophy (DM1), resulting in expression of the embryonic form of dystrophin and leading to defects in mobility and muscle architecture (Rau et al., 2015).

Interestingly, we also found alternative usage of exon 5 of the MuSC marker Integrin Alpha-7 (*Itga7*) in QKI-cKO (Supplemental Figure S4.3A). The role of integrins in establishing cell polarity has been determined in intestinal cells (Goulas et al., 2012), but their function in MuSC polarity is not currently known. *Itga7* exons 5 and 6 are mutually exclusive and encode the extracellular linker domain which binds laminins in the extracellular matrix (ECM) of muscle (Collo et al., 1993; Song et al., 1993; Ziober et al., 1993). *Itga7* exon 5, but not exon 6, is present in the *Itga7-X1* isoform which efficiently binds laminin-511, one of the predominant laminin isoforms found in muscle ECM during embryogenesis and muscle regeneration. While *Itga7-X2*, containing exon 6, but not exon 5, binds laminin-111, the other laminin isoform which is present during embryogenesis and muscle regeneration (Rayagiri et al., 2018; von der Mark et al., 2002). Laminin-211 is the predominant isoform in homeostatic adult muscle tissue and is recognized by both X1 and X2 isoforms (von der Mark et al., 2002). Interestingly, we observed a switch from the exon 6 isoform (X2) in QKI-ctrl MuSCs to the exon 5 isoform (X1) in QKI-cKO MuSCs (Supplemental Figure S4.3A). To confirm the switch to the *Itga7-X1* isoform in QKI-cKO MuSCs, we performed RT-PCR on QKI-ctrl and QKI-cKO MuSCs using a common forward primer in exon 4, and reverse primers in exon 5 and exon 6, respectively. QKI-ctrl MuSCs expressed mainly the X2 isoform (exon 6) in MuSCs, while the QKI-cKO MuSCs expressed equivalent X1 (exon 5)

and X2 isoforms (Figure 4.3A). We also confirmed the increase in *Itga7-X1* isoform in QKI-cKO MuSCs compared to QKI-ctrl by RT-qPCR of exon 5 (Figure 4.3B).

To confirm AS of the remaining MuSC polarity regulators *Dmd*, *Mark2* and *Numb* in QKI-deficient MuSCs, we isolated primary MuSCs from C57BL/6 wild type mice, cultured them *in vitro*, and transfected them with siLuc and siQKI for two days, followed by RNA isolation and RT-PCR. Primers were designed to flank the AS exon. The exclusion of *Dmd* exon 78 was observed in siQKI MuSCs compared to siLuc controls. Moreover, the inclusion of exons 9 and 15 for *Numb* and *Mark2* were confirmed (Figure 4.3C).

To determine whether QKI deficiency could also elicit these AS events in differentiating MuSCs, we transfected proliferating MuSCs with siLuc and siQKI for two days and then switched to reduced-serum differentiation media for 24 and 48h. We observed that the *Dmd*, *Mark2*, and *Numb* AS events were indeed conserved in differentiating MuSCs (Supplemental Figure S4.3B).

Notably, the large proportion of AS transcripts which utilized an alternative last exon prompted us to perform pathway enrichment analysis of these targets, and we found enrichment for ‘striated muscle contraction’, and ‘impaired skeletal muscle contractility’ terms (Supplemental Figure S4.3C). Skeletal muscle contraction requires functional repeats of small subunits called sarcomeres, which are highly ordered structures consisting of hundreds of proteins including myosin and actin filaments (Rassier, 2017). QKI has been shown to regulate RNA metabolism in the contractile machinery of cardiac smooth muscle (Chen et al., 2021a), and in the sarcomeres of zebrafish (Bonnet et al., 2017). RT-PCR analysis confirmed AS of the major sarcomere components *Capzb*, *Tnnt3*, *Tpm1*, and *Neb* in wild type primary MuSCs transfected with siQKI, but not siLuc (Supplemental Figure S4.3D). Our findings suggest that the loss of QKI also leads to AS defects in major components of the skeletal muscle sarcomere.

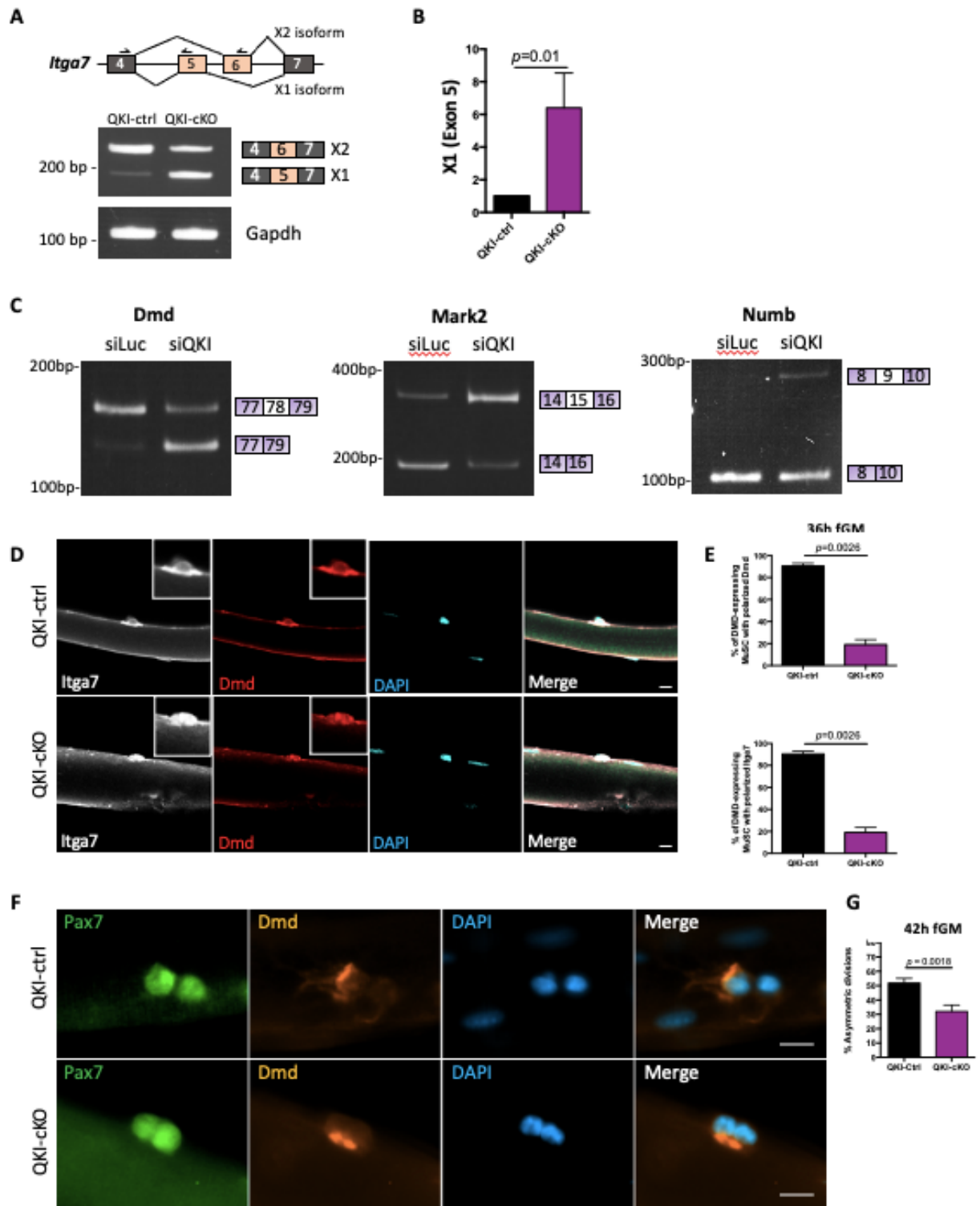


Figure 4.3. Components of MuSC polarity establishment undergo AS in QKI-deficient MuSCs.

(A) *Upper panel*: Diagram depicting splicing pattern of *Itga7* X1 and X2 isoforms. Arrows above exons 4, 5 and 6 represent primer direction. *Lower panels*: RT-PCR of *Itga7* X1 (exon 5) and X2 (exon 6) and *Gapdh* control in MuSCs isolated from QKI-ctrl and QKI-cKO mice. PCR products were separated on polyacrylamide gels and stained with ethidium bromide. The migration of DNA markers in base pairs (bp) is shown on the left, and exon inclusion/exclusion diagram is on the right. (B) Quantitative PCR for *Itga7* XI (exon 5) normalized to *Gapdh* control in MuSCs isolated from QKI-ctrl and QKI-cKO mice (n= 3 biological replicates, $p=0.01$ unpaired student's t-test). (C) RT-PCR validation of SE events of *Dmd*, *Mark2*, and *Numb* in proliferating MuSCs transfected with siLuc or siQKI. PCR products were electrophoresed on acrylamide gels and stained with ethidium bromide. The migration of DNA markers in base pairs (bp) is shown on the left, and inclusion/exclusion of the alternative spliced exon is depicted on the right. (D) Myofibers isolated from QKI-ctrl and QKI-cKO mice and cultured in fGM for 36h, stained with *Itga7* (white) and *Dmd* (red), counterstained with DAPI (blue). Scale bar represents 10 μm . (E) Quantification of *Dmd*-expressing MuSCs from (D) that had polarized localization of *Dmd* (upper panel), and *Itga7* (lower panel) (n = 3 mice per condition, 100 MuSCs quantified per mouse, unpaired student's t-test, $p=0.0026$). (F) Myofibers isolated from QKI-ctrl and QKI-cKO mice, cultured in fGM for 42h, stained with Pax7 (green) and *Dmd* (orange), and counterstained with DAPI (blue). Scale bars represent 10 μm . (G) Percentage of total divisions from (F) that were asymmetric based on inheritance of *Dmd* protein (n = 3 mice per condition, 100 MuSCs quantified per mouse, unpaired student's t-test, $p=0.0018$).

QKI deficiency leads to loss of polarization of Dmd and Itga7 proteins.

To investigate whether polarization of Dmd and Itga7 protein would be affected by the AS defects observed in QKI-deficient MuSCs, we isolated myofibers from QKI-ctrl and QKI-cKO mice and performed immunofluorescence staining prior to the first cell division (which occurs at approximately 40h) by fixing the myofibers after precisely 36h of culture. Itga7 has been shown to interact with dystrophin-associated glycoprotein complex (DGC), and thus is known to co-localize with Dmd in the MuSC (Dumont et al., 2015b). The percentage of MuSCs that expressed Dmd was unchanged in QKI-cKO compared to QKI-ctrl control MuSCs ($29.3\% \pm 6.7\%$ in QKI-ctrl and $27.7\% \pm 1.2\%$ in QKI-cKO) (Supplemental Figure S4.4A). In QKI-ctrl MuSCs, both Dmd and Itga7 were localized to one side of the cell (i.e. polarized) in 91.7% of dystrophin-expressing MuSCs (Figure 4.3D, 4.3E). We observed a significant shift in QKI-cKO MuSCs, where Dmd and Itga7 were polarized in only 16.7% of dystrophin-expressing cells (Figure 4.3D, 4.3E). Therefore, loss of QKI results in polarization defects of Dmd and Itga7 in MuSCs.

Inclusion of Itga7-X1 (exon 5) is sufficient to induce loss of MuSC polarity and reduction of myogenic progenitors.

To determine if the alternatively spliced components of asymmetric cell division could be direct targets of QKI-5, we interrogated the 200 nucleotide sequences flanking each of the AS exons of *Dmd*, *Mark2*, *Numb*, and *Itga7* for the QKI response element (QRE) sequence. We found that only exon 5 of *Itga7* had a neighbouring QRE sequence (ACUAAAY), which was located 14 nucleotides upstream of the 3' splice site in intron 4 (Figure 4.4A). To confirm QKI-5 binds this QRE sequence, we generated a biotinylated RNA spanning the fragment of *Itga7* intron 4 which contains the QRE sequence (Itga7-QRE), and a biotinylated RNA harbouring a mutated QRE sequence (Itga7-mutQRE) (Supplemental Figure S4.4B). The RNAs were bound to Streptavidin

beads and RNA ‘pull-downs’ were performed using total cell lysate from cultured C2C12 myoblasts. The bound proteins were washed with increasing NaCl concentration and eluted in sample buffer. The visualization of bound of QKI-5 was assessed by SDS-PAGE followed by immunoblotting. Indeed, the RNA containing the *Itga7*-QRE bound QKI-5 with high affinity as the interaction was maintained with 500mM NaCl, while *Itga7*-mutQRE did not bind QKI-5 (Supplemental Figure S4.4B). Therefore, QKI-5 binds to the intron 4 QRE sequence upstream of *Itga7* exon 5 to mediate AS at this location.

We next investigated whether the balance of X1/X2 *Itga7* isoforms could reproduce the polarity and myogenic progenitor defects we observed in QKI-cKO MuSCs. To re-create this defect, we opted for 2'-O-methyl antisense oligonucleotides (ASOs) targeting the *Itga7* intron 4 QRE sequence (ASO-Q1). We also identified a distal QRE sequence near the 3' end of *Itga7* intron 6 and used this ASO as control (ASO-Q2). Wild type primary MuSCs were cultured *in vitro* and transfected with ASO-Q1 and ASO-Q2 either alone or in combination, or mock transfected with water as a negative control. The cells were collected and RNA was isolated 2 days after transfection.

Quantitative PCR was performed to measure the relative inclusion of either exon 5 (X1) or exon 6 (X2) compared to an unspliced region of *Itga7* (exon 23) among the ASO-treated MuSCs. Interestingly, we recapitulated the increased expression of the X1 isoform with transfection of ASO-Q1 (2.9 ± 0.49 fold increase normalized to *Gapdh* and *Itga7* exon 23, $p = 0.0179$) (Figure 4.4B). Treatment with ASO-Q2 resulted in a slight increase in X1 expression, although to a lesser extent than ASO-Q1 (2.0 ± 0.31 fold increase normalized to *Gapdh* and *Itga7* exon 23, $p = 0.0307$). Expression of the X2 isoform (exon 6) was unaffected by treatment with ASO-Q1 or ASO-Q2 (Figure 4.4B). Semi-quantitative RT-qPCR was performed to visualize the increased expression

of X1 (exon 5) with ASO-Q1 treatment, and to confirm unchanged expression in a common region within *Itga7* exon 23. Indeed, expression of exon 5 was increased in ASO-Q1-treated MuSCs compared to the mock-transfected with water control MuSCs. The common region in exon 23 remained unchanged, indicating that ASO treatment did not affect the overall expression level of *Itga7* (Figure 4.4C). The ASO-Q1 was specific for *Itga7*, as it did not influence *Dmd* and *Mark2* AS events (Supplemental Figure S4.4C). These results indicate that masking the upstream QRE (i.e. Q1) with a targeted ASO was sufficient to promote *Itga7-X1* expression, albeit at a lower level than QKI-cKO MuSCs (Compare Figure 4.4B, 4.4C with Figure 4.3A, 4.3B).

We next examined whether the ASO-Q1-mediated increased expression of *Itga7-X1* containing the extracellular linker region could reproduce the polarity defects observed in QKI-cKO MuSCs. Myofibers were isolated from C57BL/6 wild type mice and transfected with ASO-Q1 or mock transfected with water as a negative control (CTRL). Transfection was performed 4 and 16h after addition of fiber growth media (fGM), and myofibers were fixed 36h after the addition of fGM. Co-immunostaining of *Itga7* and *Dmd* revealed a significant reduction of polarization of both proteins in ASO-Q1 transfected myofibers ($38.7\% \pm 3.4\%$) compared to CTRL cultures ($84.3\% \pm 1.9\%$) (Figure 4.4D, 4.4E).

ASO-Q1 treatment of myofibers was then extended to 72h of culture to assess the production of Myog⁺ myogenic progenitors. Myofibers were transfected twice with ASO-Q1 or water CTRL at 4 and 16h after adding fGM and fixed after 72h in culture. We observed a striking reduction in Myog⁺ myogenic progenitors per myofiber in ASO-Q1 treated myofibers (8.9 ± 1.8) versus CTRL cultures (37.6 ± 3.9), and a reduction in the total number of MuSCs per myofiber (128.0 ± 12.5 in CTRL versus 39.3 ± 4.7 in ASO-Q1) (Figure 4.4F, 4.4G). These data show that

inducing the expression of *Itga7-X1* isoform by targeting the intron 4 QRE re-creates the MuSC polarity and myogenic progenitor defects observed in QKI-cKO MuSCs.

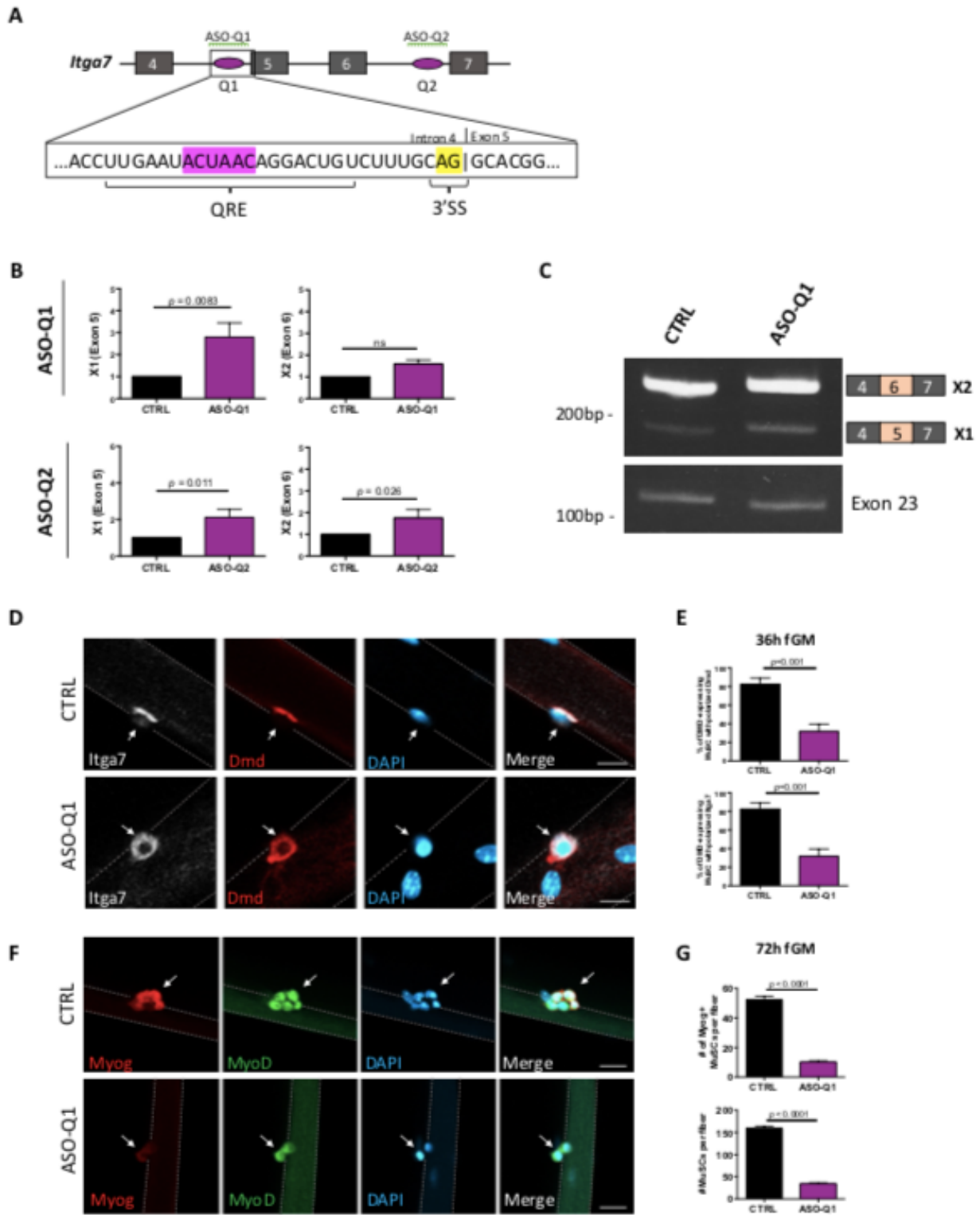


Figure 4.4 Inclusion of *Itga7-X1* (exon 5) is sufficient to induce loss of MuSC polarity and reduction of myogenic progenitors.

(A) Schematic of *Itga7* transcript from exon 4 to exon 7. QREs represented as purple ovals. Q1- upstream QRE, Q2- downstream QRE. Magnified box shows QRE site highlighted in purple, and 3' splice site highlighted in yellow. Location of ASO sequences against Q1 and Q1 (ASO-Q1 and ASO-Q2, respectively) are shown in green. (B) Quantitative PCR for *Itga7* XI (exon 5) and *Itga7* X2 (exon 6), normalized to *Gapdh* and the unchanged common region (*Itga7* exon 23) in C57BL/6 wild type primary MuSCs treated with ASO against Q1 (ASO-Q1) and Q2 (ASO-Q2) (n=3 replicates, ns - not significant, unpaired student's t-test). (C) Semi-quantitative RT-PCR for *Itga7* XI (exon 5), *Itga7* X2 (exon 6), and *Itga7* exon 23 unchanged region control in C57BL/6 wild type primary MuSCs treated with ASO against Q1 (ASO-Q1). PCR products were run on acrylamide gels and stained with ethidium bromide. The migration of DNA markers in base pairs (bp) is shown on the left, and exon inclusion diagram is shown on the right. (D) Myofibers isolated from C57BL/6 wild type mice and transfected with ASO-Q1 4h and 16h after adding culture media. Fibers were fixed 32h after transfection and immunostained for *Itga7* (white) or *Dmd* (Red), and counterstained with DAPI (blue). Scale bar represents 10 μ M. (E) Quantification of *Dmd*-expressing cells with polarized *Dmd* (upper panel) and *Itga7* (lower panel). (Error bars represent mean \pm SEM, n= 3 biological replicates, minimum 200 cells counted per group, $p=0.0044$, unpaired student's t-test). (F) Myofibers isolated C57BL/6 wild type mice and transfected with ASO-Q1 or water (CTRL) at 4h and 16h after adding culture media. Fibers were fixed 72h after addition of culture media, and immunostained for MyoD (green) and Myogenin (red) and counterstained with DAPI (blue). Scale bar represents 20 μ M. White arrows point to MuSCs. (G) Quantification of Myogenin-positive MuSCs per myofiber (upper panel) and total number of MuSCs per myofiber (lower panel). Error bars represent mean \pm SEM, n= 3 biological replicates, minimum 400 cells counted per group, $p<0.0001$, unpaired student's t-test)

4.5 Discussion

In the present manuscript, we define a role for QKI-5 and *Itga7* X1/X2 isoforms in MuSC polarity. We report that major polarity-determining factors including *Itga7* and *Dmd* undergo defective AS in QKI-deficient primary MuSCs. QKI-deficient MuSCs exhibited a loss of cell polarity and loss of the myogenic progenitor population. Treatment of wild type MuSCs with antisense oligonucleotides (ASOs) directed against the QRE in *Itga7* intron 4 led to exon 5 inclusion and expression of the *Itga7-X1* isoform known to express extracellular linker domain and interfere with polarization of both *Dmd* and *Itga7*. Our findings identify QKI-5 as a critical AS regulator of polarity in MuSCs.

The loss of cell polarity in QKI-deficient MuSCs suggests that one possible mechanism through which the pool myogenic progenitors is depleted is through a defect in asymmetric cell division.

Asymmetric cell division is essential for diversification of cell types during development and specification of stem cells in adults (Fuchs and Blau, 2020; Knoblich, 2010). In Duchenne muscular dystrophy (DMD), the ability of MuSCs to divide asymmetrically is impeded by loss of the dystrophin protein, which plays a role in establishing the cell polarity that is required for asymmetric division (Dumont et al., 2015b). The deficiency in myogenic progenitors arising from *Dmd*-deficient MuSCs is accompanied by hyperplasia of non-committed stem cells in (Chang et al., 2016; Dumont et al., 2015b; Kottlors and Kirschner, 2010). The defect in cell polarization (Figure 4.3D) and lack of myogenic progenitors formed by QKI-cKO MuSCs (Figure 4.1C) presents as a phenocopy of *Dmd*-deficient cells. Notably, however, we did not observe stem cell hyperplasia in QKI-cKO mice, but rather a reduction in the total number of MuSCs (Figure 4.1D), suggesting that the QKI-cKO phenotype may be only partly mediated by defects in AS of *Dmd*.

The MuSC surface marker *Itga7* has been shown to affect the generation of myogenic progenitor cells and muscle differentiation (Ding et al., 2020; Mayer et al., 1997; Rooney et al., 2009). The expression of *Itga7-X1* isoform in QKI-deficient MuSCs and subsequent loss of MuSC polarity provides evidence that maintaining a high *Itga7-X2/Itga7-X1* isoform ratio is a requirement for MuSC polarity.

The *Itga7-X1* (exon 5) and *Itga7-X2* (exon 6) isoforms are expressed in a mutually exclusive manner and are regulated during development. The X1 isoform is observed in embryogenesis during the development of skeletal muscle, while the X2 isoform is found in adult skeletal muscle (Collo et al., 1993; Song et al., 1993; von der Mark et al., 2002; Ziober et al., 1993). Although the X1 isoform is needed during embryonic skeletal muscle development, our findings suggest that it is ‘toxic’ or not tolerated during the regeneration of adult muscle tissue. It is known that the *Itga7* X1 and X2 isoforms have varied binding affinities to different laminin isoforms in the muscle ECM. The X1 isoform of *Itga7* preferentially binds laminin-511, while the X2 isoform binds laminin-111. The X1 isoform can also bind laminin-111 but with much lower affinity (von der Mark et al., 2002). Therefore, our findings suggest that the X2/X1 ratio in QKI-cKO or ASO-Q1 treated MuSCs is detrimental to MuSC polarity in part due to incompatible interactions with the changing landscape of extracellular laminin isoforms in adults.

The skipping of *Itga7* exon 5 in QKI-ctrl MuSCs suggests that binding of QKI-5 to its QRE within intron 4 may sterically prevent access of the U2 snRNP splicing machinery to the 3' splice site, whereas in QKI-cKO MuSCs the absence of QKI promotes splicing and inclusion of exon 5 rather than exon 6. Treatment of wildtype MuSCs with an ASO that binds to the intron 4 QRE (ASO-Q1) results in exon 5 inclusion. One possible mechanism through which ASO-Q1 increases exon 5 inclusion is through binding and masking a splicing silencer element (SSE). The use of

ASOs to restore exon expression through this mechanism has been demonstrated previously. For example, an ASO-walking technique was used to identify an SSE in the *IKBKAP* pre-mRNA responsible for the pathological skipping of exon 20 in familial dysautonomia (Sinha et al., 2018).

RBPs such as QKI and their effects on AS play an important role in disease (Lukong et al., 2008; Scotti and Swanson, 2016). For example, disruption of the *QKI* gene in a human patient resulting in haploinsufficiency led to several clinical manifestations, including severely reduced muscle tone (i.e. hypotonia) (Backx et al., 2010). Our findings provide further evidence of the important contributions of RBPs and RNA metabolism in muscle wasting disease. Several splicing aberrations are identified in muscle wasting disease (Nakka et al., 2018). For example, aberrant splicing in Myotonic dystrophy type I (DM1) is mediated through sequestration of the Muscleblind-like (MBNL) RNA binding protein to pathological CUG repeats within the DM protein kinase (*DMPK1*) RNA (Charlet et al., 2002; Philips et al., 1998; Thomas et al., 2017). Subsequent loss of MBNL function leads to AS of several muscle-specific targets, including the chloride channel *CLCN1*, wherein a premature stop codon is induced leading to hyperexcitability of myofibers (Charlet et al., 2002; Mankodi et al., 2002). Development of strategies to target such pathological splicing events include the use of ASOs. Using ASO to specifically target the 3' splice site of *CLCN1* exon 7a, or the more general CUG repeat region of *DMPK1*, improves myopathy in DM1 mouse models (Wheeler et al., 2007; Wheeler et al., 2009). Given the recapitulation of muscle disease phenotypes that we see with a single AS event of *Itga7* exon 5, we can envision the use of ASOs to target similar AS aberrations in components of asymmetric cell machinery. Indeed, splicing aberrations in *Itga7* which modulate its function are reported to be involved in myopathy (Hayashi et al., 1998; Pegoraro et al., 2002).

In summary, we report QKI-5 as a major regulator of splicing in skeletal MuSCs and as being essential for maintaining the splicing isoform pattern that drives MuSC polarity and production of myogenic progenitors. QKI-deficient mice had severe muscle regeneration defects arising from a lack of these progenitor cells. AS of *Itga7* mediated by a QRE-targeted ASO, or in QKI-deficient MuSCs, led to cell polarity defects thus identifying a role for *Itga7* isoforms in establishing cell polarity.

4.6 Materials & Methods

Mice.

C57BL/6 (Jackson Laboratory 000664) were the wild type mice used for MuSC FACS purification and myofiber isolation where indicated. QKI-cKO mice are maintained in a C57BL/6 background with two loxP sites flanking exon two of the *QKI* gene (*QKI*^{2lox/2lox}), and were generated previously (Darbelli and Richard, 2016). *QKI*^{2lox/2lox} (*QKI*-ctrl) mice were crossed with C57BL/6 mice expressing CreERT2 recombinase under the *PAX7* promoter (Jackson laboratory #017763) to generate QKI-cKO mice with tamoxifen-induced QKI deficiency specifically in MuSCs. To induce Cre recombinase, tamoxifen (TAM, T5648, Millipore-Sigma, Burlington, MA) was dissolved in corn oil (C8267, Millipore-Sigma) to 1 mg/ml, and 100 μ L was injected intraperitoneally in 6 to 8-week old mice once daily for 5 consecutive days. Experiments were conducted 10 days following the final injection of tamoxifen. Sex-and age-matched mixed populations of males and females were used for each genotype for all experiments. All mouse husbandry and experiments were conducted in accordance with the Institutional Animal Care and Use Committee (IACUC) of McGill University. All animal procedures conducted at McGill were approved by the Animal Welfare Committee of McGill University (protocol #3506).

Myofiber isolation and culture.

Wild type C57BL/6, QKI-ctrl and/or QKI-cKO mice were sacrificed and their extensor digitorum longus (EDL) muscles were dissected using standard dissection techniques. Isolated muscles were incubated with 0.4% collagenase (Sigma, c0103) in DMEM for 30 min at 37°C and 5% CO₂. Whole muscle was then triturated with a plastic disposable Bohr pipette to dissociate individual fibers from the whole muscle as described previously (Gallot et al., 2016). To mimic activating conditions, fibers were cultured in fiber growth media (fGM: DMEM plus 20% FBS, 1% chick embryo extract (Gemini Bio, 100-163P), 2.5 ng/mL bFGF (Gibco, 13256-029) 1% penicillin/streptomycin) at 37°C and 5% CO₂. For quiescent satellite cell analysis, fibers were fixed immediately following dissociation using 2% paraformaldehyde (PFA) prepared fresh in 1X PBS.

Myofiber immunofluorescence.

Cultured myofibers were fixed in 4% PFA at the indicated timepoints and washed twice with 1X PBS. Fixed myofibers were then permeabilized with 0.2% Triton X-100, 0.125M glycine in 1X PBS for 15 min at room temperature (RT). Blocking followed for 1h at RT with 2% BSA, 5% horse serum and 0.1% Triton X-100. Primary antibodies were diluted in blocking buffer to detect PAX7 (Developmental Studies Hybridoma Bank [DSHB], 1:100), MyoD (Santa Cruz Biotechnology, sc-304), Myogenin (DSHB, F5D), Dystrophin (DSHB, MANDRA1[7A10]), QKI-5 (Millipore Sigma, AB9904, AB9906, respectively). After 16h incubation at 4°C, fibers were washed 3 times with 1X PBS for 10 min. Secondary antibody (AlexaFluor anti-mouse or anti-rabbit 488nm or 568nm), or AlexaFluor-647-conjugated primary antibody against Itga7 (R&D Systems, FAB3518R) was used at a dilution of 1:400 in blocking buffer for 1h in the dark at RT.

Myofibers were washed 3 times for 10 min with 1X PBS. Finally, the myofibers were transferred to a microscope slide outlined using an ImmEdge hydrophobic barrier pen (Vector Laboratories, H-4000) and mounted with ProLong Gold Antifade Mountant with DAPI (ThermoFisher Scientific, P36935). Fiber-associated MuSCs were then visualized on a Zeiss Axio Imager M1 microscope (Carl Zeiss, Thornwood NY) or LSM800 Airyscan confocal microscope and resulting images were analyzed using Zeiss' ZEN Digital imaging suite software.

Primary MuSC isolation.

Skeletal muscle tissue was isolated from the abdominal and diaphragm muscles of wild type C57BL/6, QKI-ctrl and/or QKI-cKO mice and MuSCs were isolated as previously described using fluorescence activated cell sorting (FACS) (Pasut et al., 2012). Briefly, dissected muscles were minced with dissection scissors and digested with collagenase/dispase solution (2.4U/ml collagenase D, 2.4U/ml Dispase II in Ham's F10 media) at 37°C for 1h. Digested tissue was triturated and filtered through a 40 μ M cell strainer. Cells were pelleted for 18 min at 1800 rpm and resuspended in 1% BSA/PBS. Cells were stained for 15 min RT with Itga7-AlexaFluor-647 (R&D systems, FAB3518R) for positive selection, and PE-CD45 (Invitrogen), PE-CD11b (Invitrogen, PE-CD31 (BD Pharmigen), and PE-ScaI (BD Pharmigen) for negative selection. Hoechst was used to gate living cells. Cells were washed once with 1% BSA/PBS and pelleted prior to final resuspension and one last filter through a 40 μ M cell strainer. ITGA7+/CD45-/CDCD11b-/Sca1-/Hoechst+ Cells were sorted into full myoblast growth media using the FACSariaIII cell sorter (BD Biosciences).

MuSC growth and differentiation culture.

Purified MuSCs were seeded onto collagen-coated plates and expanded in growth media (GM: Ham's F10 media with 20% FBS, 12.5 ng/mL human recombinant bFGF [Gibco, 13256-029], and 1% Penicillin/ Streptomycin) at 37°C and 5% CO₂. Media was replenished every two days. To differentiate MuSCs into myotubes, MuSCs were grown to 90% confluency in growth media, washed twice with 1X PBS, and switched to differentiation media (DM: DMEM, 1% FBS, and 1% Penicillin/Streptomycin).

in vivo muscle regeneration and cross-sectional immunofluorescence.

The right TA muscles of QKI-ctrl or QKI-cKO mice were injected once with 50 μ L of 10 μ M cardiotoxin (Sigma, 217502) to induce muscle injury. Following three weeks, mice were sacrificed, and the injured and contralateral control TA were dissected using standard dissection techniques. Dissected TA muscles were fixed in 0.5% PFA for 2h at 4°C, and subsequently equilibrated in 20% sucrose in 1X PBS overnight at 4°C. The following day, TA muscles were rapidly frozen in liquid nitrogen-cooled isopentane and embedded in OCT compound (Fisher Scientific, 23-730-571). Frozen TA muscles were cut into 10 μ M sections using a Leitz cryostat directly onto Fisher Superfrost Plus microscope slides (12-550-150) for immunofluorescence staining. Resulting tissue sections were permeabilized for 12 minutes with 0.2% Triton X-100, 0.125M glycine in PBS at room temperature. Blocking followed with M.O.M blocking reagent (Vector Laboratories, MKB-2213-1) for 1h at RT. Primary antibodies were diluted in blocking reagent to detect PAX7 (DSHB, PAX7) and laminin (Sigma, L9393). After 16h incubation at 4°C, sections were washed 3 times with 1X PBS for 10 min. Secondary antibody (AlexaFluor anti-mouse or anti-rabbit 488nm or 568nm) was used at a dilution of 1:400 in blocking reagent for 45 min in the dark at room temperature. Sections were then washed 3 times for 10 min with 1X PBS.

Tissue sections were mounted with ProLong Gold Antifade Mountant with DAPI (ThermoFisher Scientific, P36935) and covered with a coverslip. Visualization was performed on a Zeiss Axio Imager M1 microscope (Carl Zeiss, Thornwood NY), and resulting images were analyzed using Zeiss' ZEN Digital imaging suite software.

RNA-seq sample preparation and analysis.

Primary MuSCs were purified from 6-8 week old QKI-ctrl or QKI-cKO mice (n=3 biological replicates) using FACS gating of ITGA7+/CD45-/CD11b-/Sca1-/Hoechst+ cells. Purified cells were expanded *ex vivo* in myoblast growth medium for 72h, pelleted, and bulk RNA was isolated using the PicoPure RNA extraction kit according to the manufacturer's protocol (Applied Biosystems, 4346906). RNA quality was assessed using an Agilent TapeStation 4200. RNA sequencing libraries were generated with TruSeq stranded mRNA Sample Prep Kit with TruSeq Unique Dual Indexes (Illumina). The resulting libraries were multiplexed and sequenced with 100 bp paired-end reads on the Illumina NovaSeq platform. Samples were subsequently demultiplexed with bcl2fastq v2.20 Conversion Software from Illumina. Illumina adaptor sequences were then removed using Trimmomatic v0.39 software. Trimmed sequences were subsequently aligned to the mm10/GRCm38 genome using STAR v2.7. Mapped reads were then processed using the Cufflinks software suite. FPKMs and fragment counts were scaled using the geometric means of fragment counts across all libraries. Significant changes in transcript expression were classified as having a log fold change greater than 2, base means larger than 20, and false discovery rate (FDR) less than 0.05). Expression plots were generated using CummeRbund. Alternative splicing events in QKI-cKO MuSCs were quantified using rMATS v4.0.2 and Gencode vM23 gene annotations

using untrimmed paired end reads. Events with an FDR of less than 0.05 were accepted as significant. Pathway enrichment analysis of DEGs and AS events was performed using Enrichr.

RNA isolation, cDNA Synthesis, qPCR, RT-PCR and polyacrylamide gel electrophoresis.

TRIzol (Invitrogen) was used to isolate RNA from cultured primary MuSCs per the manufacturer's instructions. 1 μ g of total RNA was used for cDNA synthesis using M-MLV reverse transcriptase (Promega, M1701), followed by qPCR analysis with targeted primers using PowerUp SYBR Mastermix (Life Technologies, A25777) run on QuantStudio7 real-time PCR system (ThermoFisher Scientific). mRNA was quantified with the $\Delta\Delta$ Ct method, normalizing to Gapdh and/or Hprt and 18s mRNA levels as indicated. Splicing assays were performed using cDNA isolated as described above and specific primers which flanked the indicated exon for PCR. Resulting PCR products were separated on a TBE-based polyacrylamide gel and DNA was stained with ethidium bromide. All PCR reactions were repeated in triplicate.

Western blotting.

Proteins from total cell lysate (150 mM NaCl, 50 mM HEPES pH 7.4, and 1% Triton X-100) were separated by SDS-PAGE and transferred onto nitrocellulose membranes using the Trans-Blot turbo transfer system (BioRad). Membranes were stained with Ponceau Red to confirm equal loading, and then blotted with the primary antibodies against MyHC (DSHB, MF-20), QKI-5 (Millipore Sigma, AB9904, AB9906, respectively) overnight at 4°C. Following 3 washes in TBST, membranes were incubated with HRP-conjugated secondary antibodies (Sigma) for 45 min and visualised on X-ray films with Western Lightning Plus ECL (Perkin Elmer).

Transfection of siRNA and ASOs in primary MuSCs.

FACS-isolated primary MuSCs were transfected with siRNA designed to target QKI (5'-GGA CUU ACA GCC AAA CAA C-3') and luciferase as a negative control (5'-CGU ACG CGG AAU ACU UGA-3'). siRNA transfections were carried out using Lipofectamine RNAiMAX reagent (ThermoFisher, 13778075) per manufacturer's instructions. Cells were harvested 48h after transfection for total RNA isolation. 2'-O-methyl antisense oligonucleotide (ASOs) were designed to target the exon 5 upstream QRE (ASO-Q1: 5'- GUCCUGUUAGUAUUCAAGGUGG -3'), and the downstream QRE (ASO-Q2: 5'- CGAUUACUGUGAGUGAUUAUCCAAC -3') to induce exon 5 inclusion. For cultured primary MuSCs, 50 nM of each ASO or water control were transfected using the Lipofectamine 3000 transfection reagent (ThermoFisher, L3000001) according to the manufacturer's instructions. Cells were harvested 48h after transfection for total RNA isolation. For myofibers, a first transfection was performed with 50nM ASOs 4h after addition of fGM. A second transfection was performed 12h after the initial transfection. Myofibers were subsequently fixed 36h or 72h following addition of culture media as indicated.

RNA Binding Assay.

Streptavidin Mag Sepharose magnetic beads (Cytiva Life Sciences, 28985738) were incubated with 1 μ g of biotinylated RNA (IDT) for 30 minutes at 4°C with end-over-end mixing.

C2C12 myoblast lysate (150 mM NaCl, 50 mM HEPES pH 7.4, 1% Triton X-100, supplemented with 40U/mL RNase inhibitor and protease inhibitors) was then added to the RNA-Streptavidin mixture and incubated at 4°C with end-over-end mixing for 1 hour. The beads were then washed 3 times with lysis buffer containing increasing salt concentrations (150, 300, and 500 mM NaCl). Protein samples were separated with SDS-PAGE and immunoblotted for QKI-5.

DECLARATION OF INTERESTS

The authors declare no competing interests.

ACKNOWLEDGEMENTS

The authors would like to thank Dr. Oscar Villareal for expert assistance with generating bioinformatics pipelines and Dr. Vahab Soleimani for critically reading the manuscript. We also thank Chris Young and Mathew Duguay at the LDI Flow Cytometry Facility for their assistance with FACS experiments. The research was funded by Canadian Institute of Health Research FDN-154303 to S.R. C.D. holds a studentship from the fonds de la recherche en santé du Québec (FRQS).

AUTHOR CONTRIBUTIONS

C.D conceptualized the project, conducted the experiments, and wrote the paper. S.R. conceptualized the project, secured funding, supervised the research, and wrote the paper.

4.7 References

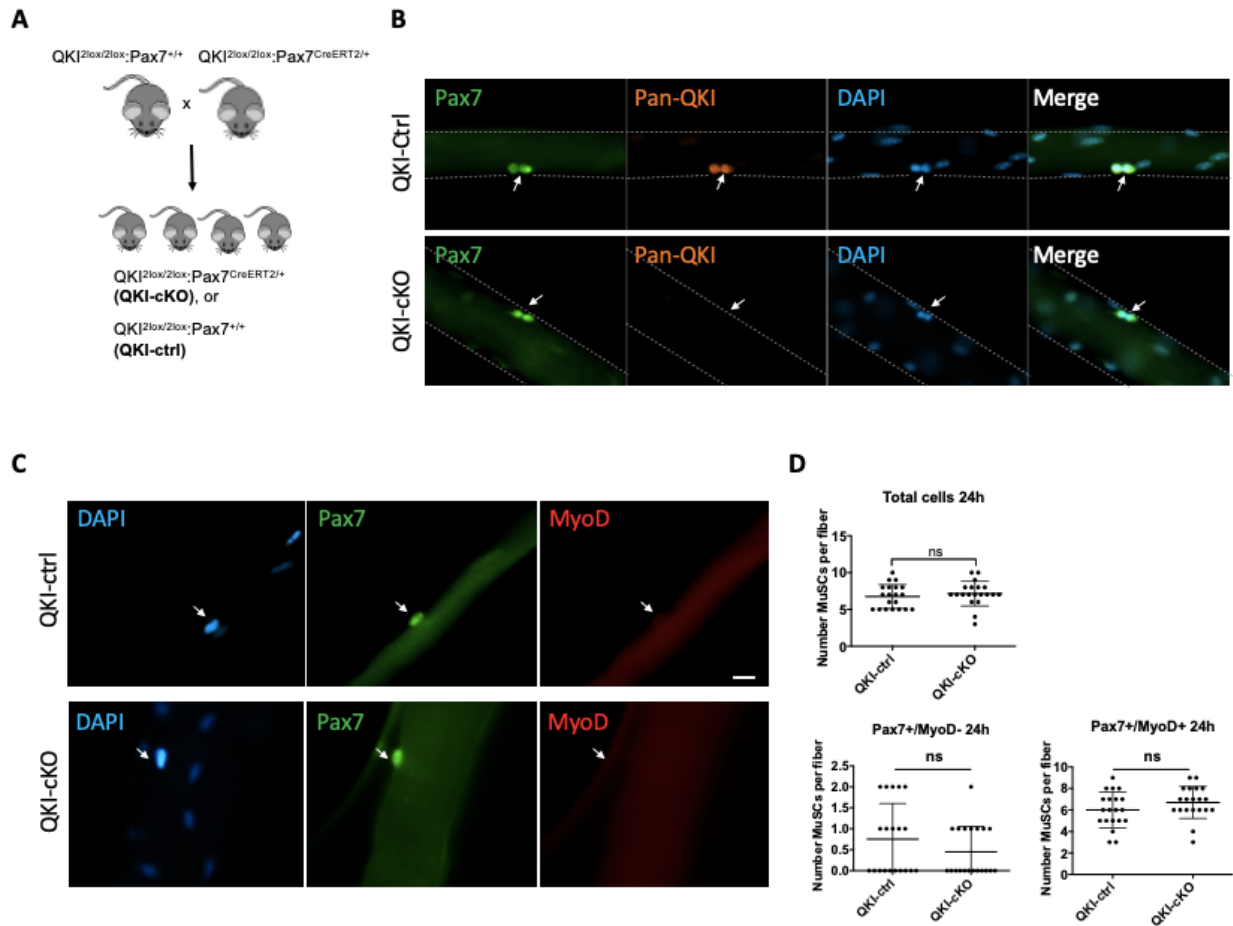
- Backx, L., Fryns, J.P., Marcelis, C., Devriendt, K., Vermeesch, J., and Van Esch, H. (2010). Haploinsufficiency of the gene Quaking (QKI) is associated with the 6q terminal deletion syndrome. *American journal of medical genetics Part A* *152a*, 319-326.
- Beuck, C., Qu, S., Fagg, W.S., Ares, M., Jr., and Williamson, J.R. (2012). Structural analysis of the quaking homodimerization interface. *Journal of molecular biology* *423*, 766-781.
- Bonnet, A., Lambert, G., Ernest, S., Dutrieux, F.X., Couplier, F., Lemoine, S., Lobbardi, R., and Rosa, F.M. (2017). Quaking RNA-Binding Proteins Control Early Myofibril Formation by Modulating Tropomyosin. *Developmental cell* *42*, 527-541.e524.
- Chang, N.C., Chevalier, F.P., and Rudnicki, M.A. (2016). Satellite Cells in Muscular Dystrophy - Lost in Polarity. *Trends in molecular medicine* *22*, 479-496.
- Chargé, S.B., and Rudnicki, M.A. (2004). Cellular and molecular regulation of muscle regeneration. *Physiological reviews* *84*, 209-238.
- Charlet, B.N., Savkur, R.S., Singh, G., Philips, A.V., Grice, E.A., and Cooper, T.A. (2002). Loss of the muscle-specific chloride channel in type 1 myotonic dystrophy due to misregulated alternative splicing. *Molecular cell* *10*, 45-53.
- Chen, E.Y., Tan, C.M., Kou, Y., Duan, Q., Wang, Z., Meirelles, G.V., Clark, N.R., and Ma'ayan, A. (2013). Enrichr: interactive and collaborative HTML5 gene list enrichment analysis tool. *BMC bioinformatics* *14*, 128.
- Chen, T., and Richard, S. (1998). Structure-function analysis of Qk1: a lethal point mutation in mouse quaking prevents homodimerization. *Molecular and cellular biology* *18*, 4863-4871.
- Chen, X., Liu, Y., Xu, C., Ba, L., Liu, Z., Li, X., Huang, J., Simpson, E., Gao, H., Cao, D., *et al.* (2021). QKI is a critical pre-mRNA alternative splicing regulator of cardiac myofibrillogenesis and contractile function. *Nature communications* *12*, 89.
- Collo, G., Starr, L., and Quaranta, V. (1993). A new isoform of the laminin receptor integrin alpha 7 beta 1 is developmentally regulated in skeletal muscle. *The Journal of biological chemistry* *268*, 19019-19024.
- Darbelli, L., and Richard, S. (2016). Emerging functions of the Quaking RNA-binding proteins and link to human diseases. *Wiley interdisciplinary reviews RNA* *7*, 399-412.
- de Bruin, R.G., Shiue, L., Prins, J., de Boer, H.C., Singh, A., Fagg, W.S., van Gils, J.M., Duijs, J.M., Katzman, S., Kraaijeveld, A.O., *et al.* (2016). Quaking promotes monocyte differentiation into pro-atherogenic macrophages by controlling pre-mRNA splicing and gene expression. *Nature communications* *7*, 10846.
- Ding, R., Horie, M., Nagasaka, S., Ohsumi, S., Shimizu, K., Honda, H., Nagamori, E., Fujita, H., and Kawamoto, T. (2020). Effect of cell-extracellular matrix interaction on myogenic characteristics and artificial skeletal muscle tissue. *Journal of bioscience and bioengineering* *130*, 98-105.
- Dumont, N.A., Wang, Y.X., von Maltzahn, J., Pasut, A., Bentzinger, C.F., Brun, C.E., and Rudnicki, M.A. (2015). Dystrophin expression in muscle stem cells regulates their polarity and asymmetric division. *Nature medicine* *21*, 1455-1463.
- Ebersole, T.A., Chen, Q., Justice, M.J., and Artzt, K. (1996). The quaking gene product necessary in embryogenesis and myelination combines features of RNA binding and signal transduction proteins. *Nature genetics* *12*, 260-265.
- Fuchs, E., and Blau, H.M. (2020). Tissue Stem Cells: Architects of Their Niches. *Cell stem cell* *27*, 532-556.

- Galarneau, A., and Richard, S. (2005). Target RNA motif and target mRNAs of the Quaking STAR protein. *Nature structural & molecular biology* *12*, 691-698.
- Gallot, Y.S., Hindi, S.M., Mann, A.K., and Kumar, A. (2016). Isolation, Culture, and Staining of Single Myofibers. *Bio-protocol* *6*.
- Goulas, S., Conder, R., and Knoblich, J.A. (2012). The Par complex and integrins direct asymmetric cell division in adult intestinal stem cells. *Cell stem cell* *11*, 529-540.
- Gurevich, D.B., Nguyen, P.D., Siegel, A.L., Ehrlich, O.V., Sonntag, C., Phan, J.M., Berger, S., Ratnayake, D., Hersey, L., Berger, J., *et al.* (2016). Asymmetric division of clonal muscle stem cells coordinates muscle regeneration in vivo. *Science (New York, NY)* *353*, aad9969.
- Hall, M.P., Nagel, R.J., Fagg, W.S., Shiue, L., Cline, M.S., Perriman, R.J., Donohue, J.P., and Ares, M., Jr. (2013). Quaking and PTB control overlapping splicing regulatory networks during muscle cell differentiation. *RNA (New York, NY)* *19*, 627-638.
- Hayashi, Y.K., Chou, F.L., Engvall, E., Ogawa, M., Matsuda, C., Hirabayashi, S., Yokochi, K., Ziober, B.L., Kramer, R.H., Kaufman, S.J., *et al.* (1998). Mutations in the integrin alpha7 gene cause congenital myopathy. *Nature genetics* *19*, 94-97.
- Knoblich, J.A. (2010). Asymmetric cell division: recent developments and their implications for tumour biology. *Nature reviews Molecular cell biology* *11*, 849-860.
- Kottlors, M., and Kirschner, J. (2010). Elevated satellite cell number in Duchenne muscular dystrophy. *Cell and tissue research* *340*, 541-548.
- Kuang, S., Kuroda, K., Le Grand, F., and Rudnicki, M.A. (2007). Asymmetric self-renewal and commitment of satellite stem cells in muscle. *Cell* *129*, 999-1010.
- Kuleshov, M.V., Jones, M.R., Rouillard, A.D., Fernandez, N.F., Duan, Q., Wang, Z., Koplev, S., Jenkins, S.L., Jagodnik, K.M., Lachmann, A., *et al.* (2016). Enrichr: a comprehensive gene set enrichment analysis web server 2016 update. *Nucleic acids research* *44*, W90-97.
- Le Grand, F., and Rudnicki, M. (2007). Satellite and stem cells in muscle growth and repair. *Development (Cambridge, England)* *134*, 3953-3957.
- Lee, J., Villarreal, O.D., Chen, X., Zandee, S., Young, Y.K., Torok, C., Lamarche-Vane, N., Prat, A., Rivest, S., Gosselin, D., *et al.* (2020). QUAKEING Regulates Microexon Alternative Splicing of the Rho GTPase Pathway and Controls Microglia Homeostasis. *Cell reports* *33*, 108560.
- Lukong, K.E., Chang, K.W., Khandjian, E.W., and Richard, S. (2008). RNA-binding proteins in human genetic disease. *Trends in genetics : TIG* *24*, 416-425.
- Mankodi, A., Takahashi, M.P., Jiang, H., Beck, C.L., Bowers, W.J., Moxley, R.T., Cannon, S.C., and Thornton, C.A. (2002). Expanded CUG repeats trigger aberrant splicing of CIC-1 chloride channel pre-mRNA and hyperexcitability of skeletal muscle in myotonic dystrophy. *Molecular cell* *10*, 35-44.
- Mayer, U., Saher, G., Fässler, R., Bornemann, A., Echtermeyer, F., Mark, H.v.d., Miosge, N., Pösch, E., and Mark, K.v.d. (1997). Absence of integrin $\alpha 7$ causes a novel form of muscular dystrophy. *Nature genetics* *17*, 318-323.
- Montarras, D., L'Honoré, A., and Buckingham, M. (2013). Lying low but ready for action: the quiescent muscle satellite cell. *The FEBS journal* *280*, 4036-4050.
- Murphy, M.M., Lawson, J.A., Mathew, S.J., Hutcheson, D.A., and Kardon, G. (2011). Satellite cells, connective tissue fibroblasts and their interactions are crucial for muscle regeneration. *Development (Cambridge, England)* *138*, 3625-3637.
- Nakka, K., Ghigna, C., Gabellini, D., and Dilworth, F.J. (2018). Diversification of the muscle proteome through alternative splicing. *Skeletal muscle* *8*, 8.

- Pasut, A., Oleynik, P., and Rudnicki, M.A. (2012). Isolation of muscle stem cells by fluorescence activated cell sorting cytometry. *Methods in molecular biology* (Clifton, NJ) *798*, 53-64.
- Pegoraro, E., Cepollaro, F., Prandini, P., Marin, A., Fanin, M., Trevisan, C.P., El-Messlemani, A.H., Tarone, G., Engvall, E., Hoffman, E.P., *et al.* (2002). Integrin alpha 7 beta 1 in muscular dystrophy/myopathy of unknown etiology. *The American journal of pathology* *160*, 2135-2143.
- Philips, A.V., Timchenko, L.T., and Cooper, T.A. (1998). Disruption of splicing regulated by a CUG-binding protein in myotonic dystrophy. *Science* (New York, NY) *280*, 737-741.
- Pilotte, J., Larocque, D., and Richard, S. (2001). Nuclear translocation controlled by alternatively spliced isoforms inactivates the QUAKING apoptotic inducer. *Genes & development* *15*, 845-858.
- Rassier, D.E. (2017). Sarcomere mechanics in striated muscles: from molecules to sarcomeres to cells. *American journal of physiology Cell physiology* *313*, C134-c145.
- Rau, F., Lainé, J., Ramanoudjame, L., Ferry, A., Arandel, L., Delalande, O., Jollet, A., Dingli, F., Lee, K.Y., Peccate, C., *et al.* (2015). Abnormal splicing switch of DMD's penultimate exon compromises muscle fibre maintenance in myotonic dystrophy. *Nature communications* *6*, 7205.
- Rayagiri, S.S., Ranaldi, D., Raven, A., Mohamad Azhar, N.I.F., Lefebvre, O., Zammit, P.S., and Borycki, A.-G. (2018). Basal lamina remodeling at the skeletal muscle stem cell niche mediates stem cell self-renewal. *Nature Communications* *9*, 1075.
- Relaix, F., and Zammit, P.S. (2012). Satellite cells are essential for skeletal muscle regeneration: the cell on the edge returns centre stage. *Development* (Cambridge, England) *139*, 2845-2856.
- Robinson, J.T., Thorvaldsdóttir, H., Winckler, W., Guttman, M., Lander, E.S., Getz, G., and Mesirov, J.P. (2011). Integrative genomics viewer. *Nature Biotechnology* *29*, 24-26.
- Rooney, J.E., Gurpur, P.B., Yablonka-Reuveni, Z., and Burkin, D.J. (2009). Laminin-111 restores regenerative capacity in a mouse model for alpha7 integrin congenital myopathy. *The American journal of pathology* *174*, 256-264.
- Scotti, M.M., and Swanson, M.S. (2016). RNA mis-splicing in disease. *Nature Reviews Genetics* *17*, 19-32.
- Shen, S., Park, J.W., Lu, Z.X., Lin, L., Henry, M.D., Wu, Y.N., Zhou, Q., and Xing, Y. (2014). rMATS: robust and flexible detection of differential alternative splicing from replicate RNA-Seq data. *Proceedings of the National Academy of Sciences of the United States of America* *111*, E5593-5601.
- Shinin, V., Gayraud-Morel, B., Gomès, D., and Tajbakhsh, S. (2006). Asymmetric division and cosegregation of template DNA strands in adult muscle satellite cells. *Nature cell biology* *8*, 677-687.
- Sinha, R., Kim, Y.J., Nomakuchi, T., Sahashi, K., Hua, Y., Rigo, F., Bennett, C.F., and Krainer, A.R. (2018). Antisense oligonucleotides correct the familial dysautonomia splicing defect in IKBKAP transgenic mice. *Nucleic acids research* *46*, 4833-4844.
- Song, W.K., Wang, W., Sato, H., Bielser, D.A., and Kaufman, S.J. (1993). Expression of alpha 7 integrin cytoplasmic domains during skeletal muscle development: alternate forms, conformational change, and homologies with serine/threonine kinases and tyrosine phosphatases. *Journal of cell science* *106* (Pt 4), 1139-1152.
- Teplova, M., Hafner, M., Teplov, D., Essig, K., Tuschl, T., and Patel, D.J. (2013). Structure-function studies of STAR family Quaking proteins bound to their in vivo RNA target sites. *Genes & development* *27*, 928-940.

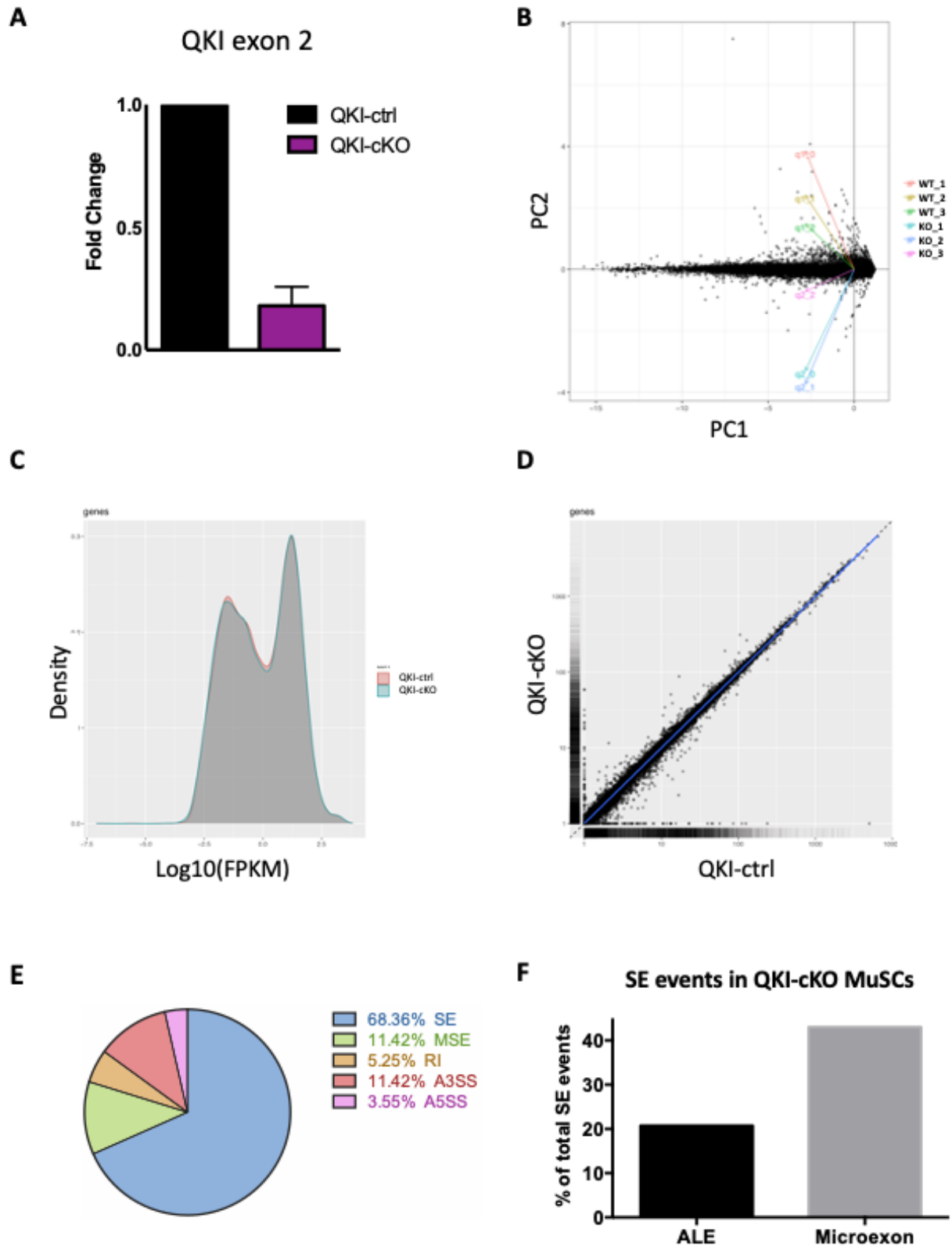
- Thomas, J.D., Sznajder Ł, J., Bardhi, O., Aslam, F.N., Anastasiadis, Z.P., Scotti, M.M., Nishino, I., Nakamori, M., Wang, E.T., and Swanson, M.S. (2017). Disrupted prenatal RNA processing and myogenesis in congenital myotonic dystrophy. *Genes & development* 31, 1122-1133.
- Trapnell, C., Roberts, A., Goff, L., Pertea, G., Kim, D., Kelley, D.R., Pimentel, H., Salzberg, S.L., Rinn, J.L., and Pachter, L. (2012). Differential gene and transcript expression analysis of RNA-seq experiments with TopHat and Cufflinks. *Nature protocols* 7, 562-578.
- Trapnell, C., Williams, B.A., Pertea, G., Mortazavi, A., Kwan, G., van Baren, M.J., Salzberg, S.L., Wold, B.J., and Pachter, L. (2010). Transcript assembly and quantification by RNA-Seq reveals unannotated transcripts and isoform switching during cell differentiation. *Nature biotechnology* 28, 511-515.
- van der Veer, E.P., de Bruin, R.G., Kraaijeveld, A.O., de Vries, M.R., Bot, I., Pera, T., Segers, F.M., Trompet, S., van Gils, J.M., Roeten, M.K., *et al.* (2013). Quaking, an RNA-binding protein, is a critical regulator of vascular smooth muscle cell phenotype. *Circulation research* 113, 1065-1075.
- von der Mark, H., Williams, I., Wendler, O., Sorokin, L., von der Mark, K., and Pöschl, E. (2002). Alternative splice variants of alpha 7 beta 1 integrin selectively recognize different laminin isoforms. *The Journal of biological chemistry* 277, 6012-6016.
- Wang, Y.X., Feige, P., Brun, C.E., Hekmatnejad, B., Dumont, N.A., Renaud, J.M., Faulkes, S., Guindon, D.E., and Rudnicki, M.A. (2019). EGFR-Aurka Signaling Rescues Polarity and Regeneration Defects in Dystrophin-Deficient Muscle Stem Cells by Increasing Asymmetric Divisions. *Cell stem cell* 24, 419-432.e416.
- Wheeler, T.M., Lueck, J.D., Swanson, M.S., Dirksen, R.T., and Thornton, C.A. (2007). Correction of CIC-1 splicing eliminates chloride channelopathy and myotonia in mouse models of myotonic dystrophy. *The Journal of clinical investigation* 117, 3952-3957.
- Wheeler, T.M., Sobczak, K., Lueck, J.D., Osborne, R.J., Lin, X., Dirksen, R.T., and Thornton, C.A. (2009). Reversal of RNA dominance by displacement of protein sequestered on triplet repeat RNA. *Science (New York, NY)* 325, 336-339.
- Wu, J.I., Reed, R.B., Grabowski, P.J., and Artzt, K. (2002). Function of quaking in myelination: regulation of alternative splicing. *Proceedings of the National Academy of Sciences of the United States of America* 99, 4233-4238.
- Yin, H., Price, F., and Rudnicki, M.A. (2013). Satellite cells and the muscle stem cell niche. *Physiological reviews* 93, 23-67.
- Ziober, B.L., Vu, M.P., Waleh, N., Crawford, J., Lin, C.S., and Kramer, R.H. (1993). Alternative extracellular and cytoplasmic domains of the integrin alpha 7 subunit are differentially expressed during development. *The Journal of biological chemistry* 268, 26773-26783.
- Zong, F.Y., Fu, X., Wei, W.J., Luo, Y.G., Heiner, M., Cao, L.J., Fang, Z., Fang, R., Lu, D., Ji, H., *et al.* (2014). The RNA-binding protein QKI suppresses cancer-associated aberrant splicing. *PLoS genetics* 10, e1004289.

4.8 Supplemental information



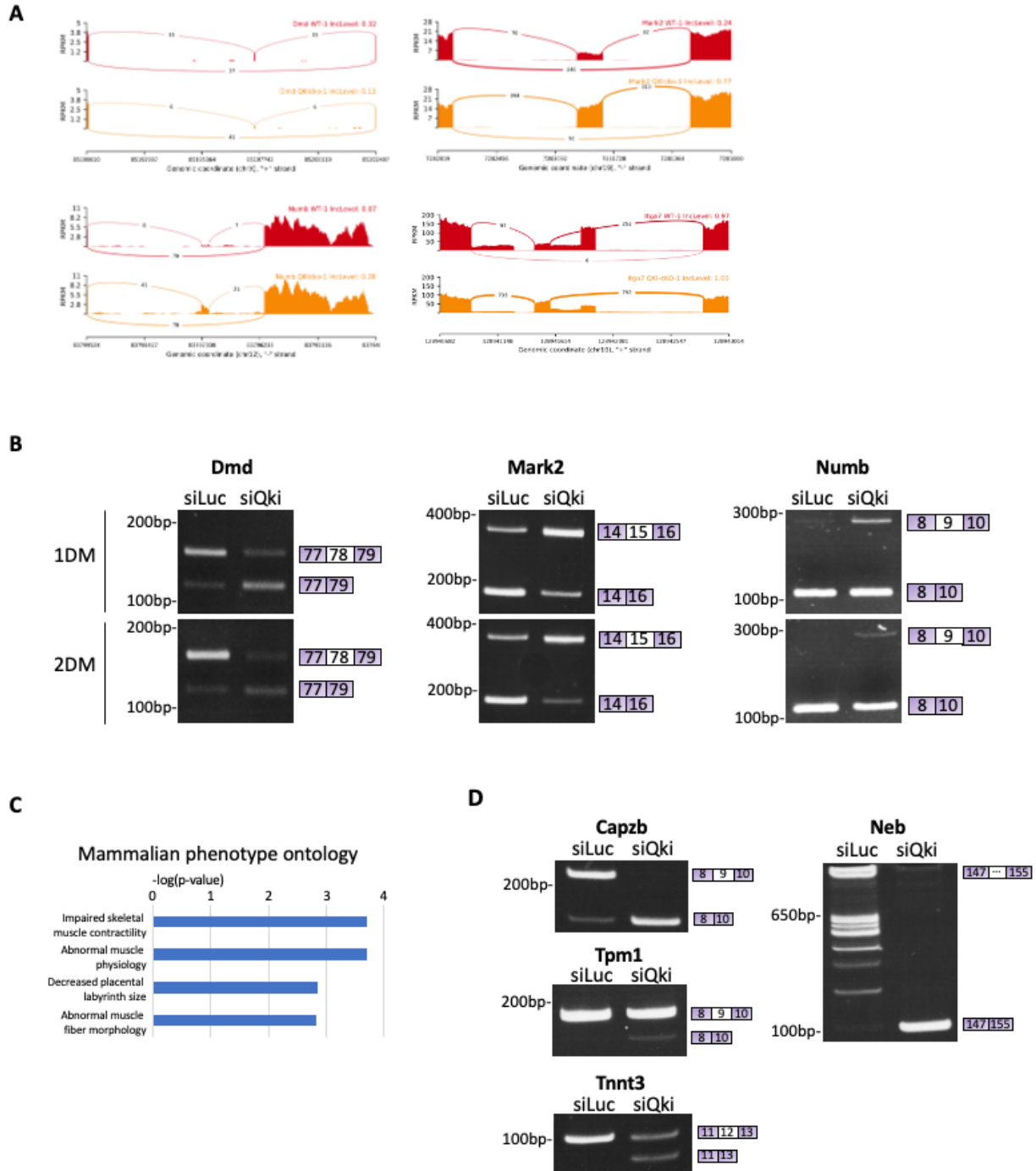
Supplemental figure S4.1.

(A) The breeding strategy for QKI-cKO and QKI-ctrl mice is illustrated. (B) Myofibers isolated from QKI-ctrl and QKI-cKO mice were cultured for 48h in fGM and were immunostained with Pax7 (green) and pan-QKI (orange) antibodies, and counterstained with DAPI (blue). MuSCs are indicated with white arrows. (C) Myofibers isolated from QKI-ctrl and QKI-cKO mice and cultured for 24h in fGM were assessed for Pax7 (green) and MyoD (red) expression. MuSCs are indicated with white arrows. Scale bar represents 10 μ m. (D) Quantification of total MuSCs from (C) (upper panel), Pax7+/MyoD- and Pax7+/MyoD+ (lower panels) (n=3 biological replicates, minimum 100 cells per group was quantified, ns - not significant).



Supplemental figure S4.2.

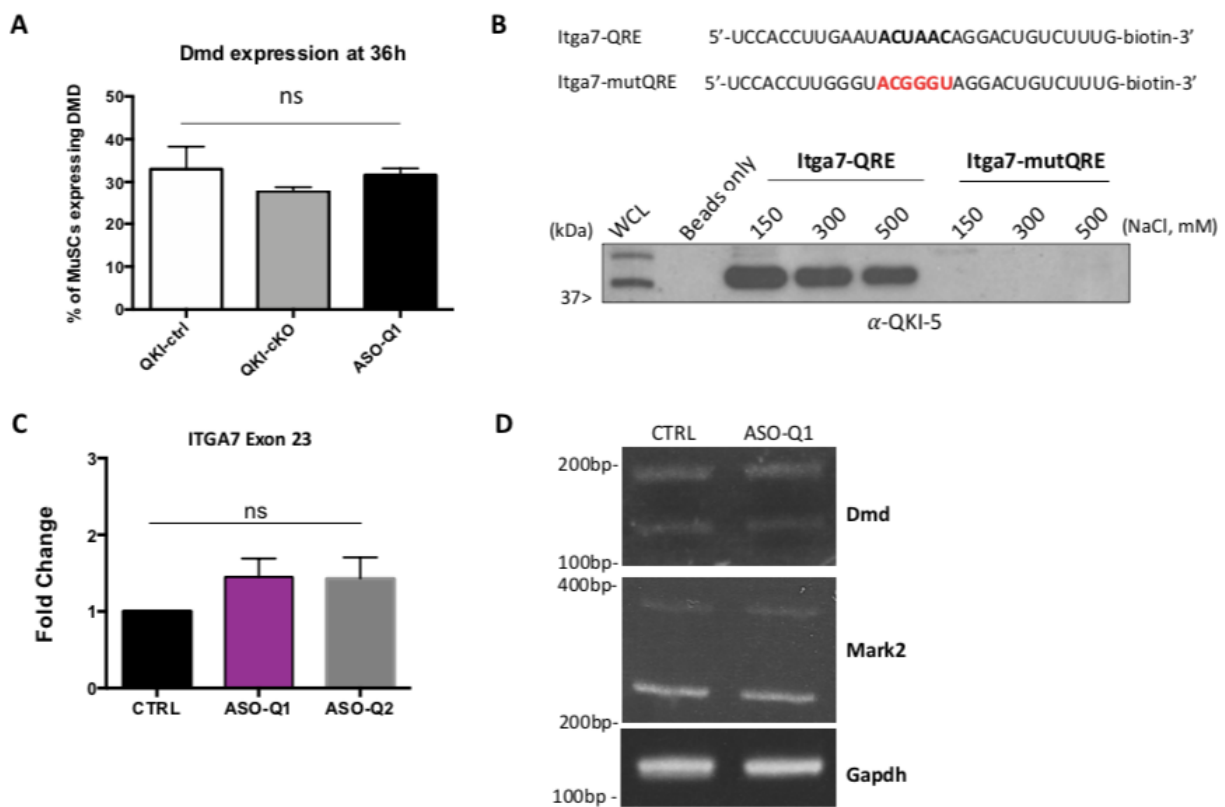
(A) Quantitative PCR confirmation of QKI knockout in MuSCs used for RNA-seq (n=3 biological replicates normalized to Gapdh levels, $p=0.0065$ unpaired student's t-test). (B) PCA plot of individual replicates. Dimensionality reduction was performed with cummeRbund software using Cufflinks output. (C) Distribution of FPKM scores across QKI-cKO and QKI-ctrl conditions from one replicate performed using cummeRbund software. (D) Pairwise scatterplot of gene expression from QKI-cKO and QKI-ctrl conditions. (E) Pie chart representing the summary of ASEs in QKI-cKO MuSCs compared to QKI-ctrl (SE: skipped exon; MSE: multiple skipped exons; RI: retained intron; A3SS: alternative 3' splice site; A5SS: alternative 5' splice site). (F) Percentage of skipped exon (SE) events which contained alternative last exon (ALE) or microexons.



Supplemental figure S4.3.

(A) Sashimi plots generated using rMATs software of asymmetric cell division factors. *Dmd*: Dystrophin; *Mark2*: Microtubule affinity regulating kinase. *Itga7*: Integrin alpha-7. WT: QKI-ctrl (red track); QKIcko: QKI-cKO (yellow track). (B) RT-PCR validation of SE events of *Dmd*,

Mark2, and *Numb* in primary MuSCs treated with siQKI or siLuc control and cultured in differentiation media for 1 day (1DM), or 2 days (2DM). (C) Pathway enrichment analysis carried out using Enrichr software of alternative last exon events in QKI-cKO versus QKI-ctrl MuSCs. (D) RT-PCR validation of AS events of select sarcomere components in proliferating MuSCs transfected with siQKI or siLuc. PCR products were run on acrylamide gels and stained with ethidium bromide. The migration of DNA markers in base pairs (bp) is shown on the left, and alternatively spliced exon is depicted on the right. Capzb: Capping actin protein of muscle Z-line subunit beta; Tpm1: Tropomyosin 1; Tnnt3: Troponin T3; Neb: Nebulin.



Supplemental figure S4.4.

(A) Quantification of proportion of Dmd-positive MuSCs in QKI-ctrl, QKI-cKO, and ASO-Q1-transfected myofibers cultured for 36h from Figure 4D. (Error bars represent mean \pm SEM, n= 3

biological replicates per group. ns - not significant, unpaired student's t-test.) (B) Biotinylated RNAs were used for RNA pull-down assays. The mutated sequence disrupting the core of the QRE is indicated in red. Immunoblotting of QKI-5 following RNA pull-down assay using C2C12 total cell lysates. Increasing NaCl concentrations in the wash buffer was used to define the high affinity RNA binding of QKI-5. (C) RT-qPCR of exon 23 of *Itga7* in ASO-treated MuSCs normalized to mock-transfected MuSCs. (Error bars represent mean \pm SEM, n = 3 independent replicates, ns - not significant, unpaired student's t-test) (D) RT-PCR validation of ASO-Q1 off-target AS events in proliferating MuSCs control (CTRL) transfected or transfected with ASO-Q1. PCR products were separated on acrylamide gels and stained with ethidium bromide. The migration of DNA markers in base pairs (bp) is shown on the left.

Chapter 5: Discussion

In summary, my work defined the function of the QKI RNA binding protein and arginine methylation by PRMT1 in MuSCs. In addition, I identified a new synergistic combination of type I PRMT inhibitors with PARP inhibitors for non-small cell lung carcinoma (NSCLC) A549 cells.

Mice with a conditional QKI deletion in their MuSCs were unable to regenerate skeletal muscle following injury compared to wildtype littermates. We performed RNAseq on purified MuSCs from the QKI conditional knockout mice and observed splicing changes in a subset of genes required for MuSC asymmetric division. We confirmed defective alternative splicing of a MuSC-specific surface marker, *Itga7*, in QKI-deficient MuSCs. These MuSCs exhibited polarity defects prior to cell division, resulting in a deficit of asymmetric cell divisions. Recapitulation of the specific *Itga7* splicing event with antisense oligonucleotides (ASOs) reproduced the polarity defects observed in QKI-deficient MuSCs.

We screened a library of FDA-approved epigenetic drugs and found that PARP inhibitors displayed strong synergy with the type I PRMT inhibitor MS023. The combination of the PRMT5 inhibitor EPZ015666 with the PARP inhibitor (BMN-673) was also synergistic. Combination treatment of MS023 and BMN-673 resulted in an increase in DNA damage which resulted in cytotoxicity. Furthermore, the MS023 and BMN-673 synergy was partially dependent on the 5'-methylthioadenosine phosphorylase (MTAP) deletion mutation that is an inherent characteristic of A549 NSCLC cells. We found that restoring MTAP expression in A549 cells attenuated the lethality of the combination treatment. Importantly, we then showed that MS023 treatment was sufficient to re-sensitize the PARP-inhibitor resistant ovarian cancer cell line PEO4 to PARP inhibition. Therefore, we identified a previously unreported synergy between PRMT inhibitors and PARP inhibitors in cancer cells.

Finally, we showed that treatment of freshly isolated MuSCs with MS023 retained them in a stem-like state in culture, allowing for *ex vivo* expansion of regeneration-competent MuSCs. We found that MS023-treated MuSCs were better at engrafting and regenerating injured muscle and were better able to repopulate the MuSC niche following regeneration, indicating an improvement in self-renewal. Importantly, we identified novel MuSC subpopulations through single cell RNA sequencing (scRNAseq) that emerged with MS023 treatment which were characterized by elevated levels of oxidative phosphorylation (OxPhos) and harboured markers of MuSC quiescence. Indeed, AMP kinase was activated in MS023-treated cells and was accompanied by increased mitochondrial biogenesis. Importantly, treatment of the preclinical mouse model for Duchenne muscular dystrophy (*mdx* mice) with MS023 resulted in improved grip strength and muscle force generation.

PRMT and PARP inhibitors synergize to kill MTAP-deficient cancer cells

In my first study, we performed a chemical screen which identified a strong synergy between MS023 and PARP inhibitors. These findings suggested that PRMT inhibitors can be an effective way of lowering the dose of PARP inhibitors used in the combination therapy to mitigate potential cytotoxicity in healthy tissues. As with any type of chemotherapy, the cytotoxic side effects must be carefully scrutinized. Importantly, we were able to kill NSCLC cells with low nanomolar-range concentrations of the PARP inhibitor BMN-673 (down to 0.3 nM) when combined with MS023. As a single agent treatment, BMN-673 had no effect at 100 times the concentration (30 nM), and was only moderately effective at killing cells at 50 nM.

Lung cancer is the leading cause of cancer-related death, and 85% of all diagnosed patients have a history of smoking (Belani et al., 2007). Non-small cell lung carcinoma (NSCLC)

dominates as the major type of lung cancer occurring in ~ 85% patients. NSCLC has a complex etiology with a wide range of known oncogenic pathways being activated among patients including mTOR signaling, receptor tyrosine kinase signalling, and cell cycle deregulation (Ding et al., 2008; Herbst et al., 2018). Therefore, finding a unified treatment that is effective in a wide range of NSCLC patients presents as a big challenge. Indeed, single agent treatment thus far has been highly toxic and impermanent (Juergens et al., 2011; Vansteenkiste et al., 2008). Thus, the identification of a synergy between PRMT inhibitors and PARP inhibitors presents a new therapeutic avenue for NSCLC.

PARPs catalyze the addition an important post-translational modification of negatively charged and branched poly(ADP-ribose) chains to various biological molecules, with known functions in DNA damage repair (Caron et al., 2019; O'Sullivan et al., 2019). The major PARP enzyme, PARP1, senses DNA lesions and binds to single strand DNA breaks, recruiting DNA damage repair (DDR) proteins such as XRCC1 (Lord and Ashworth, 2017). Given the critical role of PARP1 in DDR, inhibitors of PARP were developed to increase the efficacy of DNA-damaging agents used in cancer therapy (Zaremba and Curtin, 2007). PARP inhibitors were designed to "trap" PARP to DNA lesions by preventing the enzyme from dissociating from DNA, thereby interfering with DNA damage repair (Murai et al., 2012). Inhibitors of PARP are particularly effective in BRCA-mutant cancer cells due to their deficiencies in homologous recombination (HR) (Ashworth, 2008; Bryant et al., 2005; Farmer et al., 2005; Fong et al., 2009). Unfortunately, resistance to PARP inhibitors commonly occurs in patients with advanced cancer through increased drug efflux, reactivation of homologous recombination, restoration of replication fork stability, or loss of DNA double-strand break resection inhibition (Ronato et al., 2020). Therefore

identifying combinatory agents that can synergize with PARP inhibitors is important to re-sensitize resistant cells.

Other PARP inhibitors such as Niraparib, Rucaparib, Olaparib, and Veliparib are being tested in the clinic and differ in their ability to trap PARP to DNA lesions (Pommier et al., 2016). The PARP inhibitor used in our study, BMN-673 (also called Talazoparib) is the most potent PARP-trapping inhibitor and is 100-fold more potent than Niraparib, while Niraparib is more potent than Rucaparib and Olaparib (Murai et al., 2014). Veliparib is the least efficient at trapping PARP to DNA lesions. Interestingly, these compounds were all included in our screen, and the synergy with MS023 was inversely proportional to their PARP-trapping efficiency i.e. Veliparib was the most synergistic and Niraparib was the least. To functionally validate our screen, we used Talazoparib, which has the strongest trapping ability of all the PARP inhibitors. Therefore, future studies could examine whether this feature of PARP inhibition is related to the cytotoxic effects induced by treatment with MS023. For example, would Veliparib be more synergistic than Talazoparib given that it performed the best among the PARP inhibitors in our screen? It has been suggested that the ability to trap PARP to DNA, rather than just the ability to inhibit its PARylation activity, is a better indicator of cytotoxicity, since Talazoparib has been noted as the most cytotoxic of the PARP inhibitors mentioned above (Pommier et al., 2016). While this may remain true for single-agent therapy, it may not remain consistent when combining PARP inhibitors with other drugs.

The genetic deletion of *MTAP* occurs in ~40% of NSCLC patients (Schmid et al., 1998), therefore, a therapy that exploits the features of this deletion would benefit a broad base of patients. *MTAP* is required for the methionine salvage pathway, which metabolizes 5'-methylthioadenosine (MTA) to generate methionine and adenine (Zappia et al., 1988). In *MTAP*-negative cells, the

MTAP substrate MTA accumulates and acts as a specific and potent endogenous inhibitor of PRMT5 activity (Kryukov et al., 2016; Marjon et al., 2016; Mavrakis et al., 2016). Subsequently, MTAP-negative cells are inherently sensitive to inhibition of type I PRMTs (Fedoriw et al., 2019; Fong et al., 2019; Gao et al., 2019). Notably, due to the redundancy of PRMT1 and PRMT5 functions, it is expected that PRMT5 inhibitors would also synergize with PARP inhibitors. PARP inhibitors have been shown to synergize with PRMT5 inhibitors in acute myeloid leukemia cells (Hamard et al., 2018). Indeed, we showed that BMN-673 was also effective in combination with PRMT5 inhibitors in A549 cells.

In sum, we showed that targeting PRMTs as a combination treatment with PARP inhibitors could serve as a new therapeutic option for NSCLC and other MTAP-deficient cancers.

MS023 as a potential small molecule inhibitor for muscle wasting disease

The second part of my studies identified a role for PRMT1 in regulating the metabolism of MuSCs. The inhibition of type I PRMTs with MS023 reformed the MuSC identity to have elevated OxPhos and glycolysis, with a more stem-like transcriptional signature. The activation of Ampk was found to be critical for the enhanced proliferation phenotype, as siRNA against Ampk was sufficient to reverse the MS023 effect on proliferation. The MS023-treated cells were more efficient at regenerating injured muscle, suggesting that MS023 may be a viable option for patients with muscle wasting diseases such as Duchenne muscular dystrophy (DMD).

Therapeutic strategies for DMD have focused on gene-editing the dystrophin mutation in *ex vivo* cultured MuSCs followed by re-engraftment. An alternative approach is to target pathways within the MuSC that enhance their proliferative capacity while maintaining their ability to differentiate and complete muscle regeneration. However, the promise of the gene-editing

approach is currently impeded by the tendency of MuSCs to differentiate once isolated and cultured *ex vivo*, thus losing their stemness and ability to engraft (Fu et al., 2015a; Sacco et al., 2008). The goal of current research, therefore, is to identify small molecule inhibitors that can overcome these hurdles and prolong the window in which MuSCs can be expanded and/or gene-edited *ex vivo*, and then re-engrafted to replenish the MuSC pool in dystrophic patients.

Indeed, inhibitors have already been identified which improve MuSC expansion *ex vivo*. For instance, an inhibitor of the lysine methyltransferase SET domain containing 7 histone lysine methyltransferase (Setd7) allows for the *ex vivo* expansion of MuSCs which retain stemness, and therefore the ability to repopulate the MuSC pool in engraftment experiments (Judson et al., 2018). Setd7 is an important factor in the myogenic process. Through interaction with β -catenin, Setd7 regulates the transcription of Wnt-responsive genes required for the activation and differentiation of MuSCs (Tao et al., 2011).

Our study has therefore identified another small molecule inhibitor which may hold promise in the development of DMD therapeutics. Previous work shows that PRMT1-deficient myoblasts are highly proliferative, but lack the ability to differentiate, thus opening an opportunity to exploit the reversible nature of type I PRMT inhibitors such as MS023 and GSK3368715. These inhibitors can be used to maintain MuSCs in culture for a sufficient amount of time that would allow for gene-editing prior to engraftment. However, it has yet to be shown whether chronic exposure to PRMT inhibitors is well-tolerated *in vivo*.

The activation of Ampk, elevated energy metabolism, and self-renewal that we observed with MS023 treatment indicates that PRMTs are key metabolic regulators in MuSCs. The role of PRMT1 in the metabolism of other cell types has been demonstrated. For example, in human and mouse adipocytes, PRMT1 acts through the transcriptional co-activator PGC-1 α and regulates

thermogenic fat activation (Qiao et al., 2019). PGC-1 α was shown to be methylated by PRMT1, and this was required to stimulate mitochondrial biogenesis (Teyssier et al., 2005). These findings indicate that PRMT1 interacts with key regulators of cellular metabolism.

To our knowledge, we are the first group to characterize MuSC subpopulations that emerge in the presence of an epigenetic inhibitor and analysis of the MS023-specific clusters in the scRNAseq data allowed us to elucidate the metabolic determinants of MuSC self-renewal. The distinct metabolic signatures of self-renewing MuSC populations has been difficult to capture due to the constraints of *ex vivo* MuSC cultures (Relaix et al., 2021). Nonetheless, the metabolic states of proliferating and differentiating MuSCs have been described. When MuSCs exit quiescence and begin to proliferate, they shift from utilizing mainly OxPhos to glycolysis (Pala et al., 2018; Ryall et al., 2015). It has been shown that the initiation of terminal differentiation is mediated by the activation of pyruvate dehydrogenase (PDH), which in turn activates OxPhos while downregulating glycolysis (Hori et al., 2019). Therefore, metabolic reprogramming is inextricably tied to cell transition states of MuSCs.

PRMT1 has many substrates, yet we show that knockdown of Ampk with siRNA was sufficient to reverse the MS023-mediated increase in proliferation. Ampk is a major energy sensor in the cell that regulates energy balance and metabolic state (Hardie et al., 2016). We show that maintaining constitutive Ampk activation in cultured MuSCs through inhibition of type I PRMTs elevates OxPhos and enhances self-renewal. Interestingly, Ampk is known to regulate the transcriptional activation of genes required for mitochondrial biogenesis through activation of the Nrf1 transcription factor (Marin et al., 2017) and we show that Nrf1 mRNA and protein is elevated in MS023-treated MuSCs.

QKI mediates MuSC polarity and is critical for muscle regeneration

In the final chapter of my thesis, I identified QKI as the long sought-after regulator of *Itga7* splicing isoforms X1 and X2, and further characterized the role of QKI during *in vivo* muscle regeneration. The requirement of QKI for the establishment of polarity in the MuSC identifies for the first time the role of alternative splicing regulation in mediating asymmetric MuSC divisions. A major contributor to pathogenesis in certain muscle wasting diseases is the loss of balance between the niche-repopulating symmetric cell divisions and the progenitor creating asymmetric cell divisions (Yin et al., 2013). Loss or defects in asymmetric divisions results in fewer committed MuSCs that can terminally differentiate and generate new muscle. I have identified QKI as a key regulator of this process. Loss of QKI in MuSCs resulted in a deficiency in the number of myogenic progenitors on *ex vivo* cultured myofibers, likely due to a deficit in asymmetric MuSC divisions.

The striking regeneration defect observed with QKI deficiency is similar to what is observed with a *PAX7* genetic knockout (von Maltzahn et al., 2013), thus highlighting the importance of QKI in MuSC function. The loss of *PAX7* in MuSCs results in cell cycle arrest and deregulation of the *PAX7* transcriptional targets which are required for the myogenic program. The muscle regeneration defect is so striking that it resembled injured skeletal muscle in mice where MuSCs were ablated (von Maltzahn et al., 2013). The aberrant splicing observed in QKI deficient MuSCs was sufficient to induce a similarly striking phenotype, thereby shedding light on another important facet of the molecular machinery that is required for MuSC function.

Alternative splicing aberrations have been identified in muscle wasting diseases (Nakka et al., 2018). For instance, in myotonic dystrophy MBNL is sequestered to pathological CUG repeats in the DM protein kinase (DMPK1) RNA (Charlet et al., 2002; Philips et al., 1998; Thomas et al., 2017). As a result, MBNL is unavailable to mediate proper splicing of myotonic dystrophy type I

(DM1) and other muscle-specific targets. ASOs are being implemented as one strategy to target pathological splicing events. For example, an ASO which targets the pathological CUG repeats within the DMPK1 transcript frees MBNL to perform its normal functions in splicing and has been shown to improve myopathy in mouse models of myotonic dystrophy (Wheeler et al., 2007; Wheeler et al., 2009). One ASO drug dubbed Spinraza is approved for treatment of spinal muscular atrophy (SMA). Spinraza corrects exon 7 splicing of *SMN2*, resulting in increased functional amounts of the SMN protein that is otherwise dysfunctional in SMA patients (Finkel et al., 2016; Hua et al., 2011). We were able to recapitulate features of muscle disease by inducing a single splicing event with an ASO targeted to *Itga7*. Therefore, we can envision the use of ASOs to target similar AS aberrations in components of asymmetric cell machinery that may be involved in disease.

Chapter 6: Conclusion and Future Directions

Type I PRMT inhibition synergizes with PARP inhibitors

We have identified a synergy with the type I PRMT inhibitor MS023 and the PARP inhibitor BMN-673 that is sufficient to kill MTAP-negative NSCLC cells. Importantly, we show that this synergy is upheld in MTAP-proficient ovarian cancer cells that are resistant to PARP inhibition (PEO4).

PEO4 and PEO1 cell lines are derived from the same patient, wherein PEO1 cells contain a single BRCA2 mutation and are sensitive to PARP inhibitors due to deficiencies in HR. PEO4 are derived from PEO1 cells and contain a secondary BRCA2 mutation which restores its expression (Wolf et al., 1987), thereby restoring HR and making the cells resistant to PARP inhibitors. Importantly, PRMT1 deficiency is known to induce DNA damage with defects in HR (Yu et al., 2009), thus treatment with MS023 likely created HR defects which mimic what is seen in BRCA-mutated cancer cells, making the cells re-sensitized to PARP inhibition. An important next step would be to identify the robustness of this mechanism of synergy with MS023 and PARP inhibitors in other HR-proficient cancer cell lines.

Furthermore, given the effectiveness of the combination of MS023 and BMN-673 in cells with different genetic features (MTAP-deficiency and HR-proficiency), the exact mechanism of how these two pathways converge could potentially elucidate what other types of cancer cells would be vulnerable to their combination. One possibility is that arginine methylation on DNA damage response proteins is required for their recruitment to sites of DNA damage. Notably, PARylated proteins carry a negative charge and the highly basic RGG/RG motif that is known to be methylated by PRMTs is positively charged. It would be interesting to investigate these

interactions in the presence and absence of PRMT inhibitors and PARP inhibitors and assess the outcomes on DNA damage and repair.

It would also be important to determine whether PRMT inhibitors are effective with other PARP inhibitors that have different PARP-trapping efficiencies. Given the increase in DNA damage we observed with MS023 and BMN-673 treatment, the effectiveness of the PARP inhibitor at blocking DNA damage repair would be important in determining synergy. Indeed, PARP enzymes carry out other important functions in the cell, such as regulating transcription and apoptosis (Krishnakumar and Kraus, 2010). As such, it would be interesting to determine how much of the cytotoxicity of PARP inhibition in MTAP-negative NSCLC cells is attributed to the impairment of DNA damage repair.

Notably, the PARP inhibitors Niraparib, Rucaparib, Olaparib, and Veliparib were tested in our screen, and the synergy with MS023 was inversely proportional to their PARP-trapping efficiency i.e. Veliparib was the most synergistic and Niraparib was the least. To functionally validate our screen, we used Talazoparib, which has the strongest PARP-trapping ability of all the PARP inhibitors. Therefore, future studies could examine whether this feature of PARP inhibition is related to the cytotoxic effects induced by treatment with MS023. For example, would Veliparib be more synergistic than Talazoparib given that it performed the best among the PARP inhibitors in our screen? It has been suggested that the ability to trap PARP to DNA, rather than just the ability to inhibit its PARylation activity, is a better indicator of cytotoxicity, since Talazoparib has been noted as the most cytotoxic of the PARP inhibitors mentioned above (Pommier et al., 2016). While this may remain true for single-agent therapy, it may not apply when combining PARP inhibitors with other drugs that target different pathways.

We identified a synergy between PRMT5 inhibitors with the BMN-673 inhibitor. A new class of PRMT5 inhibition was recently developed which targets PRMT5 for degradation using proteolysis targeting chimera (PROTAC) technology (Shen et al., 2020). Therefore, it would be interesting to see if PRMT5 degradation is synergistic with PARP inhibitor treatment in MTAP-deficient cells. Indeed, Shen et al., (2020) noted that a compound which is structurally similar to the PRMT5 degrader and inhibits PRMT5 activity but does not degrade PRMT5 protein demonstrated less antiproliferative effects in MCF-7 breast cancer cell line. Therefore, it is possible that other cell types which are sensitive to PRMT degraders may not be sensitive to PRMT inhibitors and vice versa. Future studies which determine the exact effects of protein degradation versus protein inhibition in the cell would shed light on which cell types would be sensitive to either method.

MTAP-negative cells harbour a sensitivity to PRMT5 deficiency (Marjon et al., 2016). The same study identified a vulnerability of MTAP-negative cells to methionine adenosyltransferase II alpha (MAT2a) knockdown. MAT2a catalyzes the adenylation of methionine to produce S-adenosylmethionine (SAM), which serves as a universal methyl group donor for methyltransferase enzymes including PRMT5. Therefore, MTAP-negative cells require MAT2a and PRMT5 to maintain their viability. Interestingly, an inhibitor of MAT2a was recently developed and was shown to be synthetic lethal in MTAP-negative cancer cells through reduced PRMT5 activity (Kalev et al., 2021). Given that MAT2a and PRMT5 form an axis that MTAP-negative cancer cells are dependent on (Marjon et al., 2016), it would be interesting for future studies to determine whether MAT2a inhibition could replace PRMT5 inhibition in the synthetic lethality of PRMT5 and PARP inhibitors reported in our study.

Inhibiting type I PRMTs in MuSCs to enhance their therapeutic capacity

We have identified MS023 as a key inhibitor for enhancing MuSC self-renewal with improved engraftment and regenerative potential in injured muscle. It would be intriguing to determine whether other inhibitors of type I PRMTs, such as GSK3368715, would produce a similar phenotype in MuSCs. Moreover, transcriptomic profiling of PRMT1 knockout MuSCs at the single-cell level might identify which, if any, features of the self-renewal phenotype are specific to MS023 treatment. Indeed, MS023 treatment reduces aDMA of type I PRMT substrates, but has also been shown to increase binding affinity of type I PRMTs and some of its substrates in HEK293 cells (Cai et al., 2021b; Eram et al., 2016). Therefore, defining the protein interactome of PRMT1 in MS023 treated MuSCs compared to untreated MuSCs would shed some light on possible alternative mechanisms of type I PRMT inhibition.

Our data in mdx mice show that muscle force generation is improved 30 days after the final injection of MS023. It remains to be seen whether a single dose would be beneficial for a longer period of time. If multiple doses are required, further studies would need to be performed to assess safety and efficacy of repeated doses. Notably, inhibitors of PRMTs are being investigated for safety and efficacy in clinical trials (Wu et al., 2021) (Type I PRMT inhibitor GSK3368715, clinical trial NCT03666988, and PRMT5 inhibitor GSK3326595 clinical trial NCT02783300).

PRMTs are emerging major regulators of the myogenic process. A deeper interrogation of PRMT function in MuSCs can thus uncover their full potential as targets in the development of novel therapeutic strategies for muscle wasting diseases. For instance, a recent screen of small molecule inhibitors was performed to assess which targets were required for asymmetric MuSC division, and therefore required for muscle regeneration (Wang et al., 2019b). Wang et al., (2019) and colleagues discovered that inhibiting the epidermal growth factor receptor (EGFR) and Aurora

kinase A (AURKA) significantly shifted MuSCs away from asymmetric divisions and towards symmetric divisions. It would be interesting to include drugs that target PRMT1 and PRMT5 in a similar screen to determine the extent of their contribution to the balance between asymmetric and symmetric MuSC division.

We show that MS023 treatment generates previously uncharacterized subpopulations of self-renewing MuSCs, suggesting that transient or rare cell states may be amplified through treatment with other epigenetic inhibitors. Capture of short-lived MuSC transitional states has been difficult with current scRNAseq methodologies due to limited cell number, prompting a study of 365,000 single cells/nuclei pooled from over 100 publicly-available MuSC scRNAseq datasets to capture these populations (McKellar et al., 2021). Therefore, it can be envisaged that treatment with other epigenetic inhibitors which reprogram the identity of MuSCs may overcome the need to pool different datasets to study transitional MuSC states. For example, Ezh2, a component of the polycomb repressive complex (PRC2), is known to bind to the promoters of genes required for the myogenic program and prevent differentiation of MuSCs (Carette et al., 2004). Several Ezh2 inhibitors are commercially available, and it would be interesting to observe what unique features emerge in MuSC subpopulations when the block on differentiation is lifted with an inhibitor of Ezh2 and to note whether this would affect rates of MuSC self-renewal.

Furthermore, the use of small molecule inhibitors to study novel MuSC subpopulations would facilitate the association of specific molecular features with physiological cell behaviours *in vivo*. Initial scRNAseq experiments in MuSCs were mostly descriptive and confirmed what was already known about MuSC activation and how MuSCs contribute to muscle regeneration (Saber et al., 2020). Therefore, scRNAseq of MuSCs that have been reprogrammed with inhibitors can reveal previously uncharacterized MuSC trajectories or activation dynamics that would be

beneficial for muscle regeneration and may serve to identify novel treatment strategies for muscle wasting disease.

The role of QKI in MuSC polarity and muscle regeneration

We have identified QKI as a regulator of alternative splicing of key MuSC factors during *in vivo* muscle regeneration. In particular, aberrant splicing of the asymmetric cell division machinery in QKI-deficient MuSCs led to fewer myogenic progenitors, thereby partially explaining the severe regeneration defects. Given the similarity of the QKI knockout phenotype and severe muscle wasting diseases, it would be interesting to interrogate QKI isoform expression in muscle wasting disease patient samples. For example, a comparison of symptom severity in DMD patients could be correlated with reduced QKI expression or function, and perhaps the QKI-regulated network of alternatively spliced targets is deregulated leading to worsened muscle regenerative capabilities.

We showed that QKI-deficiency leads to inclusion of exon 5 in the *Itga7* mRNA, resulting in expression of the embryonic form of *Itga7* (*Itga7*-X1). While the X1 isoform is required during embryonic skeletal muscle development, we show that the switch from the X2 isoform to the X1 isoform in adult skeletal muscle is ‘toxic’ or not tolerated during muscle regeneration. A major function of the integrin family of proteins is to anchor cells to extracellular matrix proteins (Takada et al., 2007). It has been shown by other groups that the X1 and X2 isoforms of *Itga7* have different binding affinities for surrounding laminin isoforms, namely, the X1 isoform binds laminin-511 while the X2 isoform prefers laminin-111 (von der Mark et al., 2002). Our data suggest that the ratio of the X2/X1 isoforms that is established in QKI-deficient MuSCs negatively affects MuSC polarity, which may be due in part to incompatible interactions with the changing landscape of

extracellular laminin isoforms in adults. Therefore, future studies can focus on specific interactions of the *Itga7* isoforms with surrounding laminin isoforms that are present in the MuSC niche, as this may explain how the *Itga7* protein is polarized in MuSCs prior to asymmetric cell division during muscle regeneration.

QKI has been shown to have overlapping targets with the RNA binding protein polypyrimidine tract-binding protein (PTB) in the C2C12 immortalized muscle stem cell line (Hall et al., 2013). Our study focused on alternative splicing events which arose in *ex vivo* cultured QKI-deficient primary MuSCs, and it would be beneficial for future studies to determine whether these targets are affected by PTB depletion as well. Moreover, the study of what controls symmetric and asymmetric MuSCs divisions has largely been focused on the myogenic transcription factors PAX7, MyoD, and MYF5 (Kawabe et al., 2012; Kuang et al., 2007). Given the extensive involvement of QKI-regulated alternative splicing in MuSC asymmetric division machinery, it would also be interesting to investigate the role of other RNA binding proteins in MuSC function, and specifically in asymmetric MuSC division, as alternative splicing is a largely overlooked contributor to these functions. These future studies could perhaps explore the splicing machinery that controls isoform expression of *Itga7* and other MuSC asymmetric division factors, such as *Dmd*, *Numb*, *Mark2*, and *Pard3* that are required proper muscle regeneration.

Notably, we identified QKI as a regulator of *Dmd* splicing wherein QKI depletion led to exclusion of the penultimate exon 78. Alternative splicing of *Dmd* exon 78 is known to occur in patients with myotonic dystrophy (DM1), causing poor muscle architecture and mobility defects (Rau et al., 2015). Interestingly, exclusion of exon 78 in *Dmd* produces the embryonic isoform of dystrophin. As QKI depletion in adult MuSCs also generates the embryonic form of *Itga7* (exon 5 inclusion, X1 isoform), it would be interesting in future studies to examine whether QKI-mediated

exclusion of Dmd exon 78 leads to similar defects in MuSC asymmetric division. Is asymmetric MuSC machinery important in adult muscle regeneration but dispensable for embryonic development? Likewise, would other embryonic isoforms of MuSC asymmetric division machinery be toxic to adult MuSC functions? Indeed, proper isoform expression of key myogenic determinants has been shown to be crucial for developing skeletal muscle (Pistocchi et al., 2013). Therefore, it would be interesting to explore what other, if any, developmentally regulated transcripts are targets of QKI, and whether aberrant expression of their embryonic isoforms in adult MuSCs has an effect on muscle regeneration.

Stem cells and cancer cells: Key similarities and differences

Chapters 2 and 3 highlight the broad therapeutic range of type I PRMT inhibitors. In chapter 2, we show that MS023 has a potent ability to impede proliferation in cancer cells. In chapter 3, we show that treatment of MuSCs with MS023 provides a strong boost in proliferation and enhances self-renewal abilities of MuSCs. These findings raise the question of why type I PRMT inhibition leads to seemingly opposite phenotypes in stem cells than in cancer cells.

Cancer cells do share similarities with stem cells, including the shared capacity for extensive proliferation and self-renewal. Adult stem cells, including MuSCs, undergo self-renewal, a special type of cell division that gives rise to daughter cells with the same replication potential as the originating parental cell (Fuchs and Chen, 2013). Stem cell self-renewal is tightly regulated by cell intrinsic and extrinsic factors, allowing the stem cell to respond to signals that promote proliferation (Dumont et al., 2015a). For example, sonic hedgehog signaling is required for the self-renewal of normal stem cells (Amoyel et al., 2013; Zhang and Calderon, 2001). A subtype of cancer cells, often referred to as cancer stem cells (CSCs) or tumor initiating cells (TIC),

also possess features of self-renewal (Valent et al., 2012). Interestingly, it was shown that self-renewing pancreatic and rhabdomyosarcoma CSCs have elevated sonic hedgehog signaling, similarly to self-renewing normal stem cells (Li et al., 2007; Satheesha et al., 2016). However, a key difference is that CSCs lack the fine-tuned mechanisms that normal stem cells employ to regulate cell growth (Matthews et al., 2022; Rossi et al., 2020). The uncontrolled cell growth of cancer cells is often caused by inactivation of key cell cycle control genes such as Rb and p53 (Engeland, 2022). In fact, mutations which give cancer cells the ability to divide uncontrollably can also be exploited with targeted drug therapy, as surrounding healthy tissue will not carry the same genetic profile and therefore do not possess the same vulnerabilities.

Another important feature that is shared between normal stem cells and cancer stem cells is the capacity to differentiate into phenotypically diverse cell types (Batlle and Clevers, 2017). Normal stem cells are built to respond to specific cues in their environment and exit the cell cycle to initiate a tightly regulated differentiation protocol, giving rise to precisely specified cell fates with specialized functions in adult tissue. For example, MuSCs have the ability to exit the cell cycle and differentiate into specialized myoblasts that fuse to form myotubes which eventually make up the mature muscle tissue (Lobo et al., 2007; Yin et al., 2013). The characteristics of CSC differentiation differ from normal stem cells, and a unifying hierarchy for CSC differentiation remains to be elucidated. An important distinguishing feature of CSCs from normal stem cells is that most models of CSC differentiation describe two states: (1) the cancer stem cell and (2) all other oncogenic cells (Prager et al., 2019); thereby lacking the specificity and regulation seen in normal stem cells.

These key differences in the underlying mechanisms that guide the biology of cancer and stem cells could impact the differences in their responses to treatment with the same drug, such as MS023.

Inhibition of Type I PRMTs with MS023 resulted in increased self-renewal of MuSCs and retained their stemness while blocking differentiation. Other stem cell types have responded similarly to PRMT1 inhibition. For example, it was shown that tissue-specific deletion of PRMT1 in intestinal stem cells caused increased self-renewal of the crypt cells, but hampered differentiation into adult intestinal tissue (Xue et al., 2021). Therefore, during the activation of stem cells, MS023 acts to promote proliferation and self-renewal. We proposed that the enhanced proliferation phenotype of MS023-treated MuSCs is supported by elevated cellular metabolism mediated by increased AMPK activation. Interestingly, a common hallmark of cancer cells is to employ Warburg glycolysis (increased glucose uptake and glucose metabolism in the presence of oxygen) as a major source of energy for the cell (Vander Heiden et al., 2009). AMPK was shown to suppress Warburg glycolysis in lymphoma and repress tumor growth *in vivo* (Teperino et al., 2012), suggesting that AMPK activity has different metabolic outcomes depending on the cellular context. Therefore, one potential mechanism through which we observe opposite phenotypes in cancer and stem cells is via differential metabolic dependencies. Future studies could explore other possible mechanisms that are known to regulate stem cell activation and proliferation and test whether these mechanisms function differently in cancer cells to explain the responses to type I PRMT inhibition. Additionally, it would be important to examine relative expression levels of PRMTs in cancer cells and stem cells, as this may also partially explain the different response to PRMT inhibitors.

One interesting avenue to pursue could be the effect of type I PRMT inhibition on the function of RNA binding proteins (RBPs) in stem cells and in cancer. Chapter 4 of this thesis highlighted the importance of maintaining QKI-mediated splicing networks for MuSC function. Interestingly, QKI is a target of PRMT1 (Cote et al., 2003), and has known roles in cancer (Chen et al., 2012; Li et al., 2002; Yu et al., 2014). It would be intriguing to determine the effect of PRMT1 inhibition on QKI-mediated splicing networks in MuSCs, and further determine whether there are common splicing alterations in cancer cells treated with PRMT inhibitors. While many of the QKI targets identified in Chapter 4 were MuSC-specific, several targets could have effects on tumor progression. For example, LAMA2 was alternatively spliced in QKI-cKO MuSCs, and has a known role in several types of cancers including pituitary adenomas (Wang et al., 2019a) and colorectal cancer (Lee et al., 2012). Future studies can perhaps shed light on whether type I PRMT inhibition would affect the splicing pattern of these known cancer-associated genes via alteration of QKI function in cancer cells.

Chapter 7: References

- Agolini E, D.M., Bellacchio E, Alesi V, Radio FC, Torella A, Musacchia F, Tartaglia M, Dallapiccola B, Nigro V, Digilio MC, Novelli A. (2018). Expanding the clinical and molecular spectrum of PRMT7 mutations: 3 additional patients and review. *Clin Genet* 93, 675-681.
- Akawi, N., McRae J, A.M., Balasubramanian M, Blyth M, Brady AF, Clayton S, Cole T, Deshpande C, , and al., e. (2015). Discovery of four recessive developmental disorders using probabilistic genotype and phenotype matching among 4,125 families. *Nat Genet* 47, 1363-1369.
- Amoyel, M., Sanny, J., Burel, M., and Bach, E.A. (2013). Hedgehog is required for CySC self-renewal but does not contribute to the GSC niche in the *Drosophila* testis. *Development (Cambridge, England)* 140, 56-65.
- Antonyamy, S., Bonday, Z., Campbell, R.M., Doyle, B., Druzina, Z., Gheyi, T., Han, B., Jungheim, L.N., Qian, Y., Rauch, C., *et al.* (2012). Crystal structure of the human PRMT5:MEP50 complex. *Proceedings of the National Academy of Sciences of the United States of America* 109, 17960-17965.
- Arnold, L., Henry, A., Poron, F., Baba-Amer, Y., van Rooijen, N., Plonquet, A., Gherardi, R.K., and Chazaud, B. (2007). Inflammatory monocytes recruited after skeletal muscle injury switch into antiinflammatory macrophages to support myogenesis. *The Journal of experimental medicine* 204, 1057-1069.
- Backx, L., Fryns, J.P., Marcelis, C., Devriendt, K., Vermeesch, J., and Van Esch, H. (2010). Haploinsufficiency of the gene Quaking (QKI) is associated with the 6q terminal deletion syndrome. *American journal of medical genetics Part A* 152a, 319-326.
- Baghdadi, M.B., Firmino, J., Soni, K., Evano, B., Di Girolamo, D., Mourikis, P., Castel, D., and Tajbakhsh, S. (2018). Notch-Induced miR-708 Antagonizes Satellite Cell Migration and Maintains Quiescence. *Cell stem cell* 23, 859-868.e855.
- Bancroft, J.D., and Layton, C. (2013). 11 - Connective and mesenchymal tissues with their stains. In *Bancroft's Theory and Practice of Histological Techniques (Seventh Edition)*, S.K. Suvarna, C. Layton, and J.D. Bancroft, eds. (Oxford: Churchill Livingstone), pp. 187-214.
- Baralle, F.E., and Giudice, J. (2017). Alternative splicing as a regulator of development and tissue identity. *Nature reviews Molecular cell biology* 18, 437-451.
- Battle, E., and Clevers, H. (2017). Cancer stem cells revisited. *Nature medicine* 23, 1124-1134.
- Bayen, S., Saini, S., Gaur, P., Duraisamy, A.J., Kumar Sharma, A., Pal, K., Vats, P., and Singh, S.B. (2018). PRMT1 promotes hyperglycemia in a FoxO1-dependent manner, affecting glucose metabolism, during hypobaric hypoxia exposure, in rat model. *Endocrine* 59, 151-163.
- Bedford, M.T., and Clarke, S.G. (2009). Protein arginine methylation in mammals: who, what, and why. *Molecular cell* 33, 1-13.
- Belani, C.P., Marts, S., Schiller, J., and Socinski, M.A. (2007). Women and lung cancer: epidemiology, tumor biology, and emerging trends in clinical research. *Lung cancer (Amsterdam, Netherlands)* 55, 15-23.
- Ben-Porath, I., Thomson, M.W., Carey, V.J., Ge, R., Bell, G.W., Regev, A., and Weinberg, R.A. (2008). An embryonic stem cell-like gene expression signature in poorly differentiated aggressive human tumors. *Nature genetics* 40, 499-507.
- Bentzinger, C.F., von Maltzahn, J., Dumont, N.A., Stark, D.A., Wang, Y.X., Nhan, K., Frenette, J., Cornelison, D.D., and Rudnicki, M.A. (2014). Wnt7a stimulates myogenic stem cell motility and engraftment resulting in improved muscle strength. *The Journal of cell biology* 205, 97-111.

- Bertero, A., and Murry, C.E. (2018). Hallmarks of cardiac regeneration. *Nature reviews Cardiology* *15*, 579-580.
- Beuck, C., Qu, S., Fagg, W.S., Ares, M., Jr., and Williamson, J.R. (2012). Structural analysis of the quaking homodimerization interface. *Journal of molecular biology* *423*, 766-781.
- Bezzi, M., Teo, S.X., Muller, J., Mok, W.C., Sahu, S.K., Vardy, L.A., Bonday, Z.Q., and Guccione, E. (2013). Regulation of constitutive and alternative splicing by PRMT5 reveals a role for Mdm4 pre-mRNA in sensing defects in the spliceosomal machinery. *Genes & development* *27*, 1903-1916.
- Bhattacharya, D., Shah, V., Oresajo, O., and Scimè, A. (2021). p107 mediated mitochondrial function controls muscle stem cell proliferative fates. *Nature communications* *12*, 5977.
- Birnbaum, R., Yosha-Orpaz, N., Yanoov-Sharav, M., Kidron, D., Gur, H., Yosovich, K., Lerman-Sagie, T., Malinger, G., and Lev, D. (2019). Prenatal and postnatal presentation of PRMT7 related syndrome: Expanding the phenotypic manifestations. *American journal of medical genetics Part A* *179*, 78-84.
- Bjornson, C.R., Cheung, T.H., Liu, L., Tripathi, P.V., Steeper, K.M., and Rando, T.A. (2012). Notch signaling is necessary to maintain quiescence in adult muscle stem cells. *Stem cells* *30*, 232-242.
- Blanc, R.S., and Richard, S. (2017). Arginine Methylation: The Coming of Age. *Molecular cell* *65*, 8-24.
- Blanc, R.S., Vogel, G., Chen, T., Crist, C., and Richard, S. (2016). PRMT7 Preserves Satellite Cell Regenerative Capacity. *Cell reports* *14*, 1528-1539.
- Blanc, R.S., Vogel, G., Li, X., Yu, Z., Li, S., and Richard, S. (2017). Arginine Methylation by PRMT1 Regulates Muscle Stem Cell Fate. *Molecular and cellular biology* *37*.
- Boisvert, F.-M., Déry, U., Masson, J.-Y., and Richard, S. (2005a). Arginine methylation of MRE11 by PRMT1 is required for DNA damage checkpoint control. *Genes & Dev* *19*, 671-676.
- Boisvert, F.M., Cote, J., Boulanger, M.C., Cleroux, P., Bachand, F., Autexier, C., and Richard, S. (2002). Symmetrical dimethylarginine methylation is required for the localization of SMN in Cajal bodies and pre-mRNA splicing. *The Journal of cell biology* *159*, 957-969.
- Boisvert, F.M., Dery, U., Masson, J.Y., and Richard, S. (2005b). Arginine methylation of MRE11 by PRMT1 is required for DNA damage checkpoint control. *Genes & development* *19*, 671-676.
- Boisvert, F.M., Rhie, A., Richard, S., and Doherty, A.J. (2005c). The GAR motif of 53BP1 is arginine methylated by PRMT1 and is necessary for 53BP1 DNA binding activity. *Cell cycle (Georgetown, Tex)* *4*, 1834-1841.
- Bokar, J.A., Shambaugh, M.E., Polayes, D., Matera, A.G., and Rottman, F.M. (1997). Purification and cDNA cloning of the AdoMet-binding subunit of the human mRNA (N6-adenosine)-methyltransferase. *RNA (New York, NY)* *3*, 1233-1247.
- Bonnet, A., Lambert, G., Ernest, S., Dutrieux, F.X., Couplier, F., Lemoine, S., Lobbardi, R., and Rosa, F.M. (2017). Quaking RNA-Binding Proteins Control Early Myofibril Formation by Modulating Tropomyosin. *Developmental cell* *42*, 527-541.e524.
- Bortoli, S., Renault, V., Eveno, E., Auffray, C., Butler-Browne, G., and Piétu, G. (2003). Gene expression profiling of human satellite cells during muscular aging using cDNA arrays. *Gene* *321*, 145-154.
- Boscolo Sesillo, F., Fox, D., and Sacco, A. (2019). Muscle Stem Cells Give Rise to Rhabdomyosarcomas in a Severe Mouse Model of Duchenne Muscular Dystrophy. *Cell reports* *26*, 689-701.e686.

- Boswell, R.E., and Mahowald, A.P. (1985). tudor, a gene required for assembly of the germ plasm in *Drosophila melanogaster*. *Cell* 43, 97-104.
- Boutz, P.L., Chawla, G., Stoilov, P., and Black, D.L. (2007). MicroRNAs regulate the expression of the alternative splicing factor nPTB during muscle development. *Genes & development* 21, 71-84.
- Brahms, H., Raymackers, J., Union, A., de Keyser, F., Meheus, L., and Lührmann, R. (2000). The C-terminal RG dipeptide repeats of the spliceosomal Sm proteins D1 and D3 contain symmetrical dimethylarginines, which form a major B-cell epitope for anti-Sm autoantibodies. *The Journal of biological chemistry* 275, 17122-17129.
- Bulfield, G., Siller, W.G., Wight, P.A., and Moore, K.J. (1984). X chromosome-linked muscular dystrophy (mdx) in the mouse. *Proceedings of the National Academy of Sciences of the United States of America* 81, 1189-1192.
- Butler, A., Hoffman, P., Smibert, P., Papalexi, E., and Satija, R. (2018). Integrating single-cell transcriptomic data across different conditions, technologies, and species. *Nature biotechnology* 36, 411-420.
- Cai, T., Cinkornpumin, J.K., Yu, Z., Villarreal, O.D., Pastor, W.A., and Richard, S. (2021a). Deletion of RBMX RGG/RG motif in Shashi-XLID syndrome leads to aberrant p53 activation and neuronal differentiation defects. *Cell reports* 36, 109337.
- Cai, T., Yu, Z., Wang, Z., Liang, C., and Richard, S. (2021b). Arginine methylation of SARS-Cov-2 nucleocapsid protein regulates RNA binding, its ability to suppress stress granule formation, and viral replication. *The Journal of biological chemistry* 297, 100821.
- Caretti, G., Di Padova, M., Micales, B., Lyons, G.E., and Sartorelli, V. (2004). The Polycomb Ezh2 methyltransferase regulates muscle gene expression and skeletal muscle differentiation. *Genes & development* 18, 2627-2638.
- Castle, J.C., Zhang, C., Shah, J.K., Kulkarni, A.V., Kalsotra, A., Cooper, T.A., and Johnson, J.M. (2008). Expression of 24,426 human alternative splicing events and predicted cis regulation in 48 tissues and cell lines. *Nature genetics* 40, 1416-1425.
- Cerletti, M., Jang, Y.C., Finley, L.W., Haigis, M.C., and Wagers, A.J. (2012). Short-term calorie restriction enhances skeletal muscle stem cell function. *Cell stem cell* 10, 515-519.
- Chang, N.C., Chevalier, F.P., and Rudnicki, M.A. (2016). Satellite Cells in Muscular Dystrophy - Lost in Polarity. *Trends in molecular medicine* 22, 479-496.
- Chargé, S.B., and Rudnicki, M.A. (2004). Cellular and molecular regulation of muscle regeneration. *Physiological reviews* 84, 209-238.
- Charlet, B.N., Savkur, R.S., Singh, G., Philips, A.V., Grice, E.A., and Cooper, T.A. (2002). Loss of the muscle-specific chloride channel in type 1 myotonic dystrophy due to misregulated alternative splicing. *Molecular cell* 10, 45-53.
- Chen, A.J., Paik, J.H., Zhang, H., Shukla, S.A., Mortensen, R., Hu, J., Ying, H., Hu, B., Hurt, J., Farny, N., *et al.* (2012). STAR RNA-binding protein Quaking suppresses cancer via stabilization of specific miRNA. *Genes & development* 26, 1459-1472.
- Chen, C., Nott, T.J., Jin, J., and Pawson, T. (2011). Deciphering arginine methylation: Tudor tells the tale. *Nature Reviews Molecular Cell Biology* 12, 629-642.
- Chen, E.Y., Tan, C.M., Kou, Y., Duan, Q., Wang, Z., Meirelles, G.V., Clark, N.R., and Ma'ayan, A. (2013). Enrichr: interactive and collaborative HTML5 gene list enrichment analysis tool. *BMC bioinformatics* 14, 128.

- Chen, T., Damaj, B.B., Herrera, C., Lasko, P., and Richard, S. (1997). Self-association of the single-KH-domain family members Sam68, GRP33, GLD-1, and Qk1: role of the KH domain. *Molecular and cellular biology* *17*, 5707-5718.
- Chen, T., and Richard, S. (1998). Structure-function analysis of Qk1: a lethal point mutation in mouse quaking prevents homodimerization. *Molecular and cellular biology* *18*, 4863-4871.
- Chen, X., Liu, Y., Xu, C., Ba, L., Liu, Z., Li, X., Huang, J., Simpson, E., Gao, H., Cao, D., *et al.* (2021a). QKI is a critical pre-mRNA alternative splicing regulator of cardiac myofibrillogenesis and contractile function. *Nature communications* *12*, 89.
- Chen, Y.-r., Li, H.-n., Zhang, L.-j., Zhang, C., and He, J.-g. (2021b). Protein Arginine Methyltransferase 5 Promotes Esophageal Squamous Cell Carcinoma Proliferation and Metastasis via LKB1/AMPK/mTOR Signaling Pathway. *Frontiers in Bioengineering and Biotechnology* *9*.
- Chen, Y.L., Sheu, J.J., Sun, C.K., Huang, T.H., Lin, Y.P., and Yip, H.K. (2020). MicroRNA-214 modulates the senescence of vascular smooth muscle cells in carotid artery stenosis. *Molecular medicine (Cambridge, Mass)* *26*, 46.
- Chitiprolu, M., Jagow, C., Tremblay, V., Bondy-Chorney, E., Paris, G., Savard, A., Palidwor, G., Barry, F.A., Zinman, L., Keith, J., *et al.* (2018). A complex of C9ORF72 and p62 uses arginine methylation to eliminate stress granules by autophagy. *Nature communications* *9*, 2794.
- Cho, D.S., and Doles, J.D. (2017). Single cell transcriptome analysis of muscle satellite cells reveals widespread transcriptional heterogeneity. *Gene* *636*, 54-63.
- Cochrane, A., Kelaini, S., Tsifaki, M., Bojdo, J., Vilà-González, M., Drehmer, D., Caines, R., Magee, C., Eleftheriadou, M., Hu, Y., *et al.* (2017). Quaking Is a Key Regulator of Endothelial Cell Differentiation, Neovascularization, and Angiogenesis. *Stem cells* *35*, 952-966.
- Collo, G., Starr, L., and Quaranta, V. (1993). A new isoform of the laminin receptor integrin alpha 7 beta 1 is developmentally regulated in skeletal muscle. *The Journal of biological chemistry* *268*, 19019-19024.
- Conerly, M.L., Yao, Z., Zhong, J.W., Groudine, M., and Tapscott, S.J. (2016). Distinct Activities of Myf5 and MyoD Indicate Separate Roles in Skeletal Muscle Lineage Specification and Differentiation. *Developmental cell* *36*, 375-385.
- Cooper, R.N., Tajbakhsh, S., Mouly, V., Cossu, G., Buckingham, M., and Butler-Browne, G.S. (1999). In vivo satellite cell activation via Myf5 and MyoD in regenerating mouse skeletal muscle. *Journal of cell science* *112 (Pt 17)*, 2895-2901.
- Cote, J., Boisvert, F.M., Boulanger, M.C., Bedford, M.T., and Richard, S. (2003). Sam68 RNA binding protein is an in vivo substrate for protein arginine N-methyltransferase 1. *Molecular biology of the cell* *14*, 274-287.
- Côté, J., and Richard, S. (2005). Tudor domains bind symmetrical dimethylated arginines. *The Journal of biological chemistry* *280*, 28476-28483.
- Couturier, C.P., Ayyadhury, S., Le, P.U., Nadaf, J., Monlong, J., Riva, G., Allache, R., Baig, S., Yan, X., Bourgey, M., *et al.* (2020). Single-cell RNA-seq reveals that glioblastoma recapitulates a normal neurodevelopmental hierarchy. *Nature communications* *11*, 3406.
- Cura, V., Troffer-Charlier, N., Lambert, M.A., Bonnefond, L., and Cavarelli, J. (2014). Cloning, expression, purification and preliminary X-ray crystallographic analysis of mouse protein arginine methyltransferase 7. *Acta crystallographica Section F, Structural biology communications* *70*, 80-86.

- Dacwag, C.S., Ohkawa, Y., Pal, S., Sif, S., and Imbalzano, A.N. (2007). The protein arginine methyltransferase Prmt5 is required for myogenesis because it facilitates ATP-dependent chromatin remodeling. *Molecular and cellular biology* 27, 384-394.
- Darbelli, L., and Richard, S. (2016). Emerging functions of the Quaking RNA-binding proteins and link to human diseases. *Wiley interdisciplinary reviews RNA* 7, 399-412.
- Darbelli, L., Vogel, G., Almazan, G., and Richard, S. (2016). Quaking Regulates Neurofascin 155 Expression for Myelin and Axoglial Junction Maintenance. *The Journal of neuroscience : the official journal of the Society for Neuroscience* 36, 4106-4120.
- Dave, H.D., and Varacallo, M. (2019). Anatomy, Skeletal Muscle. In *StatPearls (Treasure Island (FL): StatPearls Publishing StatPearls Publishing LLC.)*.
- de Bruin, R.G., Shiue, L., Prins, J., de Boer, H.C., Singh, A., Fagg, W.S., van Gils, J.M., Duijs, J.M., Katzman, S., Kraaijeveld, A.O., *et al.* (2016). Quaking promotes monocyte differentiation into pro-atherogenic macrophages by controlling pre-mRNA splicing and gene expression. *Nature communications* 7, 10846.
- De Micheli, A.J., Laurillard, E.J., Heinke, C.L., Ravichandran, H., Fraczek, P., Soueid-Baumgarten, S., De Vlaminck, I., Elemento, O., and Cosgrove, B.D. (2020). Single-Cell Analysis of the Muscle Stem Cell Hierarchy Identifies Heterotypic Communication Signals Involved in Skeletal Muscle Regeneration. *Cell reports* 30, 3583-3595.e3585.
- Deato, M.D., Marr, M.T., Sottero, T., Inouye, C., Hu, P., and Tjian, R. (2008). MyoD targets TAF3/TRF3 to activate myogenin transcription. *Molecular cell* 32, 96-105.
- Dell'Orso, S., Juan, A.H., Ko, K.D., Naz, F., Perovanovic, J., Gutierrez-Cruz, G., Feng, X., and Sartorelli, V. (2019). Single cell analysis of adult mouse skeletal muscle stem cells in homeostatic and regenerative conditions. *Development (Cambridge, England)* 146.
- Desrosiers, R., Friderici, K., and Rottman, F. (1974). Identification of methylated nucleosides in messenger RNA from Novikoff hepatoma cells. *Proceedings of the National Academy of Sciences of the United States of America* 71, 3971-3975.
- Dhar, S., Vemulapalli, V., Patananan, A.N., Huang, G.L., Di Lorenzo, A., Richard, S., Comb, M.J., Guo, A., Clarke, S.G., and Bedford, M.T. (2013). Loss of the major Type I arginine methyltransferase PRMT1 causes substrate scavenging by other PRMTs. *Scientific reports* 3, 1311.
- Di Croce, L., and Helin, K. (2013). Transcriptional regulation by Polycomb group proteins. *Nature structural & molecular biology* 20, 1147-1155.
- Dillman, A.A., Hauser, D.N., Gibbs, J.R., Nalls, M.A., McCoy, M.K., Rudenko, I.N., Galter, D., and Cookson, M.R. (2013). mRNA expression, splicing and editing in the embryonic and adult mouse cerebral cortex. *Nature neuroscience* 16, 499-506.
- Ding, L., Getz, G., Wheeler, D.A., Mardis, E.R., McLellan, M.D., Cibulskis, K., Sougnez, C., Greulich, H., Muzny, D.M., Morgan, M.B., *et al.* (2008). Somatic mutations affect key pathways in lung adenocarcinoma. *Nature* 455, 1069-1075.
- Ding, R., Horie, M., Nagasaka, S., Ohsumi, S., Shimizu, K., Honda, H., Nagamori, E., Fujita, H., and Kawamoto, T. (2020). Effect of cell-extracellular matrix interaction on myogenic characteristics and artificial skeletal muscle tissue. *Journal of bioscience and bioengineering* 130, 98-105.
- Dominissini, D., Moshitch-Moshkovitz, S., Schwartz, S., Salmon-Divon, M., Ungar, L., Osenberg, S., Cesarkas, K., Jacob-Hirsch, J., Amariglio, N., Kupiec, M., *et al.* (2012). Topology of the human and mouse m6A RNA methylomes revealed by m6A-seq. *Nature* 485, 201-206.

- Dos Santos, M., Backer, S., Saintpierre, B., Izac, B., Andrieu, M., Letourneur, F., Relaix, F., Sotiropoulos, A., and Maire, P. (2020). Single-nucleus RNA-seq and FISH identify coordinated transcriptional activity in mammalian myofibers. *Nature communications* *11*, 5102.
- Dufresne, S.S., Dumont, N.A., Boulanger-Piette, A., Fajardo, V.A., Gamu, D., Kake-Guena, S.A., David, R.O., Bouchard, P., Lavergne, É., Penninger, J.M., *et al.* (2016). Muscle RANK is a key regulator of Ca²⁺ storage, SERCA activity, and function of fast-twitch skeletal muscles. *American journal of physiology Cell physiology* *310*, C663-672.
- Dumont, N.A., and Frenette, J. (2013). Macrophage colony-stimulating factor-induced macrophage differentiation promotes regrowth in atrophied skeletal muscles and C2C12 myotubes. *The American journal of pathology* *182*, 505-515.
- Dumont, N.A., Wang, Y.X., and Rudnicki, M.A. (2015a). Intrinsic and extrinsic mechanisms regulating satellite cell function. *Development (Cambridge, England)* *142*, 1572-1581.
- Dumont, N.A., Wang, Y.X., von Maltzahn, J., Pasut, A., Bentzinger, C.F., Brun, C.E., and Rudnicki, M.A. (2015b). Dystrophin expression in muscle stem cells regulates their polarity and asymmetric division. *Nature medicine* *21*, 1455-1463.
- Ebersole, T.A., Chen, Q., Justice, M.J., and Artzt, K. (1996). The quaking gene product necessary in embryogenesis and myelination combines features of RNA binding and signal transduction proteins. *Nature genetics* *12*, 260-265.
- Engeland, K. (2022). Cell cycle regulation: p53-p21-RB signaling. *Cell Death & Differentiation*.
- Eram, M.S., Shen, Y., Szewczyk, M., Wu, H., Senisterra, G., Li, F., Butler, K.V., Kaniskan, H.U., Speed, B.A., Dela Sena, C., *et al.* (2016). A Potent, Selective, and Cell-Active Inhibitor of Human Type I Protein Arginine Methyltransferases. *ACS chemical biology* *11*, 772-781.
- Evich, M., Stroeva, E., Zheng, Y.G., and Germann, M.W. (2016). Effect of methylation on the side-chain pKa value of arginine. *Protein science : a publication of the Protein Society* *25*, 479-486.
- Favia, A., Salvatori, L., Nanni, S., Iwamoto-Stohl, L.K., Valente, S., Mai, A., Scagnoli, F., Fontanella, R.A., Totta, P., Nasi, S., *et al.* (2019). The Protein Arginine Methyltransferases 1 and 5 affect Myc properties in glioblastoma stem cells. *Scientific reports* *9*, 15925.
- Fedoriw, A., Rajapurkar, S.R., O'Brien, S., Gerhart, S.V., Mitchell, L.H., Adams, N.D., Rioux, N., Lingaraj, T., Ribich, S.A., Pappalardi, M.B., *et al.* (2019). Anti-tumor Activity of the Type I PRMT Inhibitor, GSK3368715, Synergizes with PRMT5 Inhibition through MTAP Loss. *Cancer cell*.
- Feng, Y., Maity, R., Whitelegge, J.P., Hadjikyriacou, A., Li, Z., Zurita-Lopez, C., Al-Hadid, Q., Clark, A.T., Bedford, M.T., Masson, J.Y., *et al.* (2013). Mammalian protein arginine methyltransferase 7 (PRMT7) specifically targets RXR sites in lysine- and arginine-rich regions. *The Journal of biological chemistry* *288*, 37010-37025.
- Finkel, R.S., Chiriboga, C.A., Vajsar, J., Day, J.W., Montes, J., De Vivo, D.C., Yamashita, M., Rigo, F., Hung, G., Schneider, E., *et al.* (2016). Treatment of infantile-onset spinal muscular atrophy with nusinersen: a phase 2, open-label, dose-escalation study. *The Lancet* *388*, 3017-3026.
- Folmes, C.D., Dzeja, P.P., Nelson, T.J., and Terzic, A. (2012). Metabolic plasticity in stem cell homeostasis and differentiation. *Cell stem cell* *11*, 596-606.
- Fong, J.Y., Pignata, L., Goy, P.A., Kawabata, K.C., Lee, S.C., Koh, C.M., Musiani, D., Massignani, E., Kotini, A.G., Penson, A., *et al.* (2019). Therapeutic Targeting of RNA Splicing Catalysis through Inhibition of Protein Arginine Methylation. *Cancer cell* *36*, 194-209.e199.

- Friesen, W.J., Massenet, S., Paushkin, S., Wyce, A., and Dreyfuss, G. (2001). SMN, the product of the spinal muscular atrophy gene, binds preferentially to dimethylarginine-containing protein targets. *Molecular cell* 7, 1111-1117.
- Friesen, W.J., Wyce, A., Paushkin, S., Abel, L., Rappsilber, J., Mann, M., and Dreyfuss, G. (2002). A novel WD repeat protein component of the methylosome binds Sm proteins. *The Journal of biological chemistry* 277, 8243-8247.
- Fu, X., Xiao, J., Wei, Y., Li, S., Liu, Y., Yin, J., Sun, K., Sun, H., Wang, H., Zhang, Z., *et al.* (2015a). Combination of inflammation-related cytokines promotes long-term muscle stem cell expansion. *Cell research* 25, 1082-1083.
- Fu, X., Zhu, M.J., Dodson, M.V., and Du, M. (2015b). AMP-activated protein kinase stimulates Warburg-like glycolysis and activation of satellite cells during muscle regeneration. *The Journal of biological chemistry* 290, 26445-26456.
- Fuchs, E., and Blau, H.M. (2020). Tissue Stem Cells: Architects of Their Niches. *Cell stem cell* 27, 532-556.
- Fuchs, E., and Chen, T. (2013). A matter of life and death: self-renewal in stem cells. *EMBO reports* 14, 39-48.
- Galarneau, A., and Richard, S. (2005). Target RNA motif and target mRNAs of the Quaking STAR protein. *Nature structural & molecular biology* 12, 691-698.
- Gallot, Y.S., Hindi, S.M., Mann, A.K., and Kumar, A. (2016). Isolation, Culture, and Staining of Single Myofibers. *Bio-protocol* 6.
- Gao, G., Zhang, L., Villarreal, O.D., He, W., Su, D., Bedford, E., Moh, P., Shen, J., Shi, X., Bedford, M.T., *et al.* (2019). PRMT1 loss sensitizes cells to PRMT5 inhibition. *Nucleic acids research*.
- Gebauer, F., Schwarzl, T., Valcárcel, J., and Hentze, M.W. (2021). RNA-binding proteins in human genetic disease. *Nature reviews Genetics* 22, 185-198.
- Gerstberger, S., Hafner, M., and Tuschl, T. (2014). A census of human RNA-binding proteins. *Nature reviews Genetics* 15, 829-845.
- Geula, S., Moshitch-Moshkovitz, S., Dominissini, D., Mansour, A.A., Kol, N., Salmon-Divon, M., Hershkovitz, V., Peer, E., Mor, N., Manor, Y.S., *et al.* (2015). Stem cells. m6A mRNA methylation facilitates resolution of naïve pluripotency toward differentiation. *Science (New York, NY)* 347, 1002-1006.
- Giudice, J., and Cooper, T.A. (2014). RNA-binding proteins in heart development. *Advances in experimental medicine and biology* 825, 389-429.
- Giuliani, V., Miller, M.A., Liu, C.Y., Hartono, S.R., Class, C.A., Bristow, C.A., Suzuki, E., Sanz, L.A., Gao, G., Gay, J.P., *et al.* (2021). PRMT1-dependent regulation of RNA metabolism and DNA damage response sustains pancreatic ductal adenocarcinoma. *Nature communications* 12, 4626.
- Gonsalvez, G.B., Tian, L., Ospina, J.K., Boisvert, F.M., Lamond, A.I., and Matera, A.G. (2007). Two distinct arginine methyltransferases are required for biogenesis of Sm-class ribonucleoproteins. *The Journal of cell biology* 178, 733-740.
- Goulas, S., Conder, R., and Knoblich, J.A. (2012). The Par complex and integrins direct asymmetric cell division in adult intestinal stem cells. *Cell stem cell* 11, 529-540.
- Greer, E.L., Oskoui, P.R., Banko, M.R., Maniar, J.M., Gygi, M.P., Gygi, S.P., and Brunet, A. (2007). The energy sensor AMP-activated protein kinase directly regulates the mammalian FOXO3 transcription factor. *The Journal of biological chemistry* 282, 30107-30119.

- Grifone, R., Demignon, J., Houbron, C., Souil, E., Niro, C., Seller, M.J., Hamard, G., and Maire, P. (2005). Six1 and Six4 homeoproteins are required for Pax3 and Mrf expression during myogenesis in the mouse embryo. *Development (Cambridge, England)* *132*, 2235-2249.
- Guccione, E., and Richard, S. (2019). The regulation, functions and clinical relevance of arginine methylation. *Nature reviews Molecular cell biology* *20*, 642-657.
- Guderian, G., Peter, C., Wiesner, J., Sickmann, A., Schulze-Osthoff, K., Fischer, U., and Grimmmler, M. (2011). RioK1, a new interactor of protein arginine methyltransferase 5 (PRMT5), competes with pICln for binding and modulates PRMT5 complex composition and substrate specificity. *The Journal of biological chemistry* *286*, 1976-1986.
- Gurevich, D.B., Nguyen, P.D., Siegel, A.L., Ehrlich, O.V., Sonntag, C., Phan, J.M., Berger, S., Ratnayake, D., Hersey, L., Berger, J., *et al.* (2016). Asymmetric division of clonal muscle stem cells coordinates muscle regeneration in vivo. *Science (New York, NY)* *353*, aad9969.
- Hall, M.P., Nagel, R.J., Fagg, W.S., Shiue, L., Cline, M.S., Perriman, R.J., Donohue, J.P., and Ares, M., Jr. (2013). Quaking and PTB control overlapping splicing regulatory networks during muscle cell differentiation. *RNA (New York, NY)* *19*, 627-638.
- Hardie, D.G., Schaffer, B.E., and Brunet, A. (2016). AMPK: An Energy-Sensing Pathway with Multiple Inputs and Outputs. *Trends in cell biology* *26*, 190-201.
- Hardy, D., Besnard, A., Latil, M., Jouvion, G., Briand, D., Thepenier, C., Pascal, Q., Guguin, A., Gayraud-Morel, B., Cavaillon, J.M., *et al.* (2016). Comparative Study of Injury Models for Studying Muscle Regeneration in Mice. *PloS one* *11*, e0147198.
- Hasegawa, M., Toma-Fukai, S., Kim, J.D., Fukamizu, A., and Shimizu, T. (2014). Protein arginine methyltransferase 7 has a novel homodimer-like structure formed by tandem repeats. *FEBS letters* *588*, 1942-1948.
- Hayashi, Y.K., Chou, F.L., Engvall, E., Ogawa, M., Matsuda, C., Hirabayashi, S., Yokochi, K., Ziober, B.L., Kramer, R.H., Kaufman, S.J., *et al.* (1998). Mutations in the integrin alpha7 gene cause congenital myopathy. *Nature genetics* *19*, 94-97.
- He, Z., Duan, Z., Chen, L., Li, B., and Zhou, Y. (2020). Long non-coding RNA Loc490 inhibits gastric cancer cell proliferation and metastasis by upregulating RNA-binding protein Quaking. *Aging* *12*, 17681-17693.
- Herbst, R.S., Morgensztern, D., and Boshoff, C. (2018). The biology and management of non-small cell lung cancer. *Nature* *553*, 446-454.
- Herzig, S., and Shaw, R.J. (2018). AMPK: guardian of metabolism and mitochondrial homeostasis. *Nature Reviews Molecular Cell Biology* *19*, 121-135.
- Hindupur, S.K., González, A., and Hall, M.N. (2015). The opposing actions of target of rapamycin and AMP-activated protein kinase in cell growth control. *Cold Spring Harbor perspectives in biology* *7*, a019141.
- Hinterberger, T.J., Sassoon, D.A., Rhodes, S.J., and Konieczny, S.F. (1991). Expression of the muscle regulatory factor MRF4 during somite and skeletal myofiber development. *Developmental biology* *147*, 144-156.
- Hodson, N., West, D.W.D., Philp, A., Burd, N.A., and Moore, D.R. (2019). MOLECULAR REGULATION OF HUMAN SKELETAL MUSCLE PROTEIN SYNTHESIS IN RESPONSE TO EXERCISE AND NUTRIENTS: A COMPASS FOR OVERCOMING AGE-RELATED ANABOLIC RESISTANCE. *American journal of physiology Cell physiology*.
- Hori, S., Hiramuki, Y., Nishimura, D., Sato, F., and Sehara-Fujisawa, A. (2019). PDH-mediated metabolic flow is critical for skeletal muscle stem cell differentiation and myotube formation

- during regeneration in mice. *FASEB journal : official publication of the Federation of American Societies for Experimental Biology* 33, 8094-8109.
- Hua, Y., Sahashi, K., Rigo, F., Hung, G., Horev, G., Bennett, C.F., and Krainer, A.R. (2011). Peripheral SMN restoration is essential for long-term rescue of a severe spinal muscular atrophy mouse model. *Nature* 478, 123-126.
- Iwasaki, H., and Yada, T. (2007). Protein arginine methylation regulates insulin signaling in L6 skeletal muscle cells. *Biochemical and biophysical research communications* 364, 1015-1021.
- Iwata, N., Ishikawa, T., Okazaki, S., Mogushi, K., Baba, H., Ishiguro, M., Kobayashi, H., Tanaka, H., Kawano, T., Sugihara, K., *et al.* (2017). Clinical Significance of Methylation and Reduced Expression of the Quaking Gene in Colorectal Cancer. *Anticancer research* 37, 489-498.
- Jain, K., Jin, C.Y., and Clarke, S.G. (2017). Epigenetic control via allosteric regulation of mammalian protein arginine methyltransferases. *Proceedings of the National Academy of Sciences of the United States of America* 114, 10101-10106.
- Jeong, H.J., Lee, H.J., Vuong, T.A., Choi, K.S., Choi, D., Koo, S.H., Cho, S.C., Cho, H., and Kang, J.S. (2016). Prmt7 Deficiency Causes Reduced Skeletal Muscle Oxidative Metabolism and Age-Related Obesity. *Diabetes* 65, 1868-1882.
- Jeong, H.J., Lee, S.J., Lee, H.J., Kim, H.B., Anh Vuong, T., Cho, H., Bae, G.U., and Kang, J.S. (2019). Prmt7 promotes myoblast differentiation via methylation of p38MAPK on arginine residue 70. *Cell death and differentiation*.
- Johnson, M.A., Polgar, J., Weightman, D., and Appleton, D. (1973). Data on the distribution of fibre types in thirty-six human muscles. An autopsy study. *Journal of the neurological sciences* 18, 111-129.
- Judson, R.N., Quarta, M., Oudhoff, M.J., Soliman, H., Yi, L., Chang, C.K., Loi, G., Vander Werff, R., Cait, A., Hamer, M., *et al.* (2018). Inhibition of Methyltransferase Setd7 Allows the In Vitro Expansion of Myogenic Stem Cells with Improved Therapeutic Potential. *Cell stem cell* 22, 177-190.e177.
- Juergens, R.A., Wrangle, J., Vendetti, F.P., Murphy, S.C., Zhao, M., Coleman, B., Sebree, R., Rodgers, K., Hooker, C.M., Franco, N., *et al.* (2011). Combination epigenetic therapy has efficacy in patients with refractory advanced non-small cell lung cancer. *Cancer discovery* 1, 598-607.
- Kalev, P., Hyer, M.L., Gross, S., Konteatis, Z., Chen, C.C., Fletcher, M., Lein, M., Aguado-Fraile, E., Frank, V., Barnett, A., *et al.* (2021). MAT2A Inhibition Blocks the Growth of MTAP-Deleted Cancer Cells by Reducing PRMT5-Dependent mRNA Splicing and Inducing DNA Damage. *Cancer cell* 39, 209-224.e211.
- Kanagawa, M., Yu, C.C., Ito, C., Fukada, S., Hozoji-Inada, M., Chiyo, T., Kuga, A., Matsuo, M., Sato, K., Yamaguchi, M., *et al.* (2013). Impaired viability of muscle precursor cells in muscular dystrophy with glycosylation defects and amelioration of its severe phenotype by limited gene expression. *Human molecular genetics* 22, 3003-3015.
- Kassar-Duchossoy, L., Gayraud-Morel, B., Gomes, D., Rocancourt, D., Buckingham, M., Shinin, V., and Tajbakhsh, S. (2004). Mrf4 determines skeletal muscle identity in Myf5:Myod double-mutant mice. *Nature* 431, 466-471.
- Kawabe, Y., Wang, Y.X., McKinnell, I.W., Bedford, M.T., and Rudnicki, M.A. (2012). Carm1 regulates Pax7 transcriptional activity through MLL1/2 recruitment during asymmetric satellite stem cell divisions. *Cell stem cell* 11, 333-345.
- Kearney, P.L., Bhatia, M., Jones, N.G., Yuan, L., Glascock, M.C., Catchings, K.L., Yamada, M., and Thompson, P.R. (2005). Kinetic characterization of protein arginine deiminase 4: a

- transcriptional corepressor implicated in the onset and progression of rheumatoid arthritis. *Biochemistry* *44*, 10570-10582.
- Kim, H., Selvaraj, S., Kiley, J., Azzag, K., Garay, B.I., and Perlingeiro, R.C.R. (2021). Genomic Safe Harbor Expression of PAX7 for the Generation of Engraftable Myogenic Progenitors. *Stem cell reports* *16*, 10-19.
- Kim, J., Kundu, M., Viollet, B., and Guan, K.-L. (2011). AMPK and mTOR regulate autophagy through direct phosphorylation of Ulk1. *Nature cell biology* *13*, 132-141.
- Kim, J., Woo, A.J., Chu, J., Snow, J.W., Fujiwara, Y., Kim, C.G., Cantor, A.B., and Orkin, S.H. (2010). A Myc network accounts for similarities between embryonic stem and cancer cell transcription programs. *Cell* *143*, 313-324.
- Kim, K.H., and Roberts, C.W. (2016). Targeting EZH2 in cancer. *Nature medicine* *22*, 128-134.
- Kimmel, J.C., Hwang, A.B., Scaramozza, A., Marshall, W.F., and Brack, A.S. (2020). Aging induces aberrant state transition kinetics in murine muscle stem cells. *Development (Cambridge, England)* *147*.
- Kjøbsted, R., Hingst, J.R., Fentz, J., Foretz, M., Sanz, M.N., Pehmøller, C., Shum, M., Marette, A., Mounier, R., Treebak, J.T., *et al.* (2018). AMPK in skeletal muscle function and metabolism. *FASEB journal : official publication of the Federation of American Societies for Experimental Biology* *32*, 1741-1777.
- Knoblich, J.A. (2010). Asymmetric cell division: recent developments and their implications for tumour biology. *Nature reviews Molecular cell biology* *11*, 849-860.
- Koenig, M., Hoffman, E.P., Bertelson, C.J., Monaco, A.P., Feener, C., and Kunkel, L.M. (1987). Complete cloning of the Duchenne muscular dystrophy (DMD) cDNA and preliminary genomic organization of the DMD gene in normal and affected individuals. *Cell* *50*, 509-517.
- Kondo, T., Furuta, T., Mitsunaga, K., Ebersole, T.A., Shichiri, M., Wu, J., Artzt, K., Yamamura, K., and Abe, K. (1999). Genomic organization and expression analysis of the mouse *qk1* locus. *Mammalian genome : official journal of the International Mammalian Genome Society* *10*, 662-669.
- Kottlors, M., and Kirschner, J. (2010). Elevated satellite cell number in Duchenne muscular dystrophy. *Cell and tissue research* *340*, 541-548.
- Krishnakumar, R., and Kraus, W.L. (2010). The PARP side of the nucleus: molecular actions, physiological outcomes, and clinical targets. *Molecular cell* *39*, 8-24.
- Kryukov, G.V., Wilson, F.H., Ruth, J.R., Paulk, J., Tsherniak, A., Marlow, S.E., Vazquez, F., Weir, B.A., Fitzgerald, M.E., Tanaka, M., *et al.* (2016). MTAP deletion confers enhanced dependency on the PRMT5 arginine methyltransferase in cancer cells. *Science (New York, NY)* *351*, 1214-1218.
- Kuang, S., Kuroda, K., Le Grand, F., and Rudnicki, M.A. (2007). Asymmetric self-renewal and commitment of satellite stem cells in muscle. *Cell* *129*, 999-1010.
- Kuleshov, M.V., Jones, M.R., Rouillard, A.D., Fernandez, N.F., Duan, Q., Wang, Z., Koplev, S., Jenkins, S.L., Jagodnik, K.M., Lachmann, A., *et al.* (2016). Enrichr: a comprehensive gene set enrichment analysis web server 2016 update. *Nucleic acids research* *44*, W90-97.
- Kwon, H., Imbalzano, A.N., Khavari, P.A., Kingston, R.E., and Green, M.R. (1994). Nucleosome disruption and enhancement of activator binding by a human SW1/SNF complex. *Nature* *370*, 477-481.
- L'Honoré, A., Commère, P.H., Negroni, E., Pallafacchina, G., Friguet, B., Drouin, J., Buckingham, M., and Montarras, D. (2018). The role of Pitx2 and Pitx3 in muscle stem cells gives new insights into P38 α MAP kinase and redox regulation of muscle regeneration. *eLife* *7*.

- Ladd, A.N., Charlet, N., and Cooper, T.A. (2001). The CELF family of RNA binding proteins is implicated in cell-specific and developmentally regulated alternative splicing. *Molecular and cellular biology* *21*, 1285-1296.
- Larocque, D., Pilotte, J., Chen, T., Cloutier, F., Massie, B., Pedraza, L., Couture, R., Lasko, P., Almazan, G., and Richard, S. (2002). Nuclear Retention of MBP mRNAs in the Quaking Viable Mice. *Neuron* *36*, 815-829.
- Lassar, A.B., Davis, R.L., Wright, W.E., Kadesch, T., Murre, C., Voronova, A., Baltimore, D., and Weintraub, H. (1991). Functional activity of myogenic HLH proteins requires hetero-oligomerization with E12/E47-like proteins in vivo. *Cell* *66*, 305-315.
- Latil, M., Rocheteau, P., Châtre, L., Sanulli, S., Mémet, S., Ricchetti, M., Tajbakhsh, S., and Chrétien, F. (2012). Skeletal muscle stem cells adopt a dormant cell state post mortem and retain regenerative capacity. *Nature communications* *3*, 903.
- Lazure, F., Blackburn, D.M., Corchado, A.H., Sahinyan, K., Karam, N., Sharanek, A., Nguyen, D., Lepper, C., Najafabadi, H.S., Perkins, T.J., *et al.* (2020). Myf6/MRF4 is a myogenic niche regulator required for the maintenance of the muscle stem cell pool. *EMBO reports* *21*, e49499.
- Le Grand, F., Jones, A.E., Seale, V., Scimè, A., and Rudnicki, M.A. (2009). Wnt7a activates the planar cell polarity pathway to drive the symmetric expansion of satellite stem cells. *Cell stem cell* *4*, 535-547.
- Le Grand, F., and Rudnicki, M. (2007). Satellite and stem cells in muscle growth and repair. *Development (Cambridge, England)* *134*, 3953-3957.
- Lee, J., Villarreal, O.D., Chen, X., Zandee, S., Young, Y.K., Torok, C., Lamarche-Vane, N., Prat, A., Rivest, S., Gosselin, D., *et al.* (2020). QUAKING Regulates Microexon Alternative Splicing of the Rho GTPase Pathway and Controls Microglia Homeostasis. *Cell reports* *33*, 108560.
- Lee, J.S., Lamarche-Vane, N., and Richard, S. (2021). Microexon alternative splicing of small GTPase regulators: Implication in central nervous system diseases. *Wiley interdisciplinary reviews RNA*, e1678.
- Lee, S., Oh, T., Chung, H., Rha, S., Kim, C., Moon, Y., Hoehn, B.D., Jeong, D., Lee, S., Kim, N., *et al.* (2012). Identification of GABRA1 and LAMA2 as new DNA methylation markers in colorectal cancer. *International journal of oncology* *40*, 889-898.
- Lepper, C., Partridge, T.A., and Fan, C.M. (2011). An absolute requirement for Pax7-positive satellite cells in acute injury-induced skeletal muscle regeneration. *Development (Cambridge, England)* *138*, 3639-3646.
- Li, C., Heidt, D.G., Dalerba, P., Burant, C.F., Zhang, L., Adsay, V., Wicha, M., Clarke, M.F., and Simeone, D.M. (2007). Identification of pancreatic cancer stem cells. *Cancer research* *67*, 1030-1037.
- Li, Z., Wang, D., Lu, J., Huang, B., Wang, Y., Dong, M., Fan, D., Li, H., Gao, Y., Hou, P., *et al.* (2020). Methylation of EZH2 by PRMT1 regulates its stability and promotes breast cancer metastasis. *Cell death and differentiation* *27*, 3226-3242.
- Li, Z.Z., Kondo, T., Murata, T., Ebersole, T.A., Nishi, T., Tada, K., Ushio, Y., Yamamura, K., and Abe, K. (2002). Expression of Hqk encoding a KH RNA binding protein is altered in human glioma. *Japanese journal of cancer research : Gann* *93*, 167-177.
- Liao, H.W., Hsu, J.M., Xia, W., Wang, H.L., Wang, Y.N., Chang, W.C., Arold, S.T., Chou, C.K., Tsou, P.H., Yamaguchi, H., *et al.* (2015). PRMT1-mediated methylation of the EGF receptor regulates signaling and cetuximab response. *The Journal of clinical investigation* *125*, 4529-4543.

- Liu, F., Zhao, X., Perna, F., Wang, L., Koppikar, P., Abdel-Wahab, O., Harr, M.W., Levine, R.L., Xu, H., Tefferi, A., *et al.* (2011). JAK2V617F-mediated phosphorylation of PRMT5 downregulates its methyltransferase activity and promotes myeloproliferation. *Cancer cell* *19*, 283-294.
- Liu, K., Guo, Y., Liu, H., Bian, C., Lam, R., Liu, Y., Mackenzie, F., Rojas, L.A., Reinberg, D., Bedford, M.T., *et al.* (2012). Crystal structure of TDRD3 and methyl-arginine binding characterization of TDRD3, SMN and SPF30. *PLoS one* *7*, e30375.
- Liu, Q., Zhang, X.L., Cheng, M.B., and Zhang, Y. (2019). PRMT1 activates myogenin transcription via MyoD arginine methylation at R121. *Biochimica et biophysica acta Gene regulatory mechanisms* *1862*, 194442.
- Lobo, N.A., Shimono, Y., Qian, D., and Clarke, M.F. (2007). The biology of cancer stem cells. *Annual review of cell and developmental biology* *23*, 675-699.
- Long, C., Amoasii, L., Mireault, A.A., McAnally, J.R., Li, H., Sanchez-Ortiz, E., Bhattacharyya, S., Shelton, J.M., Bassel-Duby, R., and Olson, E.N. (2016). Postnatal genome editing partially restores dystrophin expression in a mouse model of muscular dystrophy. *Science (New York, NY)* *351*, 400-403.
- Lord, C.J., and Ashworth, A. (2017). PARP inhibitors: Synthetic lethality in the clinic. *Science (New York, NY)* *355*, 1152-1158.
- Low, S., Barnes, J.L., Zammit, P.S., and Beauchamp, J.R. (2018). Delta-Like 4 Activates Notch 3 to Regulate Self-Renewal in Skeletal Muscle Stem Cells. *Stem cells* *36*, 458-466.
- Lu, C., and Allis, C.D. (2017). SWI/SNF complex in cancer. *Nature genetics* *49*, 178-179.
- Lu, R., and Wang, G.G. (2013). Tudor: a versatile family of histone methylation 'readers'. *Trends in biochemical sciences* *38*, 546-555.
- Lukong, K.E., Chang, K.W., Khandjian, E.W., and Richard, S. (2008). RNA-binding proteins in human genetic disease. *Trends in genetics : TIG* *24*, 416-425.
- Machado, L., Esteves de Lima, J., Fabre, O., Proux, C., Legendre, R., Szegedi, A., Varet, H., Ingerslev, L.R., Barrès, R., Relaix, F., *et al.* (2017). In Situ Fixation Redefines Quiescence and Early Activation of Skeletal Muscle Stem Cells. *Cell reports* *21*, 1982-1993.
- Mankodi, A., Takahashi, M.P., Jiang, H., Beck, C.L., Bowers, W.J., Moxley, R.T., Cannon, S.C., and Thornton, C.A. (2002). Expanded CUG repeats trigger aberrant splicing of CIC-1 chloride channel pre-mRNA and hyperexcitability of skeletal muscle in myotonic dystrophy. *Molecular cell* *10*, 35-44.
- Manta, A., Stouth, D.W., Xhuti, D., Chi, L., Rebalka, I.A., Kalmar, J.M., Hawke, T.J., and Ljubcic, V. (2019). Chronic exercise mitigates disease mechanisms and improves muscle function in myotonic dystrophy type 1 mice. *The Journal of physiology* *597*, 1361-1381.
- Marin, T.L., Gongol, B., Zhang, F., Martin, M., Johnson, D.A., Xiao, H., Wang, Y., Subramaniam, S., Chien, S., and Shyy, J.Y. (2017). AMPK promotes mitochondrial biogenesis and function by phosphorylating the epigenetic factors DNMT1, RBBP7, and HAT1. *Science signaling* *10*.
- Marjon, K., Cameron, M.J., Quang, P., Clasquin, M.F., Mandley, E., Kunii, K., McVay, M., Choe, S., Kernysky, A., Gross, S., *et al.* (2016). MTAP Deletions in Cancer Create Vulnerability to Targeting of the MAT2A/PRMT5/RIOK1 Axis. *Cell reports* *15*, 574-587.
- Martin, G., Ostareck-Lederer, A., Chari, A., Neuenkirchen, N., Dettwiler, S., Blank, D., Rügsegger, U., Fischer, U., and Keller, W. (2010). Arginine methylation in subunits of mammalian pre-mRNA cleavage factor I. *RNA (New York, NY)* *16*, 1646-1659.
- Matthews, H.K., Bertoli, C., and de Bruin, R.A.M. (2022). Cell cycle control in cancer. *Nature reviews Molecular cell biology* *23*, 74-88.

- Mauro, A. (1961). Satellite cell of skeletal muscle fibers. *The Journal of biophysical and biochemical cytology* *9*, 493-495.
- Mavrakis, K.J., McDonald, E.R., 3rd, Schlabach, M.R., Billy, E., Hoffman, G.R., deWeck, A., Ruddy, D.A., Venkatesan, K., Yu, J., McAllister, G., *et al.* (2016). Disordered methionine metabolism in MTAP/CDKN2A-deleted cancers leads to dependence on PRMT5. *Science (New York, NY)* *351*, 1208-1213.
- Mayer, U., Saher, G., Fässler, R., Bornemann, A., Echtermeyer, F., Mark, H.v.d., Miosge, N., Pösch, E., and Mark, K.v.d. (1997). Absence of integrin $\alpha 7$ causes a novel form of muscular dystrophy. *Nature genetics* *17*, 318-323.
- McGreevy, J.W., Hakim, C.H., McIntosh, M.A., and Duan, D. (2015). Animal models of Duchenne muscular dystrophy: from basic mechanisms to gene therapy. *Disease models & mechanisms* *8*, 195-213.
- McInnes, L.A., and Lauriat, T.L. (2006). RNA metabolism and dysmyelination in schizophrenia. *Neuroscience and biobehavioral reviews* *30*, 551-561.
- McKellar, D.W., Walter, L.D., Song, L.T., Mantri, M., Wang, M.F.Z., De Vlaminck, I., and Cosgrove, B.D. (2021). Large-scale integration of single-cell transcriptomic data captures transitional progenitor states in mouse skeletal muscle regeneration. *Communications biology* *4*, 1280.
- Meister, G., Eggert, C., Buhler, D., Brahms, H., Kambach, C., and Fischer, U. (2001). Methylation of Sm proteins by a complex containing PRMT5 and the putative U snRNP assembly factor pICln. *Current biology : CB* *11*, 1990-1994.
- Montarras, D., L'Honoré, A., and Buckingham, M. (2013). Lying low but ready for action: the quiescent muscle satellite cell. *The FEBS journal* *280*, 4036-4050.
- Montarras, D., Morgan, J., Collins, C., Relaix, F., Zaffran, S., Cumano, A., Partridge, T., and Buckingham, M. (2005). Direct isolation of satellite cells for skeletal muscle regeneration. *Science (New York, NY)* *309*, 2064-2067.
- Morrison, S.J., and Kimble, J. (2006). Asymmetric and symmetric stem-cell divisions in development and cancer. *Nature* *441*, 1068-1074.
- Mourikis, P., Sambasivan, R., Castel, D., Rocheteau, P., Bizzarro, V., and Tajbakhsh, S. (2012). A critical requirement for notch signaling in maintenance of the quiescent skeletal muscle stem cell state. *Stem cells* *30*, 243-252.
- Mukund, K., and Subramaniam, S. (2020). Skeletal muscle: A review of molecular structure and function, in health and disease. *Wiley interdisciplinary reviews Systems biology and medicine* *12*, e1462.
- Murai, J., Huang, S.Y., Das, B.B., Renaud, A., Zhang, Y., Doroshow, J.H., Ji, J., Takeda, S., and Pommier, Y. (2012). Trapping of PARP1 and PARP2 by Clinical PARP Inhibitors. *Cancer research* *72*, 5588-5599.
- Murai, J., Huang, S.Y., Renaud, A., Zhang, Y., Ji, J., Takeda, S., Morris, J., Teicher, B., Doroshow, J.H., and Pommier, Y. (2014). Stereospecific PARP trapping by BMN 673 and comparison with olaparib and rucaparib. *Molecular cancer therapeutics* *13*, 433-443.
- Murn, J., and Shi, Y. (2017). The winding path of protein methylation research: milestones and new frontiers. *Nature reviews Molecular cell biology* *18*, 517-527.
- Murphy, M.M., Lawson, J.A., Mathew, S.J., Hutcheson, D.A., and Kardon, G. (2011). Satellite cells, connective tissue fibroblasts and their interactions are crucial for muscle regeneration. *Development (Cambridge, England)* *138*, 3625-3637.

- Nakayama, K., Szewczyk, M.M., Dela Sena, C., Wu, H., Dong, A., Zeng, H., Li, F., de Freitas, R.F., Eram, M.S., Schapira, M., *et al.* (2018). TP-064, a potent and selective small molecule inhibitor of PRMT4 for multiple myeloma. *Oncotarget* *9*, 18480-18493.
- Nakka, K., Ghigna, C., Gabellini, D., and Dilworth, F.J. (2018). Diversification of the muscle proteome through alternative splicing. *Skeletal muscle* *8*, 8.
- Nelson, C.E., Hakim, C.H., Ousterout, D.G., Thakore, P.I., Moreb, E.A., Castellanos Rivera, R.M., Madhavan, S., Pan, X., Ran, F.A., Yan, W.X., *et al.* (2016). In vivo genome editing improves muscle function in a mouse model of Duchenne muscular dystrophy. *Science (New York, NY)* *351*, 403-407.
- Ng, S.Y., Mikhail, A., and Ljubicic, V. (2019). Mechanisms of exercise-induced survival motor neuron expression in the skeletal muscle of spinal muscular atrophy-like mice. *The Journal of physiology* *597*, 4757-4778.
- Owens, J.L., Beketova, E., Liu, S., Tinsley, S.L., Asberry, A.M., Deng, X., Huang, J., Li, C., Wan, J., and Hu, C.D. (2020). PRMT5 Cooperates with pICln to Function as a Master Epigenetic Activator of DNA Double-Strand Break Repair Genes. *iScience* *23*, 100750.
- Paik, W., and Kim, S. (1980). Natural occurrence of various methylated amino acid derivatives. *Protein methylation*, 8-25.
- Pal, S., Vishwanath, S.N., Erdjument-Bromage, H., Tempst, P., and Sif, S. (2004). Human SWI/SNF-associated PRMT5 methylates histone H3 arginine 8 and negatively regulates expression of ST7 and NM23 tumor suppressor genes. *Molecular and cellular biology* *24*, 9630-9645.
- Pala, F., Di Girolamo, D., Mella, S., Yennek, S., Chatre, L., Ricchetti, M., and Tajbakhsh, S. (2018). Distinct metabolic states govern skeletal muscle stem cell fates during prenatal and postnatal myogenesis. *Journal of cell science* *131*.
- Pastore, F., Bhagwat, N., Pastore, A., Radzisheuskaya, A., Karzai, A., Krishnan, A., Li, B., Bowman, R.L., Xiao, W., Viny, A.D., *et al.* (2020). PRMT5 Inhibition Modulates E2F1 Methylation and Gene-Regulatory Networks Leading to Therapeutic Efficacy in JAK2(V617F)-Mutant MPN. *Cancer discovery* *10*, 1742-1757.
- Pasut, A., Oleynik, P., and Rudnicki, M.A. (2012). Isolation of muscle stem cells by fluorescence activated cell sorting cytometry. *Methods in molecular biology (Clifton, NJ)* *798*, 53-64.
- Pedrotti, S., Giudice, J., Dagnino-Acosta, A., Knoblauch, M., Singh, R.K., Hanna, A., Mo, Q., Hicks, J., Hamilton, S., and Cooper, T.A. (2015). The RNA-binding protein Rbfox1 regulates splicing required for skeletal muscle structure and function. *Human molecular genetics* *24*, 2360-2374.
- Pegoraro, E., Cepollaro, F., Prandini, P., Marin, A., Fanin, M., Trevisan, C.P., El-Messlemani, A.H., Tarone, G., Engvall, E., Hoffman, E.P., *et al.* (2002). Integrin alpha 7 beta 1 in muscular dystrophy/myopathy of unknown etiology. *The American journal of pathology* *160*, 2135-2143.
- Philips, A.V., Timchenko, L.T., and Cooper, T.A. (1998). Disruption of splicing regulated by a CUG-binding protein in myotonic dystrophy. *Science (New York, NY)* *280*, 737-741.
- Pilotte, J., Larocque, D., and Richard, S. (2001). Nuclear translocation controlled by alternatively spliced isoforms inactivates the QUAKING apoptotic inducer. *Genes & development* *15*, 845-858.
- Pistocchi, A., Gaudenzi, G., Foglia, E., Monteverde, S., Moreno-Fortuny, A., Pianca, A., Cossu, G., Cotelli, F., and Messina, G. (2013). Conserved and divergent functions of Nfix in skeletal muscle development during vertebrate evolution. *Development (Cambridge, England)* *140*, 1528-1536.

- Pommier, Y., O'Connor, M.J., and de Bono, J. (2016). Laying a trap to kill cancer cells: PARP inhibitors and their mechanisms of action. *Science translational medicine* 8, 362ps317.
- Prager, B.C., Xie, Q., Bao, S., and Rich, J.N. (2019). Cancer Stem Cells: The Architects of the Tumor Ecosystem. *Cell stem cell* 24, 41-53.
- Qiao, X., Kim, D.I., Jun, H., Ma, Y., Knights, A.J., Park, M.J., Zhu, K., Lipinski, J.H., Liao, J., Li, Y., *et al.* (2019). Protein Arginine Methyltransferase 1 Interacts With PGC1 α and Modulates Thermogenic Fat Activation. *Endocrinology* 160, 2773-2786.
- Radzishewska, A., Shliaha, P.V., Grinev, V., Lorenzini, E., Kovalchuk, S., Shlyueva, D., Gorshkov, V., Hendrickson, R.C., Jensen, O.N., and Helin, K. (2019). PRMT5 methylome profiling uncovers a direct link to splicing regulation in acute myeloid leukemia. *Nature structural & molecular biology* 26, 999-1012.
- Rassier, D.E. (2017). Sarcomere mechanics in striated muscles: from molecules to sarcomeres to cells. *American journal of physiology Cell physiology* 313, C134-c145.
- Rau, F., Lainé, J., Ramanoudjame, L., Ferry, A., Arandel, L., Delalande, O., Jollet, A., Dingli, F., Lee, K.Y., Peccate, C., *et al.* (2015). Abnormal splicing switch of DMD's penultimate exon compromises muscle fibre maintenance in myotonic dystrophy. *Nature communications* 6, 7205.
- Ravel-Chapuis, A., Haghbandish, A., Daneshvar, N., Jasmin, B.J., and Côté, J. (2021). A novel CARM1-HuR axis involved in muscle differentiation and plasticity misregulated in spinal muscular atrophy. *Human molecular genetics*.
- Rayagiri, S.S., Ranaldi, D., Raven, A., Mohamad Azhar, N.I.F., Lefebvre, O., Zammit, P.S., and Borycki, A.-G. (2018). Basal lamina remodeling at the skeletal muscle stem cell niche mediates stem cell self-renewal. *Nature Communications* 9, 1075.
- Relaix, F., Bencze, M., Borok, M.J., Der Vartanian, A., Gattazzo, F., Mademtoglou, D., Perez-Diaz, S., Prola, A., Reyes-Fernandez, P.C., Rotini, A., *et al.* (2021). Perspectives on skeletal muscle stem cells. *Nature communications* 12, 692.
- Relaix, F., and Zammit, P.S. (2012). Satellite cells are essential for skeletal muscle regeneration: the cell on the edge returns centre stage. *Development (Cambridge, England)* 139, 2845-2856.
- Robinson, J.T., Thorvaldsdóttir, H., Winckler, W., Guttman, M., Lander, E.S., Getz, G., and Mesirov, J.P. (2011). Integrative genomics viewer. *Nature Biotechnology* 29, 24-26.
- Rodgers, J.T., King, K.Y., Brett, J.O., Cromie, M.J., Charville, G.W., Maguire, K.K., Brunson, C., Mastey, N., Liu, L., Tsai, C.R., *et al.* (2014). mTORC1 controls the adaptive transition of quiescent stem cells from G0 to G(Alert). *Nature* 510, 393-396.
- Rodgers, J.T., Schroeder, M.D., Ma, C., and Rando, T.A. (2017). HGFA Is an Injury-Regulated Systemic Factor that Induces the Transition of Stem Cells into G(Alert). *Cell reports* 19, 479-486.
- Romitti, P.A., Zhu, Y., Puzhankara, S., James, K.A., Nabukera, S.K., Zamba, G.K., Ciafaloni, E., Cunniff, C., Druschel, C.M., Mathews, K.D., *et al.* (2015). Prevalence of Duchenne and Becker muscular dystrophies in the United States. *Pediatrics* 135, 513-521.
- Rooney, J.E., Gurpur, P.B., Yablonka-Reuveni, Z., and Burkin, D.J. (2009). Laminin-111 restores regenerative capacity in a mouse model for alpha7 integrin congenital myopathy. *The American journal of pathology* 174, 256-264.
- Rossi, F., Noren, H., Jove, R., Beljanski, V., and Grinnemo, K.H. (2020). Differences and similarities between cancer and somatic stem cells: therapeutic implications. *Stem cell research & therapy* 11, 489.
- Rudnicki, M.A., Schnegelsberg, P.N., Stead, R.H., Braun, T., Arnold, H.H., and Jaenisch, R. (1993). MyoD or Myf-5 is required for the formation of skeletal muscle. *Cell* 75, 1351-1359.

- Runfola, V., Sebastian, S., Dilworth, F.J., and Gabellini, D. (2015). Rbfox proteins regulate tissue-specific alternative splicing of Mef2D required for muscle differentiation. *Journal of cell science* *128*, 631-637.
- Ryall, J.G., Dell'Orso, S., Derfoul, A., Juan, A., Zare, H., Feng, X., Clermont, D., Koulis, M., Gutierrez-Cruz, G., Fulco, M., *et al.* (2015). The NAD(+)-dependent SIRT1 deacetylase translates a metabolic switch into regulatory epigenetics in skeletal muscle stem cells. *Cell stem cell* *16*, 171-183.
- Ryder, S.P., Frater, L.A., Abramovitz, D.L., Goodwin, E.B., and Williamson, J.R. (2004). RNA target specificity of the STAR/GSG domain post-transcriptional regulatory protein GLD-1. *Nature structural & molecular biology* *11*, 20-28.
- Ryder-Cook, A.S., Sicinski, P., Thomas, K., Davies, K.E., Worton, R.G., Barnard, E.A., Darlison, M.G., and Barnard, P.J. (1988). Localization of the mdx mutation within the mouse dystrophin gene. *The EMBO journal* *7*, 3017-3021.
- Saber, J., Lin, A.Y.T., and Rudnicki, M.A. (2020). Single-cell analyses uncover granularity of muscle stem cells. *F1000Research* *9*.
- Sacco, A., Doyonnas, R., Kraft, P., Vitorovic, S., and Blau, H.M. (2008). Self-renewal and expansion of single transplanted muscle stem cells. *Nature* *456*, 502-506.
- Sakai, H., Fukuda, S., Nakamura, M., Uezumi, A., Noguchi, Y.T., Sato, T., Morita, M., Yamada, H., Tsuchida, K., Tajbakhsh, S., *et al.* (2017). Notch ligands regulate the muscle stem-like state *ex vivo* but are not sufficient for retaining regenerative capacity. *PloS one* *12*, e0177516.
- Sanes, J.R. (2003). The basement membrane/basal lamina of skeletal muscle. *The Journal of biological chemistry* *278*, 12601-12604.
- Sartorelli, V., Puri, P.L., Hamamori, Y., Ogryzko, V., Chung, G., Nakatani, Y., Wang, J.Y., and Kedes, L. (1999). Acetylation of MyoD directed by PCAF is necessary for the execution of the muscle program. *Molecular cell* *4*, 725-734.
- Satheesha, S., Manzella, G., Bovay, A., Casanova, E.A., Bode, P.K., Belle, R., Feuchtgruber, S., Jaaks, P., Dogan, N., Koscielniak, E., *et al.* (2016). Targeting hedgehog signaling reduces self-renewal in embryonal rhabdomyosarcoma. *Oncogene* *35*, 2020-2030.
- Schmid, M., Malicki, D., Nobori, T., Rosenbach, M.D., Campbell, K., Carson, D.A., and Carrera, C.J. (1998). Homozygous deletions of methylthioadenosine phosphorylase (MTAP) are more frequent than p16INK4A (CDKN2) homozygous deletions in primary non-small cell lung cancers (NSCLC). *Oncogene* *17*, 2669-2675.
- Schweingruber, C., Rufener, S.C., Zünd, D., Yamashita, A., and Mühlemann, O. (2013). Nonsense-mediated mRNA decay - mechanisms of substrate mRNA recognition and degradation in mammalian cells. *Biochimica et biophysica acta* *1829*, 612-623.
- Scotti, M.M., and Swanson, M.S. (2016). RNA mis-splicing in disease. *Nature Reviews Genetics* *17*, 19-32.
- Seale, P., Sabourin, L.A., Girgis-Gabardo, A., Mansouri, A., Gruss, P., and Rudnicki, M.A. (2000). Pax7 is required for the specification of myogenic satellite cells. *Cell* *102*, 777-786.
- Sebastian, S., Faralli, H., Yao, Z., Rakopoulos, P., Pali, C., Cao, Y., Singh, K., Liu, Q.C., Chu, A., Aziz, A., *et al.* (2013). Tissue-specific splicing of a ubiquitously expressed transcription factor is essential for muscle differentiation. *Genes & development* *27*, 1247-1259.
- Selenko, P., Sprangers, R., Stier, G., Bühler, D., Fischer, U., and Sattler, M. (2001). SMN tudor domain structure and its interaction with the Sm proteins. *Nature structural biology* *8*, 27-31.

- Serrano, A.L., Mann, C.J., Vidal, B., Ardite, E., Perdiguero, E., and Muñoz-Cánoves, P. (2011). Cellular and molecular mechanisms regulating fibrosis in skeletal muscle repair and disease. *Current topics in developmental biology* 96, 167-201.
- Shang, M., Cappellesso, F., Amorim, R., Serneels, J., Virga, F., Eelen, G., Carobbio, S., Rincon, M.Y., Maechler, P., De Bock, K., *et al.* (2020). Macrophage-derived glutamine boosts satellite cells and muscle regeneration. *Nature* 587, 626-631.
- Shen, S., Park, J.W., Lu, Z.X., Lin, L., Henry, M.D., Wu, Y.N., Zhou, Q., and Xing, Y. (2014). rMATS: robust and flexible detection of differential alternative splicing from replicate RNA-Seq data. *Proceedings of the National Academy of Sciences of the United States of America* 111, E5593-5601.
- Shen, Y., Gao, G., Yu, X., Kim, H., Wang, L., Xie, L., Schwarz, M., Chen, X., Guccione, E., Liu, J., *et al.* (2020). Discovery of First-in-Class Protein Arginine Methyltransferase 5 (PRMT5) Degraders. *Journal of medicinal chemistry* 63, 9977-9989.
- Shi, F., Deng, Z., Zhou, Z., Jiang, C.Y., Zhao, R.Z., Sun, F., Cui, D., Bei, X.Y., Yang, B.Y., Sun, Q., *et al.* (2019). QKI-6 inhibits bladder cancer malignant behaviours through down-regulating E2F3 and NF- κ B signalling. *Journal of cellular and molecular medicine* 23, 6578-6594.
- Shinin, V., Gayraud-Morel, B., Gomès, D., and Tajbakhsh, S. (2006). Asymmetric division and cosegregation of template DNA strands in adult muscle satellite cells. *Nature cell biology* 8, 677-687.
- Sidman, R.L., Dickie, M.M., and Appel, S.H. (1964). MUTANT MICE (QUAKING AND JIMPY) WITH DEFICIENT MYELINATION IN THE CENTRAL NERVOUS SYSTEM. *Science (New York, NY)* 144, 309-311.
- Sikorsky, T., Hobor, F., Krizanova, E., Pasulka, J., Kubicek, K., and Stefl, R. (2012). Recognition of asymmetrically dimethylated arginine by TDRD3. *Nucleic acids research* 40, 11748-11755.
- Sims, R.J., 3rd, Rojas, L.A., Beck, D.B., Bonasio, R., Schüller, R., Drury, W.J., 3rd, Eick, D., and Reinberg, D. (2011). The C-terminal domain of RNA polymerase II is modified by site-specific methylation. *Science (New York, NY)* 332, 99-103.
- Sinha, M., Jang, Y.C., Oh, J., Khong, D., Wu, E.Y., Manohar, R., Miller, C., Regalado, S.G., Loffredo, F.S., Pancoast, J.R., *et al.* (2014). Restoring systemic GDF11 levels reverses age-related dysfunction in mouse skeletal muscle. *Science (New York, NY)* 344, 649-652.
- Sinha, R., Kim, Y.J., Nomakuchi, T., Sahashi, K., Hua, Y., Rigo, F., Bennett, C.F., and Krainer, A.R. (2018). Antisense oligonucleotides correct the familial dysautonomia splicing defect in IKBKAP transgenic mice. *Nucleic acids research* 46, 4833-4844.
- Soleimani, V.D., Punch, V.G., Kawabe, Y., Jones, A.E., Palidwor, G.A., Porter, C.J., Cross, J.W., Carvajal, J.J., Kockx, C.E., van, I.W.F., *et al.* (2012). Transcriptional dominance of Pax7 in adult myogenesis is due to high-affinity recognition of homeodomain motifs. *Developmental cell* 22, 1208-1220.
- Sommer, S., Lavi, U., and Darnell, J.E., Jr. (1978). The absolute frequency of labeled N-6-methyladenosine in HeLa cell messenger RNA decreases with label time. *Journal of molecular biology* 124, 487-499.
- Song, A., Wang, Q., Goebel, M.G., and Harrington, M.A. (1998). Phosphorylation of nuclear MyoD is required for its rapid degradation. *Molecular and cellular biology* 18, 4994-4999.
- Song, M., Bode, A.M., Dong, Z., and Lee, M.H. (2019). AKT as a Therapeutic Target for Cancer. *Cancer research* 79, 1019-1031.

- Song, W.K., Wang, W., Foster, R.F., Bielser, D.A., and Kaufman, S.J. (1992). H36-alpha 7 is a novel integrin alpha chain that is developmentally regulated during skeletal myogenesis. *The Journal of cell biology* *117*, 643-657.
- Song, W.K., Wang, W., Sato, H., Bielser, D.A., and Kaufman, S.J. (1993). Expression of alpha 7 integrin cytoplasmic domains during skeletal muscle development: alternate forms, conformational change, and homologies with serine/threonine kinases and tyrosine phosphatases. *Journal of cell science* *106 (Pt 4)*, 1139-1152.
- Sousa-Victor, P., and Muñoz-Cánoves, P. (2016). Regenerative decline of stem cells in sarcopenia. *Molecular aspects of medicine* *50*, 109-117.
- Sprangers, R., Groves, M.R., Sinning, I., and Sattler, M. (2003). High-resolution X-ray and NMR structures of the SMN Tudor domain: conformational variation in the binding site for symmetrically dimethylated arginine residues. *Journal of molecular biology* *327*, 507-520.
- Stouth, D.W., Manta, A., and Ljubicic, V. (2018). Protein arginine methyltransferase expression, localization, and activity during disuse-induced skeletal muscle plasticity. *American journal of physiology Cell physiology* *314*, C177-c190.
- Stouth, D.W., vanLieshout, T.L., Ng, S.Y., Webb, E.K., Manta, A., Moll, Z., and Ljubicic, V. (2020). CARM1 Regulates AMPK Signaling in Skeletal Muscle. *iScience* *23*, 101755.
- Szewczyk, M.M., Ishikawa, Y., Organ, S., Sakai, N., Li, F., Halabelian, L., Ackloo, S., Couzens, A.L., Eram, M., Dilworth, D., *et al.* (2020). Pharmacological inhibition of PRMT7 links arginine monomethylation to the cellular stress response. *Nature communications* *11*, 2396.
- Takada, Y., Ye, X., and Simon, S. (2007). The integrins. *Genome biology* *8*, 215.
- Talbot, K., Miguel-Aliaga, I., Mohaghegh, P., Ponting, C.P., and Davies, K.E. (1998). Characterization of a gene encoding survival motor neuron (SMN)-related protein, a constituent of the spliceosome complex. *Human molecular genetics* *7*, 2149-2156.
- Tang, J., Frankel, A., Cook, R.J., Kim, S., Paik, W.K., Williams, K.R., Clarke, S., and Herschman, H.R. (2000). PRMT1 is the predominant type I protein arginine methyltransferase in mammalian cells. *The Journal of biological chemistry* *275*, 7723-7730.
- Tao, Y., Nepl, R.L., Huang, Z.P., Chen, J., Tang, R.H., Cao, R., Zhang, Y., Jin, S.W., and Wang, D.Z. (2011). The histone methyltransferase Set7/9 promotes myoblast differentiation and myofibril assembly. *The Journal of cell biology* *194*, 551-565.
- Teperino, R., Amann, S., Bayer, M., McGee, S.L., Loipetzberger, A., Connor, T., Jaeger, C., Kammerer, B., Winter, L., Wiche, G., *et al.* (2012). Hedgehog partial agonism drives Warburg-like metabolism in muscle and brown fat. *Cell* *151*, 414-426.
- Teplova, M., Hafner, M., Teplov, D., Essig, K., Tuschl, T., and Patel, D.J. (2013). Structure-function studies of STAR family Quaking proteins bound to their in vivo RNA target sites. *Genes & development* *27*, 928-940.
- Teyssier, C., Ma, H., Emter, R., Kralli, A., and Stallcup, M.R. (2005). Activation of nuclear receptor coactivator PGC-1alpha by arginine methylation. *Genes & development* *19*, 1466-1473.
- Thandapani, P., O'Connor, T.R., Bailey, T.L., and Richard, S. (2013). Defining the RGG/RG motif. *Molecular cell* *50*, 613-623.
- Theret, M., Gsaier, L., Schaffer, B., Juban, G., Ben Larbi, S., Weiss-Gayet, M., Bultot, L., Collodet, C., Foretz, M., Desplanches, D., *et al.* (2017). AMPK α 1-LDH pathway regulates muscle stem cell self-renewal by controlling metabolic homeostasis. *The EMBO journal* *36*, 1946-1962.

- Thomas, J.D., Sznajder Ł, J., Bardhi, O., Aslam, F.N., Anastasiadis, Z.P., Scotti, M.M., Nishino, I., Nakamori, M., Wang, E.T., and Swanson, M.S. (2017). Disrupted prenatal RNA processing and myogenesis in congenital myotonic dystrophy. *Genes & development* 31, 1122-1133.
- Thomson, D.M. (2018). The Role of AMPK in the Regulation of Skeletal Muscle Size, Hypertrophy, and Regeneration. *International journal of molecular sciences* 19.
- Tradewell, M.L., Yu, Z., Tibshirani, M., Boulanger, M.C., Durham, H.D., and Richard, S. (2012). Arginine methylation by PRMT1 regulates nuclear-cytoplasmic localization and toxicity of FUS/TLS harbouring ALS-linked mutations. *Human molecular genetics* 21, 136-149.
- Trapnell, C., Cacchiarelli, D., Grimsby, J., Pokharel, P., Li, S., Morse, M., Lennon, N.J., Livak, K.J., Mikkelsen, T.S., and Rinn, J.L. (2014). The dynamics and regulators of cell fate decisions are revealed by pseudotemporal ordering of single cells. *Nature biotechnology* 32, 381-386.
- Trapnell, C., Roberts, A., Goff, L., Pertea, G., Kim, D., Kelley, D.R., Pimentel, H., Salzberg, S.L., Rinn, J.L., and Pachter, L. (2012). Differential gene and transcript expression analysis of RNA-seq experiments with TopHat and Cufflinks. *Nature protocols* 7, 562-578.
- Trapnell, C., Williams, B.A., Pertea, G., Mortazavi, A., Kwan, G., van Baren, M.J., Salzberg, S.L., Wold, B.J., and Pachter, L. (2010). Transcript assembly and quantification by RNA-Seq reveals unannotated transcripts and isoform switching during cell differentiation. *Nature biotechnology* 28, 511-515.
- Tripsianes, K., Madl, T., Machyna, M., Fessas, D., Englbrecht, C., Fischer, U., Neugebauer, K.M., and Sattler, M. (2011). Structural basis for dimethylarginine recognition by the Tudor domains of human SMN and SPF30 proteins. *Nature structural & molecular biology* 18, 1414-1420.
- Troy, A., Cadwallader, A.B., Fedorov, Y., Tyner, K., Tanaka, K.K., and Olwin, B.B. (2012). Coordination of satellite cell activation and self-renewal by Par-complex-dependent asymmetric activation of p38 α/β MAPK. *Cell stem cell* 11, 541-553.
- Valent, P., Bonnet, D., De Maria, R., Lapidot, T., Copland, M., Melo, J.V., Chomienne, C., Ishikawa, F., Schuringa, J.J., Stassi, G., *et al.* (2012). Cancer stem cell definitions and terminology: the devil is in the details. *Nature reviews Cancer* 12, 767-775.
- van den Brink, S.C., Sage, F., Vértesy, Á., Spanjaard, B., Peterson-Maduro, J., Baron, C.S., Robin, C., and van Oudenaarden, A. (2017). Single-cell sequencing reveals dissociation-induced gene expression in tissue subpopulations. *Nature methods* 14, 935-936.
- van der Veer, E.P., de Bruin, R.G., Kraaijeveld, A.O., de Vries, M.R., Bot, I., Pera, T., Segers, F.M., Trompet, S., van Gils, J.M., Roeten, M.K., *et al.* (2013). Quaking, an RNA-binding protein, is a critical regulator of vascular smooth muscle cell phenotype. *Circulation research* 113, 1065-1075.
- van Velthoven, C.T.J., de Morree, A., Egner, I.M., Brett, J.O., and Rando, T.A. (2017). Transcriptional Profiling of Quiescent Muscle Stem Cells In Vivo. *Cell reports* 21, 1994-2004.
- Vander Heiden, M.G., Cantley, L.C., and Thompson, C.B. (2009). Understanding the Warburg effect: the metabolic requirements of cell proliferation. *Science (New York, NY)* 324, 1029-1033.
- Vansteenkiste, J., Van Cutsem, E., Dumez, H., Chen, C., Ricker, J.L., Randolph, S.S., and Schöffski, P. (2008). Early phase II trial of oral vorinostat in relapsed or refractory breast, colorectal, or non-small cell lung cancer. *Investigational new drugs* 26, 483-488.
- von der Mark, H., Williams, I., Wendler, O., Sorokin, L., von der Mark, K., and Pöschl, E. (2002). Alternative splice variants of alpha 7 beta 1 integrin selectively recognize different laminin isoforms. *The Journal of biological chemistry* 277, 6012-6016.

- von Maltzahn, J., Jones, A.E., Parks, R.J., and Rudnicki, M.A. (2013). Pax7 is critical for the normal function of satellite cells in adult skeletal muscle. *Proceedings of the National Academy of Sciences of the United States of America* 110, 16474-16479.
- Walport, L.J., Hopkinson, R.J., Chowdhury, R., Schiller, R., Ge, W., Kawamura, A., and Schofield, C.J. (2016). Arginine demethylation is catalysed by a subset of JmjC histone lysine demethylases. *Nature communications* 7, 11974.
- Wang, M., Fuhrmann, J., and Thompson, P.R. (2014). Protein arginine methyltransferase 5 catalyzes substrate dimethylation in a distributive fashion. *Biochemistry* 53, 7884-7892.
- Wang, P., Doxtader, K.A., and Nam, Y. (2016a). Structural Basis for Cooperative Function of Mettl3 and Mettl14 Methyltransferases. *Molecular cell* 63, 306-317.
- Wang, R.Q., Lan, Y.L., Lou, J.C., Lyu, Y.Z., Hao, Y.C., Su, Q.F., Ma, B.B., Yuan, Z.B., Yu, Z.K., Zhang, H.Q., *et al.* (2019a). Expression and methylation status of LAMA2 are associated with the invasiveness of nonfunctioning PitNET. *Therapeutic advances in endocrinology and metabolism* 10, 2042018818821296.
- Wang, X., Feng, J., Xue, Y., Guan, Z., Zhang, D., Liu, Z., Gong, Z., Wang, Q., Huang, J., Tang, C., *et al.* (2016b). Structural basis of N(6)-adenosine methylation by the METTL3-METTL14 complex. *Nature* 534, 575-578.
- Wang, Y., Wysocka, J., Sayegh, J., Lee, Y.H., Perlin, J.R., Leonelli, L., Sonbuchner, L.S., McDonald, C.H., Cook, R.G., Dou, Y., *et al.* (2004). Human PAD4 regulates histone arginine methylation levels via demethyliminination. *Science (New York, NY)* 306, 279-283.
- Wang, Y.X., Bentzinger, C.F., and Rudnicki, M.A. (2013). Treating muscular dystrophy by stimulating intrinsic repair. *Regenerative medicine* 8, 237-240.
- Wang, Y.X., Feige, P., Brun, C.E., Hekmatnejad, B., Dumont, N.A., Renaud, J.M., Faulkes, S., Guindon, D.E., and Rudnicki, M.A. (2019b). EGFR-Aurka Signaling Rescues Polarity and Regeneration Defects in Dystrophin-Deficient Muscle Stem Cells by Increasing Asymmetric Divisions. *Cell stem cell* 24, 419-432.e416.
- Webb, R.C. (2003). Smooth muscle contraction and relaxation. *Advances in physiology education* 27, 201-206.
- Wheeler, T.M., Lueck, J.D., Swanson, M.S., Dirksen, R.T., and Thornton, C.A. (2007). Correction of CIC-1 splicing eliminates chloride channelopathy and myotonia in mouse models of myotonic dystrophy. *The Journal of clinical investigation* 117, 3952-3957.
- Wheeler, T.M., Sobczak, K., Lueck, J.D., Osborne, R.J., Lin, X., Dirksen, R.T., and Thornton, C.A. (2009). Reversal of RNA dominance by displacement of protein sequestered on triplet repeat RNA. *Science (New York, NY)* 325, 336-339.
- Wilkinson, M.E., Charenton, C., and Nagai, K. (2020). RNA Splicing by the Spliceosome. *Annual review of biochemistry* 89, 359-388.
- Wilson, D.P. (2011). Vascular Smooth Muscle Structure and Function. In *Mechanisms of Vascular Disease: A Reference Book for Vascular Specialists*, R. Fitridge, and M. Thompson, eds. (Adelaide (AU): University of Adelaide Press).
- Wolf, C.R., Hayward, I.P., Lawrie, S.S., Buckton, K., McIntyre, M.A., Adams, D.J., Lewis, A.D., Scott, A.R., and Smyth, J.F. (1987). Cellular heterogeneity and drug resistance in two ovarian adenocarcinoma cell lines derived from a single patient. *Int J Cancer* 39, 695-702.
- Wong, D.J., Liu, H., Ridky, T.W., Cassarino, D., Segal, E., and Chang, H.Y. (2008). Module map of stem cell genes guides creation of epithelial cancer stem cells. *Cell stem cell* 2, 333-344.

- Wosczyzna, M.N., Konishi, C.T., Perez Carbajal, E.E., Wang, T.T., Walsh, R.A., Gan, Q., Wagner, M.W., and Rando, T.A. (2019). Mesenchymal Stromal Cells Are Required for Regeneration and Homeostatic Maintenance of Skeletal Muscle. *Cell reports* *27*, 2029-2035.e2025.
- Wu, H.Y., Dawson, M.R., Reynolds, R., and Hardy, R.J. (2001). Expression of QKI proteins and MAP1B identifies actively myelinating oligodendrocytes in adult rat brain. *Molecular and cellular neurosciences* *17*, 292-302.
- Wu, J.I., Reed, R.B., Grabowski, P.J., and Artzt, K. (2002). Function of quaking in myelination: regulation of alternative splicing. *Proceedings of the National Academy of Sciences of the United States of America* *99*, 4233-4238.
- Wu, Q., Schapira, M., Arrowsmith, C.H., and Barsyte-Lovejoy, D. (2021). Protein arginine methylation: from enigmatic functions to therapeutic targeting. *Nature reviews Drug discovery* *20*, 509-530.
- Xu, J., and Richard, S. (2021). Cellular pathways influenced by protein arginine methylation: Implications for cancer. *Molecular cell*.
- Xue, L., Bao, L., Roediger, J., Su, Y., Shi, B., and Shi, Y.-B. (2021). Protein arginine methyltransferase 1 regulates cell proliferation and differentiation in adult mouse adult intestine. *Cell & Bioscience* *11*, 113.
- Yang, Y., Lu, Y., Espejo, A., Wu, J., Xu, W., Liang, S., and Bedford, M.T. (2010). TDRD3 is an effector molecule for arginine-methylated histone marks. *Molecular cell* *40*, 1016-1023.
- Yao, B., Gui, T., Zeng, X., Deng, Y., Wang, Z., Wang, Y., Yang, D., Li, Q., Xu, P., Hu, R., *et al.* (2021). PRMT1-mediated H4R3me2a recruits SMARCA4 to promote colorectal cancer progression by enhancing EGFR signaling. *Genome medicine* *13*, 58.
- Yao, J., Fetter, R.D., Hu, P., Betzig, E., and Tjian, R. (2011). Subnuclear segregation of genes and core promoter factors in myogenesis. *Genes & development* *25*, 569-580.
- Yin, H., Price, F., and Rudnicki, M.A. (2013). Satellite cells and the muscle stem cell niche. *Physiological reviews* *93*, 23-67.
- Yin, S., Liu, L., Brobbey, C., Palanisamy, V., Ball, L.E., Olsen, S.K., Ostrowski, M.C., and Gan, W. (2021). PRMT5-mediated arginine methylation activates AKT kinase to govern tumorigenesis. *Nature communications* *12*, 3444.
- Ying, H., Dey, P., Yao, W., Kimmelman, A.C., Draetta, G.F., Maitra, A., and DePinho, R.A. (2016). Genetics and biology of pancreatic ductal adenocarcinoma. *Genes & development* *30*, 355-385.
- Yu, F., Jin, L., Yang, G., Ji, L., Wang, F., and Lu, Z. (2014). Post-transcriptional repression of FOXO1 by QKI results in low levels of FOXO1 expression in breast cancer cells. *Oncology reports* *31*, 1459-1465.
- Yu, Z., Chen, T., Hebert, J., Li, E., and Richard, S. (2009). A mouse PRMT1 null allele defines an essential role for arginine methylation in genome maintenance and cell proliferation. *Molecular and cellular biology* *29*, 2982-2996.
- Zappia, V., Della Ragione, F., Pontoni, G., Gragnaniello, V., and Carteni-Farina, M. (1988). Human 5'-deoxy-5'-methylthioadenosine phosphorylase: kinetic studies and catalytic mechanism. *Advances in experimental medicine and biology* *250*, 165-177.
- Zaremba, T., and Curtin, N.J. (2007). PARP inhibitor development for systemic cancer targeting. *Anti-cancer agents in medicinal chemistry* *7*, 515-523.
- Zhang, K., Yan, F., Lei, X., Wei, D., Lu, H., Zhu, Z., Xiang, A., Ye, Z., Wang, L., Zheng, W., *et al.* (2018). Androgen receptor-mediated upregulation of quaking affects androgen

- receptor-related prostate cancer development and anti-androgen receptor therapy. *Molecular medicine reports* *17*, 8203-8211.
- Zhang, T., Gunther, S., Looso, M., Kunne, C., Kruger, M., Kim, J., Zhou, Y., and Braun, T. (2015). Prmt5 is a regulator of muscle stem cell expansion in adult mice. *Nature communications* *6*, 7140.
- Zhang, X., and Cheng, X. (2003). Structure of the predominant protein arginine methyltransferase PRMT1 and analysis of its binding to substrate peptides. *Structure (London, England : 1993)* *11*, 509-520.
- Zhang, Y., and Kalderon, D. (2001). Hedgehog acts as a somatic stem cell factor in the *Drosophila* ovary. *Nature* *410*, 599-604.
- Zhang, Y., Lu, Z., Ku, L., Chen, Y., Wang, H., and Feng, Y. (2003). Tyrosine phosphorylation of QKI mediates developmental signals to regulate mRNA metabolism. *The EMBO journal* *22*, 1801-1810.
- Zheng, S., Moehlenbrink, J., Lu, Y.C., Zalmas, L.P., Sagum, C.A., Carr, S., McGouran, J.F., Alexander, L., Fedorov, O., Munro, S., *et al.* (2013). Arginine methylation-dependent reader-writer interplay governs growth control by E2F-1. *Molecular cell* *52*, 37-51.
- Ziober, B.L., Vu, M.P., Waleh, N., Crawford, J., Lin, C.S., and Kramer, R.H. (1993). Alternative extracellular and cytoplasmic domains of the integrin alpha 7 subunit are differentially expressed during development. *The Journal of biological chemistry* *268*, 26773-26783.
- Zismanov, V., Chichkov, V., Colangelo, V., Jamet, S., Wang, S., Syme, A., Koromilas, A.E., and Crist, C. (2016). Phosphorylation of eIF2alpha Is a Translational Control Mechanism Regulating Muscle Stem Cell Quiescence and Self-Renewal. *Cell stem cell* *18*, 79-90.
- Zong, F.Y., Fu, X., Wei, W.J., Luo, Y.G., Heiner, M., Cao, L.J., Fang, Z., Fang, R., Lu, D., Ji, H., *et al.* (2014). The RNA-binding protein QKI suppresses cancer-associated aberrant splicing. *PLoS genetics* *10*, e1004289.